Research Center Borstel
Leibniz Lung Center
Priority Research Area Infections
Program Director: Prof. Dr. Ulrich E. Schaible
Group: Cellular Microbiology

Differential neutrophil responses to *Mycobacterium tuberculosis* in human and mice

Dissertation
for Fulfilment of Requirements
for the Doctoral Degree of the University of Lübeck
from the Department of Natural Sciences

Submitted by Lara Christine Linnemann
From Detmold, Germany

Hamburg, 202

First Referee:	Prof. Dr. rer. nat. Ulrich E. Schaible
Second Referee:	PD Dr. rer. nat. Kathrin Kalies
Date of Oral examination:	25.05.21
Approved for printing:	26.05.21

1 TABLE OF CONTENTS

2 SUMMARY

Despite almost one and a half centuries of research, tuberculosis (TB) caused by *Mycobacterium tuberculosis* (Mtb) remains a major health threat with approximately 10 million people affected in 2019. Though more than 90% of all infections remain latent, some patients can develop active TB resulting in severe tissue inflammation, organ destruction and death with 1.4 million being killed in 2019.

The facultative intracellular microorganism can evade immune responses and killing by the host defence. Of great concern are the growing numbers of antibiotic resistant isolates. Therefore, host-directed therapies (HDT) targeting the hosts responses need to be explored to accompany antibiotic treatment and to improve restriction of bacterial growth, pathology and transmission. Polymorphonuclear neutrophils (PMN) are prime infected cells in active TB patients and associated with enhanced susceptibility in murine TB models. Further, PMN seem to be used by the pathogen for its advantage. Mtb infection drives human PMN into necrotic cell death, which is dependent on reactive oxygen species (ROS) produced by myeloperoxidase (MPO) and subsequent phagocytosis of infected necrotic PMN by macrophages promotes Mtb growth. However, inhibition of MPO resulted in PMN apoptosis as well as reduced subsequent bacterial growth in macrophages. Based on these findings, we wanted I) to analyse ROS induced alterations in the PMN lipidome and II) to adapt this pathogenic process to the murine model in order to develop a HDT, targeting necrotic cell death of infected PMN as prerequisite for mycobacterial growth and pathology using two irreversible MPO inhibitors, ABAH and AZD5904.

Analysis of infection mediated changes of the human PMN lipidome by comparative mass spectrometry revealed metabolically induced changes based on lipid consumption by Mtb, rather than alterations caused by ROS or necrosis, which was shown by an early reduction of triacylglycerols upon Mtb infection and reduced cholesterols in infected, but apoptotic PMN. Using murine PMN isolated from distinct sources and with different maturation statuses, *in vitro* studies on effector functions, such as phagocytosis, MPO activity, ROS production and necrosis revealed, that freshly isolated bone marrow derived PMN were impaired in phagocytosis and ROS production despite active MPO and showed spontaneous infection independent necrosis, which made them unsuitable for the infection assays. Maturation of these cells by granulocyte colony stimulation factor (G-CSF) significantly enhanced the phagocytosis rate, ROS production and infection induced necrosis similar to

fully functional murine blood derived effector PMN. Inhibition of MPO activity by ABAH in matured bone marrow derived PMN did neither reduce ROS production nor necrosis upon Mtb infection, which is in contrast to human PMN. In order to test MPO inhibitors on the outcome of experimental TB, we used the susceptible C3HeB/FeJ mouse model, which resembles human pathology with increased PMN recruitment. However, neither different treatment schedules turned out to improve pathology, health score, mycobacterial burden nor antibiotic co-treatment using isoniazid (INH). Taken together, the functional differences observed between murine and human PMN are likely responsible for the failure of MPO inhibition to change the course of Mtb infection in susceptible mice and emphasizes the importance to evaluate results from animal models carefully. Therefore, exploring PMN and their effectors to develop HDT in TB must consider both *in vivo* TB models or different ways for evaluation.

3 ZUSAMMENFASSUNG

Trotz mehr als anderthalb Jahrhunderten der Forschung gehört die durch das *Mycobacterium tuberculosis* (Mtb) Bakterium ausgelöste Tuberkulose (TB) mit circa 10 Millionen neuinfizierten Menschen in 2019 zu den größten Gesundheitsbedrohungen der Menschheit. Obwohl mehr als 90% der Infektionen latent bleiben, können einige Patienten eine aktive TB entwickeln, welche zu schweren Entzündungen, zur Zerstörung von Organen und unbehandelt letztlich zum Tode führt. Dies wird durch 1,4 Millionen Tote im Jahre 2019 verdeutlicht.

Das fakultative intrazelluläre Bakterium ist perfekt angepasst, um der Immunantwort und einer Elimination durch den Wirt zu entgehen. Der Anstieg von Antibiotika resistenten Mtb-Stämmen verschärft diese Situation weiter. Daher besteht ein großes Interesse an Wirts-orientierter Therapie (HDT – ‚Host-directed therapy'). Hier rückt die Immunantwort des Wirts in den Fokus der Behandlung um Entzündungen, bakterielles Wachstum und die Weiterverbreitung zu reduzieren. Ein besonderes Interesse liegt dabei auf Neutrophilen Granulozyten, da diese die größte infizierte Zellpopulation in Patienten stellen. Im Mausmodell stehen diese zudem in einem direkten Zusammenhang mit der Schwere der Infektion. Neutrophile scheinen darüber hinaus von Mtb zu ihrem Vorteil ausgenutzt zu werden. Eine Mtb Infektion löst einen nekrotischen Zelltod in menschlichen Neutrophilen aus, welcher abhängig ist von der Produktion von reaktiven Sauerstoffspezies (ROS – reactive oxigen species) durch das Enzym Myeloperoxidase (MPO). Der nekrotische Zelltod befördert dazu das Wachstum von Mtb in Zellen, welche die nekrotischen Zellreste phagozytierten. Die Inhibition von MPO resultiert in einem apoptotischen Zelltod sowie einem reduzierten Wachstum des Erregers in nachfolgenden Zellen. Basierend auf diesen Erkenntnissen möchte diese Studie I) ROS induzierte Veränderungen des Neutrophilen Lipidoms untersuchen, sowie II) die Ergebnisse der pathogenen Prozesse in ein Mausmodell übertragen. So könnte eine HDT entwickelt werden, welche den nekrotischen Zelltod als Voraussetzung für mykobakterielles Wachstum und Entzündungen in den Fokus nimmt. Zur Verwendung kommen hier die irreversiblen MPO Inhibitoren ABAH und AZD5904.

Die Analyse von Veränderungen des humanen neutrophilen Lipidoms durch vergleichende massenspektrometrische Untersuchungen wies eher auf metabolisch basierte Veränderungen durch die Mtb Infektion hin, anstatt auf ROS induzierte Oxidation hin. Dies zeigte sich durch eine frühe, signifikante Reduktion der Triacylglycerasen in Mtb infizierten Zellen und eine

spätere Reduzierung von Cholesterolen in infizierten, aber apoptotischen Zellen. Um eine murine Zellpopulation zu identifizieren, welche sich am besten für die Infektionsversuche eignet, wurden verschiedene Neutrophil Populationen untersucht. Es zeigte sich, dass diese unterschiedliche Effektorfunktionen, wie Phagozytose, ROS Produktion und Infektionsinduzierte Nekrose aufwiesen. Unreife Knochenmarks-Neutrophile waren in diesen Effektorfunktionen beeinträchtigt, wodurch sie sich für die nachfolgenden Untersuchungen nicht eigneten. Die Reifung der Knochenmarkszellen mit Granulozyten-Kolonie-stimulierendem Faktor (G-CSF) erhöhte die Phagozytoserate, ROS Produktion und Mtb induzierte Nekrose signifikant, sodass diese Zellen mit voll funktionsfähigen murinen Blut-Neutrophilen vergleichbar waren. Eine MPO Inhibition reduzierte allerdings nicht die ROS Produktion oder Nekrose in den Zellen, was in Kontrast zu den Studien mit humanen Neutrophilen steht. Um den Effekt einer MPO Inhibition auf experimentelle TB zu untersuchen, wurden TB empfängliche C3HeB/FeJ Mäuse infiziert, welche die humane Pathologie einer erhöhten Rekrutierung von Neutrophilen wiederspiegeln. Allerdings konnten weder unterschiedliche Behandlungspläne, noch eine Kombinationstherapie mit dem Antibiotika Isoniazid die Pathologie oder den Gesundheitszustand der Tiere verbessern. Abschließend deuten die funktionalen Unterschiede zwischen humanen und murinen Neutrophilen darauf hin, dass eine MPO Inhibition nicht stattgefunden hat oder andere Mechanismen im Mausmodell im Vordergrund stehen. Dazu wird die Wichtigkeit einer gründlichen und vorsichtigen Evaluation von Tierversuchsergebnissen unterstrichen. Um die Effektormechanismen von Neutrophilen in einer HDT zu nutzen, müssen daher beide *in vivo* Modelle beachtet oder unterschiedliche Methoden der Evaluation herangezogen werden.

4 INTRODUCTION

4.1 Tuberculosis

4.1.1 The burden of Tuberculosis

Tuberculosis (TB) is an airborne, infectious disease caused by *Mycobacterium tuberculosis* (Mtb). Despite more than a century of scientific research TB is still one of the major public health threats in the world. It ranks among the top 10 causes of death and is the leading killer from one single pathogen. Around 10 million people fell ill with TB and 1.4 million people died in 2019 due to an Mtb infection. It is estimated that roughly one quarter of the world's population is latently infected with Mtb (LTBI) but only 5-10% of those LTBI patients are expected to develop active tuberculosis during their lifetime. The lack of an effective vaccine and the increasing numbers of antibiotic resistant infections challenge healthcare systems, especially in low- and middle-income countries. Around half a million drug resistant cases were diagnosed in 2019, from which only 57% can be treated successfully [1].

4.1.2 A short history of Tuberculosis: 'the white plaque'

From all infectious agents, Mtb is among those which had the broadest impact on human history. The Greek physician Hippocrates of Koz (460 – 370 BC) was probably the first, who discriminated TB as phthisis ("consumption" or "wasting away") from other forms of lung diseases and identified the malady as one of the most common causes of death in his period [2]. Aristoteles was extraordinary perceptive, when he suspected the cause of the disease being contagious, rather than hereditary, as Hippocrates has suggested [3]. However, the perception of a TB related genetic endowment was a common misconception, accepted until the 19th century, even though some physicians already suspected invisible microorganism as the contagious agent of TB [4]. Until its final classification, diseases with tuberculosis like symptoms were numerous and had many names like consumption, scrofula (describing the swelling of the lymph nodes), Pott's disease (named after Percivall Pott, who was the first describing arthritic TB of the spine) and the white plaque. On one hand, this term described the anaemia induced paleness of the patients, but was also used as a metaphorical association for the innocence and youth of infected children and young people that were affected in great numbers. In 1679, Francis Sylvius was the first to describe the characteristic granuloma found in infected lungs [3]. The term describes the most common

pathological characteristics: roundish lesions, usually enclosed in the tissue but filled with infectious pus and necrotic cells. After the discovery of the causative agent, *Mycobacterium tuberculosis,* by Robert Koch on the 24th of March 1882, the disease was finally named tuberculosis [5], and the era of TB research was initiated.

4.1.3 Epidemiology

TB remains a major public health threat, despite the discovery of antibiotics, effective against Mtb. Until the middle of the 20th century TB was common across the globe, while nowadays the incidences of active TB cases vary broadly between countries. The most affected areas are found in East Asia (44%), Sub-Saharan Africa (24%) and the Western Pacific (18%). These low to middle income countries share common features which drive the distribution of Mtb infections: poor housing, overcrowding, low ventilated and densely packed workplaces, poverty and malnutrition [1]. Further, a moderate lack of nutrients, which affects more people than acute famine, can already significantly increase the risk of developing active TB [6]. Other environmental factors are: an underdeveloped and poorly financed health care system, displacement, political instability or humanitarian crises [7]. Armed conflicts can lead to a dramatic increase of TB incidences. The Soviet Union break up [8] or the ongoing Syrian civil war [9] has brutally shown how the instability of a political system promotes an increase in TB incidences. With an ongoing deterioration of hygiene and living conditions LTBI people are more likely to develop active TB, leading to increased reoccurrence and Mtb dissemination. Considering poor or absent healthcare systems with insufficient therapeutic regimens, the evolution of resistant Mtb strains is almost pre-set. Subsequent displacement of refugees can finally spread the infection into neighbouring countries [7], [9].

4.1.4 Treatment of active tuberculosis

The standard regiment to treat drug susceptible TB requires 6-month treatment with a cocktail of multiple first-line antibiotics, typically including: Isoniazid, Rifampicin, Pyrazinamide and Ethambutol [10]. Drug toxicity induced adverse side effects and extended duration of treatment are additional stressors for the patients and often lead to non-compliance. This is a major driving force behind an alarming increase in rifampicin-resistant (RR-TB) and multidrug-resistance tuberculosis (MDR-TB) over the last decade. The latter is defined by the resistance against rifampicin and one other first line antibiotic [1]. In 2018

alone, half a million new rifampicin-resistant cases were reported from which 78% were even MDR cases. Affected by this development were India, with 27% of new cases being reported as RR-/MDR-TB, China with 14% and the Russian federation with 7%. Especially the development of RR-/MDR-TB from previously treatment-susceptible patients is a major cause of concern. Globally this development is seen in 18% of treated cases. However, the local occurrence of RR-/MDR-TB show great variations and reaches an alarming 50% in the countries of the former Soviet Union [11] (**Figure 1**). Due to a lack of alternatives, an aggressive chemotherapeutic treatment, lasting over two years, remains the only effective option. Additional resistance against two second-line agents results in extensively drug-resistant TB (XDR-TB), which, in some cases, becomes untreatable [11].

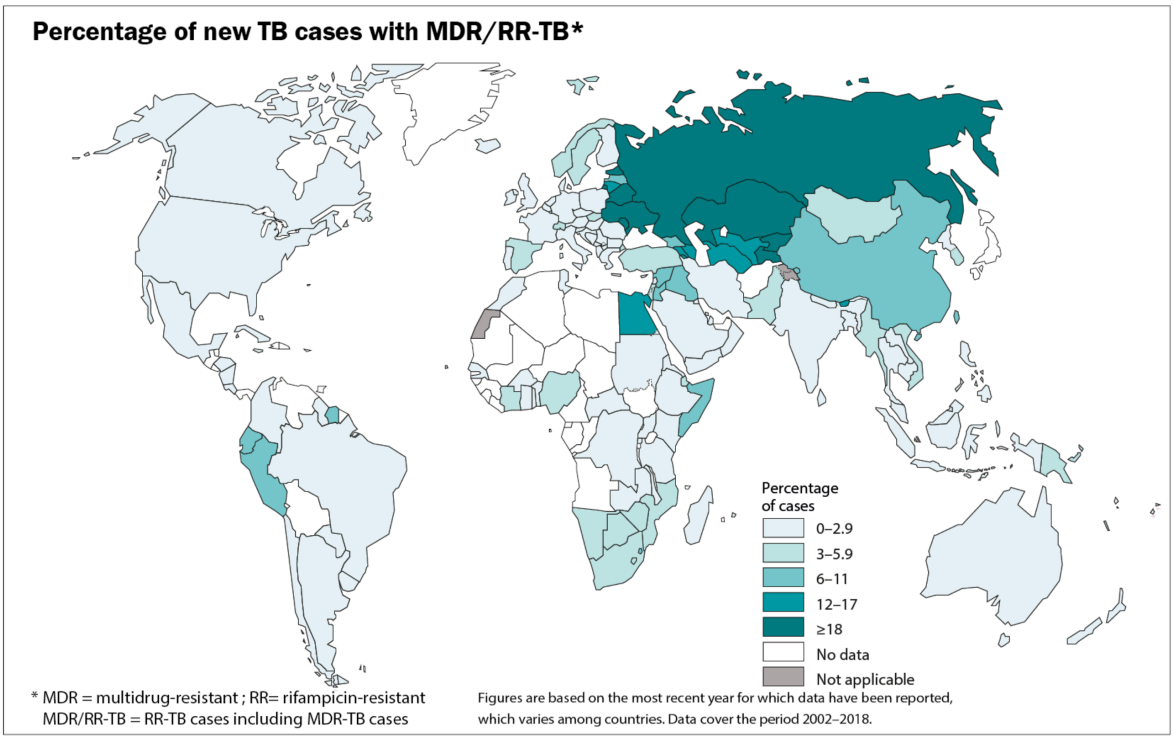

Figure 1 Incidence of MDR/RR-TB cases worldwide. Global multidrug- and rifampicin-resistant TB cases are depicted as percentage of total TB cases. Taken and modified from WHO's 'Global Health Observatory Map Gallery'. downloaded:14.10.2020 http://gamapserver.who.int/mapLibrary/Files/Maps/Global_TB_cases_new_mdr_rr_2017.png

4.1.5 The microorganism & it's virulence factors

Mycobacteria are bacillary rod shaped, obligate aerobe pathogens. More than 190 distinct species have been identified so far. A medical classification divides mycobacteria into the

following three groups: 1) non-tuberculous, ubiquitous occurring and fast growing environmental mycobacteria (NTM), for example the soil-living *Mycobacterium abcessus;* 2) *Mycobacterium leprae,* the causative agent of leprosy; 3) TB-inducing pathogenic mycobacteria termed *Mycobacterium Tuberculosis Complex* (MTBC), which includes the human pathogenic *M. tuberculosis, M. africanum* and *M. canetti* and causative agents for TB in other mammals like *M. bovis* in cattle*, M. pinnipedii* in seals and *M. microti* in voles.

MTBC strains are slow growing, acid-fast bacteria characterized by a thick waxy cell wall, which provides protection and is critical for the pathogen's survival. Its main components are cross-linked polymers, formed by peptidoglycan, incorporated, highly branched arabinogalactan polysaccharides and long-chain mycolic acids [12]. Mtb is adapted to an intracellular lifestyle, which further allows the pathogen to resist environmental stress like oxygen limitation, nutrient depletion and antimicrobial effector molecules, such as reactive oxygen species (ROS) and proteases. Additionally, Mtb has developed several virulence effector mechanisms to manipulate host cells and immune functions, like the inhibition of autophagy, acquisition of cytosolic access and induction of host cell death [13]. The induction of host cell death primarily relies on Mtb's ability to inhibit plasma membrane repair, destruction of mitochondrial membranes and inhibition of the formation of the apoptotic envelope [14]. One important virulent factor is the early secreted antigenic target-6 (ESAT-6) exported via the typeVII secretion system ESX-1. It is a system to release proteins with immune-escaping functions. It has many direct and indirect effects upon infection, like the immediate induction of matrix metalloprotease 6 in epithelial cells, thereby attracting monocytes and macrophages [15] or releasing proteins, that induce phagosome rupture [16]. Additionally, ESAT-6 has been associated with the induction of necrosis in PMN, which subsequently enhances inflammation and tissue destruction [17].

4.2 Pathology of Tuberculosis

The majority of 70% of Mtb infections become pulmonary. Yet, extrapulmonary TB can affect almost every other part of the body, most likely bones and joints, the nervous system or the pleural cavity [18]. However, the lung pathology of TB reflects the course of infection in other organs. While some invaded bacteria are kept life-long in encapsulated granulomas, which is then called latent TB (LTBI), primary TB or the reactivation of LTBI can cause detrimental outcomes. The progression of the disease is initiated by a sudden increase in bacterial replication, leading to extensive inflammation and necrosis. Progressing TB further

develops caseating granulomas. These caseous, pus containing lesions consist of necrotic cells and destroyed tissue material and are highly infectious. The burst of encapsulated inflammatory pus into adjacent tissue, leads to dissemination and, ultimately, respiratory spreading of the pathogen. In severe cases, the pathology results in cavitation and, thus, destruction of the organ and reduced lung function [19].

4.2.1 Initial infection and establishment of the cellular immune responses

Primary infection with Mtb starts in the lower respiratory tract with the inhalation of Mtb containing nuclear droplets, also called aerosols, after being in close contact to an infectious person (**Figure 2 A**). Once in the lung, the pathogen is phagocytosed by alveolar macrophages that serve as a first permissive niche for the pathogen (**Figure 2 B**). Phagocytosis is initiated through I) Mtb-specific evolutionary highly conserved Pathogen-Associated Molecular Patterns (PAMP), which are recognized by the immune cell's Pattern Recognition Receptors (PRR), like Toll-like Receptors (TLR), complement receptors and C-type lectins (Hossain), II) Fc-receptor mediated by anti-Mtb antibodies or by III) C5a opsonizing complement labelling [20]. PAMPs include a variety of specific, highly conserved pathogenic structures, such as lipopolysaccharide (LPS), peptidoglycans, bacterial DNA and others. Even though macrophages are highly specialized to kill phagocytosed bacteria, they fail to eliminate the pathogen when in a resting state and due to the immune evading abilities of the bacterium. Thereby, alveolar macrophages can serve as a trojan horse for Mtb, facilitating first entry, providing a nice for replication and, thus, persistence in the host. Despite this inability to eliminate the pathogen, phagocytosis and subsequent stimulation of PRR like C-type lectin receptors, Toll-like receptors, Fc-Receptors or nucleotide-binding oligomerization domain like (NOD) receptors induce the production of an array of inflammatory cytokines and chemo attractants. IL-8, IL-12, TNFα and IFNγ as well as leukotrienes and prostaglandins are important early mediators to recruit and activate other innate immune cells, mainly polymorphonuclear neutrophils (PMN), monocytes, dendritic cells (DC), and fibroblasts from the blood circulation to the site of infection (**Figure 2 C**) [21], [22], [23].

4.2.2 Adaptive immunity against *M. tuberculosis*

Next to macrophages, T cells are considered the second important pillar of immunity against Mtb. In the absence of functional lymphocytes there is no to little protection against the infection, which becomes terribly apparent in the elevated susceptibility of HIV infected patients, which have a substantial reduction of $CD4^+$ T cells [24]. As soon as Mtb derived antigens are transported to the lymph nodes by antigen presenting cells, a population of Mtb specific T cells is primed and starts to proliferate (**Figure 2 D**). This is the point, at which the infection is considered to be established and can be detected via immunologic tests. A major role is carried out by IFNγ producing $CD4^+$ T lymphocytes, which is particularly important for the activation of macrophages [25]. For a long time, the contribution of $CD8^+$ T cells was considered minor in the defence against Mtb. However, this perception has changed. Upon recognition of anti-Mtb antigens, presented via Major histocompatibility complex I (MHCI), they produce Il-2, TNFα and IFNγ and can induce apoptosis of infected cells, which subsequently limits Mtb growth [26].

The role of the humoral immune response and antibody producing B cells is still under investigation and debate and often neglected in the face of the importance of T cells and macrophages. However, their presence in the infection has been confirmed in several studies. A high number of $B221^+$ B cells, that accumulate adjacent to Mtb containing lesions, was identified in the lungs of infected mice [27]. Further, the implication of the B cell response on the course of infection was shown to be dose dependent. A high aerosol challenge with Mtb lead to an exacerbated pathology in a mouse model that lack B cells, accompanied by increased PMN accumulation and inflammation [25]. In a guinea pig model of TB, which is highly susceptible, B cells were found to replace the early induced T cell response [28]. However, whether the susceptibility is based on the increased B cell presence or a reduced T cell response, remains elusive. Especially the use of anti-Mtb antibodies and the role of B cells in shaping the immune response became a growing topic. Fc-receptor mediated phagocytosis was shown to enhance subsequent phago-lysosome fusion and the presentation of mycopeptides to T cells [29], [30], which in turn promoted the abundance of IFNγ producing T cells [31], [32]. Additionally, LTBI patients with a high sera level of anti-Mtb IgG3 antibodies were increasingly protected from TB reactivation [33], which was supported by various mouse models [34], [35]. B cells were further shown to regulate PMN infiltration in an Il-17 dependent way [20]. Thus, B cells are important in influencing immunity and cytokine responses during TB, but further studies need to be done to answer remaining questions.

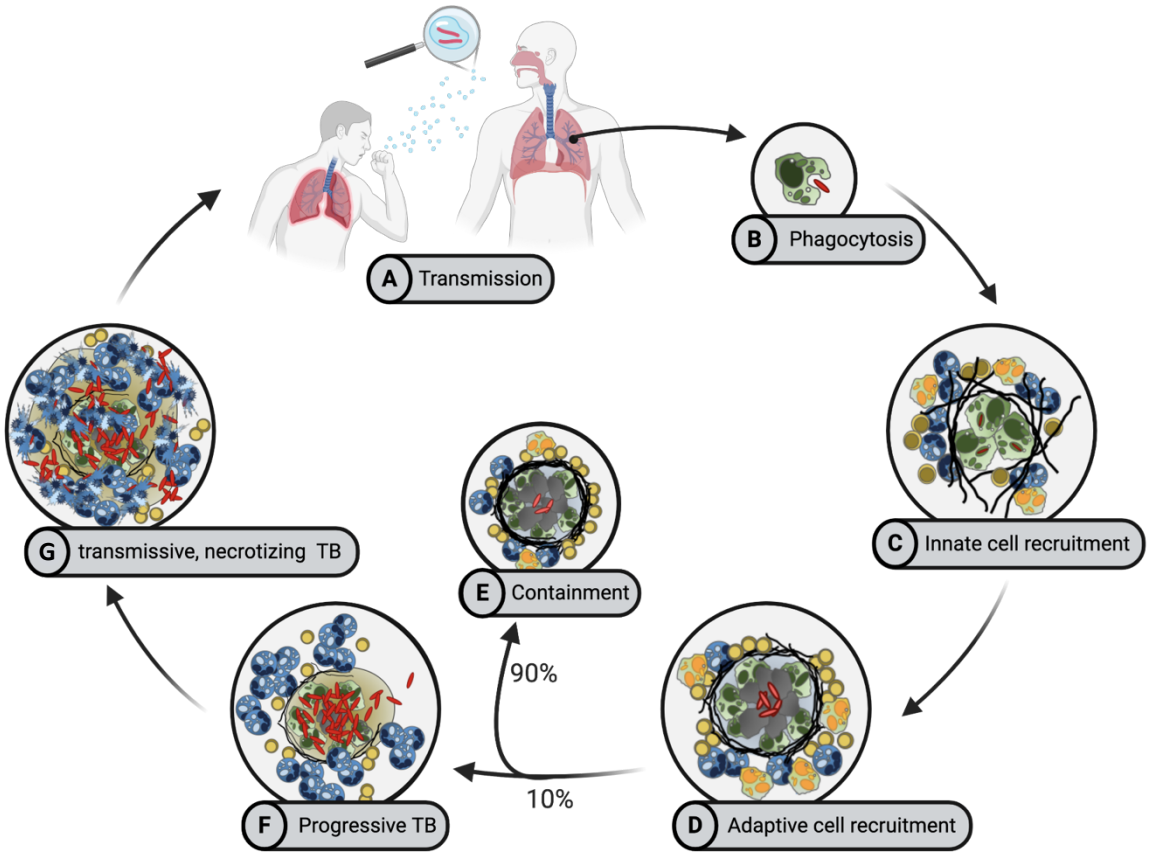

Figure 2 **Dissemination of *M. tuberculosis* and disease development**. After initial infection via inhalation of contagious aerosol (A Transmission), *M. tuberculosis* is phagocytosed by alveolar macrophages (B Phagocytosis) that migrate into the tissue. Early cell recruitment after infection induced cytokine/chemokine response includes macrophages, DCs, PMN and fibroblasts (C Innate cell recruitment). Adaptive cell recruitment (D) is initiated after presentation of Mtb antigens to T cells. 90% develop a latent TB, characterized by encapsulation of the infectious area (E Containment). Only 10% of latently infected patients develop progressing TB (F), marked by enhanced Mtb replication, PMN recruitment and exacerbated inflammation. Increased necrotizing processes lead ultimately to pulmonary spreading of the infection (G). *Created in parts with Biorender.com*

4.2.3 Granuloma formation

After initiation of the infection, tuberculosis can develop into several directions, based on the genetic background of the host and environmental or epigenetic factors. The progression of the disease is not linear and hardly follows textbook descriptions but certain key immunological responses could be identified and are common among most etiopathologies. The major hallmark of an Mtb infection is the development of granulomas. The core of a classical granulomatous structure is formed by a caseous centre, which consists of coagulative necrotic tissue and cells. The main cell population surrounding this centre is a

sphere of macrophages. The granuloma is finally encapsulated by a variety of DCs, lymphocytes and PMN and enclosed by accumulating fibroblasts and a fibrous cuff consisting of collagen (**Figure 2 E)** [19]. Depletion of TNFα or IFNγ can lead to inability to form granulomas [21]. Studies with TNFα deficient mice have supported these findings, as these mice have an impaired granuloma development and are additionally hypersusceptible to Mtb infection [36]. Therefore, it was assumed that granuloma formation is essential for resistance against Mtb. Today it is known that the hyper susceptibility is rather the effect of an impaired macrophage activation, which require TNFα, than due to poor granuloma formation. However, for around 90% of Mtb infected people the infection remains at this latent stage, which suggests at least some protective or containing function of the granuloma by reducing spreading and dissemination of the bacterium throughout the body (**Figure 2 E)**. Nonetheless, the benefits of granuloma formation are also under constant debate, given the <10% latently infected individuals which develop active tuberculosis from pre-existing granulomas that serve in these cases as Mtb reservoirs (**Figure 2 F)**. The enclosed area of a granuloma possibly provides a niche where bacteria can thrive and grow, mostly protected from antimicrobial effects of effector cells and molecules. The events that suddenly lead to a relapse with increased growth of the bacteria and development of active TB are not always known. However, coinfections, like HIV or Malaria, and genetic or acquired immunodeficiencies (i.e. Type II diabetes mellitus) have been identified to promote reactivation [11].

Independent of the relapse cause, one common factor could be identified that is intrinsically tied to the pathology of animal and human active TB. This is, the abundance and response of PMN, which could be linked to the development of the course of infection. It has become evident that PMN numbers highly correlate with the infection outcome, and drive necrotic lung pathology, liquefication of granuloma and finally lead to transmission of the disease and ultimately to the collapse of lung functions (**Figure 2 G)** [37]–[39].

4.3 Neutrophils in health and disease

Polymorphonuclear neutrophils (PMN) are a highly interesting, but also enigmatic cell population in the context of infectious diseases. For a long time, PMN were mainly regarded as simple, short-lived killer cells. The last decades of PMN research have changed this view and increased the awareness of their significance in influencing and shaping the immune response. Their importance is particularly highlighted in patients with transient or acute

neutropenia, which is the complete or temporary absence of PMN, resulting in severe immunodeficiencies. Thereby, these patients are at high risk of uncontrolled, life-threatening infections [40].

In human peripheral blood, 50 – 70% of circulating leukocytes are PMN, while in mice they only account for 10 – 25% [41]. Under healthy conditions, peripheral PMN numbers are in a steady state and after a half-life of 1 – 4 days, the cells rehome to the bone marrow and succumb to an apoptotic cell death. The life span prolongates, when the cell is activated. Tissue resident PMN can be further be found in high numbers in liver, spleen and lung [41]. It is hypothesized, that the occurrence in these organs is linked with the need of quick recruitment in case of acute inflammation [42]. In case of infectious inflammation, their main task is to restrict early pathogen replication, spreading and, additionally, alarming the immune system by releasing a broad array of alarmins, cytokines and chemokines. Their immediate antimicrobial as well as their damaging effector functions are based on an array of microbicidal agents, proteolytic enzymes, and a highly effective machinery to produce reactive oxygen species (ROS) [43]. Details on ROS production and their implication in bacterial clearance will be discussed below in more detail.

Nonetheless, besides their antimicrobial effector functions they have been shown to be able to adopt properties from antigen presenting cells (APC), like expression of MHCII and T cell co-stimulatory molecules CD80 and CD86 upon stimulation with GM-CSF [44], [45]. Specialized B cell helper PMN have been described to stimulate antigen production in B cells in the marginal zone of lymph nodes [46] and they were identified to regulate NK cell development in the bone marrow [47]. Altogether, they are important immune mediators by orchestrating recruitment and effector functions of other leukocytes. However, besides these positive implications, PMN effector functions can also result in unregulated inflammation, tissue destruction and even contribute to septic shock or respiratory distress upon overactivation and exaggerated accumulation [48], [49]. Thus, it is a fine line that separates a beneficial from a harmful PMN response and emphasize the fine balance that is required in the response of these cells.

4.3.1 Migration and recruitment of PMN

Upon infection, PMN are quickly recruited from the circulation to the site of inflammation. CXCL1 (C-X-C motive chemokine ligand) in mice or CXCL8 (formerly Il-8) in humans is

an early secreted chemokine, produced by monocytes and endothelial cells to prime and recruit PMN from the vasculature [50]. The recruitment into tissue is initiated by changes in the receptor molecules of the vascular endothelium upon stimulation by inflammatory signals which include different cytokines, histamines and cysteinyl-leukotrienes [51], [52]. Thereby, endothelial cells almost immediate express the adhesion molecules P- and E-selectin, which bind glycosylated ligands on the PMN's surface, resulting in tethering or capturing and finally rolling of circulating PMN across the endothelial surface. These initial cell-cell contacts serve as activation signals for PMN and initiate subsequent tissue migration. The transmigration or diapedesis of PMN into the tissue occurs at endothelial tight-junctions and relies, among other factors, on interactions between endothelia-expressed intercellular adhesion molecules (ICAMs) and PMN expressed macrophage-1 antigen (MAC1). In the tissue, PMN migrate along a gradient of chemoattractants, like CXCL2, CXCL4 and CCL5 (C-C motive ligand), complement factor C5a, leukotriene B4 or bacterial derived molecules to the site of inflammation [53]. Migration can be terminated with the production of anti-inflammatory and pro-resolving cytokines and mediators, like Il-10 and Il-1R.

4.3.2 Neutrophil effector functions

Upon pathogen encounter and further stimulation by pro-inflammatory cytokines and growth factors, a multi-step process is initiated in which turn, the PMN become fully activated. The antimicrobial armoury of PMN is stored intracellular in specific granules, which protect the cell from their cytotoxic properties. They have been classified into (I) Primary azurophilic, (II) secondary specific and (III) tertiary gelatinase granules (**Figure 3**), and are released specifically during different effector function like intracellular pathogen killing, degranulation or neutrophil extracellular trap (NET) production [42].

Intracellular killing of pathogens, which is the main effector function following pathogen encounter, can be classified into three major steps: receptor mediated phagocytosis, production of highly reactive oxygen species (ROS) and fusion of PMN granules with the phagocytic vacuole. Yet, this doesn't follow a chronological order, but is rather simultaneously occurring. Like all phagocytes, PMN recognize PAMPs or opsonizing host molecules, like IgG or C5a complement. During phagocytosis, the content of azurophilic granules, such as antimicrobial peptides, myeloperoxidase (MPO), phospholipases and serine proteases, is released into the forming phagocytic cap [54]. Secondary specific

granules, which mainly contain lactoferrin, cathelicidin and lysozymes release their content also into the forming phagosome, but additionally into the extracellular space. Further, tertiary gelatinase granules are released into the surrounding, which contain extracellular matrix degrading proteins like collagenase, gelatinases, and matrixmetalloproteinase-9 [55] (**Figure 3**).

Degranulation is the release of mainly secondary and tertiary granules and their containing effector molecules. It further facilitates the release of cytokines and chemoattractants into the tissue [42].

The formation of NETs is another highly efficient way to immobilize and kill pathogens. It is a targeted process, in which the PMN DNA, packed with anti-microbicidal enzymes and peptides, is released towards the pathogens [42].

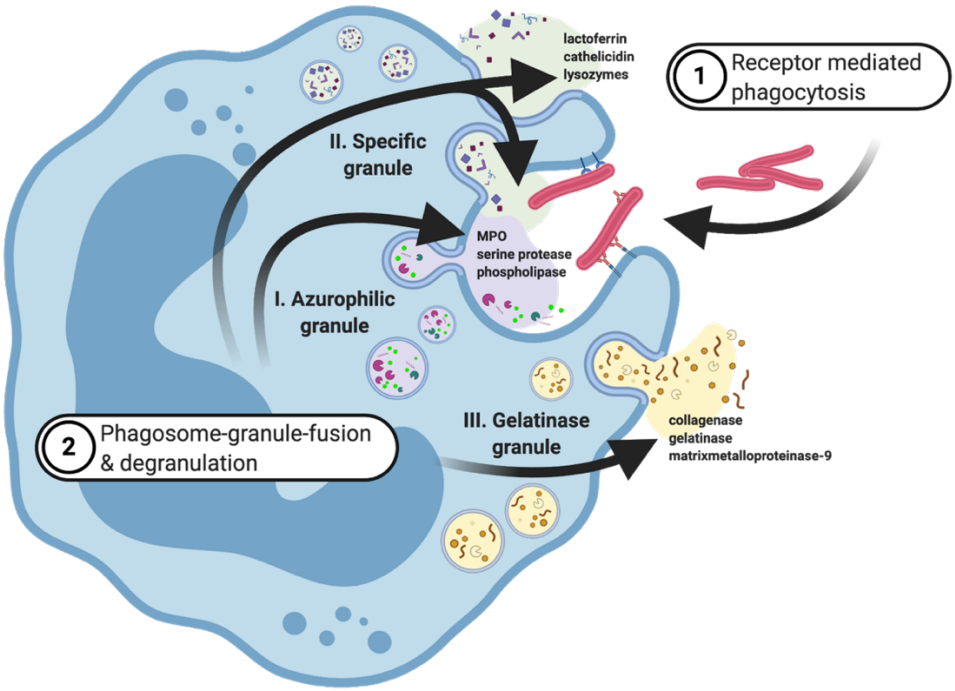

Figure 3 **Phagocytosis by PMN.** Phagocytosis is initiated by receptor mediated uptake of the bacterium (1). This is followed by phagosome-granule-fusion (2), which is the release of primary azurophilic (I.) and secondary specific (II.) granules into the phagocytic cup. Simultaneously, secondary specific (II.) and tertiary, gelatinase (III.) granules are released into the surrounding and the intercellular space. *Created with Biorender.com*

A special role has to be attributed to the serine proteases in azurophilic granules in shaping the immune response. PMN express a number of serine proteases, which include for example

cathepsin G, neutrophil elastase, lactoferrin, and proteinase 3. Serine proteases positively contribute to the immune response in many ways. They have been shown to proteolytically modify chemokines into their active form and certain surface molecules like G-protein-coupled-receptors require protease activity to become active [56]. The importance of these proteases is further highlighted in serine protease-deficient mice, that were more susceptible to death and sepsis than wild type littermates upon bacterial infection [57], [58]. Another implication was found in PMN recruitment and migration. Inhibition of serine proteases lead to a reduction of PMN invasion into tissue [59] and *in vitro* incubation of PMN with protease inhibitors results in reduced adhesion [60]. While the general role of serine proteases for migration is still controversial [49], neutrophil elastase and cathepsin G were shown to possibly play an important role. During the cell-cell interaction of vascular PMN and epithelial cells, they cleave adhesion molecules like ICAM [61], [62], thereby inducing the formation of gaps, through which the PMN can invade the tissue.

However, a nonregulation of these proteases can cause detrimental effects which is shown by increased tissue damage through degradation of cellular matrix and is best documented in human pulmonary diseases [63]–[66]. Thus, due to their high reactiveness, the protease activities have to be carefully balanced which is done by highly specific endogenous protease inhibitors [49]. This is particularly exemplified in mice that genetically lack serpinb1, a serine protease inhibitor, leading to an impaired bacterial clearance and a high mortality rate upon *Pseudomonas aeruginosa* infection [67].

Conclusively, the implications of serine proteases show the importance of a controlled confinement and release of PMN effector molecules, to prevent uncontrolled tissue destruction and inflammation.

4.3.3 The correlations of MPO, ROS and necrosis

Generation of ROS is a key feature of the antimicrobial properties of PMN. It is a multistep process that mainly occurs during phagocytosis. The main enzyme to facilitate ROS production is MPO, a glycosylated 146 kDa homodimer, each dimer incorporating a heme group [68]. The enzyme is in turn dependent on the activity of the nicotinamide adenine dinucleotide phosphate (NADPH) oxidase complex, which provides the substrates for MPO.

The process of ROS production relies initially on the assembly of the NADPH oxidase complex in the membrane of the forming phagosome [69]. This complex constantly transfers electrons from NADPH into the phagosome's lumen, thereby generating $NADP^+$ and

superoxide (O_2^-). The voltage-gated proton channel Hv1 provides a constant influx of protons (H^+) (**Figure 4**, **A, B**), which are used by the superoxide dismutase (SOD) to convert O_2^- into hydrogen peroxide (H_2O_2). This product is the main substrate to generate ROS by MPO (**Figure 4**, **1)**. Simplified, H_2O_2 reacts with the ferric centre of active MPO (often termed Fe^{3+}-MPO or ferric MPO), forming the so-called complex compound I, in which oxygen is covalently bound to the heme iron. Compound I is the primary catalytic enzyme that can reduce halides, mostly chloride (Cl^-), upon a two electron reduction to hypochlorous acid (HOCl). Thereby, compound I is reverted into active, ferric MPO. When excessive H_2O_2 is present, compound I can also transform into the chloride oxidation inactive compound II [70], [71]. This can be reversed to the active ferric MPO by O_2^- or other reducing molecules, which can also reduce ferric MPO into so called compound III. This in turn, can also be reverted to ferric MPO, but is also able to react with other electron donors as well as electron acceptors. Thus, the MPO complex is highly versatile and in constant movement (**Figure 4, 2**). However, the main product HOCl exerts its full potential upon a lowered pH, which is present in phagosomes, where it can react with chloride to molecular chlorine (Cl_2). Cl_2 is highly reactive but relatively short-lived. Further chlorination of an array of possible reactants lead to formation of other long-lived ROS, like aldehydes and chloramines, that can even act in remote distance of the producer cell [72]. ROS are able to induce severe oxidative stress like peroxidation of sulfhydryl groups, iron-sulphur centres, sulphur-ether groups, heme groups and unsaturated fatty acids leading to membrane disintegration of the microorganism or DNA damage [73]. The importance of the implications of ROS are further highlighted in patients with chronic granulomatous disease (CGD). They have an increased susceptibility towards infectious diseases based on a mutation of the NADPH oxidase, leading to an impaired ROS production [74], [75].

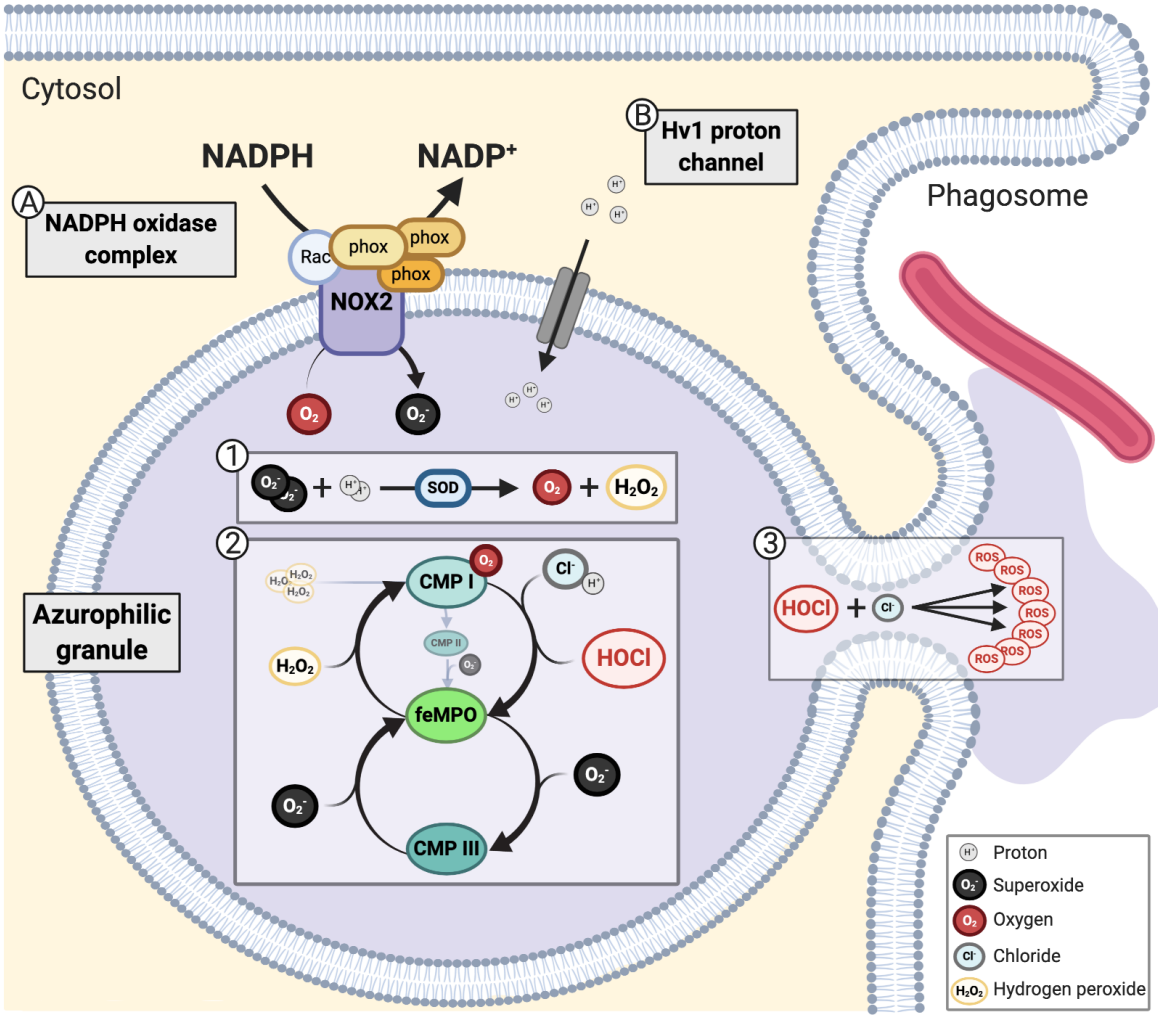

Figure 4 **ROS production in azurophilic granules of PMN upon infection.** The process of ROS production is initiated with the assembly of the NADPH oxidase complex, which main components are NOX2, several phox subunits and Rac GTPase (A). This complex reduces NADPH into $NADP^+$, thereby generating superoxide (O_2^-) from oxygen (O_2). The second substrates, required for subsequent ROS production, are protons (H^+), pumped into the granule space by the Hv1 proton channel (B). The superoxiddismutase (SOD) converts O_2^- and H^+ into O_2 and hydrogen peroxide (H_2O_2) (1). H_2O_2 is the main substrate for ferric MPO (feMPO). In a multistep process, feMPO converts in a reaction with H_2O_2 into Compound I (CMP I), which reduces halides like chloride (Cl^-) into hypochlorous acid (HOCl), thereby turning back into feMPO. feMPO can additionally switch upon reaction with O_2^- into compound III (CMP III) and back. In case of excessive H_2O_2, CMP I can also be converted into Compound II (CMP II), which is further reduced to feMPO. This acts a buffering mechanism for the chemical reactions (2). Upon a lower pH HOCl can further react with chlorine to hyperreactive chloride (Cl_2) (3). *Created with Biorender.com*

Unfortunately, the oxidative damaging effects of ROS are not restricted to invading pathogens but can also severely harm the host. Implications for the fatal effects of an imbalance of anti- and pro-oxidants have been found for several other infectious and autoimmune diseases. For example, a high concentration of MPO was associated with the

development of myelin damaging plaques in multiple sclerosis [76]. Most viral lung infections also show detrimental, increased PMN accumulation and ROS levels upon infection. The most prominent example nowadays being COVID-19. Upon infection with SARS-CoV-2 a high PMN to lymphocyte ratio could be associated with an increased mortality of the patients. It was further hypothesized, that an imbalance between anti- and pro-oxidative molecules is responsible for the severity of the pathology. Thereby, the excessive production of ROS interferes with the function of lymphocytes, pulmonary cells and red blood cells and drive systemic dissemination of the inflammation, thrombosis and alveolar damage [77], [78].

The negative aspects of excessive ROS also seem to dominate the pathology of a progressive Mtb infection. Additional to the increased PMN accumulation seen in susceptible mice and humans with active TB, *in vitro* cultures of human PMN have shown that virulent Mtb strains induce ROS dependent necrosis of the infected cells, allowing the mycobacterium to escape from the PMN's microbicidal armamentarium. In contrast, PMN from CGD patients with an impaired ROS production did not succumb to necrosis. Pharmacological inhibition of MPO and, thus, ROS production reverted PMN necrosis to less inflammatory apoptosis [79].

4.3.4 Cell death and efferocytosis of PMN

The removal of dead cells from the tissue is an essential process to resolve inflammation, as the accumulation of dead cells and debris can lead to the development of autoimmune and other diseases. A major mechanism to remove debris is a process called efferocytosis, which describes the engulfment of dead and dying cells by myeloid efferocytes, mostly macrophages. However, the cell death itself has already a great impact on the cell's proximity and on subsequent efferocytosis [80][81].

The most common cell death under healthy conditions is apoptosis, which is either initiated by intrinsic stress or by the activation of extrinsic cell death receptors. It is followed by the activation of a cascade of caspase activity, DNA condensation, shrinkage of the cell and ultimately production of apoptotic vesicles which encapsulate the intracellular content. Hence, after phagocytosis of a pathogen, it is an efficient way for the short-lived PMN to further contain the infection and prevent exaggerated inflammatory signalling and tissue destruction by enclosure of cytotoxic effector molecules [82].

A non-apoptotic cell death, is marked by rupturing of the cell membrane and the release of intracellular content into the tissue. This is usually described as necrosis or necrotic cell death. In contrast to NETosis, it is an uncontrolled mechanism, driving inflammation by the release of pro-inflammatory cytokines, serine proteases and other cytotoxic effector molecules. Thus, the uncontrolled release of pro-inflammatory and tissue degrading molecules can significantly disturb and interfere with an orchestrated immune response [83].

Efferocytosis is mediated by 'find me' and 'eat me' signals. The release of PAMPs and host cell-derived damage associated molecular patterns (DAMPs) are major 'find me' signals released by necrotic cells. In general DAMPs are characterized by their usually solely intracellular occurrence, which includes genomic and mitochondrial DNA, cytoplasmic molecules like S100 alarmins, cytokines and other molecules. Independent of the cell death, all dying cells express so called 'eat me' signals which discriminate them from neighbouring healthy cells which express certain 'don't eat me' signals. One prominent 'eat me' signal is phosphatidylserine (PS). PS is usually located intracellularly while sphingomyelin and phosphatidylcholine are found as counterparts on the outer leaflet of healthy cells. This organization is maintained by the ATP driven enzyme flippase. Upon cell death induction and functional loss of many cellular pathways, PS is exposed extracellularly, which labels the cell for efferocytosis [84]. Other 'eat me' signals include membrane bound LPC, which can be opsonized by IgM and is thereby marked for Fc-receptor dependent recognition by efferocytes [85]. Soluble 'find me' signals, which are released during apoptosis to attract efferocytes, can be modified membrane lipids, like sphingosine-1-phosphate (S1P), lysophosphatidylcholine (LPC), nucleotides like ATP and chemokines like CX_3CL1, among other [81]. They have downstream effects on recruited efferocytes. For example, S1P was reported to induce an increase in apoptosis sensors on the macrophage's surface, and, thus, elevating efferocytosis [86]. Further, efferocytosis of apoptotic cells, restrained the production of pro-inflammatory mediators by macrophages [80]. A proceeding neutrophilic apoptotic cell death further promoted Mtb control by macrophages, while PMN necrosis drove Mtb growth within macrophages [17]. This indicates, that the mycobacteria, freed from phagosomes by necrotic cell death, can directly interact with targets of the next cell to execute its virulence mechanisms, e.g. inhibition of phagosome maturation. The enclosure into apoptotic vesicle may prevent this interaction, thereby increasing elimination of the mycobacteria by efferocytic macrophages (**Figure 5**).

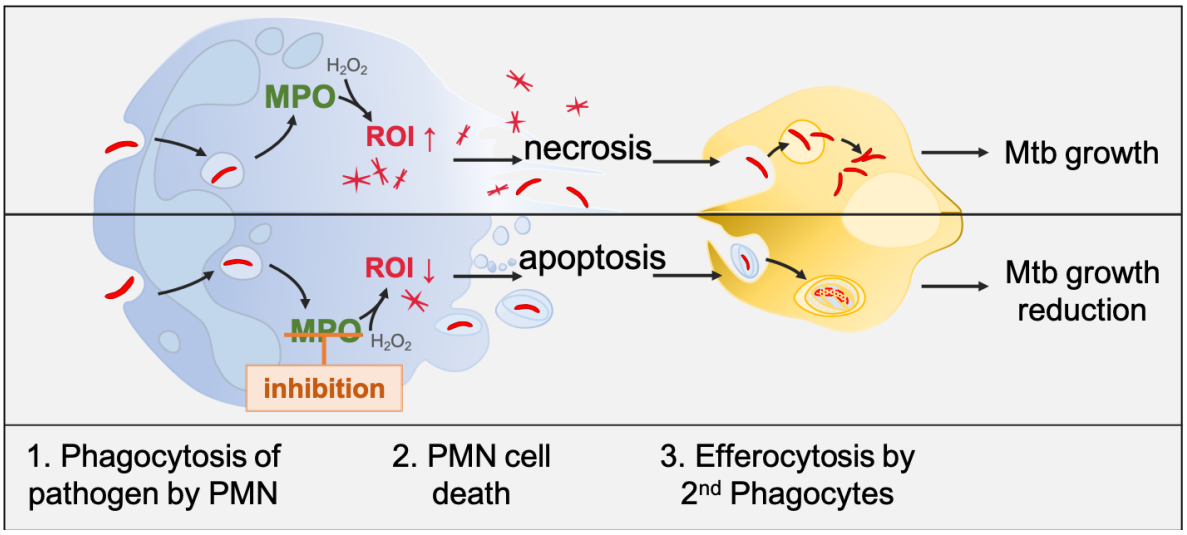

Figure 5 **Implication of PMN in Mtb growth and death.** Mtb induces a ROS dependent, necrotic cell death of human PMN. This drives Mtb growth in subsequent secondary phagocytes like macrophages. Inhibition of MPO and, thus, the production of ROS, leads to apoptosis of the PMN and to the enclosure of the bacteria in apoptotic vesicles. This subsequently limits Mtb growth in secondary phagocytes [17].

Conclusively, an imbalance of apoptotic and necrotic cells, as well as an impairment of efficient efferocytosis has been associated with severe inflammatory pathologies. In turn, apoptosis and subsequent efferocytosis is an important, non-inflammatory way to remove dying cells and prevent progression of inflammation [87], [88].

4.3.5 Lipidperoxidation and other implications of lipids in the immune response

Lipid peroxidation (LPO) is a double-edged sword among chemical cellular processes. If regulated, like in the case of an enzymatic induced process, it is an important purposeful biological effector, leading to the generation of signalling molecules that regulate host responses.

The enzymes lipoxygenase, cyclooxygenase and Cytochrome P450 are for example important in generating small lipid mediators (SLM) by oxidization of the polyunsaturated fatty acid (PUFA) arachidonic acid. SLM which are small signalling molecules, exert their activity in autocrine or paracrine activities through G-protein coupled receptors and are, thus, involved in numerous biological processes. For example, leukotriene B4 (LTB4) and prostaglandin E2 (PGE2) were shown to be highly involved in PMN recruitment during inflammation. Opposite effector functions of different SLM are maintenance of cellular

homeostasis, they regulate proliferation, differentiation and anti- and proinflammatory immune responses [89]. In contrast to the mediated and controlled enzymatic oxidation of lipid substrates which include mainly free and ester forms of PUFA and cholesterols, the uncontrolled and undirected oxidation via free radical-mediated or free radical-independent, non-enzymatic activities can cause disturbances in membrane organization, functional loss and signalling impairment of molecules [90], [91]. Oxidation of lipids results in a chain reaction, where one radical can modulate a number of molecules after initiation of the process. At low levels, these alterations may have no harmful effect, but excessive LPO can significantly change the immune response, increase pathological stress and disorder and even induce cell death [92].

Apart from directed or undirected LPO, host lipids provide an important nutrient source for intracellular Mtb [93]–[95]. This is indicated by an immediate upregulation of genes that are associated with lipid metabolism upon entering the host [96] and by a change of the mycobacterium cell wall lipid composition when entering dormancy [97]. Further, Mtb strains with defects in their lipid metabolism show a loss of virulence [96]. For example, a defect in a cholesterol oxidase enzyme of Mtb resulted in an attenuated infection of mice [98]. Cholesterol has been shown to be an important carbon and energy source. The molecule is initially oxidised at its alkyl side-chain or its steroid ring until it is completely degraded. Other important energy sources are fatty acids, which are mainly found in diacylglycerols (DAG) and triacylglycerols (TAG). Their metabolization starts with the ß-oxidation of *methyl-branched* or uneven fatty acid side chains and results in a carbon product, usually succinate or pyruvate, that can be provided for energy production via the tricarboxylic acid cycle (TCA cycle). Other end products of lipid oxidation may not be used as energy sources but can be directly incorporated into the mycobacterium's cell wall [99].

However, the full extend and mechanisms that are exploited by Mtb to use host derived lipids as carbon sources remain in some aspects elusive. Thus, the impact of the ROS dependent necrotic cell death on the host cells lipidome after Mtb infection, is an important analytical step to further investigate the effects and alterations of host lipids and their possible influence on the mycobacterium in the context of TB.

4.3.6 Neutrophil implications in human TB

Evidence for the implications of PMN in human active TB have been continuously found. Their quick recruitment to the site of infection is, regarding their early effector functions in

activation of the immune response, probably highly important to contain the initial infection [100]. However, in the context of a reactivated and active TB, PMN were shown to rather exacerbate inflammation and tissue destruction, than support clearance of the bacteria.

PMN were found to be the main and most heavily infected cell population in the sputum and bronchoalveolar lavage (BAL) of active TB patients, implying their quick response and continuous recruitment to the infectious sites [101]. Additionally, peripheral blood derived hPMN from active TB patients show upregulated surface activation markers [38], [102]. Finally, PMN driven RNA signatures in the blood [103] and sera level of pro-inflammatory S100A8/A9 alarmins [104] or CXCL8 [50] have been found to correlate with the radiological health score and the pathology of infected patients. As microbicidal phagocytes, one of their major functions is to eliminate pathogens. However, human PMN (hPMN) have been shown to be unable to kill phagocytosed bacteria *in vitro*. Instead, they quickly succumb to a necrotic cell death [79].

4.3.7 The lessons learned from the animal model

Several animal models support the implication of a PMN driven pathology found in humans. The use of genetically different mouse strains revealed distinct disease patterns upon Mtb infection, revealing fundamental differences in the immune response and pathology development between the strains [105]–[108]. Based on these findings, mice can broadly be classified into super susceptible, intermediate susceptible and relative resistant mouse strains, depending on their genetic background [109]. Interestingly, the early immune response against Mtb in mice was shown to be quite comparable between genetically different strains [109]. Following aerosol infection, mice develop an acute immune response against Mtb. This is in parts comparable with the initial immune response in humans, though in direct comparison, the process is of course quicker and more pronounced. After approximately 2 weeks, the infection spread to the lymph nodes, which initiates adaptive T cell responses [110]. From this point forward, genetic dependent differences become evident. The widely used mice with genetic B/6 background, were shown to be relatively resistant towards Mtb infection. After around 4 weeks of infection, the number of bacteria in the lung reaches a plateau and the animals survive the infection for more than 20 weeks, despite slow progressing pathology [111]. A similar picture was seen in the BALB/c model, which is regarded as intermediate susceptible and succumb to the infection after approximately 10 weeks [109]. The most prominent susceptible mice have a CBA, DBA/2,

AJ or C3H background [112]. From those the strain C3HeB/FeJ has been shown to be very susceptible to an infection with Mtb and succumb within less than 10 weeks to the infection [112].

The species dependent differences are further pronounced in the development of granuloma. They have been categorized into three distinct phenotypes, according to cellular composition, degree of pathology and the ability to control bacterial replication [113]. Susceptible C3HeB/FeJ mice develop three distinct granulomatous lesions. Lesion type I are human like granuloma, with a central dominance of neutrophils and a necrotic to caseous core, which is encapsulated by fibrotic tissue [113]–[115]. These lesions can occasionally develop central cavities, leaving no intact lung tissue. Lesion type II granuloma show similarities to type I lesions, consisting in their majority of neutrophils that are invading primarily alveolar space. During progression, these areas also turn into highly neutrophilic areas and usually contain a necrotic core. In contrast to type I lesions, these inflammatory areas are not encapsulated by fibrotic tissue, and can metastasize across large areas of the lung. It has to be noted, that particularly type II lesions had little to none lymphocytes present [113]. Type III granuloma are dominated by invading lymphocytes and macrophages, only occasionally appearing PMN and little fibrosis. Interestingly only the type III granuloma can be found in resistant B/6 mice [28], [111].

Detailed analysis of the C3HeB/FeJ mice showed, that the overall increased tissue necrosis and decreased ability to restrict mycobacterial replication could be traced back to a distinct gene locus on chromosome 1 and was therefore called *sst1* (*s*u*s*ceptible for *t*uberculosis) [117]. In turn, B/6 mice were shown to express a resistant allele of this locus. Backcrossing transfer of the resistant B/6 *sst1* locus onto the TB susceptible C3H background subsequently increased their survival and prevented necrotic granuloma formation. However, susceptibility cannot be solely explained with the phenotype of the *sst1* locus. For example, the B6.C3H-sst1 mouse, which shows a susceptible necrotic granulomatous phenotype, is still more resistant to the infection than the C3HeB/FeJ mice. Another factor contributing to the increased susceptibility is a reduced inflammatory cytokine response of macrophages, which was shown to be *sst1* independent [117]. Indeed, resistance was shown to be multigenic trait and several other resistance loci have been identified in different mouse strains [118]–[120].

However, the increased susceptibility of the mouse strain C3HeB/FeJ and other susceptible strains could always be related to an increased PMN infiltration in the lungs of infected

animals [121][107]. Antibody dependent depletion of PMN resulted not only in reduced inflammation and bacterial burden but also in increased T cell responses, suggesting an additional antagonistic effect of PMN recruitment on the adaptive immune response [107]. In contrast, resistant mouse strains like the widespread C57Bl/6 mice show limited PMN recruitment, tissue necrosis [107] and fail to establish a hypoxic environment upon infection with virulent Mtb [122].

4.4 Host-directed therapy: a loophole against antibiotic resistance?

The major goals of anti-tuberculosis treatment are: 1) the reduction of replicating bacteria in the patient, which reduces pathology and further transmission, 2) the elimination of persisting bacilli to prevent relapse and 3) the prevention of antibiotic drug resistance.

Evolution of drug resistance is unavoidable under the selective pressure of antibiotic treatment. One contributing factor is the limited diffusion of antimicrobial effector molecules or chemotherapeutic drugs into the infected centre, thereby limiting anti-microbial substances to sub lethal concentrations, which in turn, can promote the development of drug resistant mycobacteria [123]. Therefore, unless an effective vaccine is developed, supplementary treatment options to antimicrobial drugs should be exploited. The current development of Host-Directed Therapy (HDT) might improve this situation, by increasing treatment efficacy and reduced treatment time. The basic idea is the modulation of the immune response and host cell functions by drugs which don't target the bacterium directly. Some HDT strategies, which are under current investigation, include: (1) targeting the granuloma structure to increase drug accessibility, (2) autophagy induction and enhancement of intracellular killing, (3) promotion of cell-mediated immune responses by T cells, (4) suppression of Mtb growth by monoclonal anti-Mtb antibody therapy and (5) enhancement of anti-inflammatory responses that reduce tissue destruction [124].

Summarized, the vast amount of research, that describe the pro-inflammatory, pathogen driving implications of PMN and PMN necrosis in mouse and humans and their potency to serve as biomarkers in point of care diagnosis, make them highly interesting targets for HDT. With regard to the Mtb infection induced, MPO driven ROS dependent necrosis of PMN [17], [79], this seems like a promising target. Additionally, the inhibition of MPO, which converted the cell death to apoptosis increased Mtb killing in subsequent efferocytes [17]. Thus, targeting MPO-ROS driven necrosis seems to be a promising way to address important

requirements of anti-mycobacterial treatment: Reduction of bacterial replication, pathology and transmission. In conjunction with an antibiotic chemotherapy this might shorten treatment time and allow a reduction of the dose and the amount of required antibiotics.

4.5 Objectives

The aim of this study was to investigate the role of PMN during active TB. The evaluation of MPO as HDT in mice can serve as an important step towards the development of usable HDT for TB in humans. Therefore, based on previous *in vitro* studies with hPMN on MPO inhibition [17], one major goal was to retro-translate these findings into the mouse model to evaluate the Mtb growth reducing and anti-inflammatory effects *in vivo*. Further, the implications of a necrotic cell death and, thus, ROS induced changes on the lipidome were analysed *in vitro* with hPMN. In particular these questions were the centre of these studies:

1) Analysis of the influence of Mtb induced, ROS dependent necrosis on the lipidome of hPMN
2) *In vitro* analysis of MPO inhibition in murine PMN
3) Evaluation of *in vivo* inhibition of MPO in a susceptible murine model for TB

5 MATERIAL

5.1 Antibodies

5.1.1.1 Flow cytometry antibodies

Antigen	Clone	Species	Conjugate	Dilution	Manufacturer
CD11b	M1/70	rat IgG2a κ	PacBlue	1:400	BioLegend
CD11c	N418	hamster IgG	Pe-Cy7	1:200	BioLegend
CD3	APC-Cy7	rat IgG2b κ	17A2	1:200	BioLegend
CD4	APC	rat IgG2b κ	RM4-5	1:200	BioLegend
CD49b	DX5	rat IgM	PE	1:200	BioLegend
CD69	H1.2F3	rat IgG1 κ	PerCP	1:200	BioLegend
CD8a	53-6.7	rat IgG2a κ	BV510	1:200	BioLegend
IFNγ	XMG1.2	rat IgG1 κ	PacBlue	1:100	BioLegend
Ly6G	1A8	rat IgG2a κ	APC	1:400	BioLegend
MHCII (1-A/1-E)	M5/114.15.2	rat IgG2a κ	BV510	1:100	BioLegend
MPO	2D4	rat IgG1 κ	FITC	1:100	BioLegend
TNFα	MP6-XT22	rat IgG1 κ	Pe-Cy7	1:100	BioLegend

5.1.1.2 Antibodies for T cell re-stimulation

Antigen	Clone	Species	Conjugate	Dilution	Manufacturer
CD3	145-2C11	hamster	-	5 μg/mL	BioLegend
CD28	37.51	hamster	-	5 μg/mL	BioLegend

5.1.1.3 Primary antibodies

Antigen	Clone	Species	Dilution	Manufacturer
MPO	polyclonal	rabbit	1:200	Thermo Fischer Scientific

5.1.1.4 Secondary antibodies

Antigen	Clone	Species	Conjugate	Dilution	Manufacturer
Biotin-SP-conjugated F(ab')$_2$ α-Rb-IgG	-	goat	biotin	1:500	Jackson Immuno Research

5.1.2 Flow cytometry panels

5.1.2.1 Flow cytometry panel for *in vitro* stain: PMN effector functions

Laser	Filter	Fluorophore	Panel 2 - T cell	Concentration
405 nm	450/50 525/50	PacBlue	CD11b	1:200
488 nm	525/50 585/40 655-730 750 LP	FITC dsRed PerCP	DHR123 Mtb 7-AAD	1 µM MOI 3,5 1:100
633 nm	655-730 750 LP	APC	Ly6G	1:200

5.1.2.2 Flow cytometry panel for *in vivo* stain: PMN and myeloid cells

Laser	Filter	Fluorophore	Panel 2 - T cell	Concentration
405 nm	450/50 525/50	PacBlue BV510	CD11b MHCII (1-A/1-E)	1:400 1:100
488 nm	525/50 585/40 655-730 750 LP	FITC PerCP PE-Cy7	DHR123 7-AAD CD11c	1:200 1:200
633 nm	655-730 750 LP	APC APC-Cy7	Ly6G CD3	1:400 1:200

5.1.2.3 Flow cytometry panel for *in vivo* stain: T cells and cytokines

Laser	Filter	Fluorophore	Panel 2 - T cell	Concentration
405 nm	450/50 525/50	PacBlue BV510	IFNy CD8a	1:50 1:200
488 nm	525/50 585/40 655-730 750 LP	FITC PE PerCP PE-Cy7	MPO CD49b CD69 TNFa	1:50 1:200 1:200 1:50
633 nm	655-730 750 LP	APC APC-Cy7	CD4 Ly6G CD3	1:200 1:200 1:200

5.2 Cell surface marker

5.2.1 Myeloid cell populations

	SSC-A	FSC-A	CD11b	CD11c	MHCII	Ly6G
alveolar macrophages	med	med	-	+	-/med/+	-
interstitial macrophages	high	high	+	-/med/+	-/med/+	-
myeloid/conventional DC	med	med	+	+	+	-
Neutrophils	high	high	+	-	-	+

5.2.2 NK-, NKT- and T cell populations

	SSC-A	FSC-A	CD3	CD49b	CD4	CD8	CD69
NK cells	low	low	-	+	-	-	-
NKT cells	low	low	+	+	-	-	-
$CD4^+$ cells	low	low	+	-	+	-	-
$CD8^+$ cells	low	low	+	-	-	+	-
activated NKT cells	low	low	+	+	-	-	+
activated $CD4^+$ cells	low	low	+	-	+	-	+
activated $CD8^+$ cells	low	low	+	-	-	+	+

5.3 Bacteria strains

Species	Strain	Genotype	Antibiotics	Supplier
Mycobacteria tuberculosis	H37Rv	wildtype	none	W.R. Jacobs - Albert Einstein College of Medicine, New York
Mycobacteria tuberculosis	H37Rv	Discosoma sp. Red fluorescent protein (DsRed)	Hygromycin (50 µg/ml)	T. Parish - Queen Mary Univ. of London London, England

5.4 Buffer and medium

Buffer & Medium		
Ammonium chloride solution	155 mM	NH4Cl
(Erythrocyte lysis buffer)	0,1 mM	EDTA
	10 mM	KHCO3
		in Aqua dest.
		adjust to pH 7,2 - 7,4
Bone marrow isolation buffer	0,10%	NaHCO3

	0,05%	FCS
	0,20%	1 M Hepes
		in HBSS w/o Ca and Mg
Cell isolation medium	2%	FCS
	1 mM	EDTA
		in PBS
Citrate buffer	9,9 mM	Citric Acid
		in Aqua dest.
		adjust to pH 6,0 with 1 M NaOH
	0,05%	Tween20
Complete RPMI (cRPMI)	10%	FCS
	1%	L-Glutamine
	1%	HEPES 1M
	1%	Natriumpyruvate
	0,10%	2-Mercaptoethanol
		in RPMI1640 w/o Ca
FACS buffer	1%	FCS
	0,10%	NaN3
	2 mM	EDTA
		in PBS
Human cell culture medium	10%	autologous donor serum
	1%	L-Glutamine
		in RPMI1640 w/o Ca and phenol red
Mouse cell culture medium	10%	autologous donor serum
	1%	L-Glutamine
		in RPMI1640 w/o Ca and phenol red
TBS (10x)	150 mM	NaCl
	50 mM	Tris-HCl
		in Aqua dest.
		adjust to pH 7,4
Organ digestion buffer	50 mg/mL	Liberase TL
	50 mg/mL	DNAseI
		in RPMI1640 w/o Ca
PBS (10x)	18 mM/L	KH2PO4
	27 mM/L	KCl

	100 mM/L	Na2HPO
	1,37 M/L	NaCl
		in Aqua dest.
Protein extraction buffer	0,35 M	succrose (D+)
	1 mM	CaCl2
	10 U/mL	Heparin
		in HBSS w/o Ca and Mg
WTA	0,01%	Tween 80
	0,05%	BSA
		in ddH20
7H9 liquid medium	10%	OADC
	0,05%	Tween
		in Difco™ 7H9 Medium
7H11 agar medium	19 g	Difco™ 7H11 Agar
	1 g	Asparagin
	5 mL	Gylcerol
		in 1 L Aqua dest.

5.5 Chemicals

Chemicals	**Company**
2-Isopropanol	Carl Roth
3,3', 5,5'-Tetramethylbenzidin	Sigma-Aldrich
7-AAD	BioLegend
Acetic acid	Carl Roth
Acetyl chloride	Carl Roth
Acetone	Walter CMP
Albumin Bovine Fractions V, protease free (BSA)	Serva
Ammonium chloride	Carl Roth
Aqua bidistillata	B. Braun
Calcium chloride	Sigma-Aldrich
Carbolfuchsin	BD Bioscience
chloroform, LC-MS grade	Sigma-Aldrich
Citric acid	Sigma-Aldrich
DAB-staining soluton	Sigma-Aldrich
DHR123	Invitrogen
Difco™ 7H11 Agar	BD Bioscience
Difco™ 7H9 Medium	BD Bioscience
Dimethylsulfoxid (DMSO)	Sigma-Aldrich

Dinatriumhydrogen phosphat	Sigma-Aldrich
DNAseI	Roche
Entellan	VWR
Entellan®	Merck
Eosin	Carl Roth
Ethanol	Walter CMP
Ethylendiamintetraessigsäure (EDTA)	Sigma-Aldrich
Fetal Bovine Serum (FBS)	Biochrom
Glycerol	Sigma-Aldrich
HBSS w/o Ca and Mg	Capricorn Scientific
Heparin	B Braun
HEPES buffer solution 1 M	Pan Biotech
Histopaque	PAN Biotech
Isopentane	VWR
Kalium chloride	Carl Roth
Kalium hydrogen phosphat	Sigma-Aldrich
Ketamin Ketamidor®	WDT
L-Gutamine 200 mM	PAN Biotech
Liberase TL	Roche
Methanol, LC-MS grade	Sigma-Aldrich
Methyl-*tert*-butyl ether, LC-MS grade	Sigma-Aldrich
Methylenblue	Carl Roth
Meyer's Haemalaun	Carl Roth
Natrium chloride	Carl Roth
Natriumazide	Merck
Natriumchloride	Merck
Natriumhydrogencarbonat	Merck
Natriumhydroxide	Carl Roth
Natriumpyruvate	Pan Biotech
Oleic Albumin Dextrose Catalase (OADC)	BD Bioscience
Paraffin	McCorkick Scientific
Paraformaldehyde (PFA)	Carl Roth
Percoll human, density 1,077 g/mL	PAN Biotech
Phosphate buffered Saline (PBS) 10x, w/o Ca and Mg	PAN Biotech
Potassiumbicarbonate	Sigma-Aldrich
RPMI1640, w/o L-Glutamine, w/o phenol red	PAN Biotech
Sodium Pyruvate 100 nM	PAN Biotech
ß-mercaptoethanol (50mM)	PAN Biotech
Sucrose D(+)	Carl Roth
Sulfuric Acid	Merck
SYTOX™ Green nucleic acid stain	Invitrogen
Tris	Carl Roth
Triton X-100	Carl Roth
Trizol	Invitrogen

Tween 20	Sigma-Aldrich
Tween80	Sigma-Aldrich
Water, LC-MS grade	Sigma-Aldrich

5.6 Consumables

Consumables	Company
Aqua dest.	Merck Millipore
Cannulas (18G, 20 G, 27G, 28G)	BD
Cell culture flasks (T25)	Sartedt
Cell strainer (70 µm, 100 µm)	Corning
cOmplete Proteinase inhibitor cocktail (EDTA-free)	Roche
Conical tube (15 mL, 50 mL)	Corning
Coverslips	Thermo Fischer Scientific
Cuvettes	Sarstedt
Disposable Hemocytometer (Neubauer chaimber)	Nano Entek
Dry ice	
EDTA tube	Sarstedt
FACS tube (5 mL popypropylen round bottom tube)	Corning
FCS	Biochrom
Flat bottom cell culture plate (96 well, 48 well, 24 well 6 well)	Corning
micropipettes (10 µL, 20 µL)	Hirschmann
Minilys tubes	Cayman
Parafilm	BEMIS
Pasteurpipettes (glas)	Brand
Petri dish (10 cm)	Sarstedt
Pipette Art-Tips with filter (20 µL, 100 µL 200 µL, 1000 µL)	Thermo Fisher Scientific
Pipette Tips (20 µL, 100 µL 200 µL, 1000 µL)	Sarstedt
Reaction tubes (0,5 mL, 1 mL, 2 mL)	Sarstedt
Round bottom cell culture plate (96 well)	Corning
Serum-Gel Z tube	Sarstedt
Steritop® Filter	Millipore
Stripette (2 mL, 5 mL, 10 mL, 25 mL)	Greiner Bio-One
Super Frost® Plus Slides	Thermo Fisher Scientific
Syringe pre-filter	Sarstedt
Syringes (1 mL, 5 mL, 10 mL)	BD
Tissue molds	VWR
Tissue Tek	Leika
ViCell™ XR sample vials	Beckman Coulter
Whirl-Pak® bag	Nasco

5.7 Drugs and antibiotics

Drug	Supplier

ABAH	Sigma-Aldrich
AZD5904	MCE - MedChemExpress
Isoniazid	Fluka
Hygromycin B	PAN Biotech

5.8 Equipment

Equipment	Company
BD FACSCanto™ II Cell analyzer	BD
Centrifuge 5417R	Eppendorf
Cooling centrifuge Heraeus Miltigue 3SR Plus	Invitrogen
Cryostat CM3050S	Leica
Desktop Computer	Apple
FastPrep machine	MP
Feeding tube for oral gavage	Schreiber / Aesculap
Foreceps	Schreiber / Aesculap
Heater and magnet mixer	IKA® RET basic
Heracell 240 incubator	Thermo Fisher Scientific
Light Microscope Olympus BX41	Olympus
MACSQuant®Analyzer 10 Flow Cytometer	Milteny Biotec
MESO® Quick Plex SQ 120	MSD
Mikroskop Eclipse TS100	Nikon
Mikrotom RM215RT	Leica
Multichannel pipettes Finnpipette® (50 µL; 300 µL)	Thermo Fisher Scientific
Newbauer chamber	Marienfeld-superior
Paraffin casting station LEICA EG1140c	Leica
Parrafin Stretch Bath 1052	GLF
Photometer 6320D	Jenway
Pipette Set (10 µL; 20 µL, 100 µL, 200 µL, 1000 µL)	Thermo Fisher Scientific
Q exactive Orbitrap mass spectrometer	Thermo Fisher Scientific
Scale	VWR
Scale ED822	Sartorius
Scissors	Schreiber / Aesculap
Shandon-Chamber	Thermo Fisher Scientific
Spin tissue processor STP120	Thermo Fisher Scientific
Steamer	Tefal
Steril work bench MSC-Advantage™ class II	Thermo Fisher Scientific
Synergy™ Multi-Mode Microplate reader	Biotec® Agilent
Thermo SPD SpeedVac	Thermo Fischer Scientific
ViCell® Counter	Beckman Coulter
Vortex Mixer Uzubio VTX-3000L	LMS®
Water Bath GFL 1052	GFL
water bath sonificator (Bandelin Sonorex DigiPlus)	Bandelin

5.9 Kits

Kit	Order No.	Company

LEGENDplex™ Mouse proinflammatory chemokine panel	740451	BioLegend
MESO SCALE DISCOVERY'S Multi-Array®	customized	MSD
Mouse Myeloperoxidase DuoSet ELISA	DY3667	R&D systems
Pierce™ BCA™ Protein-Assay	22660	Thermo Fisher Scientific
Cytofix/Cytoperm™ Fixation Permeabilization Kit	554714	BD
EasyStep™ Mouse Neutrophil Enrichment	19762	StemCell
LDH cytotoxcicity detection kit	11644793001	Roche
ABC peroxidase staining kit	32052	Thermo Fisher Scientific

5.10 Proteins

Protein	Company
recombinant murine G-CSF	Preprotech

5.11 Software

FlowJo™ V.10.7.1
Biorender.com
BioTek Gen5™ Data Analysis Software
Ledendplex™ Data Analysis Software
Microsoft Excel
Microsoft Word
Microsoft PowerPoint

6 METHODS

6.1 Serum, cell and organ isolation

6.1.1 Ethical statements

The isolation and experimental work with human blood cells was approved by the ethical committee of the University of Lübeck, Germany (22-202A). Peripheral human blood was collected from healthy volunteers, aged between 18 and 65. Written consent and authorization for the use of the samples was obtained by each individual.

All animal experiments were approved by the Ethics committee for the animal experiments of the Ministry of agriculture Environment, and rural areas of the state of the Schleswig-Holstein, Germany (V 244 - 16731/2020(58-5/17)). For isolation of serum, bone marrow, blood cells and organs all mice were euthanized according to Paragraph §2(2) of the German 'Tierschutz-Versuchstier Verordnung' (TierSchVerV) using CO_2.

6.1.2 Isolation of murine samples

After euthanization, the mice were dunked in 70% EtOH for sterilization and the peritoneal cavity was opened. Blood was collected from the vena cava using a 1 mL syringe with a 27G needle in order to generate serum or to collect peripheral blood leukocytes. In case organs were harvested after an *in vivo* experiment, the diaphragm was cut to open the pleural cavity. A cardiac perfusion was performed by injecting 20 mL ice cold PBS into the left ventricle using a syringe with a 18G needle, while the right atrium was cut open to release the injected PBS. Afterwards, all organs of interest were collected and further processed.

6.1.3 Preparation of murine autologous serum

For the preparation of murine autologous serum blood was taken from the vena cava as described before and transferred into a Serum-Gel Z tube and shortly stored on ice. To precipitate the serum, tubes were centrifuged for 10 min at 4°C with 4000 xg. Serum, which accumulates on top of the gel layer, was collected from the tubes and immediately stored at -80°C until further use with a maximum storage time of 7 days.

6.1.4 Preparation of murine peripheral blood leukocytes for PMN isolation

For the isolation of peripheral blood leukocytes, blood was collected as described before from the *vena cava*, transferred into EDTA containing tubes and stored on ice until further usage. For the lysis of erythrocytes, the blood sample was transferred to a 15 mL conical tube containing 9 times the volume ammonium chloride solution. The tube was inverted and incubated 15 min on ice. Following, the sample was centrifuged, the supernatant discarded and the remaining pellet was washed twice with cell isolation buffer (6 min, 4°C, 300 xg). The purified peripheral blood leukocytes were then further used for PMN isolation (see below).

6.1.5 Preparation and cultivation of murine bone marrow cells for PMN isolation

Bone marrow was isolated from the lower extremities (femur, tibia and Ilium/Ischium). The bones were dissected and freed from excessive muscle and tissue using a tissue cloth. The epiphyses were cut off and saved in a 70 µm cell strainer that was placed on a 50 mL conical tube. Following, the bone marrow was flushed out through into the cell strainer with bone marrow isolation buffer using a syringe with a 28-G needle. For each bone a volume of approximately 5 mL was used. The epiphyses were minced with scissors and remaining cells were pushed through the cell strainer with the puncheon of a syringe. The cell strainer was finally flushed with bone marrow isolation buffer till a total volume of 50 mL was reached. After centrifugation (6 min, 4°C, 300 xg) the pellet was resuspended in 1 mL cell culture medium supplemented with 10 ng/mL recombinant murine granulocyte colony-stimulating factor (ms G-CSF) and counted. Bone marrow cells were cultivated at a density of $4x10^6$ cells/mL in ms G-CSF supplemented cell culture medium for 48h at 37°C with 5% CO_2. Following this maturation period, the bone marrow cells were washed, counted and further used for PMN isolation.

6.1.6 Isolation of murine PMN

Murine PMN were isolated using the immunomagnetic negative isolation kit 'EasySep™ Mouse Neutrophil Enrichment' from StemCell. The protocol was followed according to the manufacturer's instructions. In short, bone marrow cells or peripheral blood leukocytes were washed in PBS, supplemented with 2% FCS and 1 mM EDTA, and counted. In an appropriate volume to the cell number, a mix of biotinylated antibodies targeting unwanted

cells was added to the cell suspension. Labelled cells were then detected with tetrameric antibody complexes that, in a next step, were bound to magnetic beads. By placing the reaction tube into an EasySep™ magnet unwanted cells were withheld and the flow-through contained the purified, untouched PMN which were transferred into a new tube. After washing (6 min, 4°C, 300 g) and counting the purified PMN were used for *in vitro* cell culture assays at indicated cell numbers.

6.1.7 Isolation of human peripheral neutrophils

For the isolation of human peripheral blood neutrophils (hPMN) all required reagents were preheated to 37 °C prior to the isolation. Carefully, 20 mL Histopaque were overlaid with 30 mL blood. After centrifugation at 800 xg at RT for 25 min without breaks, serum was aspirated and a part was saved for later opsonization of bacteria. The remaining serum was heat inactivated at 56°C for 30 min and used as serum supplement in human cell culture medium. Granulocytes were transferred to a new conical tube and washed (485 xg, RT, 5 min). The pellet was re-suspended in 1-2 mL RPMI1640 and layered onto a freshly prepared 85% - 80 % - 75% - 70% - 65% Percoll / PBS gradient. After centrifugation at 800 xg at RT without breaks, PMN accumulated between 75% and 80% Percoll and were collected with a 20G needle. Neutrophils were washed, resuspended in human cell culture medium (RPMI, + 10% autologous, heat inactivated donor serum, + 5% L-glutamine) and counted for the following experiments.

6.2 Microbiological assays

6.2.1 Culturing of *M. tuberculosis*

The mycobacterial strain H37Rv NY was used for all cell culture and *in vivo* experiments. In case of *in vitro* FACS analysis or immunochemical analysis, a genetic modified fluorescently labelled strain expressing a DsRed vector was used. Frozen aliquots were thawed and cultured in Middlebrook 7H11 broth supplemented with 5% OADC (Oleic acid, Albumin, Dextrose, Catalase). In case of fluorescent labelled strains, the appropriate selection antibiotic was added to the culture medium. Details on the used antibiotic selections can be found in chapter **Bacteria strains**.

After 3 – 4 days, a tenth of the culture was passaged to new medium. For *in vitro* infections bacteria from passages 2 – 4 were used. The bacteria were washed twice with PBS (3500 xg,

10 min, 4°C) and resuspended in 1 mL PBS. Following, single cell suspensions were obtained by passing the suspension 5 times through a 27G needle. The OD was measured in a 1:10 dilution in 4% Paraformaldehyde (PFA). The concentration of bacteria per mL was calculated with the following equation based on the measured OD_{580}.

$$\boldsymbol{bacteria\ [x10^8/mL] = OD_{580} * 5x10^8 * 10}$$

6.2.2 *In vitro* infection of cell cultures

Bacteria that were used for infection were opsonized prior to the assay with autologous serum for 30 – 45 min at 37°C at a ratio of 1:1. For *in vitro* infection assays, $1x10^5$ cells were seeded in a volume of 100 µL cell culture medium and infected with a MOI of 3 or 5.

6.3 Cell cultures & cell culture assays

6.3.1 MPO inhibitor treatment *in vitro*

PMN that were treated *in vitro* with ABAH or AZD5904 were seeded in the required medium. ABAH was dissolved at a concentration of 500 mM in DMSO and a final concentration of 500 µM was added to the cell cultures. AZD5904 was dissolved at a concentration of 150 mM in DMSO and added as a final concentration of 300 µM to the medium.

6.3.2 Determination of the phagocytosis rate of PMN

To assess the phagocytosis rate of murine PMN, cells were infected with virulent H37Rv Mtb, expressing a red fluorescent reporter Protein (DsRed). Cells were measured 2 hpi with fluorescence-activated cell sorting (FACS) for DsRed positivity using a MACSQuant® Analyzer10 Flow Cytometer and data was analysed using FlowJo.

6.3.3 PMN necrosis assay (LDH release assay)

For the evaluation of necrosis, release of lactate dehydrogenase (LDH) was measured using an LDH cytotoxicity detection kit from Roche (11644793001). The protocol was followed

according to the manufacturer's instructions. In short, 50 µL of cell culture supernatant or extracellular protein fraction were collected and transferred to a new 96-well F-bottom plate. After adding of 50 µL Reaction Reagent from the kit to each well, the plate was incubated for 30 min at room temperature, protected from light. Absorbance at 490 nm was determined. The percental amount of LDH activity was calculated using a 100% value from cells lysed with 0,5% Triton X-100.

6.3.4 PMN necrosis assay (Sytox green assay)

For the analysis of necrosis of hPMN, $1x10^5$ cells were cultured per well in 100 µL in a 96 U-bottom cell culture plate with the medium described for lipidome analysis. The cells were infected and treated as described before and the medium was supplemented with 5 µM SYTOX™ Green nuclear staining buffer, which bind DNA upon membrane disintegration. Fluorescence was then measured with an excitation of 504 nm and emission at 523 nm with a Synergy™ Multi-Mode Microplate reader (Biotec). The percental necrosis rate was calculated by using a baseline measurement after infection of the cells and a 100% necrosis value, which was generated by lysis of the cells with 0,5% Triton X-100.

6.3.5 Colony forming unit assay

To determine bacterial numbers in cell cultures or organ lysates, colony forming units of the bacteria were evaluated. For the analysis of *in vitro* cultures cells were lysed at 2 hpi with 0,5% Triton X-100 in PBS. For *in vivo* determination of the CFU, organs were homogenized in WTA buffer, either using a Whirl-Pak to dissociate the organ or in Minilys tubes, in which organs were grinded using a FastPrep machine (MP Biomedical). From the tissue homogenates 4-log serial dilution in PBS containing 0,05% Tween 80 were prepared. Dilutions were plated on 7H11 Agar plates and Mtb cultures were counted after a 3 – 4-week incubation at 37°C.

6.3.6 Cell culture for lipidome analysis

Human peripheral blood PMN were analysed to look for infection induced differences in their lipidome. For the extraction of lipids, $5x10^6$ hPMN/mL were seeded in RPMI1640 supplemented with 1% L-Glutamine and 10% heat inactivated autologous donor serum. The cells were either uninfected, infected with Mtb H37Rv at MOI 3 or treated with ABAH and

incubated for 2 or 6 h at 37°C with 5% CO_2. All samples were prepared as technical duplicates or triplicates. To analyse the effect of MPO inhibition, one sample of infected cells was treated with 500 µM ABAH. After incubation, 1/10th of the volume was taken twice to generate a CFU control and cytospins for microscopic analysis. In parallel, an LDH release measurement was performed on a separate plate as described before. After incubation, the cell culture was transferred into a 2 mL Eppendorf tube and centrifuged at 4000 xg at 4°C for 10 min. Afterwards, the pellet was washed twice with 1 mL PBS (4000 xg, 4°C, 10 min). Finally, the pellet was resuspended in 50 µL PBS and transferred into 270 µL MeOH/1,84% BHT (butylated hydroxytoluene).

6.4 Animal experiments

6.4.1 Aerosol infection of mice

Animals were infected with the virulent *Mtb* strain H37Rv NY in an aerosol inhalation system (Glas-Col) with an intermediate infection dose of 100 – 150 CFU. The animals were placed in individual metal cages that were put in an aerosol chamber. Inside the camber, the system regulated the main air flow at around 1.68 m^3/h and the compressed air flow for nebulization at around 0,28 m^3/h. Thereby, nebulization of an infectious solution in the chamber allowed a natural infection by inhalation of Mtb. The detailed program of the aerosol infection can be found in **Table 1**.

Table 1 Aerosol infection program

	Time [sec]
preheating	900
Nebulizing time	2400
Extraction time	2400
Decontamination	900

To prepare the infection solution, an aliquot from a frozen stock culture with a defined number of 1,2x10^8 bacteria was used. First, a single cell suspension was prepared by passing

the thawed suspension 7 times through a 27G needle. According to the intended infection dose the infection solution was prepared in 6 mL Aqua dest. From this solution, 5,5 mL were used for the infection of the animals. The remaining 500 µL were used to prepare a serial dilution up to 10^{-5} in 0,05% Tween80 in PBS and plated on 7H11 Agar plates. The CFU was counted after a 3 – 4 weeks incubation period. After the infection program was finished, the mice were removed from the infection chamber and the system was decontaminated by nebulizing 6 mL disinfectant using the same program as before.

Table 2 Scoring system for Mtb infected animals

Score	Activity	Bodyweight	General conditions	Behaviour
1	Very active	No change or increase	Fur glossy and glowing, clean orifices of the body, eyes clear and glossy	Normal
2	Active	Loss of < 10%	Reduced or abnormal body hygiene, uneven fur	Little changes
3	Less active	Loss of 10 - 20%	Dull, unkempt fur, unkempt orifices, elevated tonicity	Unusual, reduced motor functions or hyperkinetic
4	Not active	Loss of 20 - 30%	Dirty fur, clotted orifices, abnormal body position, eyes cloudy, elevated tonicity	Self-isolation, lethargic, pronounced hyperkinetic, coordination disorder, behavioural stereotypes
5	lethargic	Loss of > 30%	Cramps, paralysis in extremities and torso, breathing noises, cold body	Pain during handling, self-amputation (auto aggression)

6.4.2 Health scoring of the animals

Health status of the animals was scored weekly to daily during the treatment period. Criteria included the animal's activity, bodyweight, general condition and its behaviour. Detailed

description of the criteria can be found in **Table 2**. For each criteria a score from 1 to 5 was given and the mean of all four criteria was taken as overall score. If an animal dropped below 3 in its overall score it was removed from the experiment and sacrificed according to the German Protection of Animals Act.

6.4.3 Animal drug treatment

All drug solutions were prepared freshly 30 min before application. During all experiments, mice were weighted prior to drug administration and received 10 mL/kg of the required solution.

Animals were treated *intraperitoneal* with either 40 or 80 mg/kg 4-Aminobenzoic acid hydrazide (ABAH). For the lower concentration, a 256 mM solution of ABAH in DMSO was prepared. This was further diluted 1:10 in PBS before given *intraperitoneal* to the animals. For the preparation of 80 mg/kg ABAH, 8 mg/mL ABAH were dissolved in 30% Captisol® in 0,9% NaCl. The solution was sonicated for 10 min and heated in a water bath for 15 – 20 min at 37°C until applied to the animals.

In order to treat the animals *per os*, ABAH was dissolved in 30% Captisol®, 0,9% NaCl with 1% Tween80. To solubilize the drug, 8 mg/mL ABAH were dissolved in 25% of the final Volume with 4% Tween-80 in in 0,9% NaCl. The solution was then sonicated for 10 min. The remaining 75% of the final volume was added, which contained 40% Captisol® [w/v] (CyDex) in 0,9% NaCl. The solution was then warmed up in a water bath for 15 – 20 min at 37°C until applied to the animals. In case co-treatment with 10 mg/kg INH was applied, the Captisol® containing solution was supplemented with 4 mg/mL INH, leading to a final concentration of 1 mg/mL, equating for 10 mg/kg INH.

AZD was solubilized as described for *per os* ABAH administration but a concentration of 4,5 mg/mL was used.

6.5 Immunologic analysis

6.5.1 Extracellular protein extraction

Extracellular proteins were extracted to evaluate tissue necrosis and MPO concentration and activity, potentially affected by MPO inhibitor drugs. After the harvest, organs were shortly washed in PBS and immediately incubated in protein extraction buffer 4 times the volume

of the organs weight. The samples were incubated on ice for 2 h. After that, the organs were removed from the buffer and the solution was centrifuged (5 min, 4°C, 500 xg) to remove tissue debris and loose cells. The supernatant was transferred to a new 50 mL conical tube. To precipitate the proteins, four times the supernatants' volume of ice-cold acetone was slowly added to the tubes and incubated for 1h at -20°C. Following, the tubes were centrifuged (15 min, 4 °C, 3500 xg) and the protein pellet was resuspended in 300 µL PBS.

6.5.2 BCA protein content determination

Protein concentrations were estimated in lung lysate, extracellular protein fractions and serum. The commercially available 'Pierce™ 660 nm Protein assay' (Thermo Scientific™; 22660) was used. 10 µL of sample were applied to a 96-well F-bottom plate. The addition of the ready-to-use protein assay reagent to each well induced a colour change that indicates the protein concentration via absorbance at 660 nm. To calculate the concentration the values from a standard curve were used.

6.5.3 Measuring MPO activity

To estimate the peroxidase activity of MPO in biological samples, the reaction of MPO with 3,3', 5,5'-Tetramethylbenzidin (TMB) was utilized. TMB is a substrate for the peroxidase-catalysed reaction and allows an estimation of the activity through measurement of the colour change by photometry. For the analysis of MPO activity from *in vitro* cultures, the activity was measured in intra- and extra cellular fractions. To separate the fractions, cell cultures were centrifuged (5 min, 4 °C, 500 xg) after the incubation period and 50 µL of the supernatants were transferred to a new 96-well F-bottom plate. The cells were then washed by adding 100 µL PBS and followed by centrifugation (5 min, 4 °C, 500 xg). Supernatants were discarded and cell pellets were resuspended and lysed in 100 µL PBS with 0,5% Triton X-100. From this cell lysate 50 µL were taken to a new 96-well F-bottom plate. 50 µL TMB solution was added to each well and the reaction was stopped after 10 min with 50 µL 2 M H_2SO. Changes in the absorbance can be used to estimate the MPO activity.

To evaluate the activity of MPO in tissue samples, the MPO activity assay was combined with the previously described MPO ELISA. After the incubation of the sample solutions on the ELISA plate, 100 µL TMB solution was added to each well. Absorbance was then

acquired in a kinetic mode at 650 nm for 5 to 10 min. To convert the absorbance measurement into units of enzyme activity per mL, the change in absorbance was calculated using the following equation:

$$\Delta A_{650} = [\frac{A_{650}(time\ 5\text{min}) - A_{650}(time\ 10\text{min})}{4\ min}]$$

The reaction rate of MPO was further determined by dividing the change of absorbance with the extinction coefficient of TMB ($3.9\text{x}10^4 M^{-1}cm^{-1}$) multiplied with the pathlength of sample in the well.

$$MPO\ activity\ \left[\frac{Units}{mL}\right] = \frac{\Delta A_{650}}{3.9\text{x}10^4 M^{-1}cm^{-1} * 0{,}4\ cm} * \frac{0{,}1\ mL}{sample\ volume}$$

6.5.4 Determination of MPO protein concentration (MPO ELISA)

To evaluate the concentration of MPO protein in samples, the mouse Myeloperoxidase DuoSet ELISA Kit (R&D; DY3667) was used. The protocol was followed according to the manufacturer's instructions. In short, an ELISA plate was coated over night at RT with 800 ng/mL capture anti-MPO antibody. The plate was washed with ELISA washing buffer and blocked for 1 h with 1% BSA in PBS at RT. The plate was washed three times and 100 µL sample solution was applied. For *in vitro* cultures, 100 µL cell culture supernatant or 100 µL lysed cell pellet was used. The protocol for the preparation of these samples is described in the abstract 'Measuring MPO activity'. For the evaluation of tissue MPO concentration, 100 µL of extracellular protein fraction was used. The sample solutions were incubated for 2 h at RT in the plate followed by four washing steps. Detection antibody was added at a working concentration of 50 ng/mL and incubated for 2 h at RT or oN at 4 °C. The plate was washed three times with ELISA washing buffer and 100 µL StrepHRP solution was added for 20 min at RT. After another washing step, 100 µL substrate solution was added for 15-20 min at RT and the reaction was finally stopped with 50 µL 2 M H_2SO. The absorbance was acquired at 540 nm. A linear standard curve with recombinant murine MPO ranging from 0 to 16000 ng was used to calculate the concentration of MPO in the samples.

6.5.5 LEGENDplex™ cytokine analysis

To analyse the cytokine and chemokine concentration in lung lysate from infected mice flow cytometry was used (for the preparation of lung lysate see chapter *colony forming unit assay*). The 'LEGENDplex™ mouse proinflammatory chemokine panel' kit from BioLegend (740451) was used for the assay. It is a beat-based immunoassay, working in principle like a sandwich immunoassay. The protocol and analysis were performed following the manufacturer's instructions. In short, antibody directed capturing labels cytokines with beats of different size and granularity. In a next step, cytokine specific, biotinylated antibodies were added, which bind the analytes on the beads. Streptavidin-labelled fluorophores were then used to label the beat-sample-detection antibody complexes. A standard curve generated with the samples was used for determination of cytokine concentrations. The samples were measured with a BD FACSCanto™ II Cell analyser. The evaluation was performed using the 'LEGENDplex™ Data Analysis Software' from BioLegend. Results were normalized against the protein content of the whole lung lysate.

6.5.6 MSD U-plex cytokine analysis

MESO SCALE DISCOVERY'S Multi-Array® (MSD) technique allows a multiplex analysis of chemokines and cytokines, based on electrochemiluminescence. We used a customized panel including IFNγ, TNFα, CXCL-1, MIP-2, IL-6, IL-2, IL-1ß, Il-17, MIP-1a and IL-22 to analyse lung lysate of infected mouse lungs (for the preparation see chapter *colony forming unit assay*). The protocol was followed manufacturer's instructions. In short, biotinylated antibodies against each analyte were coupled with individual U-PLEX linkers in a first step. These linkers were coated on a plate, on which each well had a distinct binding area for each linker. Afterwards, the samples were incubated on the plate. For detection, antibodies labelled with electro chemiluminescent labels (MSD GOLD SULFO-TAG) are used to complete the immunoassay. The measurement uses electricity to stimulate light emission by the SULFO-TAGs. Light intensity can be used to quantify the analytes in the samples. For each analyte a standard curve is prepared during the assay, which allows an estimation of the sample's concentration. For the measurement of the plate a MESO® Quick Plex SQ 120 was used.

6.6 Phenotypic analysis of cell populations using flow cytometry

6.6.1 Preparation of tissue derived single cell suspensions

For the preparation of single cell suspensions from an organ, it was initially placed in a 24-well plate and cut with scissors. The pieces were then transferred to a 50 mL conical tube, containing 2 mL organ digestion buffer and incubated on a shaker at 600 rpm for 90 min at 37°C. Afterwards, the tubes were placed on ice and the tissue was pressed through a 100 µm cell strainer into a new tube, using the stamp from a syringe. The cell strainer was flushed with 30 mL ice cold PBS and remaining droplets were collected from underneath the cell strainer. The suspension was centrifuged (5 min, 4°C, 500 xg) and the supernatant discarded. Erythrocytes were lysed by resuspending the cell pellet for 3 min at RT in ammonium chloride buffer. The reaction was stopped with 10 mL cRPMI (see Methods) and the cells were washed by centrifugation (5 min, 4°C, 500 xg) with 10 mL cRPMI. To evaluate the cell number, cells were finally resuspended in 1 mL RPMI and counted using a ViCell counter (Beckman Coulter). The cells were further processed for FACS analysis.

6.6.2 Surface marker staining

For *in vitro* cell culture analysis, $1x10^5$ cells/well were used. For the analysis of organ lysates $1x10^6$ cells/well were used. Cells were centrifuged (5 min, 4 °C with 500 xg) and the supernatant was discarded. To prevent unspecific binding of antibodies, cells were incubated for 10 min at RT in 50 µL Fc-blocking buffer, containing 1% a-CD16/32, 1% Rat serum and 1% Syrian hamster serum. Following, 50 µL of surface staining was added and the cells were incubated for another 15 min on ice. The individual staining panels can be found in the material section ('FACS panels'). Cells were washed twice with 200 µL FACS buffer (5 min, 4 °C with 500 xg) and finally resuspended in 200 µL FACS buffer and analysed with a MACS Quant Analyzer 10 from BD.

6.6.3 Intracellular cytokine analysis

For the analysis of intracellular cytokine expression, murine lung cells were seeded in cRPMI medium containing 5 µg/mL Brefeldin A solution at a concentration of $1x10^6$ cells/well on a 96-F bottom plate that had been previously coated with 5 µg/mL recombinant mouse anti-CD3e and 5 µg/mL recombinant mouse anti-CD28 antibodies in PBS. The cells were then incubated for 4,5 h at 37°C with 5% CO_2. After the incubation the cells were

mixed by pipetting and transferred to a 96-well U-bottom plate. First, cell populations were stained following the protocol for surface marker staining. Next, the cells were resuspended in 100 µL Cytofix/Cytoperm buffer (BD) and kept at 4 °C over night. Following, the cells were washed twice by centrifugation (5 min, 4 °C, 300 xg) with 200 µL Cytofix washing buffer. For the intracellular staining, antibodies were diluted in Cytoperm/Cytofix buffer and 50 µL was added to each well. Cells were incubated for 15 min on ice and washed twice with 200 µL Cytofix washing buffer (5 min, 4 °C, 300 xg). For analysis the cells were resuspended in 200 µL FACS buffer and measured with a MACS Quant Analyzer 10 from BD.

6.7 Histopathological and immunochemical analysis

6.7.1 Cryo conservation & sectioning

Organs from infected mice were fixated over night at 4°C in 4% PFA. The next day, the fixated samples were washed with PBS and incubated in 5% saccharose for 60 min at RT. The following incubation steps were each for 60 min in a mixture of 5% saccharose with 20% saccharose in three different ratio: 2:1, 1:1 and 1:2. Subsequently, the samples were incubated overnight in 20% saccharose at 4°C. A final 30 min incubation was performed in 20% saccharose mixed with an infiltration solution (TissueTek) in a ratio 2:1. 30 min prior to the freezing process a beaker glass filled with cold isopentane was placed onto dry ice. The tissue samples were then placed into tissue moulds and filled with TissueTek. The Tissue mould were put into the isopentane for a couple of minutes to harden. The frozen cryo blocks were then stored at -20°C until further use. Cryo blocks were cut into 5 µm sections. From each organ, 5 consecutive sections on individual slides were prepared. Then 300 µm of the organ were cut off and another 5 µm consecutive section was added to each slide. Thereby each slide contained sections of two different levels of the organs. For the preparation of the sections, a cryostat (Leica) with cooling function was used.

6.7.2 Paraffin embedding & sectioning

Organs from infected mice were fixated over night at 4°C in 4% PFA. The next day, the fixated samples were washed and stored in PBS. In a first step, the organs were dehydrated in an increasing Ethanol row (Autotechnikon Microm, STP 120, Thermo Fisher) after being transferred to paraffin. The exact steps of the procedure can be found in **Table 3**.

Following, the organs were embedded in 65°C heated paraffin into blocks using a paraffin casting station (Leica; EG1140C). After hardening, the blocks were cut using a rotation microtome (Leica; RM 2155). To apply the sections on SuperFrost® microscopy slides, the sections were expanded in 37°C in a paraffin stretch bath (Leica; 1052) and taken out with the slide. On each slide 2 – 3 sections were applied. Afterwards the slides were dried over night at 37°C. Prior to further processing or staining the slides were de-paraffinized starting with a two times 10 min incubation in Xylol. This process was followed by 2 min incubation steps in a decreasing concentration of Ethanol (2x 100%, 2x 96%,2x 70%). Finally, the slides were washed two times for 2 min in A. dest. and were ready for further processing.

Table 3 Workflow of the Autotechnikon Microm for paraffin embedding

Step	time [h]
4% PFA	1
70% Ethanol	1
80% Ethanol	1
90% Ethanol	1
96% Ethanol	1
100% Ethanol	3 x 1
Xylol	2 x 1
Parafin (65°C)	2 x 1,5

6.7.3 H&E staining

Haemalaun & Eosin staining allows a general differentiation of cells by staining the nucleus deep purple and the cytoplasm light pink. For this staining cell cultures or deparaffinated tissue sections were used. First, the samples were incubated for 1 min (cell cultures) or 5 min (tissue sections) in Meyer's Haemalaun. After washing of exceeding dye with tap water,

samples were incubated for 1 min in Eosin. Afterwards the samples were washed and dehydrated in a series of 70% EtOH, 96% EtOH, 100% EtOH and Xylol. The slides were finally covered with coverslips using Entellan.

6.7.4 Acid fast staining

This staining was used for cytospinned cell culture samples. Slides were incubated for 3 min in carbolfuchsin and afterwards rinsed with tab water. Following, the slides were dipped three times into TB-decolonizer to wash off excess dye. Afterwards, the samples were washed and dehydrated in a series of 70% EtOH, 96% EtOH, 100% EtOH and Xylol. The slides were finally covered with coverslips using Entellan.

6.7.5 Ziehl-Neelson staining

The Ziehl-Neelson staining method colorizes Gram bacteria in bright pink and cells in blue. This allows a qualitive analysis about the infiltrating cells into the tissue and the existing bacterial load. In a first step, paraffin embedded tissue sections on microscopy slides were de-paraffinized as described in the 'Paraffin embedding & section' chapter. Slides were then washed in Aqua dest. and placed on a staining bench. The tissue sections were covered with Ziehl-Neelson carbofuchsin solution. To fixate the dye in the tissue, the slides were heated three times with an oil lamp. Afterwards, the excess dye was washed out with Aqua dest. and the slides were shortly dipped in 5% HCL in 70% Ethanol. After flushing in Aqua dest., the tissue sections were stained for 1 min with 1:10 methylenblue in Aqua dest. After washing off the excess dye, the sections were dehydrated with 2 min incubation steps in an increasing Ethanol row (96% EtOH, 100% EtOH) and finally placed for 2 min in Xylol. The slides were finally covered with coverslips using entellan.

6.8 Immunohistochemistry

6.8.1 MPO-DAB staining

MPO was immunoenzymatically stained using 3,3'-Diaminobenzidine (DAB). First, paraffin sections were de-paraffinized as described in the 'Paraffin embedding & section' chapter. Then, a chemical antigen retrieval was performed. Slides were placed in citrate buffer and incubated for 30 min in a steamer. Afterwards, the cuvette was let to cool down and the slides were washed twice with TBS. The slides were placed in Shandon Chambers

and incubated for 10 min in 1% H_2O_2 in TBS to block endogenous peroxidases, followed by washing steps (three times for 5 min with TBS). Blocking and permeabilization were performed in parallel by a 10 min incubation in 0,1% Triton-X/3% BSA/5% normal goat serum in TBS. Following, the anti-MPO antibody was added in a 1:150 dilution in TBS over night at 4°C. The next day the slides were washed as before. The second goat α-rabbit-F(ab)2 biotinylated antibody was given 1:500 in TBS/3%BSA and the slides were incubated for 45 min at RT. After the incubation period, an ABC peroxidase staining Kit (Thermo Fisher Scientific; 32052) was used to prepare the biotinylated secondary antibodies for the enzymatic staining reaction. The reagent was prepared following manufacturer's instructions and incubated for 45 min at RT on the slides. The slides were washed as before and removed from the Shandon chambers. Then, each organ slide was covered for 15 min with a DAB-staining solution (Sigma), prepared following manufacturer's instructions. The reaction was stopped by placing the slides in aqua dest. Finally, a Hemalaun stain was performed as described before to visualize the nuclei.

6.9 Biochemical analysis

6.9.1 Lipid extraction of human PMN

Recovery of lipids from the samples was performed following a methyl-*tert*-butyl ether/methanol extraction protocol (Schwudke, 2008). Prior to the extraction, all used glass ware was washed three times with LC-MS grade water, LC-MS grade MeOH and LC-MS-grade chloroform or MTBE, depending on the finally applied substance. Afterwards, the glass ware was dried using Nitrogen. All samples were substituted with 10 µL of a self-prepared synthetic lipid standard that was added to each tube and vortexed. Details on the composition and concentrations can be found in table X. Following, 1 mL MTBE with 0,8% AcOH was added to the samples and incubated in a shaker at 600 rpm at RT for 1h. 250 µL MS-H_2O were added to each tube, vortexed and placed in a shaker for another 5 min. Following, the samples were centrifuged for 5 min at 4°C at 15000 rpm. This procedure divides the samples into a lipid containing organic and a watery phase. 800 µL of the upper, organic phase were transferred into a new tube and dried in a speedVac (Temp.: no; 1 ramp) for approximately 2 – 2,5 h. Then, the dried lipids were resuspended in 50 µL storage solution ($CHCl_3$/MeOH/2-Isopropanol [60:30:4,5]). For lipid analysis, 5 µL of the lipid solution were added to 245 µL MS-Mix, from which 20 µL were used to perform the measurement.

6.9.2 Cholesterol extraction from lipid extracts

For extraction of cholesterols from lipid extracts, the 10 µL of the organic phase were transferred to a new tube and dried in a speedVac (Temp.: no; 1 ramp) until no moisture was left. Acetyl chloride was added to chloroform in a relation of 1:5 and 100 µL were added to the dried samples. Then they were incubated for 1 h at RT, with opened lids to evaporate the chloroform. The rest was again dried in a speedVac (Temp.: no; 1 ramp) for approximately 20 minutes. Following, the samples were resuspended in 50 µL MS-Mix and 20 µL of a 1:10 dilution in MS-Mix were used for shotgun lipid profiling.

6.9.3 Shotgun lipid profiling

Lipid extracts diluted in MS-Mix were analysed in technical replicates with shotgun lipidomic approach using a nano-electrospray ion source. Samples were automatically injected with the autosampler TriVersa NanoMate (Advion, Ithaca, USA) and analysed with a Q Exactive Plus (Thermo, Bremen, Germany). Samples were measured over a period of 15 min, starting with 5 min in negative ion mode and followed by 10 min positive ion mode analysis. Cholesterols were analysed over a time period of 10 min in positive ion mode. Identification of lipid classes and species was performed by the biochemical department at Researchcentre Borstel using LipidXplorer (Herzog, 2011 & 2012). The import settings can be found in the supplementals. The mean amount in pmol from technical replicates was normalized against the total identified lipid classes or the total identified lipidome in the samples.

6.10 Statistical analysis

Statistical analysis was performed using GraphPad Prism® (version 8.4.3.). The analysis of more than two groups at one timepoint was performed using ordinary one-way ANOVA with Turkey's multiple comparison post-test. An ordinary two-way ANOVA with Turkey's multiple comparison post-test was used for experiments, comparing different groups with more timepoints. Statistical significance was reached with a p value of < 0.05. Significance was marked with stars * $p \leq 0{,}05$; ** $p \leq 0{,}01$; *** $p \leq 0{,}001$.

7 RESULTS

7.1 Analysis of the hPMN lipidome

ROS mediated oxidation of cellular lipidome can have profound effects on cellular functions and immune regulation [125]. LPO products can act as lipid mediators or can be presented as antigens on MHCI like CD1 molecules, that can subsequently influence T cell responses, by either silencing or enhancing the T cell response [126], [127]. Further lipids and lipid products are mycobacterium's primary energy source [94], [96], thus a thorough analysis of Mtb induced PMN lipidome changes is a fundamental first step to understand the role of lipids during the infection. For the first time, the lipidome of hPMN upon infection with Mtb was analysed. The analysis was performed by mass spectrometry of *in vitro* hPMN culture. Uninfected hPMN were compared with Mtb infected with or without MPO inhibitor (ABAH) treatment.

7.1.1 Phenotype of Mtb infected hPMN upon MPO inhibition

As described before, Mtb infection drives PMN into necrotic cell death in a ROS dependent manner. Thus, in a first step the hPMN phenotype triggered by an infection with Mtb was confirmed. Throughout the performed experiments, the bacterial load, determined by CFU assay, was stable (**Figure 6 a**). Analysis of the cell death was performed using a SYTOX™ green nucleic acid stain assay. Mtb infection induced necrosis at 6 hpi, which was prevented upon ABAH treatment, thereby confirming earlier results which describe the Mtb induced necrosis as MPO driven (**Figure 6 b**) [17], [79]. The protein concentration of the samples was slightly reduced upon Mtb infection, regardless of additional MPO inhibitor treatment, but not in a significant manner (**Figure 6 c**).

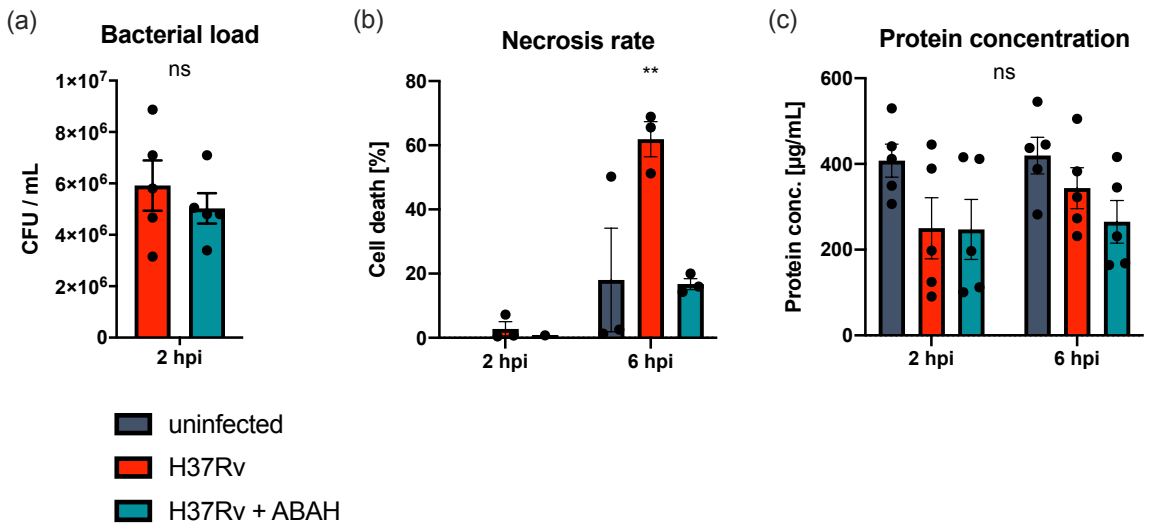

Figure 6 Infection rate, protein concentration and necrosis of H37Rv infected, hPMN *in vitro* culture. Peripheral blood hPMN were infected with H37Rv Mtb (MOI 3) and cultured for 2 and 6 h. The infection rate, determined via the CFU, was assessed at 2 hpi (a). Necrosis was analyzed using a SYTOX™ green nucleic acid stain at 2 and 6 hpi (b). The protein concentration was slightly lowered by the infection, but not significantly (c). Depicted are 3 - 5 independent experiments. Error bars indicate mean with SEM, (a, c) 2-Way ANOVA with Tukey's multiple comparison. (b) unpaired t-test. *p ≤ 0,05; **p ≤ 0,01; ***p ≤ 0,001.

In order to confirm necrotic cell death induction by Mtb infection, cells were cytospinned and stained according to acid-fast staining (AFS) protocol. The phenotype of uninfected hPMN did not change during the 6 h incubation time. Mtb infected hPMN showed typical signs of necrosis, as soon as 2 hpi. At 6 hpi, significant necrosis was observed, marked by cell ghosts and free DNA with free bacteria (red arrows). ABAH treated, infected cells also showed Mtb induced morphological changes. However, apoptotic cells were more abundant than in non-treated samples, which was marked by condensation of the DNA and shrinkage of the cells and Mtb enclosed in apoptotic vesicles (green circles) (**Figure 7**).

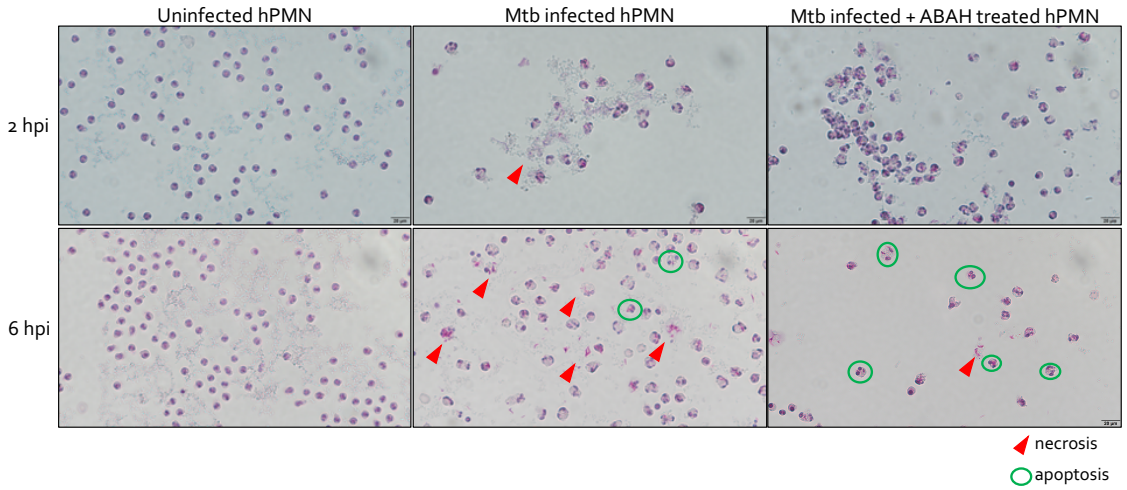

Figure 7 **Morphological differences of hPMN after infection with H37Rv Mtb.** hPMN were infected with H37Rv Mtb (MOI 3) and cultured for 2 and 6 h. Cells were cytospinned and stained using the AFS protocol. Depicted are pictures from one representative experiment.

7.1.2 Analysis of distinct lipid types and lipid classes in uninfected hPMN

We applied MS/MS analysis using a Q Exactive Orbitrap mass spectrometer (ThermoFisher) to analyse the lipidome of *in vitro* cultured hPMN. In total, hPMN isolated from five different donors were used, which included three men and two women, aged between 25 and 65.

In a first step, uninfected hPMN were analysed. The identified lipids were classified into four major lipid types, each with distinct lipid classes. In total, 10 phospholipid classes, 3 neutral lipid classes, 2 sphingolipid classes and one cholesterol class could be identified. Further differentiation was made by the identification of distinct lipid species. These were identified by the difference in length and molecular composition of their fatty acid chains. Based upon this classification, 225 phospholipids, 29 neutral lipids, 20 sphingolipids and 1 cholesterol species were found. In total 275 lipid species were identified (**Figure 8 a**). The lipid type with the highest variation regarding the amount of lipid classes were phospholipids, from which the highest species variability was found in phosphatidylethanolamines (PE/PE-O) with in total 100 identified species, followed by phosphatidylcholines (PC/PC-O) with 64 distinct species (**Figure 8 b**). Of note, the same amount and numbers for lipid classes and species were found for Mtb infected and MPO inhibitor treated hPMN.

The percentage of each lipid class of the total amount of identified lipids did not differ much between 2 and 6 hpi in uninfected hPMN. The numerous PE/PE-O species only make less than 10%, while PC/PC-O account for around 28% of the total lipidome. The biggest portion of the total identified lipids are cholesterols with approximately 37%. However, one difference was observed for phosphatidylglycerol (PG), which showed an increase of 4,39% during this time period (**Figure 8 c**)

(a)

Lipid type	*Abbreviation*	*Lipid class*	*Scan polarity*	*number of identified species*
Phospholipids				
	PC	Phosphtatidylcholines	positive	24
	PC-O		positive	40
	PS	Phosphatidylethanolamine	negative	13
	PI	Phosphatidylinositol	negative	19
	PG	Phosphatidylglycerol	negative	3
	PE	Phosphatidylethanolamine	negative	50
	PE-O		negative	50
	LPE	lysophosphatidylethanolamine	negative	16
	LPC	Lysophosphatdycholine	positive	9
	PA	Phosphtatidic acids	negative	1
Total	10			225
Neutral lipids				
	CE	cholesteryl esters	positive	2
	TAG	Triacylglycerole	positive	25
	DAG	diacylglycerol	positive	2
Total	3		Total	29
Sphingolipids				
	SM	Sphingomyelin	positive	16
	CER	ceramide	positive	4
Total	2		Total	20
Sterols				
	Chol	Cholesterols	positive	1
Total	1			**275**

(b)

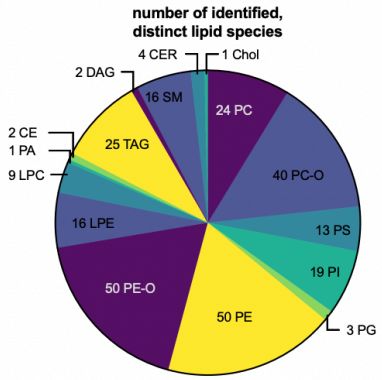

(c)

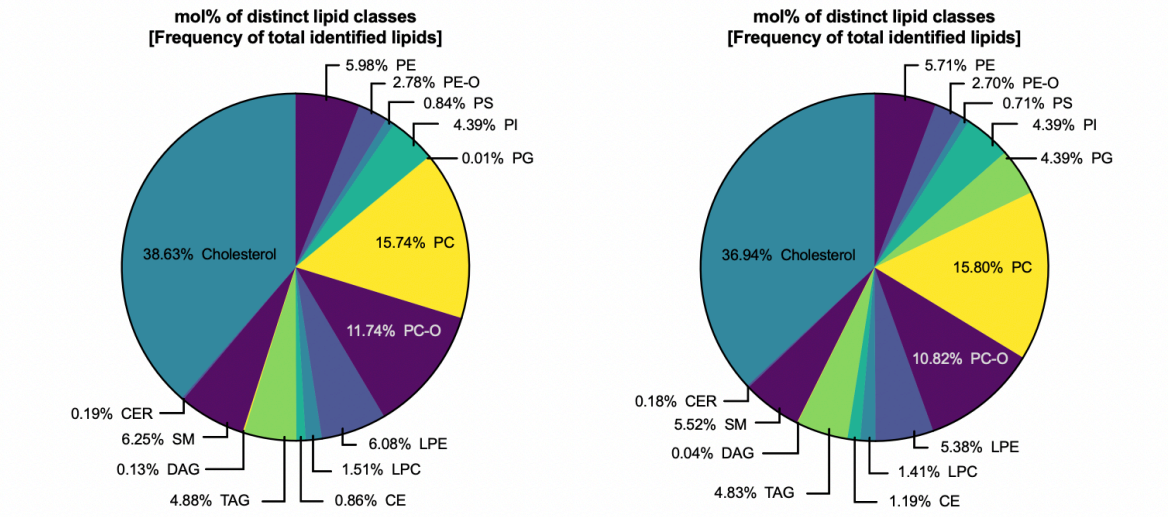

Figure 8 Composition of the hPMN lipidome. Peripheral blood hPMN were incubated for 2 and 6 hpi. Mass spectrometry allowed identification of distinct lipid types, lipid classes and lipid species of uninfected hPMN (a). The number of lipid species per lipid class is pictured in (b). The percentage of distinct lipid classes at 2 and 6 hpi is shown in mol% as frequency of total identified lipids (c).

7.1.3 Analysis of Mtb induced changes in the lipid types of the hPMN lipidome

In order to analyse possible Mtb induced changes in the hPMN lipidome, the percentage of the four lipid classes was analysed in regard to the total of identified lipids in mol% and additionally normalized to the total amount of protein of each sample in pmol lipid/µg protein (**Figure 9**). The analysis of multiple normalization modes is required, because mass spectrometry is highly sensitive and small changes can already have a huge impact. Thus, if the results are comparable, the normalization against multiple controls strengthens the data generated during MS/MS measurement.

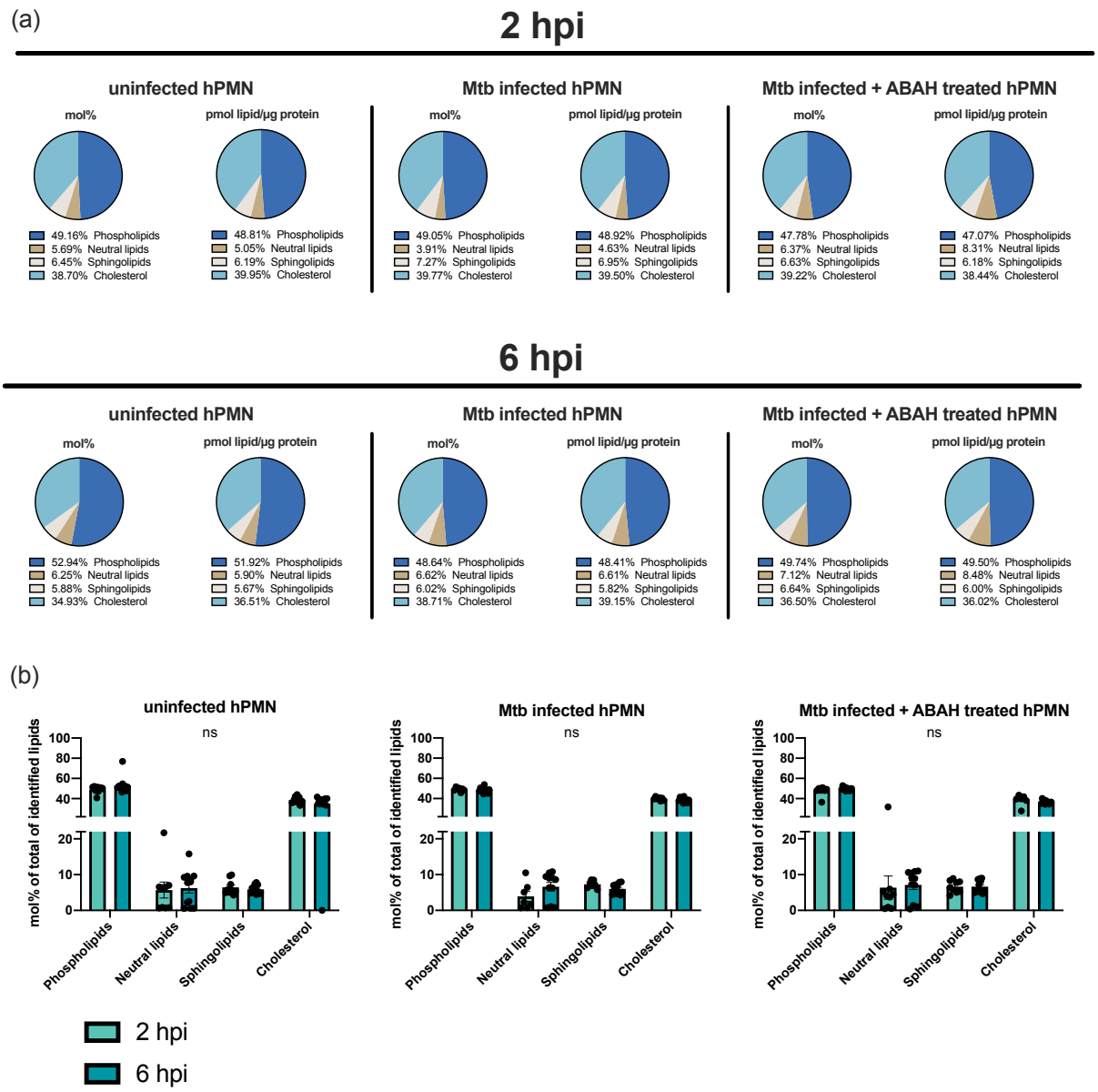

Figure 9 Differences in lipid type distribution upon Mtb infection and MPO inhibitor treatment. Lipids were isolated form hPMN *in vitro* cultures at 2 and 6 hpi. The results from the MS/MS measurement were either normalized against total amount of lipids (mol%) or the protein concentration of the respective sample (µmol lipid/µg protein) (a). Time dependent differences are shown for mol% (b). Depicted are results from 5 independent experiments. Error bars indicate mean with SEM, 2-Way ANOVA with Tukey's range test.

Comparison of the differently treated samples showed changes at 2 hpi, while at 6 hpi no differences in the distribution of the lipid types could be detected. In Mtb infected hPMN a slight reduction in neutral lipids was detected: 3,91% of the total lipidome were identified as neutral lipids, compared to 5,69% in uninfected cells and 6,37% in infected and ABAH treated cells. The results of the normalization to µg protein support this observation (**Figure 9 a**). At 6 hpi this difference was absent and 6,62% of the lipidome of Mtb infected cells were neutral lipids (**Figure 9 a**). The difference was also present upon direct comparison of 2 vs. 6 hpi. However, no statistical significance for changes in neutral lipid types could be detected for Mtb infected PMN (**Figure 9 b**).

7.1.4 Analysis of Mtb induced changes in the lipid classes of the hPMN lipidome

To analyse the time dependent change of each lipid class, the data was again, normalized as mol% or pmol lipid/µg protein. The earlier observed increase in PG species was confirmed to be statistically significant and was found in all samples, independent of infection or treatment (**Figure 10**). The normalization to mol% showed, that the Mtb infection induced a statistically significant decrease in triacylglycerates (TAG) (**Figure 10 a**). This was also observed for the quantification against total protein, however not in a statistically significant manner (**Figure 10 c**). Interestingly, cholesterol was significantly reduced upon ABAH treatment, but not upon Mtb infection at 6 hpi (**Figure 10 b, d**).

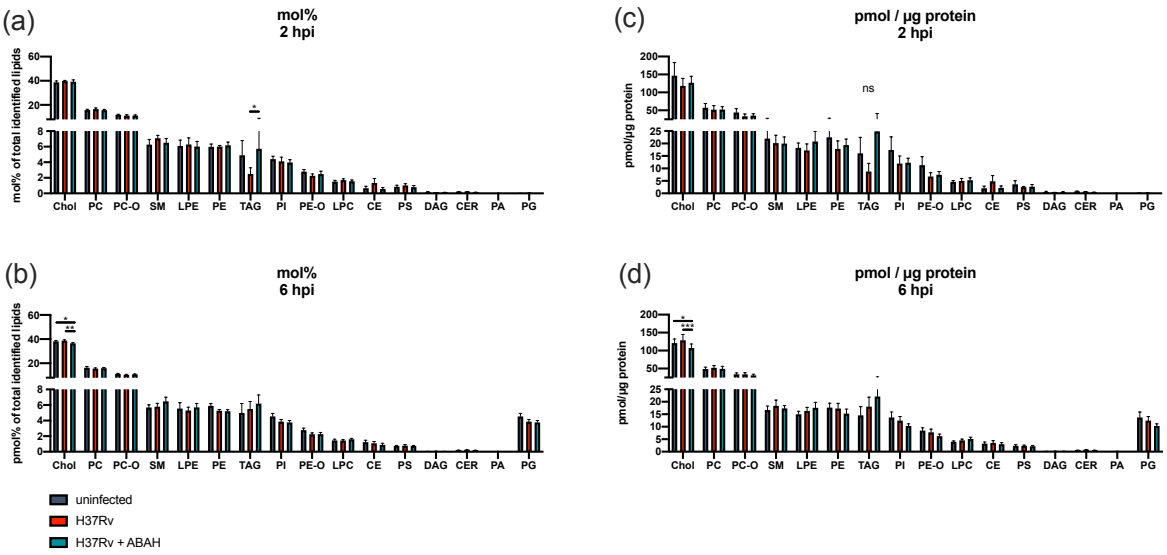

Figure 10 Time dependent change of lipid classes between different hPMN cultures. Lipids were isolated from hPMN *in vitro* cultures at 2 and 6 hpi, which were either uninfected, infected with H37Rv or infected and treated with the MPO inhibitor ABAH. Lipid classes are depicted as mol% of total identified lipids at 2 hpi (a) and 6 hpi (b) or normalized to the protein content as pmol/µg protein for 2 hpi (c) and 6 hpi (e). Depicted are 5 independent experiments. Error bars indicate mean with SEM, 2-Way ANOVA with Tukey's multiple comparison. *$p \leq 0{,}05$; **$p \leq 0{,}01$; ***$p \leq 0{,}001$.

7.1.5 Analysis of selected lipid species

All identified lipid classes were further analysed for differences in their lipid species, based on the composition and length of their fatty acid chains. Interestingly, hardly any statistically significant differences between the groups or over time were detected. However, due to the interesting infection induced changes in the frequency of TAG, the composition of its species was further looked at. The lipid species are normalized against the total amount of TAG lipids. A time dependent decrease from longer to shorter fatty acid chains could be observed, e.g. seen in the reduction of TAG 54:4 and TAG 54:4. However, this was independent of the infection status of the cells, but a little more pronounced upon Mtb infection (**Figure 11**). Details on other lipid species compositions can be found in supplementary material **12.4.**

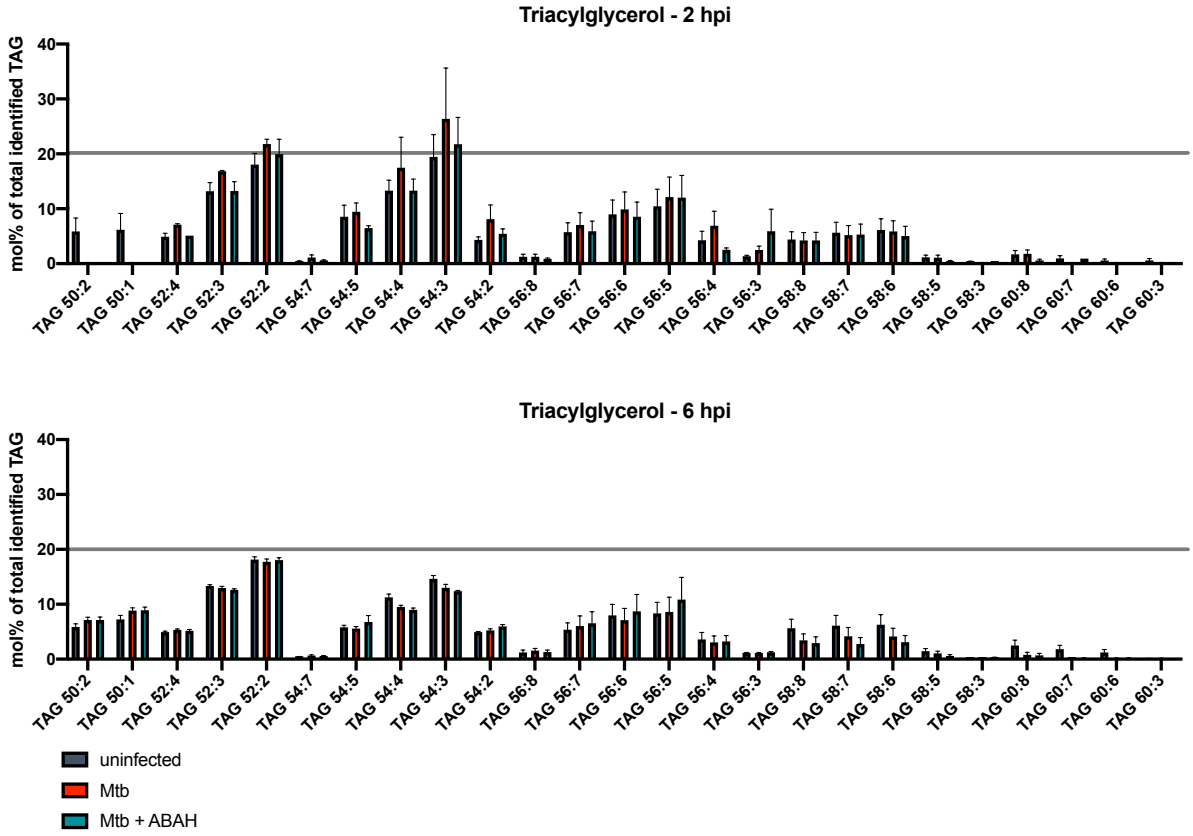

Figure 11 TAG lipid species distribution in hPMN upon H37Rv Mtb infection. Lipids were isolated from hPMN *in vitro* cultures at 2 and 6 hpi, which were either uninfected, infected with H37Rv or infected and treated with the MPO inhibitor ABAH. For detailed analysis of TAG lipid species, normalization to the total amount of TAG lipids was made. Depicted are 5 independent experiments. Error bars indicate mean with SEM.

7.2 Comparison of distinct murine PMN populations *in vitro*

Distinct murine PMN populations were analysed for their suitability in Mtb infection assays *in vitro*. PMN collected from peripheral blood were compared with freshly isolated PMN from the bone marrow and PMN that were isolated from bone marrow that was matured for 48 h in the presence of recombinant murine granulocyte colony stimulatory factor (G-CSF). After infection with Mtb, phagocytosis rates, ROS production and necrosis were analysed. We observed striking differences between the distinct murine PMN populations, that have not been described before.

7.2.1 CD11b is upregulated on matured bone marrow derived PMN

PMN were isolated using a column-free, negative selection and enrichment Kit for murine PMN (StemCell). For enrichment, phenotyping, depletion studies and flow cytometry analysis, murine PMN can be characterized according to the surface expression of Ly6G since they represent the only myeloid cell line expressing Ly6G mRNA according to gene databank analysis [128]. For further characterization of PMN activity the surface marker CD11b was chosen. The α_M-integrin CD11b is a multifunctional surface receptor expressed by a variety of leukocytes, including macrophages, B and NK cells. On PMN, CD11b forms the heterodimeric integrin $\alpha_M\beta_2$, together with CD18, which is essential for adhesion to endothelia and extravasation from the blood stream into tissue as well as for phagocytosis and degranulation of PMN [129], [130]. Peripheral blood PMN have been shown to have a significantly elevated CD11b expression after entering a post mitotic and thereby a metabolically inactive state. These cells are the first to arrive at sites of inflammation and show an elevated phagocytosis rate in comparison to PMN that are still pre mitotic [130]. Other studies have supported the finding of a $CD11b^{high}$ neutrophil population that is rapidly infiltrating sites of inflammation and its occurrence in bone marrow blood and tissue coherently fluctuates among these organs upon inflammatory stimuli [131]. Therefore, we tried to utilize the expression level of CD11b as an indicator for the activation and maturation status.

After exclusion of debris and doublets, enriched PMN isolated from blood or bone marrow, which was kept naïve or matured for 48 h with G-CSF, were analysed for their purity by gating for $Ly6G^+$ cell at 2 hpi (**Figure 12 a**). The highest frequency of leukocytes as determined by $Ly6G^+$ cells were found in PMN isolates from the bone marrow with around

80%. Blood derived isolates showed a slightly reduced purity of around 70%. The proportion of Ly6G^{-} to Ly6G^{+} PMN was significant in unmatured bone marrow derived PMN (**Figure 12 b**).

The expression of CD11b on Ly6G^{+} cells was highest on matured bone marrow derived PMN with a median fluorescence of 123, followed by blood derived PMN with a median fluorescence of 80. Unmatured bone marrow PMN showed a reduced CD11b expression with a median fluorescence of 50. In all three PMN populations, the median expression of CD11b did not change upon different MOI (**Figure 12 c**).

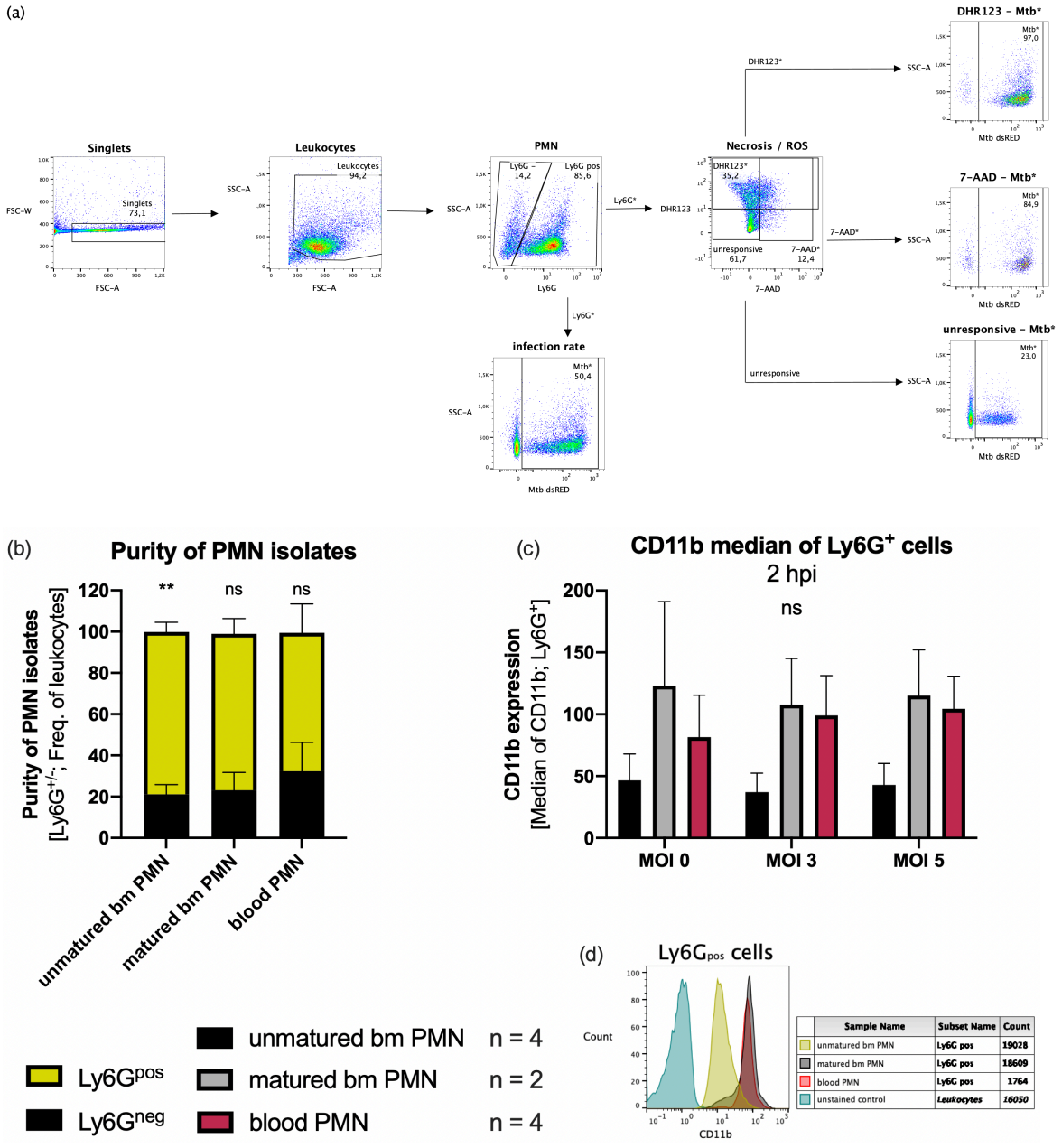

Figure 12 Purity of PMN isolates and their surface expression of CD11b. PMN were isolated from the blood (blood PMN), the bone marrow (unmatured bm PMN) or from bone marrow that

was cultivated for 48h in G-CSF containing medium (matured bm PMN), infected with a MOI 3 or 5 of H37Rv dsRed, incubated for 2 h and stained for flow cytometry analysis. After debris and doublet exclusion (a, singlets; leukocytes), PMN were defined as $Ly6G^+$ and the $Ly6G^+$ PMN populations were analysed regarding their frequency of leukocytes. $Ly6G^+$ cells, were further analysed for their infection rate (Mtb $dsRed^+$, Frequency of $Ly6G^+$), necrosis (7-AAD^+, Frequency of $Ly6G^+$) and ROS production ($DHR123^+$, Frequency of $Ly6G^+$). Further, the infection rate of necrotic (Mtb $dsRed^+$, Frequency of $Ly6G^+$/7-AAD^+), ROS positive (Mtb $dsRed^+$, Frequency of $Ly6G^+$/$DHR123^+$) or unresponsive (Mtb $dsRed^+$, Frequency of $Ly6G^+$/$DHR123^-$/7-AAD^-) PMN was analysed. In the gating scheme, a '*' symbolizes a positive cell culture ('+') (a). The purity of each uninfected cell population is depicted as $Ly6G^+$ to $Ly6G^-$ PMN (b). Further the expression of CD11b on $Ly6G^+$ cells as median of CD11b fluorescence was analysed upon different infection rates at 2 hpi (c). Histogram of CD11b expression of one representative sample from infected, matured bone marrow PMN (d). Depicted are two to four independent experiments. Error bars indicate SEM, 2-Way ANOVA with Tukey's range test. *$p \leq 0,05$; **$p \leq 0,01$; ***$p \leq 0,001$.

7.2.2 Phagocytosis rate of different murine PMN populations

Efficient phagocytosis of bacteria is a key feature of fully competent antimicrobial PMN. Cells were infected with fluorescent, virulent Mtb dsRed and the number of cells which had engulfed mycobacteria were quantified by flow cytometry. After exclusion of debris and doublets, $Ly6G^+$/$dsRed^+$ cells were measured (**Figure 13 a**). Unmatured bone marrow derived PMN showed a phagocytosis rate of 20 and 25% upon a MOI 3 or 5, respectively. Maturation of bone marrow with G-CSF significantly increased the capability of PMN to phagocytose bacteria, resulting in 60 – 70% of $Ly6G^+$/Mtb $dsRed^+$ cells. The same percentage of Mtb dsRed positive cells was found in peripheral blood derived PMN. CFU analysis supported the results of increased phagocytosis by matured bone marrow PMN when compared to unmatured PMN (**Figure 13 b**), however, not in a significant manner.

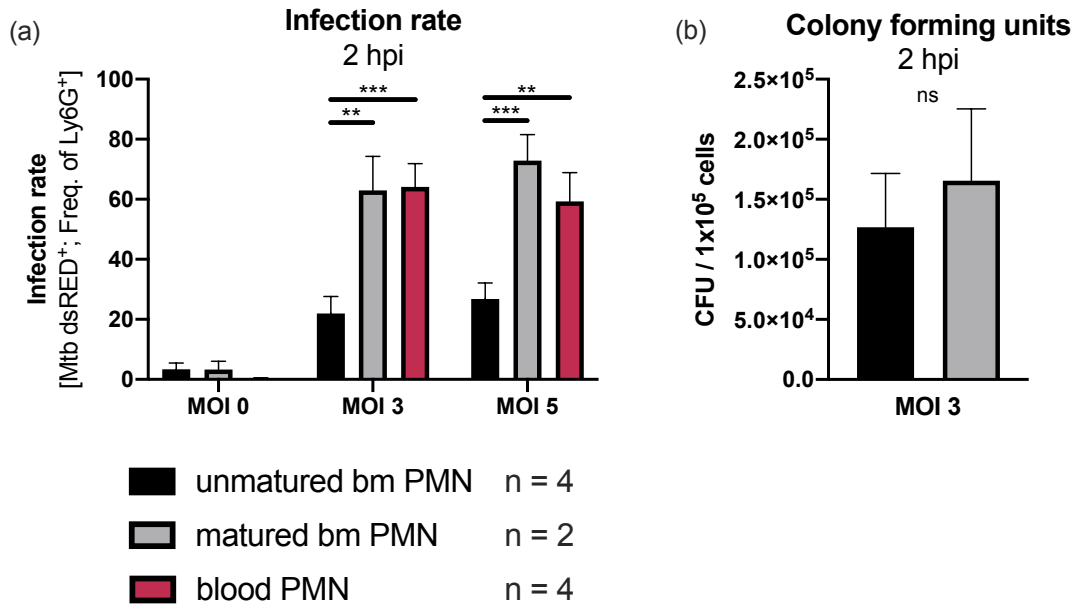

Figure 13 Phagocytosis rate of distinct murine PMN populations upon H37Rv dsRed infection *in vitro*. PMN were isolated from the blood (blood PMN), the bone marrow (unmatured bm PMN) or from bone marrow cells that was cultivated for 48h in G-CSF containing medium (matured bm PMN), infected with a MOI 3 or 5 of H37Rv dsRed, incubated for 2 h and stained for flow cytometry analysis or used for CFU assay. Phagocytosis rates were determined as frequency of Mtb DsRed$^+$ cells from Ly6G$^+$ PMN using flow cytometry at 2 hpi (a). Additionally, the infection level was determined by using CFU assay at 2 hpi using a MOI of 3 (b). Depicted are two to four independent experiments. Error bars indicate SEM, 2-Way ANOVA with Tukey's range test (a) and unpaired t-test (b). *p ≤ 0,05; **p ≤ 0,01; ***p ≤ 0,001.

7.2.3 ROS production in matured bone marrow derived PMN upon Mtb infection

The conversion of DHR123 into its fluorescent form rhodamine 123 by was utilized to quantify the production of ROS in infected murine PMN populations. Time kinetics showed a significant increase in ROS production in matured bone marrow derived PMN upon infection at 2 hpi, which declined over time (**Figure 14 b**). That effect was absent in unmatured bone marrow derived PMN, which did not increase ROS production above the baseline level of uninfected cells, neither upon infection nor over time (**Figure 14 a**). Peripheral blood derived PMN had a slight increase in ROS production upon MOI 5 at 2 hpi, but also showed higher interexperimental variations (**Figure 14 c**). In each cell population, ROS production was almost completely restricted to Mtb dsRed$^+$ cells, underlining that the respiratory burst was infection induced (**Figure 14 d - f**).

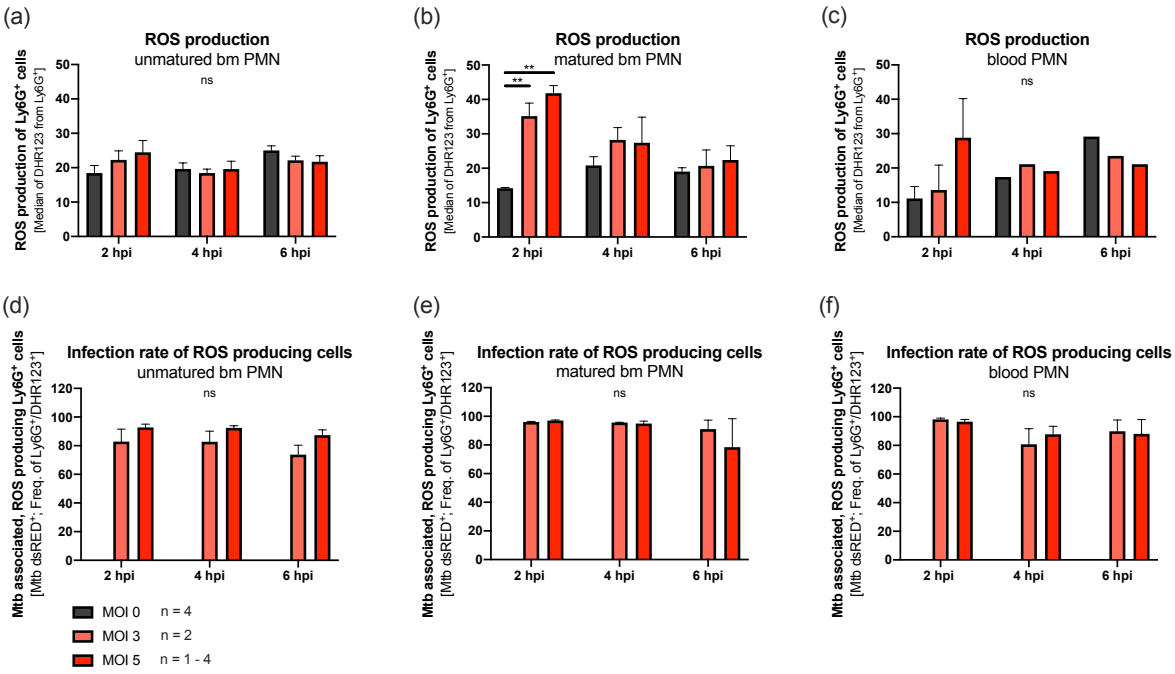

Figure 14 ROS production of distinct murine PMN populations upon H37Rv dsRed infection *in vitro*. PMN were isolated from the blood (blood PMN), the bone marrow (unmatured bm PMN) or from bone marrow that was cultivated for 48h in G-CSF containing medium (matured bm PMN), infected with a MOI 3 or 5 of H37Rv dsRed, incubated for 2, 4 and 6 h and stained for flow cytometry analysis. Production of intracellular ROS ($DHR123^+$) was analysed as frequency of $Ly6G^+$ cells in unmatured (a), G-CSF matured bone marrow (b) and blood derived PMN (c). Further, ROS production was analysed regarding their association with Mtb $dsRed^+$ (Mtb $dsRed^+$; Frequency of $Ly6G^+/DHR123^+$) (d - f). Depicted are one to four independent experiments. Error bars indicate SEM, 2-Way ANOVA with Tukey's range test (a) and unpaired t-test (b). $*p \leq 0{,}05$; $**p \leq 0{,}01$; $***p \leq 0{,}001$.

7.2.4 Necrosis of different PMN populations upon Mtb infection

A common way to measure cell death by flow cytometry is to utilize the fluorescent DNA-binding dye 7-AAD, which is membrane impermeable and only binds nucleic acid, when the plasma membrane is ruptured or disintegrated, thus, in necrotic cells. Another way is to measure the activity of the solely intracellular LDH, which is only released upon membrane disintegration and subsequently accumulates in the cell supernatant.

Flow cytometry analysis showed that both bone marrow derived PMN populations had a very low necrosis rate not exceeding 10 – 15% of all leucocytes analysed (**Figure 15 a, b**). Surprisingly, Mtb infection only slightly elevated the overall necrosis rate. Nevertheless, a majority of 70 – 80% of necrotic $Ly6G^+$ cells were infected with Mtb, indicating an

association between infection and necrosis (**Figure 15 d, f**). Necrosis rates of blood derived PMN increased over time and were also clearly infection induced (**Figure 15 c, f**).

LDH analysis showed a different picture. In unmatured bone marrow derived PMN the difference between infected and uninfected cells was small. In contrast, in G-CSF matured bone marrow PMN infection induced a significant increase in necrosis at 4 and 6 hpi, while uninfected PMN hardly showed any necrosis (**Figure 15 g, h**). Therefore, uninfected, unmatured bone marrow derived PMN had a high background necrosis, independent of the infection rate. In blood derived neutrophils, necrosis was also increased upon infection though not in a statistically significant manner (**Figure 15 i**).

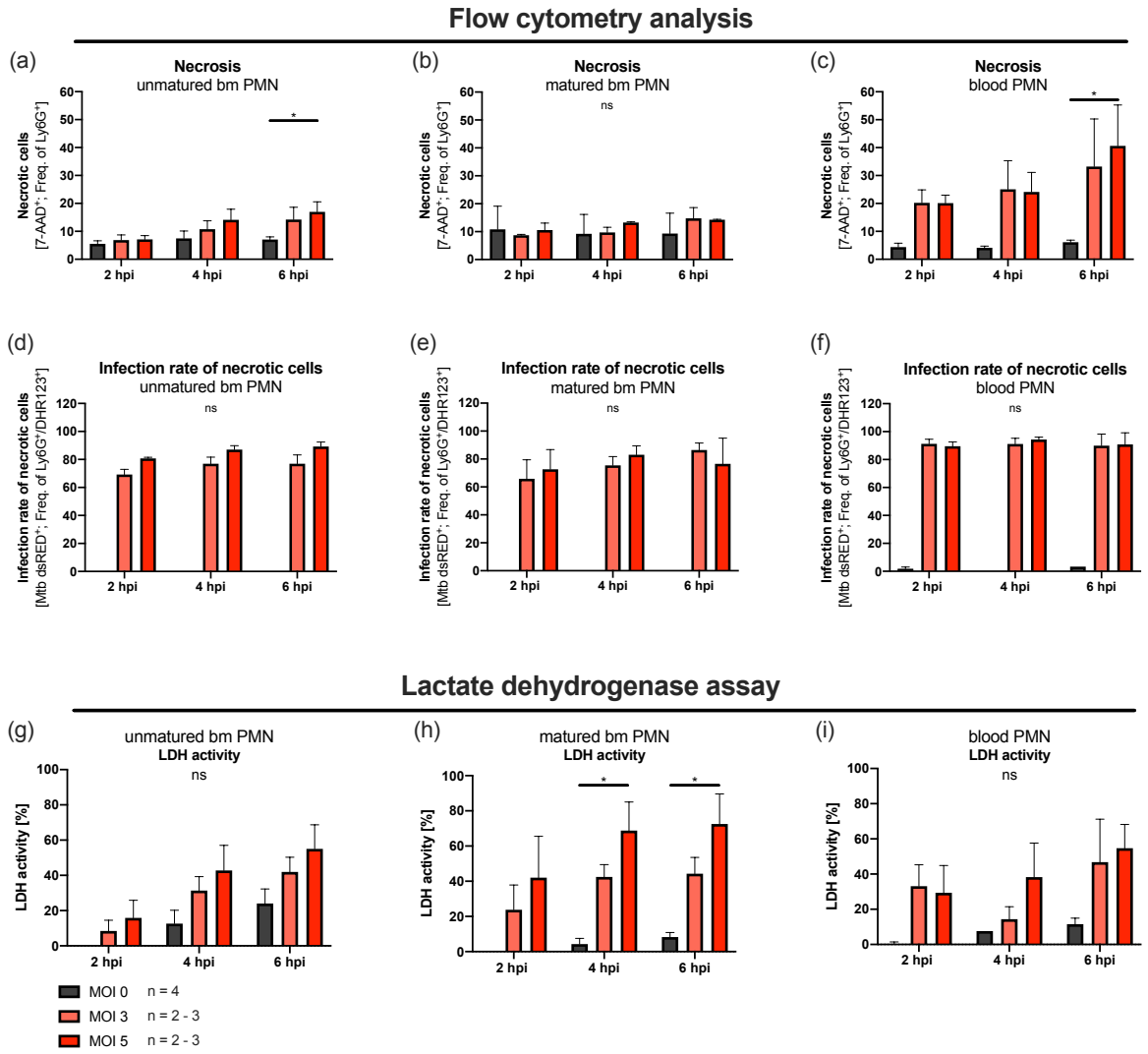

Figure 15 Necrosis rates of distinct murine PMN populations upon H37Rv dsRed infection *in vitro*. PMN were isolated from the blood (blood PMN), the bone marrow (unmatured bm PMN) or from bone marrow that was cultivated for 48h in G-CSF containing medium (matured bm PMN), infected with a MOI 3 or 5 of H37Rv dsRed, incubated for 2, 4 and 6 h, stained for flow cytometry or used for supernatant LDH activity assays. Necrosis (7-AAD$^+$) was analysed

as frequency of Ly6G$^+$ cells in unmatured (a), G-CSF matured bone marrow (b) and blood derived PMN (c). Further, necrosis was analysed regarding their association with Mtb dsRed$^+$ (Mtb dsRed$^+$; Frequency of Ly6G$^+$/7-AAD$^+$) (d - f). Quantification of extracellular LDH activity was performed from supernatants (g – i). Depicted are two to four independent experiments. Error bars indicate SEM, 2-Way ANOVA with Tukey's range. *p ≤ 0,05; **p ≤ 0,01; ***p ≤ 0,001.

For a deeper analysis of the flow cytometry data, unresponsive, DHR123$^-$/7-AAD$^-$ cells were analysed further (**Figure 16**). The majority of 80 – 90% of unmatured bone marrow PMN hardly showed any effector functions upon infection (**Figure 16 a**). In G-CSF matured bone marrow and blood PMN the number of unresponsive cells was significantly reduced upon Mtb infection, while uninfected samples maintained a high percentage of unresponsive cells (**Figure 16 b, c**). In general, only around 50% of unresponsive cells were Mtb dsRed$^+$, which is than for example necrotic 7-AAD$^+$ (**Figure 15 d - f**) or ROS producing DHR123$^+$ cell populations (**Figure 14 d - f**). Again, unmatured bone marrow derived PMN had a lower association with Mtb dsRed than matured bone marrow or blood derived PMN (**Figure 16 d - f**).

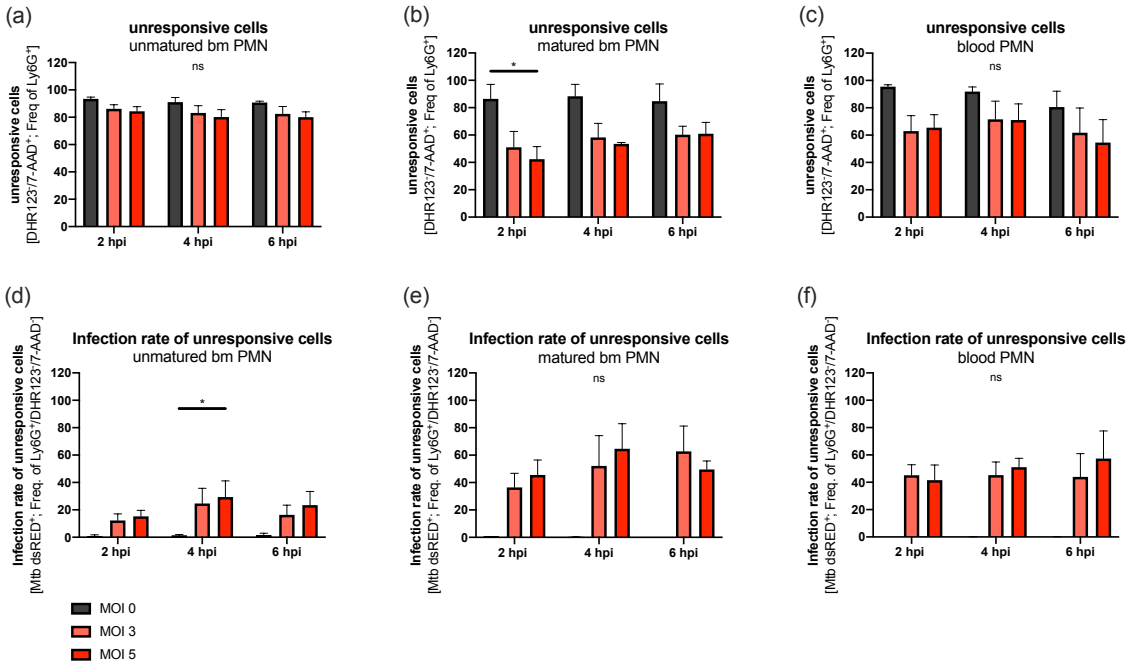

Figure 16 Proportion of unresponsive cells of distinct murine PMN populations upon H37Rv dsRed infection *in vitro*. PMN were isolated from the blood (blood PMN), the bone marrow (unmatured bm PMN) or from matured bone marrow cells that were cultivated for 48h in G-CSF containing medium (matured bm PMN), infected with a MOI 3 or 5 of H37Rv dsRed,

incubated for 2, 4 and 6 h, stained for flow cytometry analysis. The proportion of unresponsive ($DHR123^-/7\text{-}AAD^-$) cells was analysed as frequency of $Ly6G^+$ cells in unmatured (a), G-CSF matured bone marrow (b) and blood derived PMN (c). Further, necrosis was analysed regarding their association with Mtb $dsRed^+$ (Mtb $dsRed^+$; Frequency of $Ly6G^+/DHR123^-/7\text{-}AAD^-$) (d - f). Depicted are two to four independent experiments. Error bars indicate SEM, 2-Way ANOVA with Tukey's range. *$p \leq 0,05$; **$p \leq 0,01$; ***$p \leq 0,001$.

7.2.5 Evaluation of different murine PMN population in an *in vitro* infection assay

To evaluate the different PMN populations, the data was rearranged for direct comparison of phagocytosis and ROS production at 2 hpi and necrosis at 6 hpi. As already described, G-CSF matured bone marrow and blood derived PMN 60 – 70% were associated with Mtb at 2 hpi, while only 20 – 25% of unmatured bone marrow derived PMN were infected (**Figure 17 a**). In matured bone marrow PMN, the oxidative burst was highest and significantly elevated at 2 hpi (**Figure 17 b**). Necrosis measurement at 6 hpi varied between the two assays that were used. Flow cytometry analysis revealed a significantly increased necrosis of 20% in blood derived PMN, compared to 5 – 7% necrosis in unmatured bone marrow PMN (**Figure 17 c**). Analysing necrotic cell death via LDH release, matured bone marrow PMN showed the highest necrosis rate with around 70%. Around 55% of the blood derived PMN and unmatured bone marrow PMN were necrotic. The necrosis rate was not significantly different comparing the different populations infected with different MOI. (**Figure 17 d**).

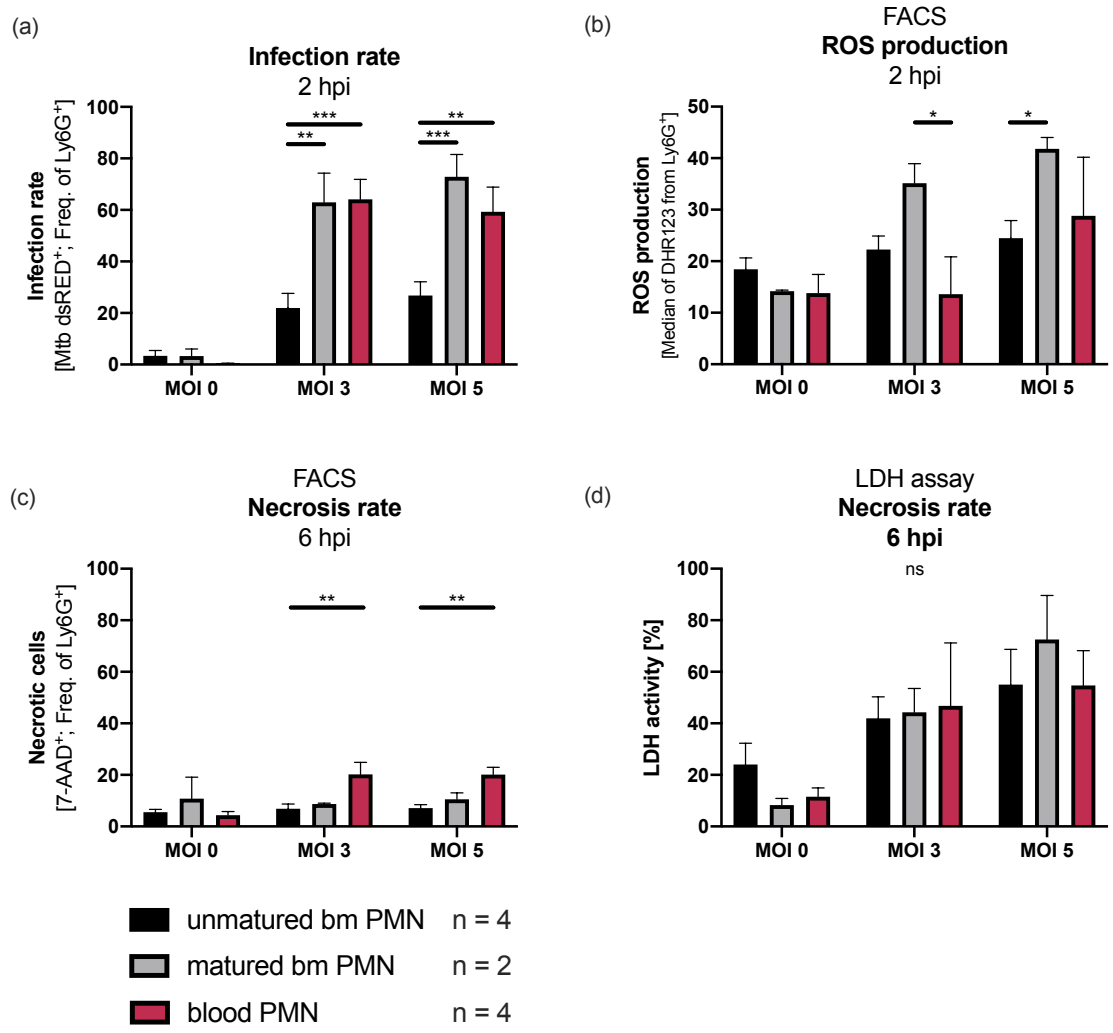

Figure 17 Direct comparison of different murine PMN populations. PMN were isolated from the blood (blood PMN), the bone marrow (unmatured bm PMN) or from bone marrow that was cultivated for 48h in G-CSF containing medium (matured bm PMN), infected with a MOI 3 or 5 of H37Rv dsRed, incubated for 2, 4 and 6 h, stained for flow cytometry analysis or used for supernatant LDH activity assays. Phagocytosis rates (Mtb DsRed$^+$) were analysed as frequency of Ly6G$^+$ PMN using flow cytometry at 2 hpi (a). ROS production (DHR123$^+$, Frequency of Ly6G$^+$) of different PMN populations was compared using flow cytometry at 2 hpi (b). Necrosis (7-AAD$^+$, Frequency of Ly6G$^+$) of different PMN populations was compared using flow cytometry (c) and analysed measuring LDH activity (d) at 6 hpi. Depicted are two to four independent experiments. Error bars indicate SEM, 2-Way ANOVA with Tukey's range. *p ≤ 0,05; **p ≤ 0,01; ***p ≤ 0,001.

Maturation of bone marrow increased the main antibacterial responses of PMN, which are phagocytosis and ROS production, as well as the subsequent necrotic cell death. Blood derived PMN were comparable in phagocytosis and necrosis, but showed a reduced ROS production compared to matured bone marrow PMN. However, this cell population

displayed vast variations between different experiments, indicating a more unpredictable quality of individual isolates. Additionally, due to the small blood volume of mice, the amount of isolated blood PMN is relatively low with only 1-2x10^6 recovered PMN per mouse. To acquire larger numbers of cells, several mice would be required to be sacrificed. In contrast, bone marrow cells can be harvested in great numbers, resulting in approximately 1x10^7 PMN collected per mouse. Thus, in following experiments the effect of MPO release, activity and inhibition was only analysed in unmatured and matured bone marrow derived PMN.

7.3 MPO inhibition in murine PMN *in vitro*

7.3.1 MPO protein release of unmatured and G-CSF matured bone marrow PMN

MPO concentration was determined by ELISA at 2 hpi in supernatants and cell pellets of unmatured and matured bone marrow derived PMN after infection with Mtb H37Rv to further compare these two murine PMN populations. Further, the effect of MPO inhibition using ABAH and AZD5904 was evaluated. Total amounts of MPO were comparable between unmatured (**Figure 18 a**) and G-CSF matured bone marrow PMN (**Figure 18 b**), but slightly higher after maturation with G-CSF. Infection increased the total amount of MPO protein in both PMN populations, but not in a significant manner. This was mainly due to an increased release of MPO into the supernatant upon infection while the amount of MPO in the cell pellet remained stable between the populations and infection rates. In unmatured bone marrow derived PMN treatment with MPO inhibitors did not have any effect on the total amount of MPO protein, where the amount of released and intracellular MPO remained stable. However, in G-CSF matured PMN cell culture, MPO inhibitor treatment increased the amount of releases MPO into the supernatants, while the untreated cell culture hardly showed any MPO release (**Figure 18 b**).

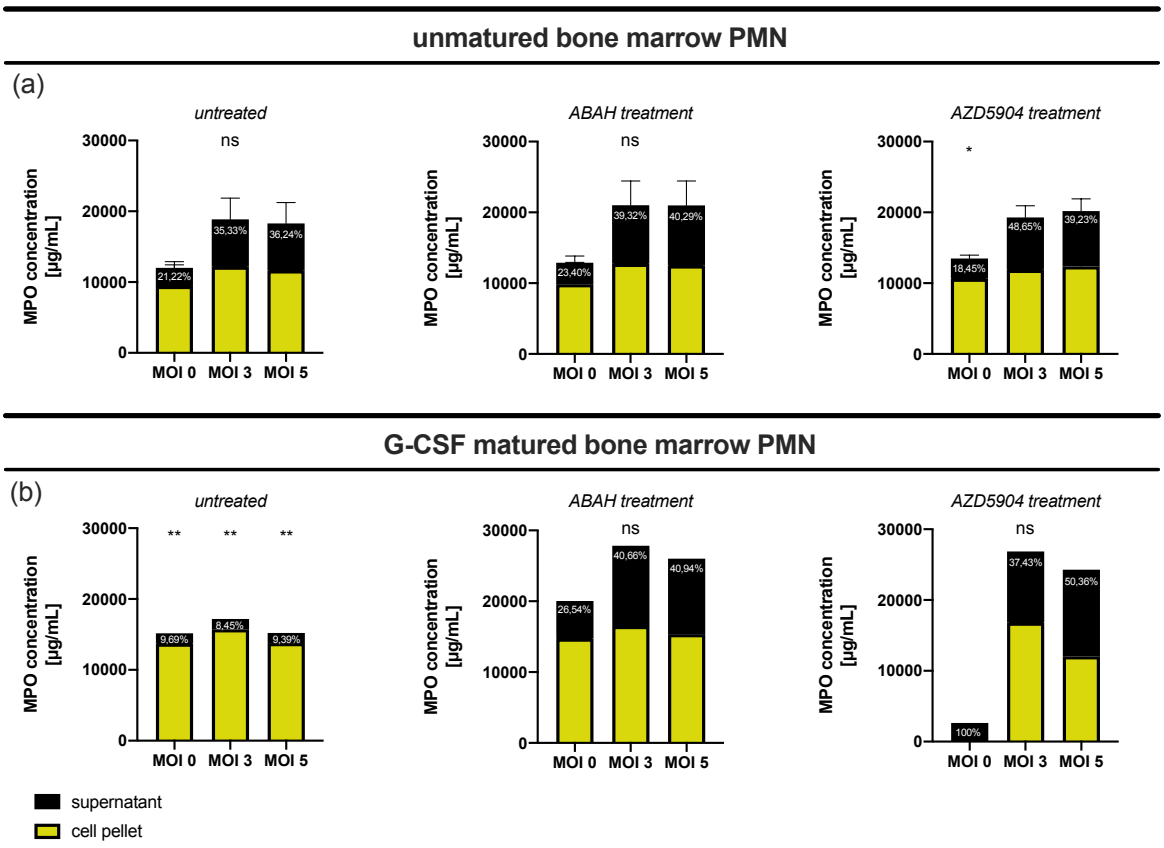

Figure 18 MPO concentration in murine bone marrow PMN populations at 2 hpi. PMN were isolated from the bone marrow (unmatured bm PMN) or from matured bone marrow cells that were cultivated for 48h in G-CSF containing medium (matured bm PMN), infected with an MOI 3 or 5 of H37Rv dsRed, treated with 500 µM ABAH or 300 µM AZD5904 and incubated for 2 h. MPO concentration was analysed in cell pellets (yellow) and supernatants (black) using an MPO ELISA. Percentages represent the amount of released MPO, calculated from the total amount measured in the cell culture. Depicted are one (matured bone marrow PMN) to two (unmatured bone marrow PMN) independent experiments, comprising 2 - 4 technical replicates. Error bars indicate SEM, 2-Way ANOVA with Tukey's range is comparing MPO protein concentration in supernatant to cell pellet. *p ≤ 0,05; **p ≤ 0,01; ***p ≤ 0,001.

7.3.2 Effect of MPO inhibition on MPO protein activity

Enzyme activity of MPO was analysed in the cell pellets and supernatants utilizing 3,3',5,5'-tetramethyl-benzidine (TMB), which acts as a chromogenic substrate for MPO. Kinetic measurement allowed the calculation of MPO activity as µmol/min/mL.

Infection significantly increased the activity of extracellular MPO into the supernatant of untreated, unmatured (**Figure 19 a**) and G-CSF matured bone marrow PMN (**Figure 19 b**) at 2 hpi. In both populations, the extracellular MPO activity remained stable until 6 hpi, while intracellular MPO activity decreased between 2 and 6 hpi, to an almost undetectable

level. MPO inhibitor treatment using ABAH almost completely abolished MPO activity in the supernatants, independent of the maturation status of the cells. Surprisingly, no MPO inhibition could be detected upon AZD5904 treatment, neither in PMN supernatants, nor in the cell pellet fraction. Interestingly, ABAH treatment did not reduce the MPO activity in the cell pellet and therefore should be considered membrane impermeable. Comparison of unmatured and matured PMN populations showed no significant differences in MPO activity, indicating that maturation did neither influence MPO expression nor activation.

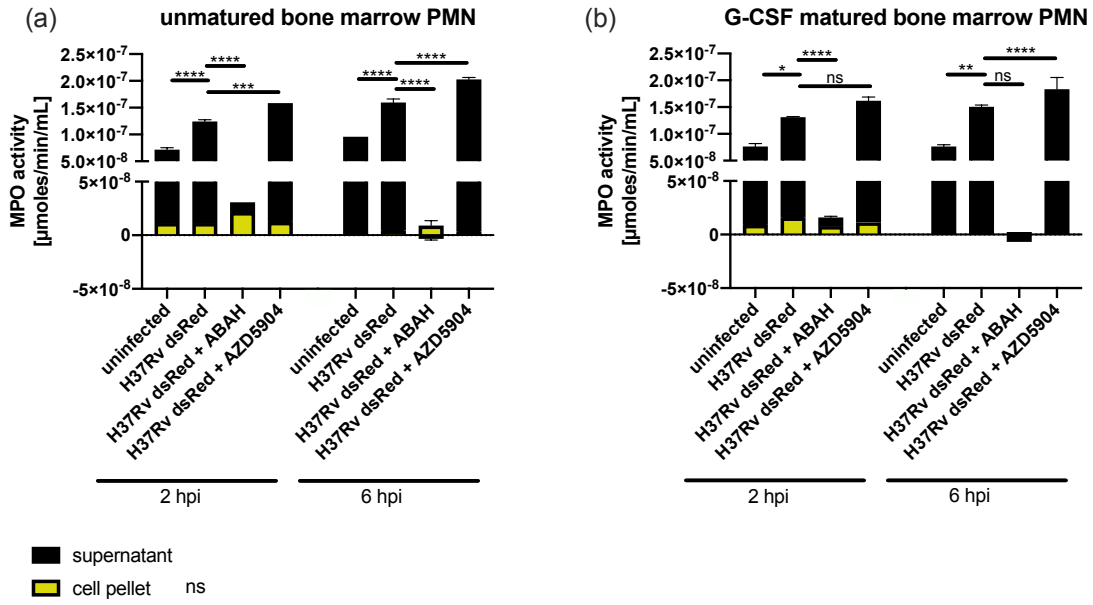

Figure 19 MPO activity upon ABAH and AZD5904 treatment in murine bone marrow derived PMN *in vitro*. PMN were isolated from the bone marrow (unmatured bm PMN) or from bone marrow that was cultivated for 48h in G-CSF containing medium (matured bm PMN), infected with a MOI 3 of H37Rv dsRed, treated with 500 µM ABAH or 300 µM AZD5904 and incubated for 2 and 6 h. MPO activity was analysed in the supernatants and cell pellets of unmatured (a) and G-CSF matured bone marrow PMN (b) using a TMB MPO activity assay. Depicted are two independent experiments. Statistics were calculated using an ordinary 2-Way ANOVA with Tukey's range test. Depicted are only the results for supernatant comparison. In the cell pellets, no significant differences (ns) were detected. *p ≤ 0,05; **p ≤ 0,01; ***p ≤ 0,001.

7.3.3 The effect of MPO inhibition on ROS production in G-CSF matured bone marrow derived PMN *in vitro*

Since unmatured bone marrow PMN showed impaired phagocytosis and ROS production, we only used G-CSF matured bone marrow PMN for further studies. We wanted to

investigate the effect of MPO inhibition on downstream ROS production. The MPO inhibitor ABAH had almost no effect on ROS production in murine PMN. Only when the cells were infected with a MOI 5, ABAH slightly reduced ROS production, however not in a significant manner (**Figure 20 c**). This is not surprising, regarding the earlier observed exclusively extracellular activity of ABAH (**Figure 19**), which was shown with the MPO activity assay and considering the fact, that ROS detection was performed intracellularly. AZD5904 had no effect on intracellular ROS production at all, independent of different MOI (**Figure 20 b, c**).

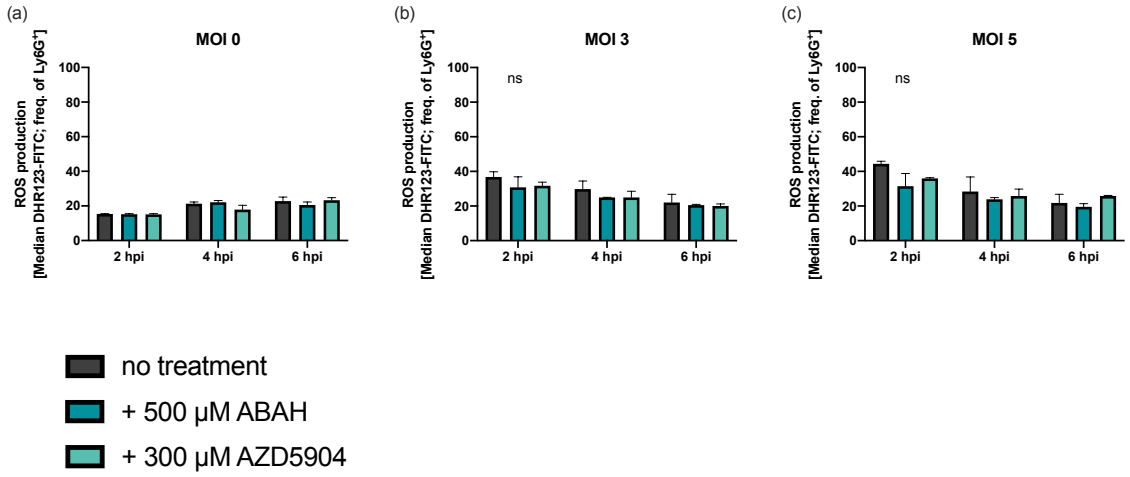

Figure 20 Effect of MPO inhibition on ROS production *in vitro*. PMN were isolated from bone marrow that was cultivated for 48h in G-CSF containing medium, left uninfected (a), were infected with a MOI 3 (b) or 5 (c) of H37Rv dsRed, treated with 500 µM ABAH or 300 µM AZD5904, incubated for 2, 4 and 6 h and stained for flow cytometry analysis. Production of intracellular ROS was as $Ly6G^+/DHR123^+$ cells. Depicted are two independent experiments. Statistics were calculated using an ordinary 2-Way ANOVA with Tukey's range test. *p ≤ 0,05; **p ≤ 0,01; ***p ≤ 0,001.

7.3.4 The effect of MPO inhibition on necrosis in G-CSF matured bone marrow derived PMN *in vitro*

Based on previous findings in human PMN [17], we hypothesized that MPO inhibition would result in a reduced necrotic cell death. Therefore, the effect of ABAH and AZD5904 on the necrotic cell death matured bone marrow derived PMN was analysed *in vitro* using LDH measurement.

LDH release detection showed high and distinct necrosis rates upon infection, as previously observed (**Figure 15**). However, no reduction of necrosis was detected in Mtb infected, MPO inhibitor treated cells (**Figure 21**).

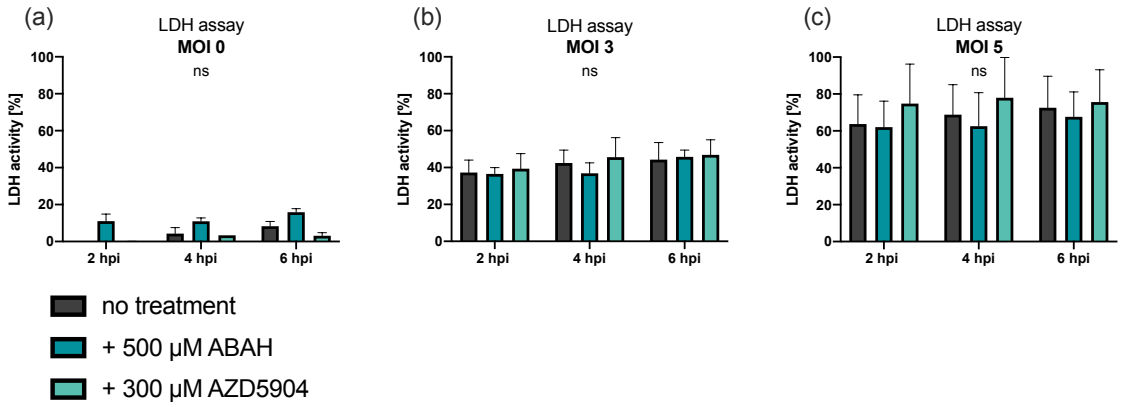

Figure 21 Effect of MPO inhibition on necrosis in matured bone marrow PMN *in vitro* upon Mtb infection. PMN were isolated from matured bone marrow that was cultivated for 48h in G-CSF containing medium, left uninfected (a), were infected with a MOI 3 (b) or 5 (c) of H37Rv dsRed, treated with 500 µM ABAH or 300 µM AZD5904, incubated for 2, 4 and 6 h. Necrosis was measured using the activity of extracellular LDH in the supernatants. Depicted are two independent experiments. Statistics were calculated using an ordinary 2-Way ANOVA with Tukey's range test. *$p \leq 0{,}05$; **$p \leq 0{,}01$; ***$p \leq 0{,}001$.

Taken together, the data show that matured bone marrow derived PMN exhibited all major effector functions like phagocytosis, infection induced ROS production, necrosis and MPO release. ABAH was shown to effectively reduce extracellular MPO activity. However, this had no secondary effect on the cells as necrosis and ROS production were not reduced in comparison to infected, untreated cells.

7.4 In vivo effect of MPO inhibition in Mtb infected mice

Exacerbated inflammation and tissue destruction are hallmarks of TB pathogenesis. The Mtb induced, necrotic cell death of PMN was identified as one important factor of these processes [107], [132]. Studies on murine demyelinating diseases revealed beneficial, systemic effects of MPO inhibition [76]. Thus, despite the failure of MPO inhibition to limit necrosis of Mtb infected PMN in vitro, efficient inhibition of extracellular MPO may still have an effect on other inflammatory innate cells within the granuloma. Therefore, we evaluated how pharmacological inhibition of MPO can affect experimental TB pathogenesis in Mtb infected C3HeB/FeJ mice.

7.4.1 Intraperitoneal MPO treatment of H37Rv infected C3HeB/FeJ mice

In a first experimental set up C3HeB/FeJ mice received a high infection dose of 100 – 150 mycobacteria, determined at day 1 post infection (p.i.). The animals were treated for a period of 9 or 10 days, starting at day 25 and 32 p.i., respectively. Using a similar infection dose, Driver *et al.* showed, that C3HeB/FeJ mice start to develop necrotic lesions between day 30 and 40 p.i., which are initially composed of macrophages and lymphocytes, accompanied by a rapid accumulation of granulocytes in the alveolar space [115]. Therefore, the treatment start was chosen to coincide with the onset of necrosis development, as the aim of this study was to evaluate the potential of MPO inhibition during acute TB.

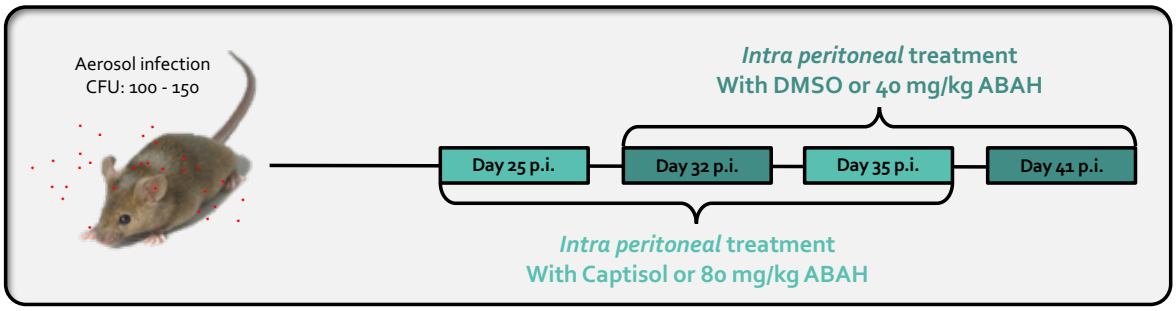

Figure 22 Experimental set-up of *intraperitoneal* treatment. C3HeB/FeJ mice were infected with an infection dose of 100 – 150 Mtb H37Rv via aerosol inhalation, determined at day 1 p.i. In a first set-up mice were treated i.p. with 40 mg/kg ABAH dissolved in DMSO. Treatment was started at day 32 p.i. and continued for 9 days, twice a day (dark turquoise, late treatment). In a second set-up mice were treated i.p. with 80 mg/kg ABAH dissolved in 20% Captisol®. Treatment was started at day 25 p.i. and continued for 10 days, twice a day (light turquoise, early treatment).

In a first treatment schedule, treatment was administered twice a day *intraperitoneally* (i.p.), at concentrations of 40 mg/kg ABAH, dissolved in DMSO, starting at day 32 p.i. (late treatment, dark turquoise). The same concentration of DMSO was used as a vehicle for a control group. In a second treatment schedule, the concentration of ABAH was doubled to 80 mg/kg, dissolved in 20% Captisol® solution and the start of the treatment was preponed to day 25 p.i. (early treatment, light turquoise) (**Figure 22**).

Animals from both treatment schedules had a similar health score at the start of the treatment, suggesting they were in a comparable state of the infection. The mean health score for the MPO inhibitor early treated groups rose from 1 at day 25 p.i. to 1,25 at day 35 p.i. Mice that received the treatment later showed a comparable increase with a health score mean of 1,35 at day 35 p.i. Until the end of the late treatment, the score elevated to 2, due to the prolonged infection period (**Figure 23 a**).

During the treatment period, early treated animals showed a mean weight loss of 4,31% while animals receiving the late treatment lost in average 5,01% of their weight (**Figure 23 b**). Direct comparison of the weight loss of the two vehicle treated groups showed no major differences However, Captisol® treated animals showed reduced weight loss after 9-day period treatment (**Figure 23 c**).

Interestingly, the bacterial burden of lung and spleen, analysed via the formation of CFU showed no differences between day 35 p.i. and day 41 p.i. respectively (**Figure 23 d, e**).

Thus, regardless of the time point during infection when treatment started, the vehicle used or the concentration of the MPO inhibitor, intraperitoneal administration of ABAH did not affect the infection outcome of the infection, like weight loss, health score or bacterial burden of lung and spleen.

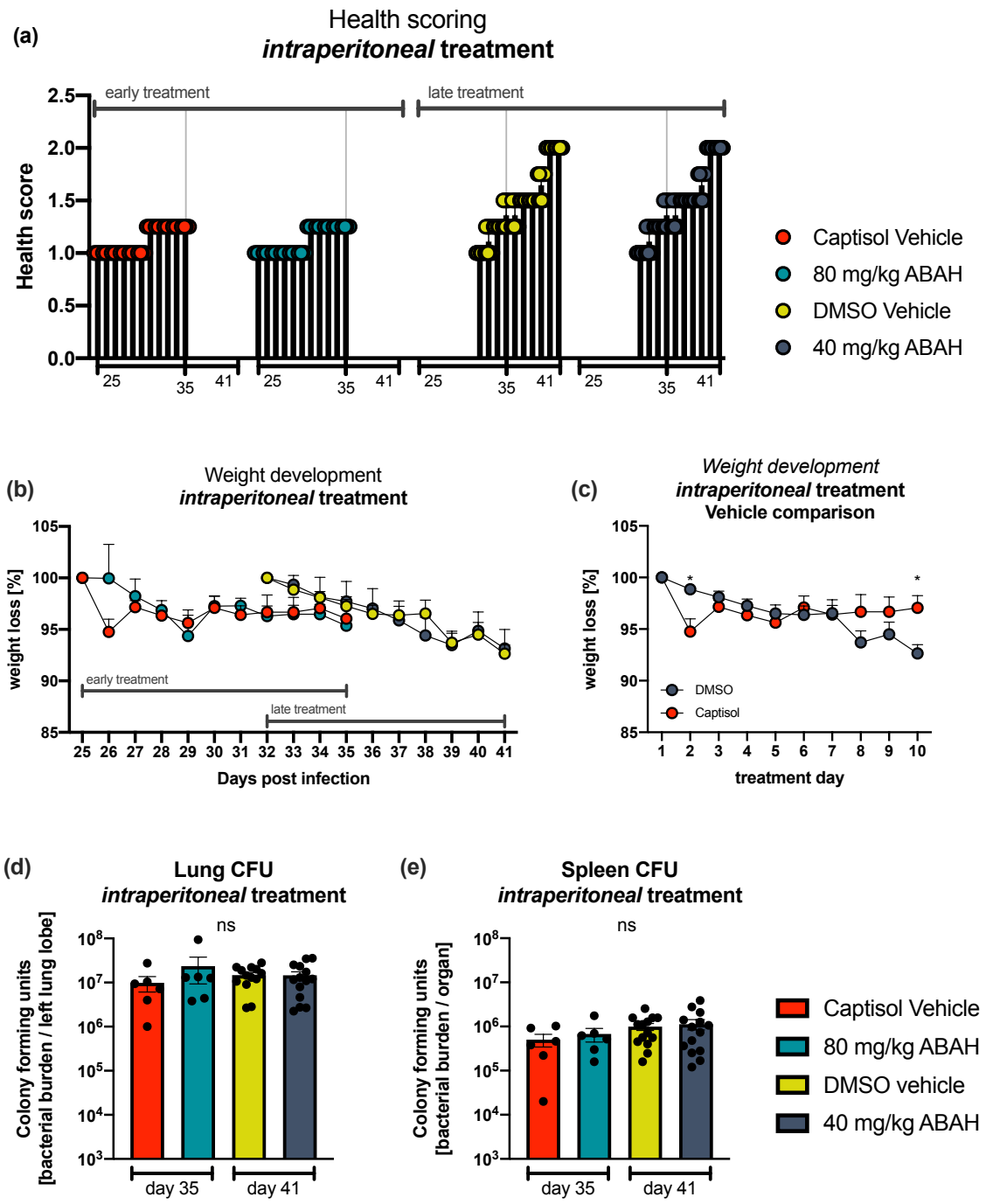

Figure 23 Weight loss, health score and lung bacterial burden of different *intraperitoneal* MPO inhibitor treatment schedules of Mtb infected C3HeB/FeJ mice. C3HeB/FeJ mice were infected with a dose of 100 – 150 Mtb H37Rv via aerosol inhalation, treated for a 9- or 10-day period with 80 mg/kg (early treatment) or 40 mg/kg (late treatment) ABAH and sacrificed at day 35 and day 41 p.i., respectively. Health score (a), weight development (b, c) and mycobacterial growth in lung (d) and spleen (e) were analysed. Health and weight scoring were done at each day of the treatment from day 25 to 35 p.i. (early treatment) or day 32 to 41 p.i. (late treatment) (a - c). Mycobacterial growth was determined at the end of the treatment period at day 35 and 41 p.i. (d, f), respectively. Depicted are one (early treatment) to two (late treatment) independent experiments. Error bars indicate SEM, 2-Way ANOVA with Tukey's range test. *p ≤0,05; **p ≤ 0,01; ***p ≤0,001.

7.4.2 Histopathological analysis of lungs from *intra peritoneal* MPO inhibitor treated, H37Rv infected C3HeB/FeJ mice

In order to analyse the histopathological alterations in infected mouse lungs, the organs were embedded in paraffin. Lung sections were then stained with different protocols. From each mouse, the same lung lobe was used for histopathological analysis, however, the level and angle of each analysed section was different due to the handling procedure. Shown are mice from MPO inhibitor treated mice and their vehicle control group.

The Ziehl-Neelsen (ZN) stain allowed an overview of the general granuloma development and inflammatory infiltrations (**Figure 24 a**, red circles). There was a vast variation in the granuloma development between individual mice, even within the same treatment group. While some mice showed extended granulomatous lesions, in the analysed organ parts other showed only small ones. The most striking difference was the increased number of infiltrations in the late treatment group. However, no quantitative data could be drawn from that observation, due to the differences between the individual analysed sections. Further, no distinct granuloma formation was observed as described by Driver *et al.* (2012) or Irvin *et al.* (2015), which made it difficult to confine, specify and evaluate infected areas. Detailed analysis of ZN staining did not reveal major differences, neither between the treatment schedules nor the different groups. Some mice from the early treatment groups had higher numbers of bacteria in the lung. However, this observation was not confirmed by the CFU data. Nevertheless, all groups showed strong clustering of the acid-fast mycobacteria at granulomatous lesions, often enclosed in macrophages (**Figure 24 b**, yellow arrows). Further, no differences in MPO expression were observed in the lungs of infected mice. Of note, the administration of ABAH did not reduce the expression of MPO (**Figure 24 c**). Isotype control stains can be found in supplementary material **Figure 39**.

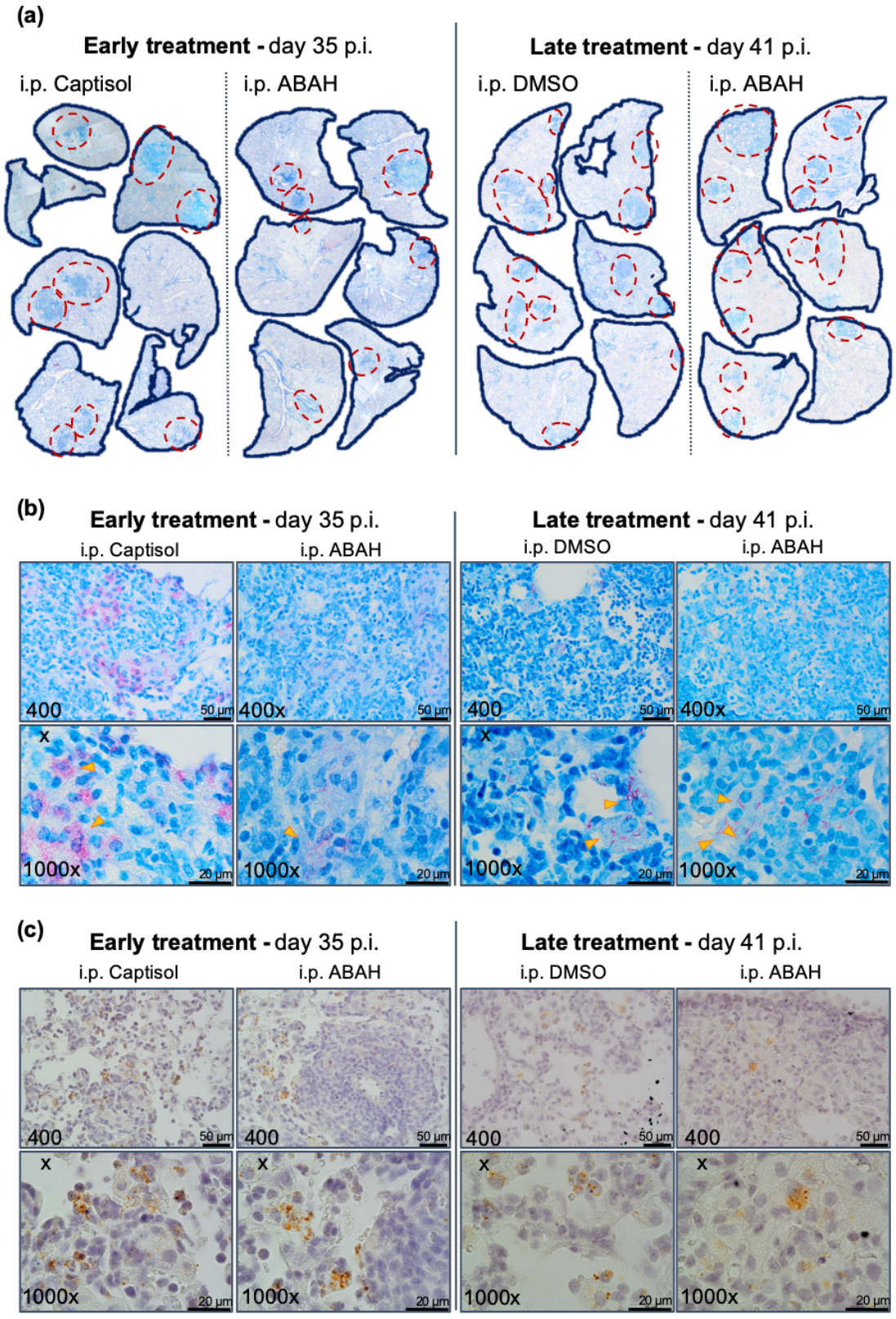

Figure 24 Histopathological and immunohistological analysis of MPO inhibitor treated C3HeB/FeJ mice. C3HeB/FeJ mice were infected with an infection dose of 100 – 150 Mtb H37Rv via aerosol inhalation, treated for a 9- or 10-day period with 80 (early treatment) or 40 mg/kg (late treatment) ABAH and sacrificed at day 35 and day 41 p.i., respectively. Lungs were removed and processed for histological analysis by Ziehl-Neelsen (ZN) stain and

immunostaining for MPO. ZN stained lung slides allowed an overview on granuloma development (a). Detail pictures of ZN staining, show clustering of bacteria (yellow arrows), often enclosed in macrophages (b). Detail pictures of MPO (red arrows) staining did not show any differences between the groups (c). Depicted are representative shots of each group.

7.4.3 *Per os* MPO inhibitor treatment of H37Rv infected C3HeB/FeJ mice

To evaluate another route of MPO inhibitor application, the animals were treated *per os* by oral gavage in a second experimental set-up. The animals were treated twice a day with either 80 mg/kg ABAH or 45 mg/kg AZD5904 dissolved in a 30% Captisol® solution (single treated). A second set of mice was used to study the combined effect of an antibiotic plus HDT treatment (co-treatment). In these groups the animals received the inhibitors in combination with a low dose (10 mg/kg) of the first-line antibiotic isoniazid (co-treated). The standard treatment of mice with INH is usually 25 mg/kg [133], [134]. The low-dose antibiotic treatment was chosen, to reduce the effects of the antibiotic induced reduction of the bacterial load and avoid thereby a masking of possible effects of the MPO inhibitors. As control groups Captisol® solution with or without INH was used (**Figure 25**).

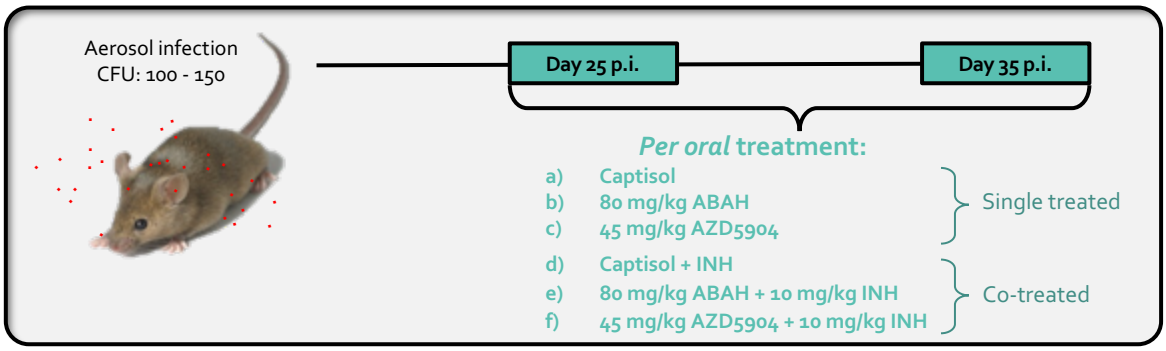

Figure 25 Experimental overview for *per os* treatment of mice. C3HeB/FeJ mice were infected with an infection dose of 100 – 150 Mtb H37Rv via aerosol inhalation, determined at day 1. Starting at day 25 p.i., *per os* treatment was administered twice a day to 6 different groups: a) 30% Captisol®, b) 80 mg/kg ABAH, c) 45 mg/kg AZD5904, d) 30% Captisol® + 10 mg/kg INH, e) 80 mg/kg ABAH + 10 mg/kg INH, f) 45 mg/kg AZD5904 + 10 mg/kg INH.

7.4.4 Weight and health scores of *per os* treated, H37Rv infected C3HeB/FeJ mice

AZD5904 single treated mice showed an increased weight loss compared to ABAH or vehicle treated mice, which became statistically significant during the last 4 days of treatment (**Figure 26 a**). In average, AZD5904 treated mice lost 14,04 % of their bodyweight

during the treatment period. In contrast, ABAH treated mice lost 6,87% while untreated mice lost 9,16% during that time period. In mice that were co-treated with INH, the significant weight loss difference between AZD5904 treated mice and other groups was absent and the weight loss was comparable between all groups (**Figure 26 b**), indicating the additional INH treatment abrogated the weight loss of AZD5904 treated mice. In detail, Captisol® plus INH treated animals lost 10,43% of their bodyweight during treatment, ABAH plus INH treated animals, 9,26%, and AZD5904 plus INH treated animals lost 11,71%. This was confirmed, when each single treated group was directly compared with their co-treated counter group, where no differences could be detected (**Figure 26 c**).

The health scores did not differ between the groups. Only AZD5904 mice showed a slight increase towards the end of the treatment. It rose from 1 at day 25 p.i. to 1,62 at day 35 p.i., while the other groups kept a score from 1,25 – 1,5 (**Figure 26 d**).

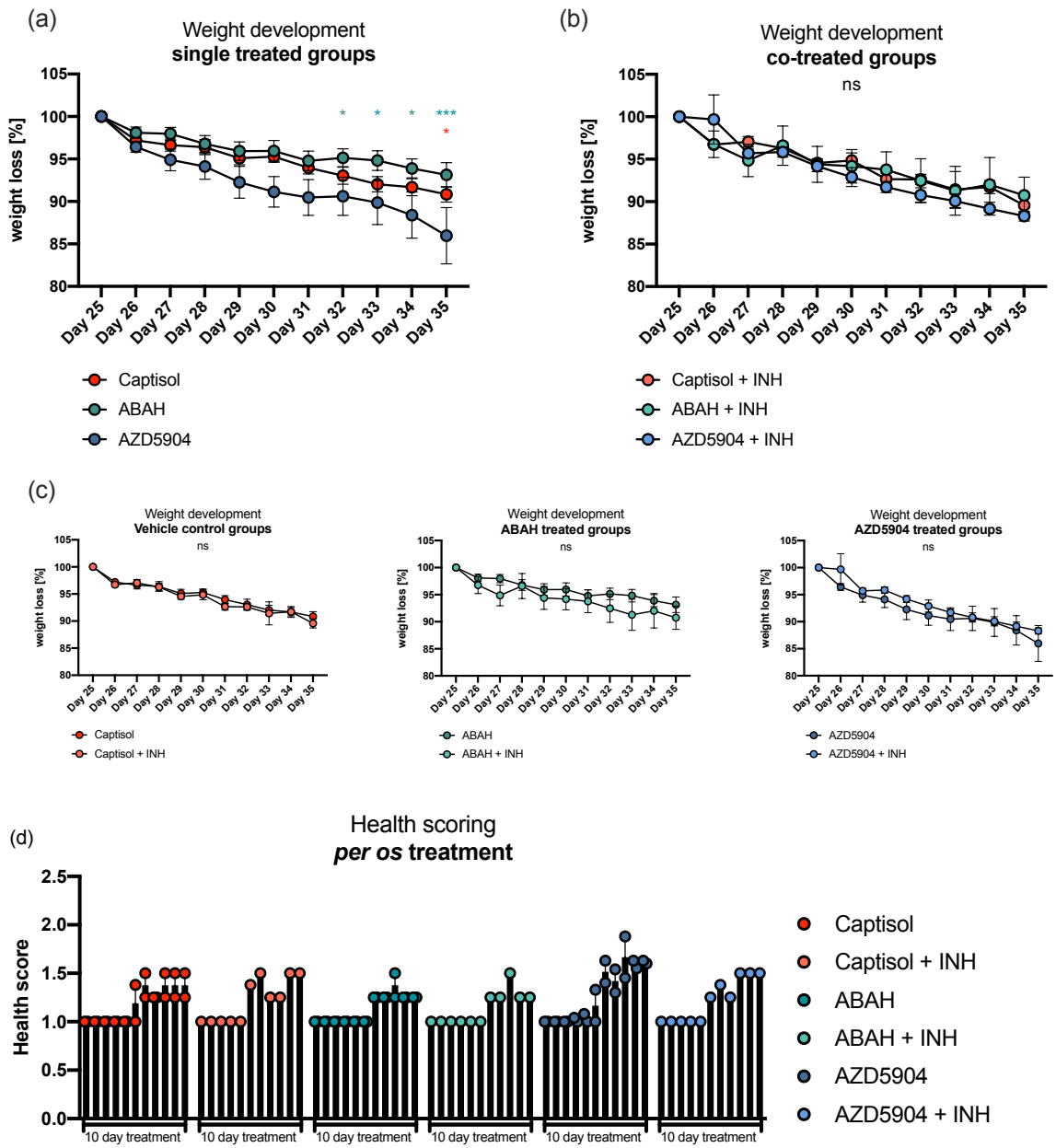

Figure 26 Weight and health scoring of *per os* treated, H37Rv infected C3HeB/FeJ mice. C3HeB/FeJ mice were infected with an infection dose of 100 – 150 Mtb H37Rv via aerosol inhalation, treated for a 10 day period with 80 mg/kg ABAH, 45 mg/kg AZD5904 (single treatment) or in combination with 10 mg/kg INH (co treatment) and sacrificed at day 36 p.i. Bodyweight (a – c) and health score (d) were monitored during the course of treatment. Health and weight scoring were done at each day of the treatment. Depicted are one (co treated) to two (single treatment) independent experiments. Error bars indicate SEM, 2-Way ANOVA with Tukey's range test. *p ≤ 0,05; **p ≤ 0,01; ***p ≤ 0,001

7.4.5 Macroscopic pathological alterations of lungs from *per os* MPO inhibitor treated, H37Rv infected C3HeB/FeJ mice

During dissection, the lung pathology was macroscopically visualized. Exemplary a photo of each treatment group is shown in **Figure 27**, which was taken before the lung was removed. In most lungs, granulomas and inflammatory infiltrates were visible (yellow arrows). Of note, AZD5904 single treated mice had well developed abscesses. Mice, that received additional INH treatment appeared to have lungs with less numbers of lesions.

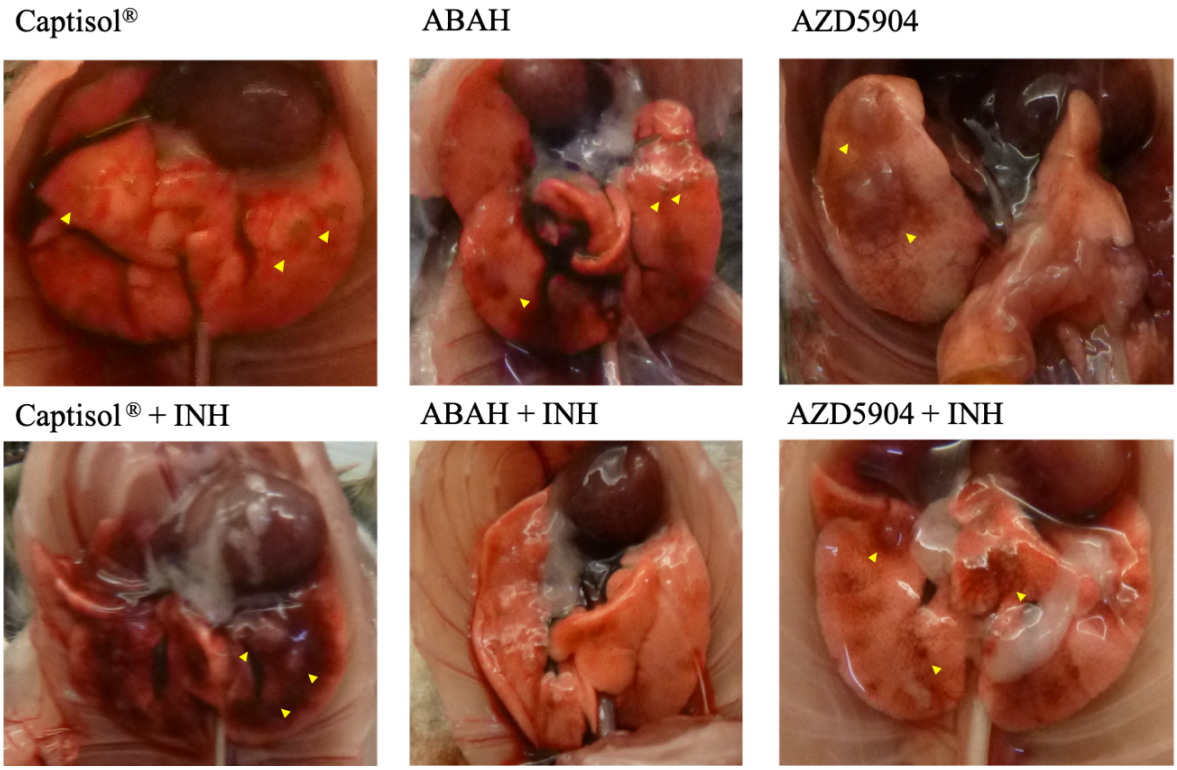

Figure 27 Macroscopic pathological changes in the lungs of H37Rv infected C3HeB/FeJ mice. C3HeB/FeJ mice were infected with an infection dose of 100 – 150 Mtb H37Rv via aerosol inhalation, treated for a 10 day period with 80 mg/kg ABAH, 45 mg/kg AZD5904 alone or in combination with 10 mg/kg INH and sacrificed at day 36 p.i. Pictures were taken before cardiac perfusion and organ removal. Yellow arrows indicate visible granulomatous areas in the lung of the mice. Depicted is one representative mouse from each group.

7.4.6 Histopathological analysis of lungs from *per os* MPO inhibitor treated, H37Rv infected C3HeB/FeJ mice

ZN staining was used to get a general overview about the granuloma development and cell infiltration. There were no significant differences in the numbers of visible granulomas.

Further, the infiltration showed great variations in their morphology, with some being very large and showing a classical granulomatous structure and other being merely some unstructured cellular infiltrations. Most importantly, this observation was made independent of the different treatments. No quantitative data could be drawn from the microscopic analysis, due to the earlier mentioned handling procedure. Detailed analysis of the granulomatous area showed clustering of bacteria across an inflamed area (yellow arrows, **Figure 28**). Some mycobacteria seem to be enclosed in cells, while other are free in in the tissue. However, no visible differences could be detected between the groups.

MPO staining showed a clear expression of MPO in lung tissue (red arrows) in all groups (**Figure 29**). There was no visible reduction of MPO expression upon MPO inhibitor treatment. Some Macrophages also stained positive for MPO. Isotype control stains can be found in supplementary material **Figure 39**.

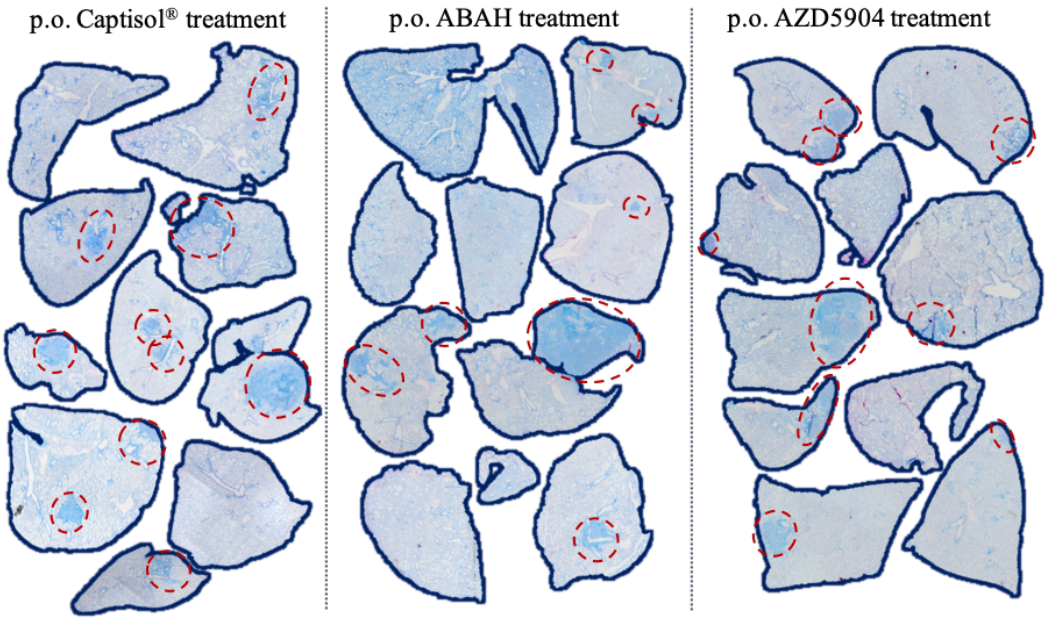

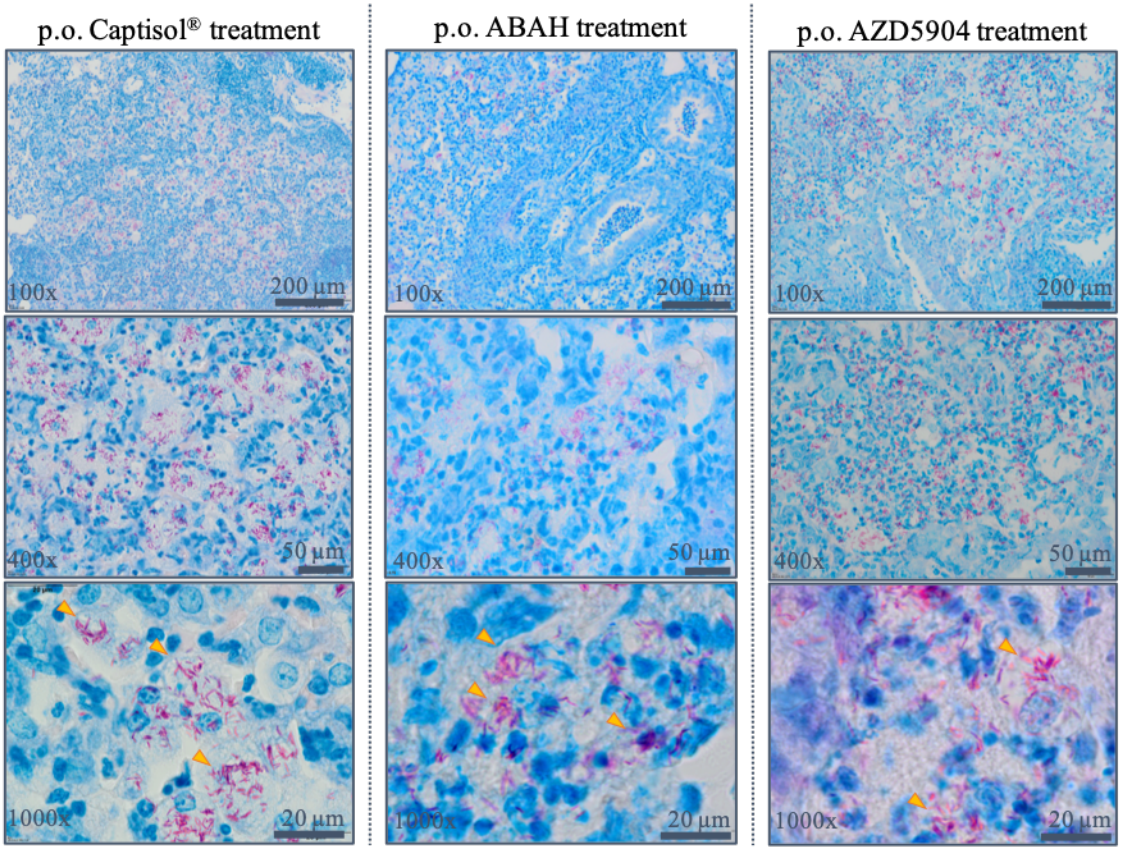

Figure 28 Histopathological analysis of lungs from H37Rv infected and *per os* treated C3HeB/FeJ mice. C3HeB/FeJ mice were infected with an infection dose of 100 – 150 Mtb H37Rv via aerosol inhalation, treated for a 10 day period with 80 mg/kg ABAH, 45 mg/kg AZD5904 alone or in combination with 10 mg/kg INH and sacrificed at day 36 p.i. Organs were removed, embedded in paraffin and stained with ZN protocol. Overview pictures were taken to analyze granuloma formation. Detailed pictures allow mycobacterial detection (yellow arrows). Depicted are representative lung slices individual mice.

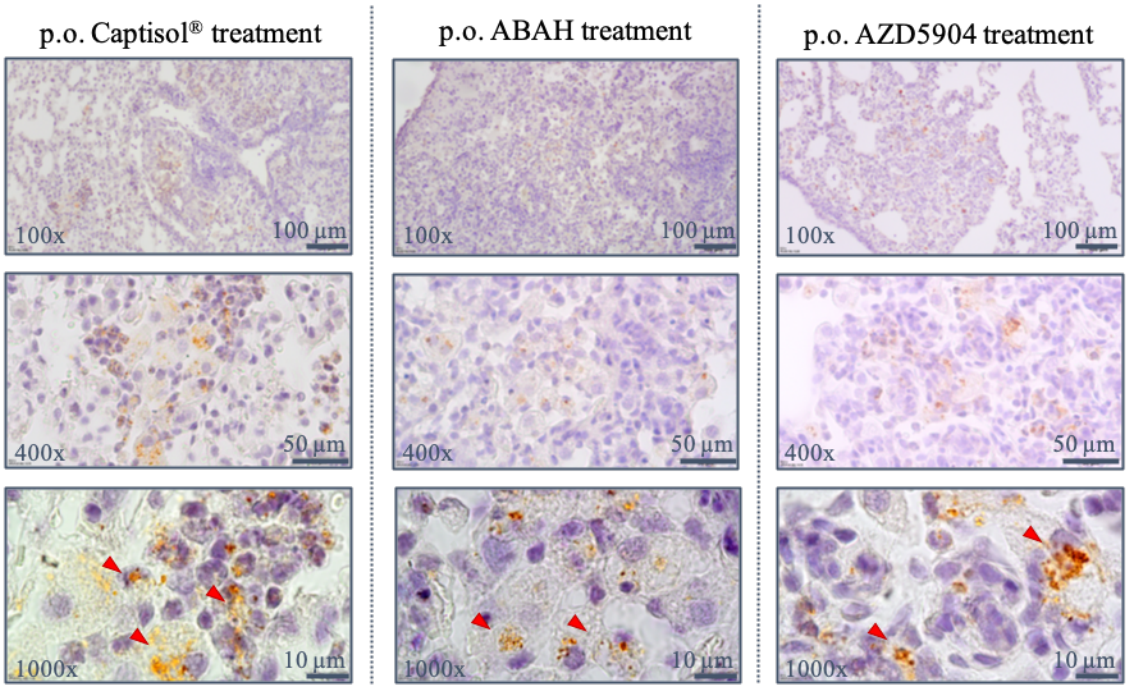

Figure 29 Immunohistological analysis of H37Rv infected, *per os* treated C3HeB/FeJ mice. C3HeB/FeJ mice were infected with an infection dose of 100 – 150 Mtb H37Rv via aerosol inhalation, treated for a 10-day period with 80 mg/kg ABAH, 45 mg/kg AZD5904 alone or in combination with 10 mg/kg INH and sacrificed at day 36 p.i. Organs were removed, embedded in paraffin and immunostained with anti-MPO antibody. Pictures show MPO expression (red arrows). Depicted are representative lung slices individual mice.

7.4.7 Mycobacterial burden of MPO inhibitor and MPO inhibitor plus IHN treated mice

Bacterial burden was determined by analysing the CFU in lung, spleen and liver of Mtb infected mice under the different treatment regiments. The highest burden was found in the lung of Captisol® treated mice, reaching 10^8 bacteria in the left lung lobe at day 35 p.i. This was a slight increase compared to 10^6 to 10^7 in the pre treatment group at day 25 p.i. Single MPO inhibitor treatment only slightly reduced the bacterial burden. INH single treatment however, did reduce the CFU to 10^5 at day 35 p.i., but as seen for the single treated groups, no further reduction of the bacterial burden was observed when MPO inhibitors were additionally administered to INH treatment (**Figure 30 a**). The same overall results were found in the spleen (**Figure 30 b**). In the liver the bacterial burden did not exceed the number of bacteria found at day 25 p.i., reaching 10^4 bacteria per organ (**Figure 30 b, c**).

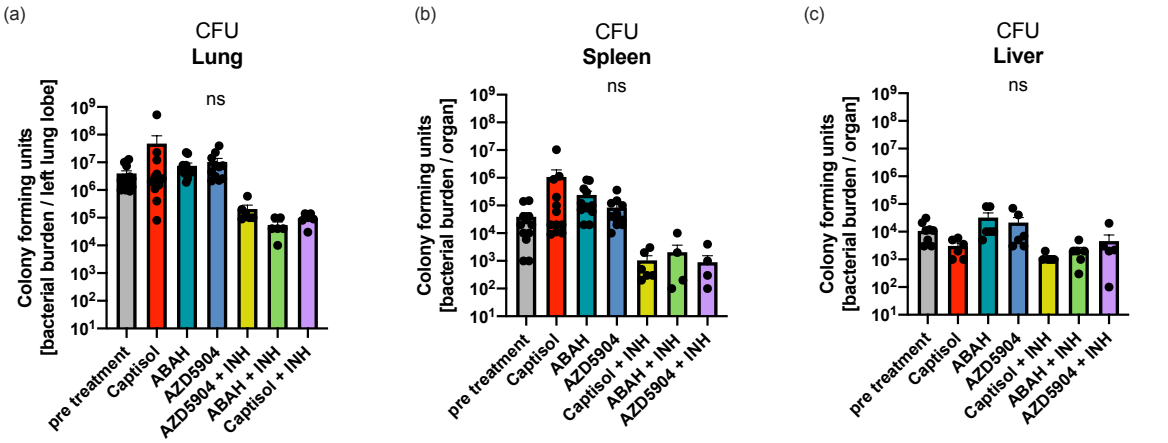

Figure 30 Organ CFU in H37Rv infected C3HeB/FeJ mice upon MPO inhibitor and HDT treatment. C3HeB/FeJ mice were infected with an infection dose of 100 – 150 Mtb H37Rv via aerosol inhalation, treated for a 10-day period with 80 mg/kg ABAH, 45 mg/kg AZD5904 alone or in combination with 10 mg/kg INH and sacrificed at day 36 p.i. Organs were removed and mycobacterial growth was analyzed by CFU assay in lung (a), spleen (b) and liver (c) at day 25 p.i. (pre treatment group) or at day 35 p.i. Depicted are one (co treated) to two (single treatment) experiments. Error bars indicate mean with SEM, 2-Way ANOVA with Tukey's range test.

7.4.8 Characterization of PMN and their effector functions from lungs of *per os* MPO inhibitor treated mice

C3HeB/FeJ mice are described to develop a PMN driven, proinflammatory necrotic granulomatous phenotype upon pulmonary Mtb infection [107], [115]. Thus, the abundance of PMN, MPO expression, ROS production and necrosis can be taken as an indicator for the pathological state of the granulomatous lesions in the lung. Therefore, these parameters were analysed in single cell suspensions from the lungs prepared at day 25 p.i. and day 35 p.i. by FACS.

For the analysis of PMN, two panels were applied to evaluate the frequencies of MPO and ROS expressing PMN and their necrosis. In the first panel, cells were gated into $CD3^+$ lymphocytes and $CD3^-$ myeloid cells, after exclusion of debris and doublets. From this population, PMN were gated as $Ly6G^+/CD11b^+$. This cell population was further analysed for their cell death ($7\text{-}AAD^+$) and intracellular ROS production ($DHR123^+$). (for the gating strategy see **Figure 31**). MPO expression was analysed in a second panel. After exclusion of debris and doublets, $Ly6G^+/SSC\text{-}A^{high}$ were further analysed for their MPO expression (for the gating strategy see **Figure 31**). Of note, PMN frequencies were comparable between the two gating strategies (data not shown).

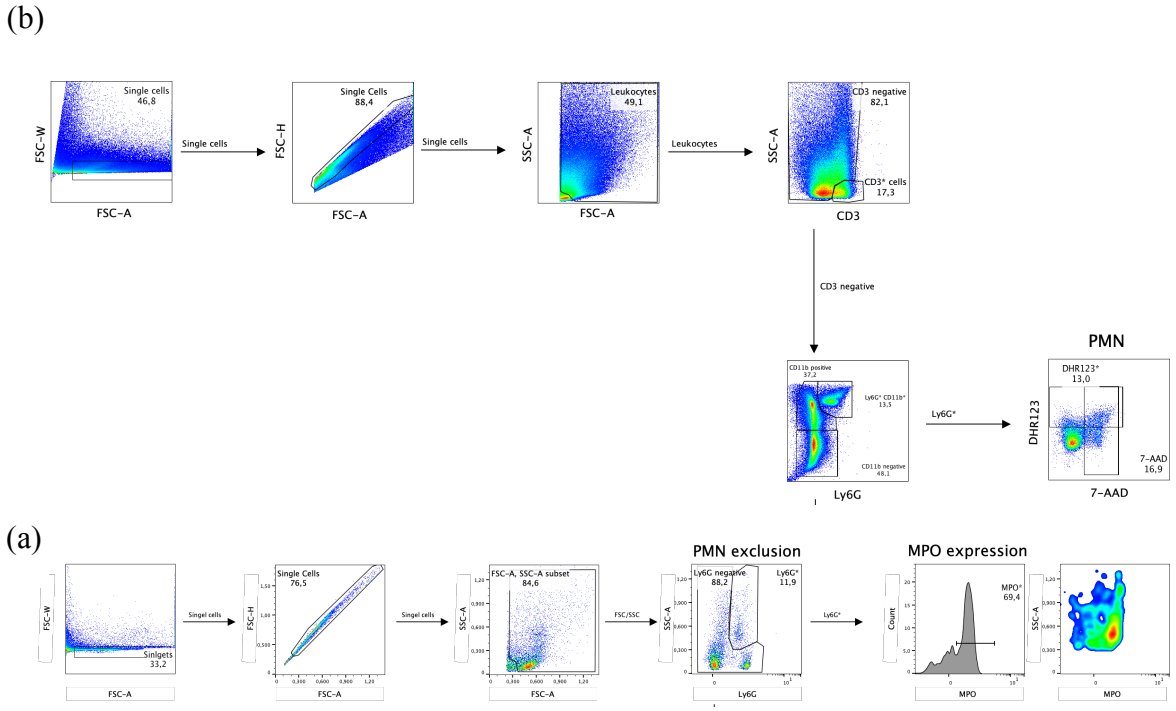

Figure 31 Gating scheme for PMN FACS analysis. FACS analysis was performed on single cell suspensions of H37Rv infected C3HeB/FeJ mice at day 25 p.i. and 35 p.i. Two panels were

used to analyze ROS production, MPO expression and necrosis. After exclusion of debris, doublets and $CD3^+$ cells PMN were gated as $Ly6G^+/CD11b^+$ cells. Those cells were further analyzed for $DHR123^+$ (ROS production) and 7-AAD+ (necrotic cell death) (a). In a second panel, after exclusion of debris, doublets, PMN were gated as $Ly6G^+/SSC\text{-}A^{high}$ and further analyzed for MPO^+ expression (b). Graphs are depicted in linear or biexponential format. In the graphs the symbol '*' represents '+' (positive population). Shown is one representative sample.

The frequency of $Ly6G^+$ PMN did not significantly change during treatment time, comparing day 25 p.i. and day 35 p.i. Mice that received ABAH or AZD5904 plus INH showed a slightly lower frequency of PMN but not in a statistically significant manner (**Figure 32 a**). MPO expressing PMN were significantly reduced upon MPO inhibitor treatment, when compared to the Captisol® and Captisol® + INH vehicle control groups (Fig, **Figure 32 b**). In contrast, the frequency of ROS positive PMN was significantly elevated in the lungs of mice with the MPO inhibitor treatment (**Figure 32 c**). The frequency of necrotic PMN was also significantly enhanced in MPO inhibitor treated mice (**Figure 32 d**), while INH co treated mice showed the same level of necrotic cell death as Captisol® treated mice. Interestingly, the number of necrotic, MPO and ROS positive cells, were always higher in animals at day 25 p.i., before treatment start.

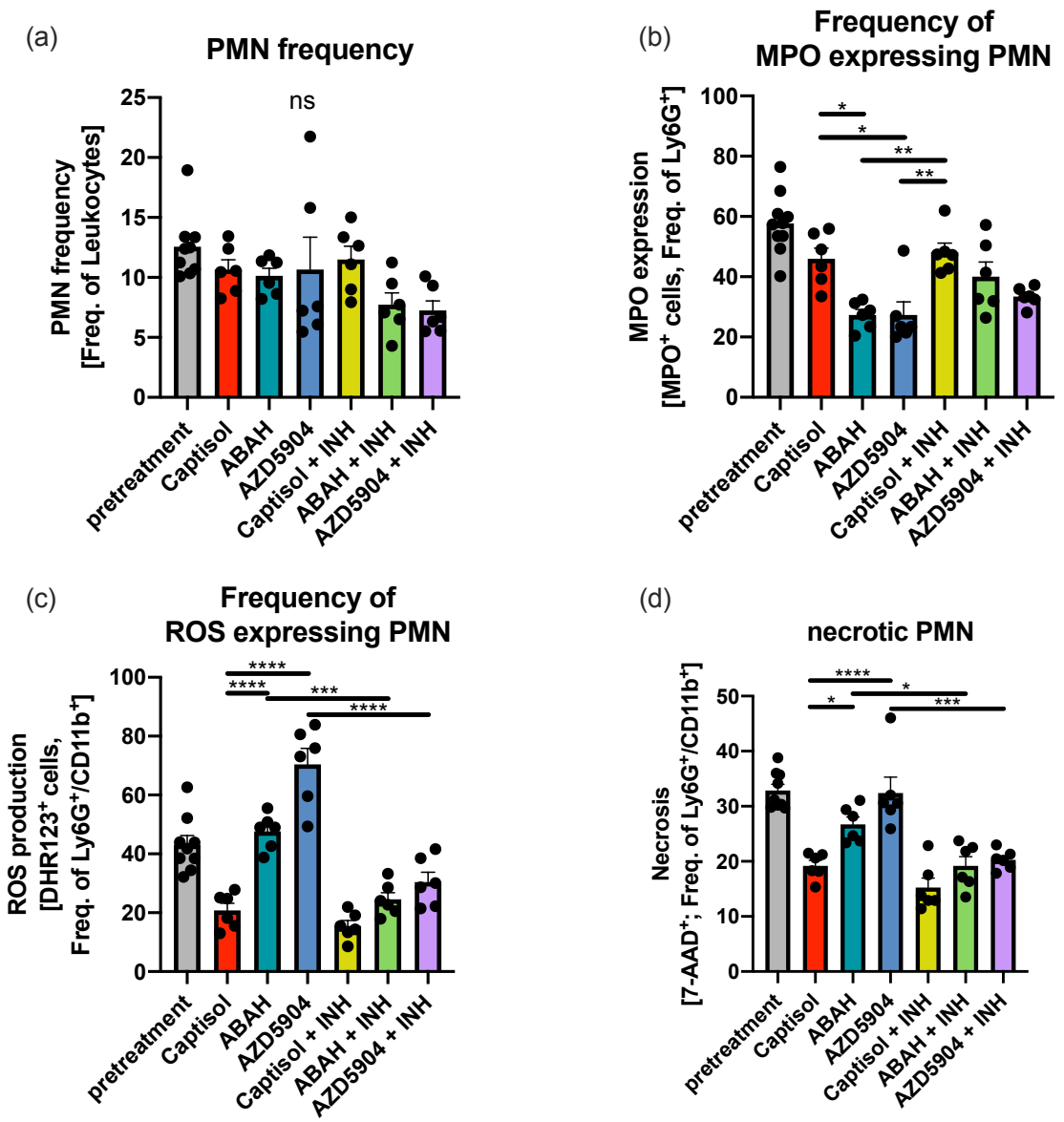

Figure 32 Characterization of lung PMN of H37Rv infected C3HeB/FeJ mice. C3HeB/FeJ mice were infected with an infection dose of 100 – 150 Mtb H37Rv via aerosol inhalation, treated for a 10-day period with 80 mg/kg ABAH, 45 mg/kg AZD5904 alone or in combination with 10 mg/kg INH and sacrificed at day 25 p.i. and 36 p.i., respectively. Organs were removed and single cell suspensions were stained for flow cytometric analysis. Initially, the frequency of PMN ($Ly6G^+/CD11b^+$ or $Ly6G^+/SSC\text{-}A^{high}$) (a) was analysed. In a next step, expression of MPO (MPO^+) (b), ROS ($DHR123^+$) (c) and necrosis ($7\text{-}AAD^+$) (d) was analyzed in PMN. Depicted is one experiment with 6 – 10 mice per group. Error bars indicate mean with SEM, 2-Way ANOVA with Tukey's range test. *$p \leq 0{,}05$; **$p \leq 0{,}01$; ***$p \leq 0{,}001$

7.4.9 MPO concentration and activity in the lungs of *per os* MPO inhibitor treated mice

In order to get a complete picture of tissue necrosis in Mtb infected lungs, extracellular protein was separated from cellular fractions of the organs. LDH activity, as marker for cell death, was analysed in extracellular protein fractions. MPO protein concentration and enzymatic activity were determined in extracellular protein fractions versus total lung lysates and serum.

Of note, the highest concentration of LDH was found before the start of the treatment at day 25 p.i., while at day 35 p.i. the activity was significantly lower. However, no differences were detected between the groups at day 35 p.i. (**Figure 33**).

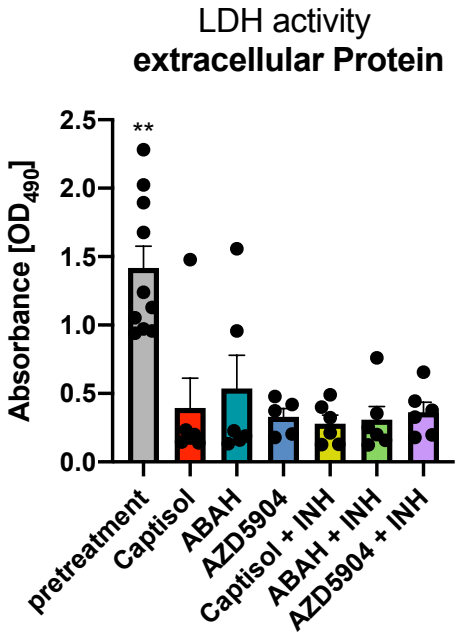

Figure 33 Extracellular LDH activity in extracellular protein fractions of H37Rv infected C3HeB/FeJ mice. C3HeB/FeJ mice were infected with an infection dose of 100 – 150 Mtb H37Rv via aerosol inhalation, treated for a 10-day period with 80 mg/kg ABAH, 45 mg/kg AZD5904 alone or in combination with 10 mg/kg INH and sacrificed at day 25 p.i. and 36 p.i., respectively. Organs were removed and extracellular proteins were extracted from whole lung lobes. The LDH activity was analyzed in the extracellular protein fractions. Depicted is one experiment with 6 – 10 mice per group. Error bars indicate mean with SEM, ordinary 1-Way ANOVA with Tukey's range test. *p ≤ 0,05; **p ≤ 0,01; ***p ≤ 0,001.

The concentration of MPO protein was normalized to the amount of total protein per mg. Regarding extracellular lung protein, the group analysed at day 25 p.i. had a statistically

significant enhanced MPO concentration, which was not reflected by the analysis of whole lung lysate protein fractions where the MPO concentration was comparable to the groups analysed at day 35 p.i. MPO inhibitor single treated groups had slightly elevated extracellular lung MPO protein concentrations, compared to the Captisol® treated control group (**Figure 34 a**). In total lung lysate fractions this difference was more pronounced, but not statistically significant (**Figure 34b**). INH plus MPO inhibitor treatment did not change MPO protein concentration at day 35 p.i., neither in extracellular protein fractions, nor in total lung lysate (**Figure 34 a, b**). In serum the MPO protein concentration doubled during the treatment time from day 25 p.i. to 35 p.i. However, treatment with ABAH, INH plus Captisol® or INH plus ABAH did not alter the presence of MPO protein in the serum (**Figure 34 c**). Despite repeated analysis, no MPO protein concentration could be detected in AZD single and co-treated samples. Interestingly, the average MPO protein concentration at day 35 p.i. was the lowest in serum with $2{,}17 \times 10^{-4}$ µg MPO/µg BCA protein, followed by total lung lysate with $2{,}05 \times 10^{-3}$ µg MPO/µg BCA protein, and was found to be the highest in extracellular protein fractions, with $3{,}15 \times 10^{-3}$ µg MPO/µg BCA protein.

The MPO activity was normalized to the amount of MPO protein. No differences were detected between the different treatment regimen. However, the highest activity at day 35 p.i. in serum with $3{,}83 \times 10^{-7}$ Units/min in average, followed by a high activity in extracellular protein fractions with $3{,}48 \times 10^{-7}$ Units/min and the lowest in total lung lysate with $1{,}41 \times 10^{-7}$ Units/min (**Figure 34 d-f**).

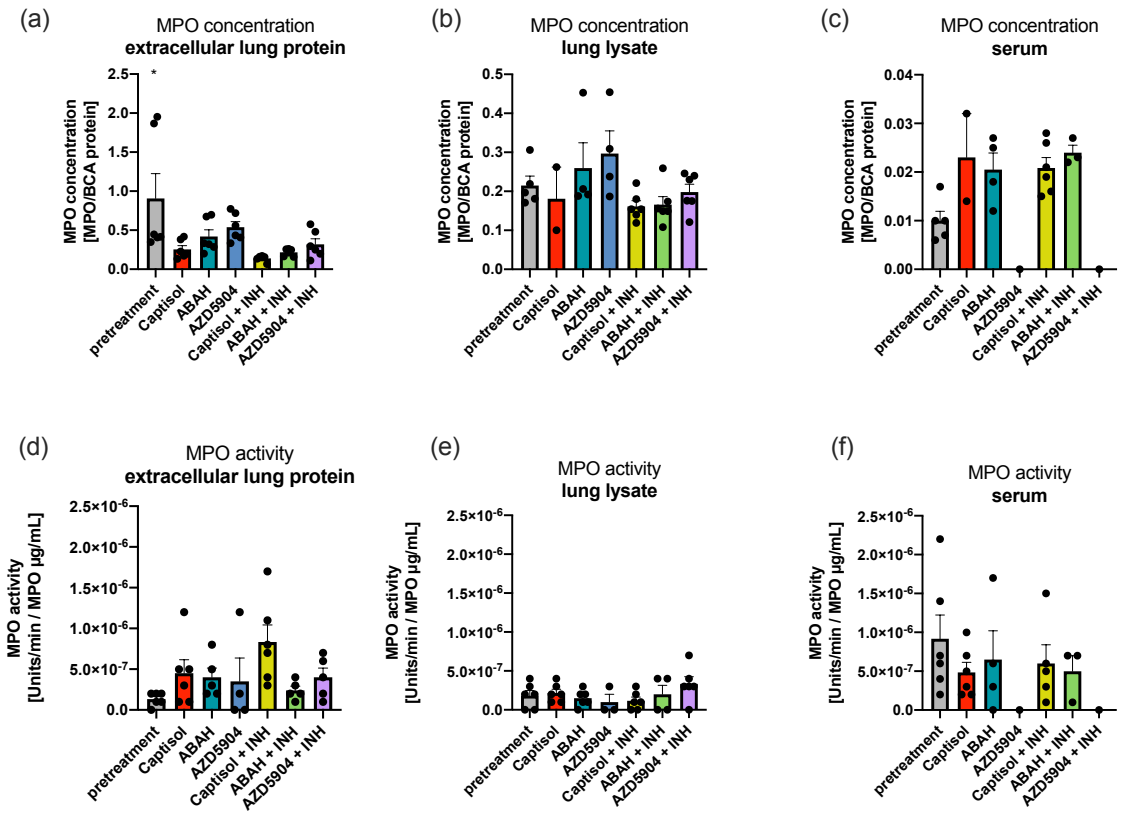

Figure 34 MPO protein concentration and activity in different organ samples from H37Rv infected C3HeB/FeJ mice. C3HeB/FeJ mice were infected with an infection dose of 100 – 150 Mtb H37Rv via aerosol inhalation, treated for a 10-day period with 80 mg/kg ABAH, 45 mg/kg AZD5904 alone or in combination with 10 mg/kg INH and sacrificed at day 25 p.i. and 36 p.i., respectively. Organs were removed and MPO protein concentration and activity were measured in fractions of extracellular lung protein (a, d), whole lung lysate (b, e) and serum (c, f). MPO protein concentrations are normalized to total protein content of each sample. MPO activity was normalized against the MPO protein concentration measured in each sample. Depicted is one experiment with 6 – 10 mice per group. Error bars indicate mean with SEM, ordinary 1-Way ANOVA with Tukey's range test. *p ≤ 0,05; **p ≤ 0,01; ***p ≤ 0,001.

7.4.10 Innate and adaptive immune response in the lungs of H37Rv infected C3HeB/FeJ mice

Macrophages are an important pillar of cell mediated immunity to overcome the disease, but rely on the activation by $CD4^+$ T cells to eliminate phagocytosed mycobacteria. Therefore, we analysed other innate and adaptive immune cells in single cell suspensions from Mtb infected lungs at day 25 and day 35 p.i.

7.4.10.1 Innate cellular immune response

After exclusion of debris, doublets and $Ly6G^+$ cells, dendritic cells (DC) were characterized as $CD11b^+/CD11c^+/MHCII^+$, interstitial macrophages were defined as $CD11b^+/CD11c^-/MHCII^{-/+}$ and alveolar macrophages were identified as $CD11b^-/CD11c^-/MHCII^{-/+}$. (for gating strategy see supplemental material 12.2). NK cells were characterized in a second panel as $CD3^-/CD49b^+$ (for gating strategy see supplemental material 12.3). Neither MPO inhibitor treatment alone, nor MPO inhibitor plus INH treatment changed the frequency of DCs, alveolar macrophages, interstitial macrophages or NK cells in comparison to their respective control group. However, upon INH plus MPO inhibitor treatment the frequency of DCs was statistically significant reduced (**Figure 35 a)** and the frequency of alveolar macrophages statistically significant elevated. (**Figure 35 b**). Only upon AZD5904 plus INH treatment the frequency of interstitial macrophages was significantly reduced (**Figure 35 c**). Additional INH treatment had no effect on the frequency of NK cells (**Figure 35 d**).

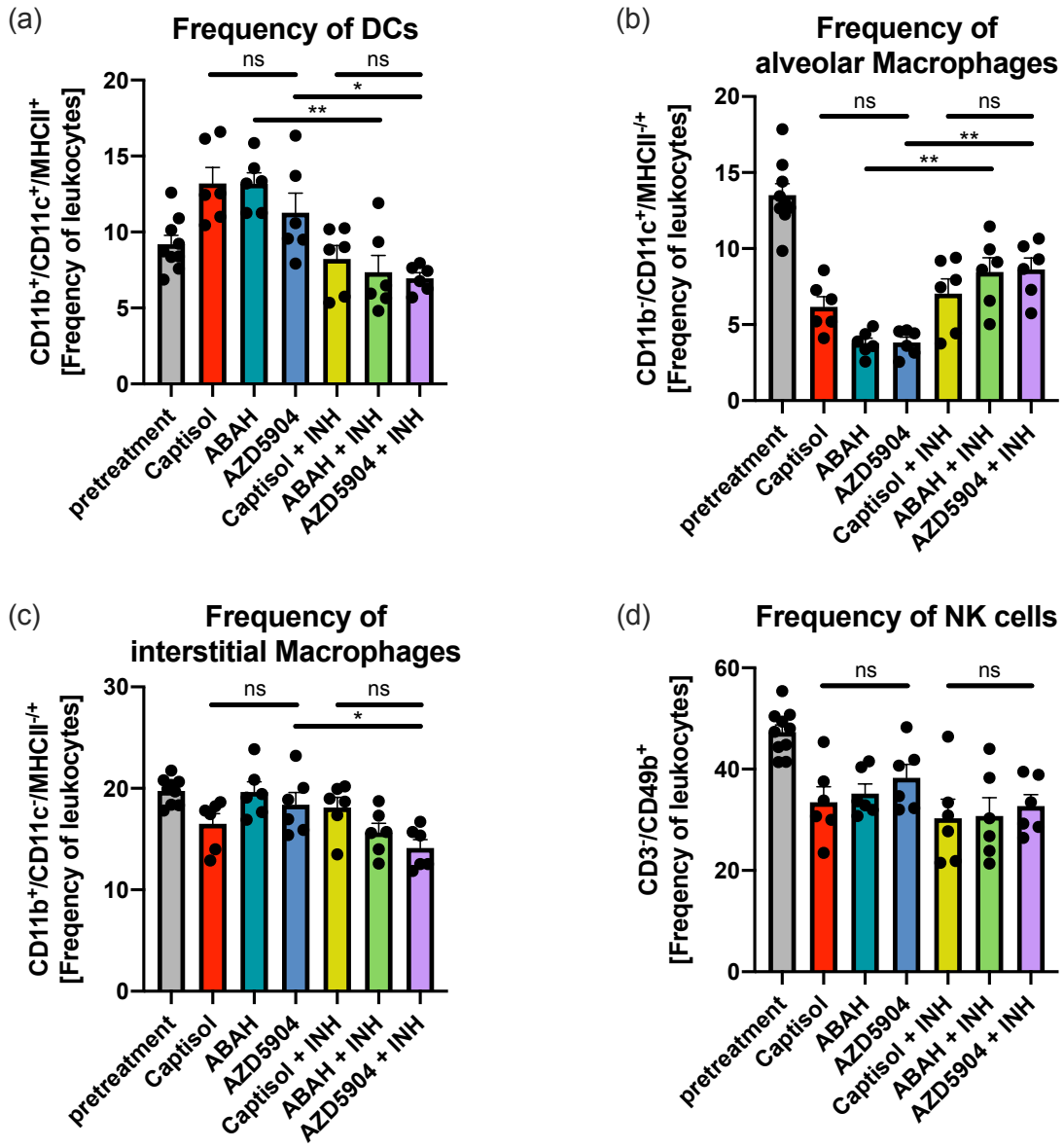

Figure 35 Frequency of myeloid cell populations in H37Rv infected C3HeB/FeJ mice. C3HeB/FeJ mice were infected with an infection dose of 100 – 150 Mtb H37Rv via aerosol inhalation, treated for a 10-day period with 80 mg/kg ABAH, 45 mg/kg AZD5904 alone or in combination with 10 mg/kg INH and sacrificed at day 25 p.i. and 36 p.i., respectively. Organs were removed and single cell suspensions from the lungs were stained for flow cytometric analysis. The frequency of dendritic cells (DC) (a), alveolar macrophages (b), interstitial macrophages (c) and NK cells (d). DCs were characterized as $CD11b^{+}/CD11c^{+}/MHCII^{+}$, alveolar macrophages as $CD11b^{-}/CD11c^{-}/MHCII^{-/+}$, interstitial macrophages as $CD11b^{+}/CD11c^{-}/MHCII^{-/+}$ and NK cells as $CD3^{-}/CD49b^{+}$. Depicted is one experiment with 6 – 10 mice per group. Error bars indicate mean with SEM, ordinary 1-Way ANOVA with Tukey's range test. *$p \leq 0{,}05$; **$p \leq 0{,}01$; ***$p \leq 0{,}001$.

7.4.10.2 Adaptive cellular immune response

After exclusion of debris, doublets and Ly6G$^+$ cells, CD3$^+$ lymphocytes were separated by gating from CD3$^-$ myeloid cells. Lymphocytes were further gated into CD3$^+$/CD49b$^+$ NKT cells and CD49b$^-$/CD4$^+$ or CD8$^+$ T cells, respectively. The expression of CD69 was further used to identify the activated cells (for gating strategy see supplemental material 12.3) [135].

The frequency of CD4$^+$, CD8$^+$ and NK T cells was not significantly changed between any of the different treatment groups (**Figure 36 a - c**). However, MPO inhibitor treatment significantly increased the frequency of activated CD4$^+$ and CD8$^+$ T cells, while the groups with INH or INH plus MPO inhibitors showed significantly lower frequencies of activated cells (**Figure 36 d, e**). Activity of NKT cells was not altered by any treatment (**Figure 36 f**). Of note, the proportion of activated NK T cells was high, with 30 – 40 % of all NKT cells being CD69$^+$, compared to CD4$^+$ and CD8$^+$ T cells from which 5 – 15 % expressed the activation marker.

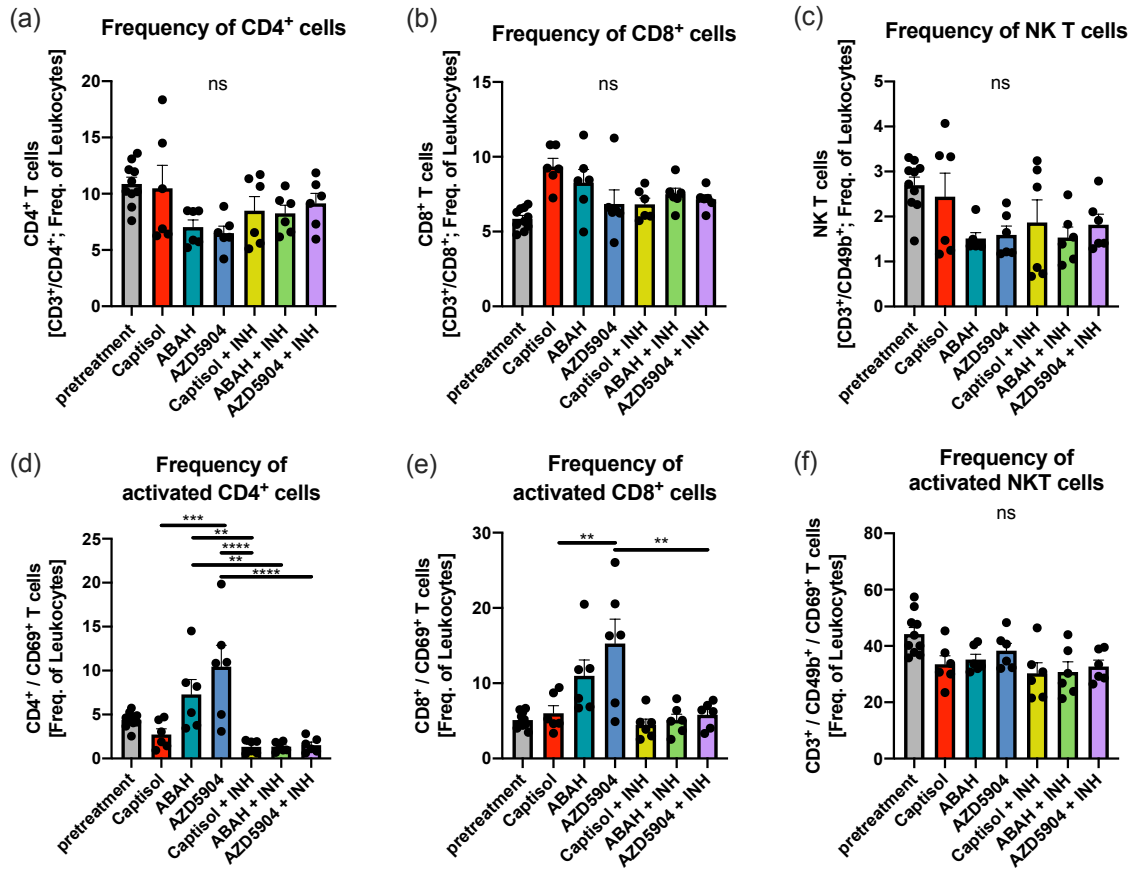

Figure 36 Frequency of adaptive cell populations in H37Rv infected C3HeB/FeJ mice. C3HeB/FeJ mice were infected with an infection dose of 100 – 150 Mtb H37Rv via aerosol inhalation,

treated for a 10-day period with 80 mg/kg ABAH, 45 mg/kg AZD5904 alone or in combination with 10 mg/kg INH and sacrificed at day 25 p.i. and 36 p.i., respectively. Organs were removed and single cell suspensions from the lungs were stained for flow cytometric analysis. The frequency of $CD4^+$ (a), $CD8^+$ (b) and NK T cells (c) were evaluated. $CD4^+$ T cells were characterized as $CD3^+/CD4^+$, $CD8^+$ T cells as $CD3^+/CD8^+$ and NK T cells as $CD3^+/CD49b^+$. CD69 was used to assess the frequency of activated cells (d – f). Depicted is one experiment with 6 – 10 mice per group. Error bars indicate mean with SEM, ordinary 1-Way ANOVA with Tukey's range test. *$p \leq 0,05$; **$p \leq 0,01$; ***$p \leq 0,001$.

In vitro stimulation of T cell populations with CD3/28 antibodies was used to evaluate the IFNγ and TNFα responses of these cells. $CD4^+$ and $CD8^+$ T cells showed significantly higher frequencies of TNFα producing cells upon single treatment with AZD5904, compared with the Captisol® treated control group. Groups that received INH or INH plus MPO inhibitors treatment had a lower frequency of TNFα expressing $CD4^+$ and $CD8^+$ T cells (**Figure 37 a, b**). NKT cells showed an increase in the frequency of TNFα expressing cells from day 25 p.i. to 35 p.i. in all groups, without reaching significance (**Figure 37 c**).

Surprisingly, $CD4^+$ IFNγ producers were almost absent at day 35 p.i. in all treatment groups (**Figure 37 d**), while $CD8^+$ T cells showed a high frequency of IFNγ positive cells. Further, treatment with MPO inhibitors plus INH significantly increased the frequency of IFNγ producing $CD8^+$ T cells, compared to Captisol® treated animals (**Figure 37 e**). A comparable picture was seen for NKT cells, where INH treatment increased IFNγ production, but not in a significant manner (**Figure 37 f**).

7.4.11 Cytokine / chemokine response in lungs of H37Rv infected C3HeB/FeJ mice

The cytokine and chemokine responses were evaluated in lung lysates of inhibitor only treated mice at day 35 p.i. Cytokines and chemokines were analysed using the LEGENDplex™ or MSD system.

TNFα and IFNγ concentrations in lung lysates were not significantly changed by the treatment but showed a slight reduction upon ABAH treatment. The interleukin IL-1β and Il-17, indicators for ingoing inflammation, were slightly reduced upon ABAH treatment. Il-22, which is associated with inflammation resolution was not changed. The Chemokines

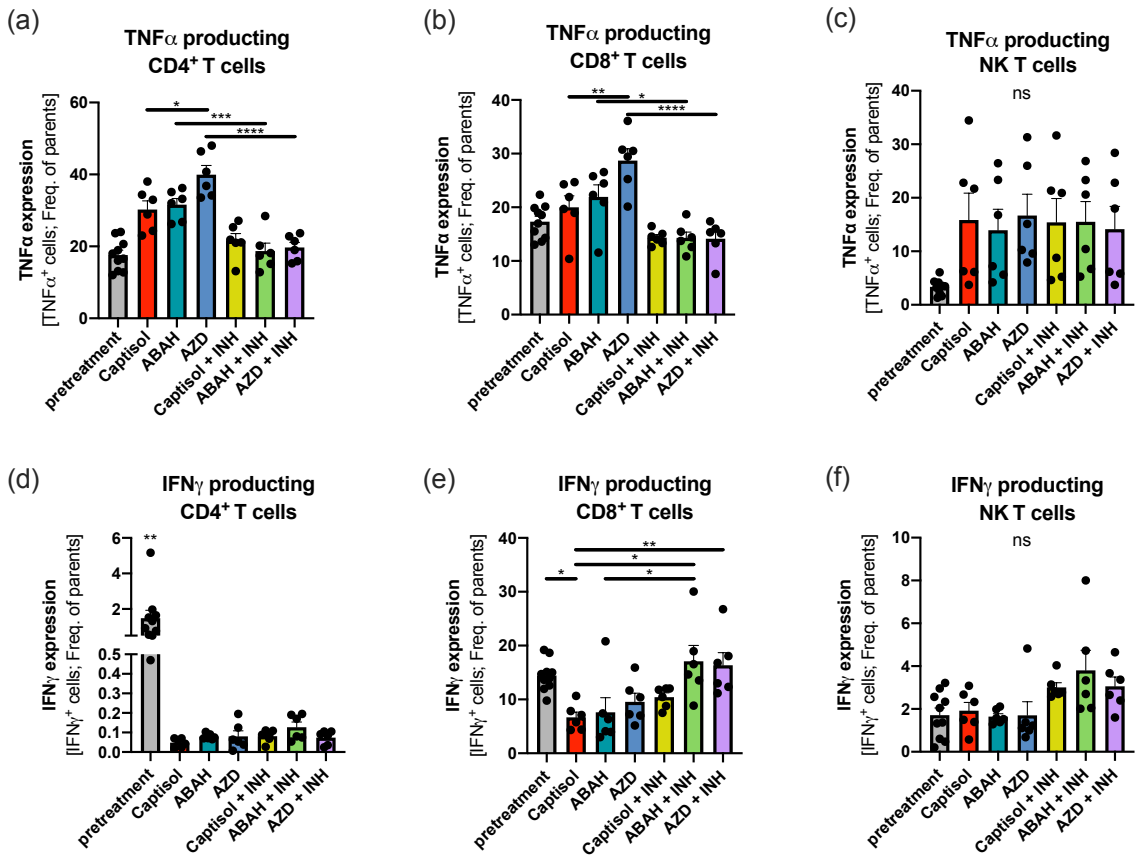

Figure 37 Cytokine production of adaptive cell populations in lungs of H37Rv infected C3HeB/FeJ mice. C3HeB/FeJ mice were infected with an infection dose of 100 – 150 Mtb H37Rv via aerosol inhalation, treated for a 10-day period with 80 mg/kg ABAH, 45 mg/kg AZD5904 alone or in combination with 10 mg/kg INH and sacrificed at day 25 p.i. and 36 p.i., respectively. Organs were removed and single cell suspensions from the lungs were stained for flow cytometric analysis. The production of IFNγ and TNFα was analysed in $CD4^+$ (a, d), $CD8^+$ (b, e) and NK T cells (c, f). Depicted is one experiment with 6 – 10 mice per group. Error bars indicate mean with SEM, ordinary 1-Way ANOVA with Tukey's range test. *p ≤ 0,05; **p ≤ 0,01; ***p ≤ 0,001.

CCL3, CCL4 and CCL5 have multiple functions, but have been described to be upregulated upon Mtb infection. All bind to CCR5, which is expressed on PMN and macrophages. Their concentration was, however, not significantly changed upon infection. Only CCL5 was slightly downregulated upon ABAH and AZD5904 treatment. The concentration of the PMN recruitment associated chemokine CXCL1 was not changed upon treatment, while concentrations of the PMN activating CXCL5 was slightly reduced in MPO inhibitor treated mice. CXCL9 and CXCL10 which are associated with structured granuloma formation and Mtb specific T cell recruitment were not changed (**Figure 38**).

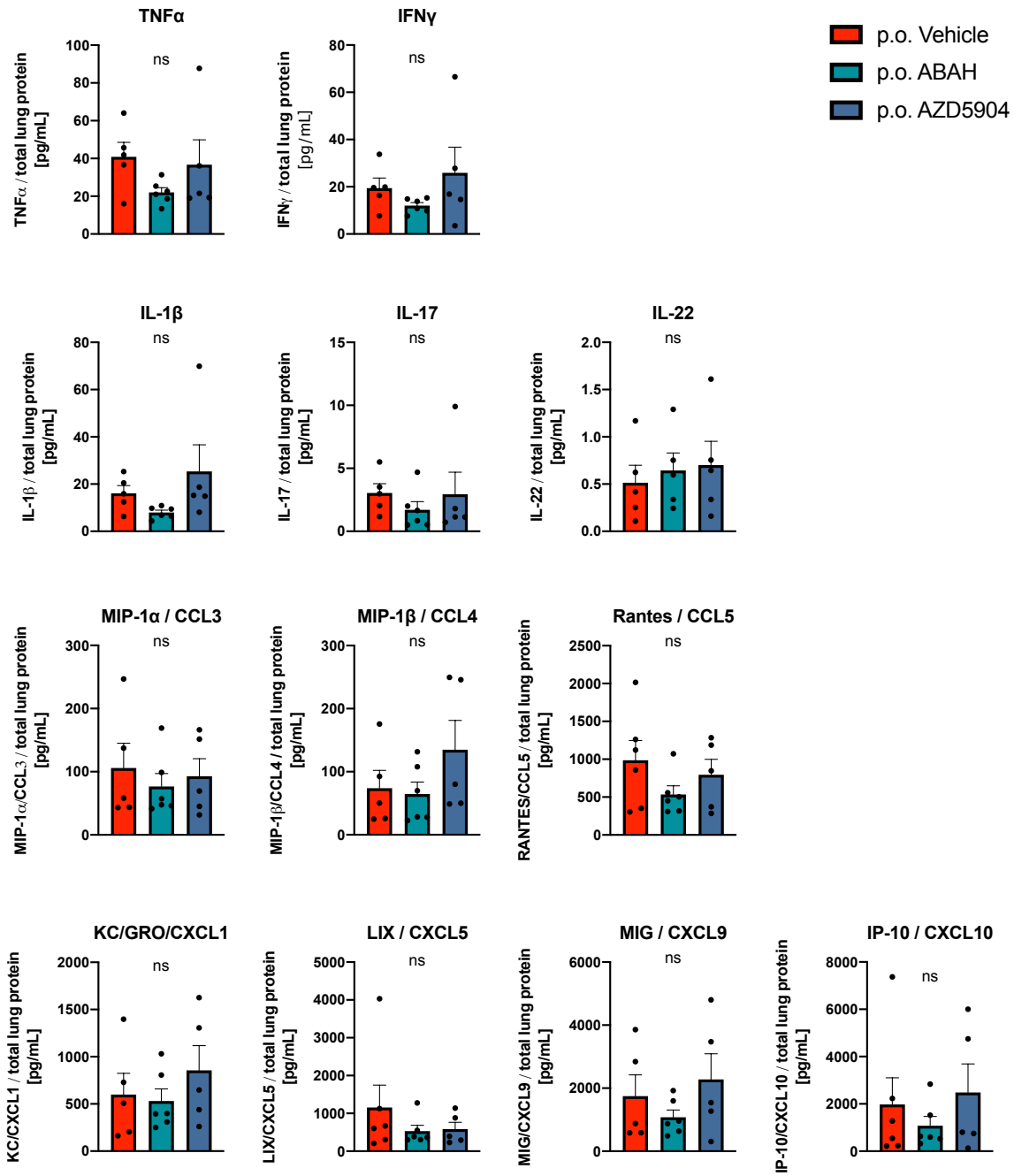

Figure 38 Cytokine and chemokine response in lungs of H37Rv infected C3HeB/FeJ mice. C3HeB/FeJ mice were infected with an infection dose of 100 – 150 Mtb H37Rv via aerosol inhalation, treated for a 10-day period with 80 mg/kg ABAH, 45 mg/kg AZD5904 alone and sacrificed at 36 p.i. Organs were removed and cytokines and chemokines were analyzed in whole lung lysates using the LEGENDplex™ or MSD system. Depicted is one experiment with 5 – 6 mice per group. Error bars indicate mean with SEM, ordinary 1-Way ANOVA with Tukey's range test. *p ≤ 0,05; **p ≤ 0,01; ***p ≤ 0,001.

8 DISCUSSION

The role of PMN during chronic inflammatory or infectious diseases has attracted growing interest over the past years. PMN are important early innate immune cells, that can be recruited quickly to a site of infection and initiate the immune response. However, uncontrollably recruited and activated in great numbers, their effector functions can lead to inflammation and tissue destruction. In TB this effect has been associated with increased pathology and worsened outcome for the patients. Most importantly, human PMN infected with Mtb *in vitro* were shown to succumb to a MPO dependent, ROS induced, necrotic cell death, thereby promoting Mtb growth and inflammation [17], [79]. Thus, understanding the function of PMN during TB is an important pillar for improving therapy and to develop new treatment regiments.

This study aimed to answer relevant questions regarding PMN effector function upon Mtb infection. First of all, we analysed the lipidome of uninfected vs. Mtb infected hPMN and how the infection might change the cells lipid composition. Although the ROS induced necrosis, did not seem to influence the lipidome of the cells, the infection itself induced some interesting changes, pointing towards a consumption of host lipids as nutrient source by the mycobacterium. In a next step, different murine PMN types were compared for their *in vitro* phenotype upon Mtb infection, in order to find the most suited population for the following assays. The results of the PMN population, harvested from different organs, strongly indicated distinct effector functions like phagocytosis, ROS production and necrosis. The PMN population which turned out to be best for the infection assays was analysed for the effects of MPO inhibition *in vitro.* Surprisingly, MPO inhibition did not reduce intracellular ROS production or necrosis. Lastly, we evaluated a putative PMN targeting host-directed therapy (HDT) in susceptible C3HeB/FeJ mice, which develop PMN driven, necrotic granulomas [115]. Although we could not detect an improvement, by inhibiting MPO *in vivo,* the study provides important insight into the differences between human and murine TB.

8.1 Mtb induced changes of the hPMN lipidome

The necrotic cell death of hPMN upon Mtb infection has the potential to alter lipid structures and change the composition of the lipidome. Lipids are major molecular components of the

cellular membrane system and serve as small mediators determining immune signalling pathways [136]. Further, lipids provide an essential nutrient source for Mtb [93]–[95]. The molecular structure of lipids makes them highly susceptible to environmentally induced changes like lipid peroxidation (LPO) induced by ROS or other oxidative effector molecules. The spontaneous free radical oxidation is usually started at an unsaturated fatty acid residue within the molecule. This can result in a chain reaction, producing additional free radicals and thereby oxidizing adjacent lipid molecules. This process can lead to severe cellular damage, for example in the case when LPO react with DNA, sugars and proteins, thereby altering cellular homeostasis, even inducing cytotoxic effects like membrane disintegration [89]. Further, LPO products can serve as signalling molecules and are often associated with pathogenicity, like for example in neurodegenerative diseases [89]. Here we provide a MS/MS based analysis of the lipidome of hPMN and the influence of an Mtb infection vs. Mtb infection with parallel MPO inhibition using ABAH, which leads to a reduction of necrosis.

The composition of the lipidome of uninfected resting hPMN, was comparable to earlier studies of the human lung lipidome [137], analysis of bronchoalveolar lavage [138] or isolated hPMN [139] regarding lipid types, lipid classes and the number of identified lipid species (**Figure 8**). Although these studies used different analytic methods and different samples, as whole lung lysate consist not only of PMN, the overall consistency of the data indicates a robust and precise measurement in our hands. Over time, the major change was a significant increase in Phosphatidylglycerol (PG) at 6 hpi. Of note, this was a significant change in all three groups, independent of infection or ABAH treatment (**Figure 10**). Thus, it seems to be a process independent of the infection or treatment, solely based upon the incubation *in vitro*. PGs have been described to be mainly located in the mitochondrial membrane and moreover, the organelle is capable of synthesizing this lipid class *de novo* [140]. PGs are not indispensable for the survival of cells, as a deletion of a PG synthesizing gene has shown. However, its loss has been associated with temperature sensitivity and growth retardation [141]. Thus, the upregulation of PG might be an adaptation for a better survival of the cells *in vitro,* in order to adapt to the experimental conditions. Further, another role for PG was described in lipid-gated ion channels. Ion channels are important for a number of basic cellular processes, like excitement, activation and signalling. As the name suggests, these membrane bound channels, regulate ion transport into the cell. In case of lipid-regulated channels, certain lipid species have to bind to the transmembrane or a subunit domain of these molecular complexes to activate or regulate the channel [142]. Recently it

has been shown, that PG bind and stabilize PG dependent ligand-gated ion channels [143]. As no further analysis was conducted to look at PG-ion channel dependent effector functions, it is only speculation, that the upregulation of PG species is somehow connected and important for cellular processes during the *in vitro* incubation of PMN. However, the upregulation of PG in all samples indicates an important role for this lipid class and a possible connection to cell culture adaptation or ion transport into mitochondria and its subsequent processes.

Comparison of the uninfected, infected and infected plus ABAH treated cells revealed only little changes in the lipid composition. Even though, necrosis of *in vitro* cultured and H37Rv infected hPMN was significantly enhanced at 6 hpi (**Figure 6**), this tremendous impact on cell membrane integrity had only minimal influence on the PMN lipidome. Most obvious was an early, significant reduction in neutral lipids upon Mtb infection at 2 hpi, compared to non-infected PMN as well as infected, but ABAH treated PMN (**Figure 9**). Detailed analysis of the identified lipid classes revealed, that this effect was based on a reduction of triacylglycerols (TAGs) (**Figure 10**). Interestingly, this effect proceeded the necrotic cell death, which only occurred after the 2 hpi time point. Thus, there seems to be an early, Mtb driven alteration of the lipid composition regarding TAGs upon infection of hPMN, which can be inhibited or reverted by MPO inhibition. A possible explanation for the reduced proportion of TAG might be found in the energy metabolism of the bacteria. As a facultative intracellular living organism, Mtb has to acquire all its nutrients from its host cell. Indeed, it has been shown that complex lipids are an important nutrient source for Mtb cell membranes. Thus, host cell membranes and storage lipids provide important precursors for the lipid metabolic pathways required by Mtb [93]. The molecular structure of TAG contains three fatty acids residues and the oxidation of the fatty acids is a highly conserved and efficient pathway to generate energy for a cell. In line, the degradation of neutral lipids by the host cell is able to deprive Mtb of this important energy source, and, thus reduce mycobacterial growth [144]. Further, a great part of the Mtb genome encodes for lipid metabolism associated genes. Approximately 250 distinct enzymes have been identified, that are involved in fatty acid metabolism. For comparison, *Escherichia coli* only encodes for around 50 [145].

There are other studies, mainly performed in macrophages, that highlight the influence Mtb might have on the lipidome of its host cell. Due to its intracellular lifestyle, Mtb has developed several ways to alter the lipid homeostasis in macrophages. During the course of

infection, Mtb supports the development of mature macrophages into so called foamy macrophages, which are characterized by increased number of TAG containing lipid droplets [92]. Mtb can be found in large numbers adjacent to the lipid droplets in these foamy macrophages. These cells are suspected to promote persistence in the host [95]. Another mechanism, that was recently discovered, is an Mtb induced impairment of the Acetyl-CoA Carboxylase 2 (ACC2), a major driver for fatty acid oxidation in the host cell. Thereby, accumulation of TAG is elevated, which can then be used by the mycobacterium for replication and survival. In turn, the inhibition of this Mtb driven mechanism, reduced bacterial growth [147]. Altogether, this supports the assumption that the reduced frequency of TAG in hPMN might be based on an energy requirement by Mtb. Although direct TAG consumption by Mtb can't be confirmed with this experiment, it would be interesting to further investigate this topic. The Mtb knockout strain with a deletion for *Mtb triaglycerol synthase 1* (*tgs1*), which are unable to metabolize host derived TAG [95], could be an interesting tool to answer the question whether Mtb's metabolic need for TAG drives the reduction in TAG concentrations in PMN.

Interestingly, a second alteration in the lipidome of hPMN was seen when comparing uninfected and Mtb infected hPMN to Mtb infected, ABAH treated hPMN at 6 hpi. Upon Mtb infection and supplemental ABAH treatment the frequency of cholesterols was significantly reduced, compared to uninfected and Mtb infected hPMN. This effect may be related to the apoptotic phenotype, as Mtb infected cells, which were left untreated, succumbed to necrosis and uninfected cells, did not show any signs of cell death (**Figure 10**). Like TAGs, cholesterols can act as an important energy source for Mtb [98], [148]. It was shown to be important to circumvent host defence mechanisms, thereby leading to persistence of the pathogen. In IFNγ activated macrophages, which have the ability to sequester mycobacteria in nutrient deprived lysosomal compartments, Mtb can metabolize the sterols of cholesterols as a carbon and energy source. Thus, it was hypothesized that the intracellular conditions found in activated macrophages, drives the cells to metabolize cholesterols, while upon resting conditions, the bacterium can use other energy sources [149]. The enclosure of Mtb in apoptotic vesicles might be a similar, nutrient limiting force, comparable to the situation in phagolysosomes. The limited availability of other energy sources, may pressure Mtb to switch from neutral lipids to cholesterols as primary energy source, which might explain the reduced cholesterol concentration in apoptotic hPMN. Again, infection studies with Mtb strains, impaired in metabolizing cholesterol, could answer this question. However, it might also be a host driven response to the infection that

lead to the reduction of cholesterols, that somehow is linked to the apoptotic cell death and not necessarily to the infection or ABAH treatment.

Although we initially aimed to also analyse ROS induced LPO, the method applied only allowed a broad overview on the main lipid types, classes and species. For detailed analysis of LPO products different analytical standards would be required. This could not be further conducted, due to initial experimental obstacles, which delayed this study. However, taken together, our data indicates minimal but quickly induced changes of the PMN lipidome upon Mtb infection, probably due to metabolic processes. For a deeper understanding of the underlying mechanisms further studies have to be conducted to reveal the interactions between the host and the pathogen. Of note, the discussion was based upon studies, that mainly used macrophages. Considering the fundamental differences between these two cell populations regarding effector functions and life span, the conclusions that are drawn here are only a first impression of what might take place in PMN upon Mtb infection regarding the host cell lipid composition. Comparative analysis of macrophages and PMN could provide interesting new results in this context. Nevertheless, this study provides the first insight into PMN lipid biology in regard to Mtb infection induced alterations.

8.2 Murine PMN populations from different origin have distinct effector functions

Studies on human PMN usually use cells, isolated from the peripheral blood. In contrast, for *in vitro* experiments with murine PMN, the cells are usually isolated from bone marrow, peripheral blood or the peritoneal cavity [150]. The PMN from these sources can differ in their phenotypes and stages of development, thus representing distinct populations. As prerequisite for subsequent studies, the responses to Mtb of PMN from bone marrow and blood were analysed in a comparative manner.

8.2.1 Freshly isolated, murine bone marrow PMN have impaired effector functions

Initially, freshly isolated, unmatured bone marrow derived PMN were used to analyse effector functions of murine PMN. They can be easily harvested in great numbers and are often used in literature [150]–[152]. Freshly isolated bone marrow derived PMN were described as functional fully competent in regard of ROS production. Of note, the study used extracellular stimulation and not phagocytosis induced activation [151]. However, we

expected no major obstacle using this cell population for our assays. Surprisingly, no substantial increase in ROS production was detected in this PMN population (**Figure 14**). Further, no increase in necrosis upon Mtb infection could be observed, using LDH activity measurement of the supernatant. Instead, already uninfected cells, showed a high necrosis rate, which limited the infection induced effects even further (**Figure 15**). This was different from earlier studies, which demonstrated elevated necrosis upon Mtb infection *in vitro* in hPMN [17], [79] and even *in vivo* in mice, in which lung necrosis was associated with PMN numbers [115].

A crucial event in activating mycobactericidal effector functions of PMN is phagocytosis of a pathogen [54]. The lack of effector functions of unmatured bone marrow derived PMN pointed towards an inability in phagocytosis. Using a fluorescent labelled Mtb strain and flow cytometry, we could indeed show, that unmatured bone marrow PMN had a very limited phagocytosis rate of only 20 – 25% (**Figure 13**). This could explain the reduced effector functions, like ROS production and necrosis. We used a MOI of 3 or 5, to infect PMN *in vitro*, which means that 3 to 5 bacteria were added per cell to the culture. Regarding this numbers and experience from other *in vitro* assays using hPMN or macrophages, this phagocytosis rate is exceptionally low.

PMN originate from the bone marrow. Therefore, it is not surprising, that it contains a huge population of unmatured and precursor PMN. It seems likely, that the majority of the bone marrow population is unable to phagocytose due to their maturation status. Therefore, we applied a protocol to pre-stimulate and, thus, mature freshly isolated bone marrow with recombinant murine G-CSF. PMN isolated from these pre-stimulated bone marrow cells were hypothesised to be more mature and to have increased effector functions.

8.2.2 STIMULATION OF BONE MARROW WITH G-CSF INCREASES PMN EFFECTOR FUNCTIONS

G-CSF has been used before to mature granulocytes and hematopoietic progenitors. It was shown to be indispensable for survival of bone marrow derived granulocytes, which succumbed to apoptosis upon its absence, but not important for migration from the bone marrow to the circulation. This was shown in G-CSF deficient mice, that showed normal PMN numbers in circulating blood [153]. G-CSF can promote proliferation and differentiation of PMN and acts as chemoattractant for tissue resident PMN [154], [155]. Moreover, Fine et al. reported upregulation of CD11b on bone marrow cells upon G-SCF

stimulation *in vitro,* followed by a development of 60% of the bone marrow cells into PMN, which were defined as $CD11b^+/CD66a^+$. The observed increase was significant when compared to a culture without G-CSF stimulation, in which only 10% of the cells developed into PMN [131]. In humans, administration of recombinant human G-CSF significantly increased PMN abundance in the blood, in a dose dependent manner [156].

Based on these studies, we applied a similar approach for optimal expression of bone marrow derived PMN effector functions. After the isolation of bone marrow, the cells were cultivated in the presence of recombinant murine G-CSF for 48h. This G-CSF mediated *in vitro* maturation significantly increased phagocytosis, ROS production and necrosis of bone marrow derived PMN, indicating a fundamental difference between freshly isolated, unmatured and matured bone marrow derived PMN. Another approach, that was described to increase effector functions of blood derived PMN is the stimulation with recombinant IFNγ or TNFα [157], [158]. However, in our hands pre-stimulation with either recombinant IFNγ or TNFα did not enhance the phagocytosis rate or ROS production of freshly isolated, unmatured murine bone marrow derived PMN (Data not shown). The most likely explanation lies in the origin of the different cell populations that were used by us(bone marrow derived) and others (blood derived) [157], [158]. Nevertheless, it also has to be considered, that the cytokines IFNγ and TNFα induce completely different responses compared to the growth factor G-CSF.

For a long time, PMN were seen as terminally differentiated cells, that have only little to no transcription, once released into the blood stream. The implication of IFNγ and TNFα for PMN were often overlooked, as the cytokines are classically associated with T cells, NK cells and the activation of macrophages [159]. Nowadays it is now known, that PMN express more than 1000 possible binding sites for IFNγ and TNFα, which initiate several different pathways and transcriptional processes [160], [161]. The engagement with IFNγ stimulates activation and defence mechanism in PMN, like increased ROS production, antigen presentation and differential gene expression. TNFα for example, is described to induce upregulation of CD11b and to increase the production of superoxide anions, but additionally impairs migration towards a chemoattractant [161], [162]. In contrast, G-CSF is critical for PMN survival, proliferation and maturation in the bone marrow and for migration into tissue towards chemoattractants [131], [153]–[155]. Conclusively, IFNγ and TNFα failed to increased activation of freshly isolated bone marrow derived PMN, probably because the cells were still too immature to fully respond to the infection and stimulation *in vitro.*

Therefore, this pre-activation seems only to work on fully mature blood [157], [158] or matured bone marrow derived PMN. In contrast, the 48h incubation with the essential growth factor G-CSF allows the cells to reach their terminal maturation. Nevertheless, a detailed analysis of gene expression patterns of the different PMN populations after various stimulations would be important, to fully understand the reaction of distinct PMN to extracellular stimuli and the implication of their maturation status.

Interestingly the total amount of MPO in matured vs. unmatured PMN did not differ, indicating that the majority of MPO protein is pre-formed in the bone marrow, before PMN reach full maturity. Infection however, slightly increased MPO concentrations, via *de novo* synthesis (**Figure 18**). The infection dependent release of MPO into the supernatant was also comparable between both cell populations, indicating degranulation of the unmatured bone marrow derived PMN, independent of PMN phagocytosis.

Another major difference we found between these two cell populations, was the expression levels of CD11b. Matured bone marrow derived PMN expressed twice the amount of CD11b at the plasma membrane than immature cells (**Figure 12**). CD11b belongs to the β2 integrin receptors and in combination with CD18 it assembles to the surface receptor often termed Macrophage-1 antigen receptor (MAC-1) [163]. It is expressed on myeloid cells like macrophages, DC and PMN and has been shown to be required for cell-cell interactions, trans endothelial migration and complement mediated phagocytosis. Patients with a defect in MAC-1 have reoccurring fungal and bacterial infections, primarily marked by impaired migration and reduced phagocytic ability by PMN [164], [165]. *In vivo* studies with CD11b KO mice also showed limited phagocytosis rates in PMN. This is in line, with the low expression of CD11b on unmatured bone marrow PMN and might explain the reduced phagocytosis rates. However, the reduction of CD11b is not solely affecting phagocytosis, but can also act as an indicator for the activation status of the cell. Crosslinking of MAC-1 was further shown to be important for TNFα production through the NF-κB pathway [166], which is an important stimulant for phagocytosis initiation and Mtb killing by PMN [167]. The presence of MAC-1 may also be relevant for ROS production. Crosslinking of MAC-1 initiated a NADPH driven, respiratory burst in murine PMN infected with *Aspergillus fumigatus* hyphae [168]. In combination with the reduced effector functions towards Mtb, our findings support the usability of CD11b to act as an easy-to-use marker to analyse the activation status of PMN.

There are some very detailed characterizations of different PMN population in the bone marrow. High dimensional, single cell studies and mass cytometry analysis allowed a detailed description of distinct cell populations, based on expression patterns and surface markers. Evrard *et al.,* identified three specialized bone marrow derived PMN related populations based on distinct surface receptor and RNA expression. They found a highly proliferative PMN precursor, giving rise to a population of immature PMN that finally develops into mature PMN. Interestingly, a murine tumour model associated the numbers of immature PMN with increased pathology [169]. Additionally, another but highly similar unipotent neutrophil precursor has been described in humans and mice, whose increasing numbers correlated with tumour growth [170]. Despite the correlations between pathology and numbers of distinct PMN populations, these studies did not analyse subsequent effector mechanisms like phagocytosis, degranulation, ROS production or cell death, which makes it difficult to pinpoint the maturation status to effector functions identified in our study. However, the indication that an unregulated number of unmatured cells lead to a negative outcome, highly suggest false or absent effector functions.

However, it would be highly interesting to separate and characterize the distinct bone marrow populations for differential assessment of their effector functions and the effect of G-CSF mediated maturation to gain further insight into PMN biology.

8.2.3 Matured bone marrow derived PMN and blood PMN have similar effector functions

Based on these significant differences between the two PMN populations, we included murine blood derived PMN as third population in the study. This population is thought to resemble the characteristics of peripheral hPMN most closely, as they are harvested from the same organ and go through the same maturation and migratory steps [131]. Like hPMN, the murine blood PMN circulate approximately 90 h in the blood stream [171] and either migrate into the tissue upon inflammatory signals or rehome back to the bone marrow, where they are recycled [42].

In our hands blood derived PMN showed characteristics comparable to matured bone marrow derived PMN, like for example a similar phagocytosis rate of 60% and the same elevated level of CD11b expression (**Figure 17**). This indicates, that these cells are in a comparable maturation state as the *in vitro* matured bone marrow derived PMN.

Interestingly, a reduced ROS production was measured in blood PMN compared to matured bone marrow derived PMN (**Figure 14**). This might be based on the exposure of PMN to different stimuli in the circulation, by which the cells might become exhausted. Further, different PMN populations have been described in the blood as well. One study in mouse and human described around 13% of all blood derived PMN as 'primed' PMN. This cell population was characterized by elevated CD11b, CD63 and CD66a expression, an increased nuclei area and a multilobular nuclear morphology [131]. However, with regard to phagocytosis rate and ROS production levels they did not differ from the so called resting PMN, which showed a reduced expression of the mentioned marker, smaller nuclear area and reduced lobes [131]. The primed PMN are thought to be quicker recruited, because of their elevated adhesion markers. One preliminary study on septic patients however, indicated reduced phagocytic capacity of unmatured PMN in the blood. But the characterization of unmatured PMN was based solely on the shape of the nucleus, which makes the comparison to other studies difficult [172]. Considering, that PMN have a quick turn over in the blood, already small changes in diet or hormonal rhythms might change their population, which could explain the high inter experimental differences. However, it confirms again that it is important to characterize different PMN populations before studying effector functions triggered by an infectious agent.

However, this population can only be harvested in a very small number, as mice do not have a great amount of blood. Thus, large scale experiments were not possible in order to reduce the number of mice used for experiments. Because, the G-CSF mediated maturation of bone marrow produces a great number of functional fully competent murine PMN, this method should be used to generate PMN for *in vitro* assays.

8.2.4 Cell death of the different PMN populations to Mtb infection assays

Interestingly, evaluation of infection induced necrosis was highly depended on the applied assay and the analysed cell population. In blood derived PMN, necrosis measurements via flow cytometry and LDH assay were more comparable to each other, than in matured bone marrow derived PMN, which only allowed detection of necrosis by LDH activity but not flow cytometry. A likely explanation for this effect, lies in the protocol of both analytic procedures. The number of necrotic, 7-AAD positive cells determined by flow cytometry quantified only cells, which still have a relatively intact membrane, while the greater part of necrotic debris was likely lost due to the repeated washing steps during the staining

procedures. In contrast, the determination of LDH enzyme activity in the cell supernatants reveals the necrosis level of the whole cell culture without loss due to handling. In healthy cells, LDH is exclusively intracellular. Its quantification in the supernatant correlates with necrosis rates after disintegration.

These differences might indicate more efficient Mtb induced necrosis in matured bone marrow derived PMN compared to blood PMN. The effects of the increased ROS production by matured bone marrow derived PMN, might degrade these cells to a point where they became undetectable by flow cytometry. In blood derived PMN, necrosis induction might be slower, due to the reduced ROS production, thereby more cells remain detectable by flow cytometry. In support of our hypothesis, a quick increase of ROS upon encounter of a pathogen might lead to a systemic and complete elimination of infected cells, while a lower level of ROS only induces a 'mild' necrosis.

To this point, the data still supports the hypothesis of a Mtb induced, ROS dependent necrotic cell death of PMN, as high ROS levels were followed by high necrosis levels, but simultaneously highlights the difference between PMN populations used in the assay and the differences between the assays.

8.2.5 MPO inhibitor treatment did not inhibit necrosis *in vitro*

In conclusion, our data indicates that G-CSF matured bone marrow derived murine PMN are a stable and homogenous population, easy to generate in great numbers. They were further shown to have a high phagocytosis rate, show an upregulated CD11b and MPO expression, an elevated ROS production and finally succumb to a necrotic cell death upon Mtb infection, which reflect the phenotype of hPMN infected with Mtb *in vitro* [17]. Therefore, they represent a suitable population to analyse the effect of MPO inhibition upon Mtb infection in murine PMN *in vitro*.

Matured bone marrow derived PMN were infected with virulent Mtb and treated with the MPO inhibitors ABAH and AZD5904, which were used successfully to inhibit ROS production and necrosis in hPMN [17], [79], [173]. Both drugs are described to irreversible inhibit the enzyme. ABAH was described to be oxidized by active, ferric MPO, which subsequently keeps MPO in its inactive form 'Compound III' and finally leads to the functional loss of its haem group [174]. AZD5904 is described to form an adduct with the haem group of the enzyme, thereby inhibiting its function [175].

Based on these previous studies, it was surprising, that MPO inhibition resulted only in a small, but not significant reduction of ROS. Most importantly, MPO inhibition did not inhibit necrosis, which was in sharp contrast to the findings in hPMN (**Figure 6**) [17], [79]. Nevertheless, the MPO inhibition was in parts successful. Despite the inability to prevent necrosis, ABAH induced an irreversible inhibition of MPO activity in the supernatant. Intracellular enzyme activity was, however, not reduced. This effect has been seen before [76], and as there was only little MPO activity in the cell pellet, intracellular MPO activity seems to be neglectable in murine PMN (**Figure 19**).

On the contrary, AZD5904 did not reduce MPO activity, neither in the supernatant, nor intracellularly. This is in contrast to the manufacturer's description, that AZD5904 inhibits rodent PMN MPO to a comparable extend as hMPO (**Figure 19**). A possible explanation might be, that recombinant MPO was used for the manufacturer's studies, which might react differently than endogenous enzyme produced by PMN in cell culture. However, no publications can be found on murine PMN and AZD5904, leaving this assumption speculative. Despite a high degree of homology between murine and human MPO [176], some distinct morphological and structural features can be found between the species. Human anti-neutrophilic cytoplasmic autoantibodies (ANCA) against MPO do not cross react with rodent MPO and vice versa, which suggest epitopic determinants to be different between species [177]. Whether this affects binding and inhibition by the MPO inhibitors however, remains unanswered. Thus, further studies on the direct effect of MPO inhibitors on MPO and species related differences might be important, especially in the context of therapeutic development.

8.3 C3HeB/FeJ as a model for PMN targeting HDT

Despite the ineffective reduction of necrosis upon MPO inhibition *in vitro*, we observed significant inhibition of extracellular MPO activity upon ABAH treatment. As this might have a systemic effect on adjacent cells, we decided to test the effect of MPO inhibition *in vivo*. Further, other studies have shown the positive effects of MPO inhibition *in vivo* (**Table 4**). MPO has been identified as a key mediator of inflammation in experimental autoimmune encephalomyelitis (EAE), a murine model for multiple sclerosis, in which PMN, macrophages and microglia cells secrete MPO. MPO inhibition by ABAH was successfully used to reduce clinical EAE symptoms *in vivo*. Further, intracellular MPO was described as inactive until its release, indicating that an intracellular activity of MPO inhibitors might be

neglectable in this context [76]. Several other studies further confirmed the efficacy of ABAH. For example, a murine model of cerebral stroke also showed a positive effect upon ABAH induced MPO inhibition and improved subsequent cell proliferation and neurogenesis [178], [179].

AZD5904 has also been shown to be effective *in vitro* and *in vivo* for different types of diseases. For a while, it was tested with positive effects on human Parkinson patients [175]. In a model with 6-month smoke exposure of guinea pigs, different AZD5904 treatment regiments, lead to a significant decrease of protein oxidation markers [173]. Altogether this supports a possible positive effect of MPO inhibition *in vivo*, even though the inhibition was ineffective for PMN necrosis in *in vitro* assays.

Table 4 *In vivo* studies analysing the efficacy of MPO inhibition

Model		Drug	Effects	Literature
Mouse	Experimental autoimmune encephalomyelitis	ABAH	Reduced extracellular peroxidase activity	[76]
			Reduced tissue damage ad demyelination	
Mouse	Cerebral stroke	ABAH	Cell proliferation	[178]–[180]
			Neurogenesis	
Human	Parkinson	AZD5904	Reduction of disease related symptoms	[175]
Guinea pig	Smoke exposure	AZD5904	Decreased protein oxidation	
			Reduced hypertension	[173]

8.3.1 Comparison of different application routes and treatment schedules

The application route of drugs is a key component for *in vivo* treatment of animals and has to be chosen carefully. In order to analyse the effects of *in vivo* inhibition of MPO, Mtb infected C3HeB/FeJ mice were treated *intraperitoneally* with different dosages of ABAH dissolved in either DMSO or Captisol® starting at day 25 or 35 p.i., respectively. The distribution of the drug after *intraperitoneal* injection is parenteral (Greek: 'besides intestine'), meaning the drug does not have to pass the gastrointestinal tract. The administered substances are absorbed by vessels lining the peritoneum, like mesenteric vessels of the gastrointestinal tract before being disseminated systemically [181].

Comparison of the two *intraperitoneal* vehicle treated groups showed no major differences in weight loss and health scores, indicating that both vehicle substances can be equally used for this treatment, without obvious adverse effects (**Figure 23**). The slightly increased weight loss seen at the end of DMSO vehicle treatment is likely due to the progressed infection, as DMSO was used for the late treatment period from day 35 p.i. to 45 p.i. Nevertheless, neither different drug dosages nor changed treatment starts improved the health score or reduced bacterial burden or histopathological granuloma formation in these mice (**Figure 23**).

Although *intraperitoneal* administration is considered to be an easy and quick method to systemically apply drugs to an animal, this method has its disadvantages. The repeatedly injections can cause pain, tissue irritation, formation of fibrous tissue, and even infections. One study reported that 19,6% of *intraperitoneal* applied substances in rats are likely to be injected into the gastrointestinal tract, urine bladder, subcutaneously or retroperitoneally, despite competent staff executing the treatment [182]. However, despite needle-induced skin irritation no severe side-effects or dislocation of the drugs were observed in our hands upon *intraperitoneal* treatment, indicating a correct application.

In order to exclude application route dependent differences, C3HeB/FeJ mice were treated *per os* with the MPO inhibitors solved in Captisol® using oral gavage. This method is an enteral application, where the drugs are directly administered into the stomach of the animals, using a feeding tube. The absorption of drugs follows a similar pathway as for *intraperitoneally* drug administration. However, in contrast, the drugs have to pass the gastrointestinal tract, where they are absorbed by mesenteric vessels and pass through the liver, before being systemically distributed [181]. It has the advantage, that it is less painful for the animals, they can quickly adjust to this method and the drugs reach the intended location with more precision, as incorrect performed oral gavage would result in an immediate death by suffocation.

Nevertheless, *per os* MPO inhibitor treated animals showed no increase in the health score or reduced weight loss (**Figure 26**). Further, no reduction of the bacterial burden, PMN MPO activity, PMN necrosis or PMN ROS production could be observed. In contrast, ROS production and necrosis were even enhanced in lung resident PMN (**Figure 32**). This still might indicate, that the level of ROS does correlate with necrosis. However, because the inhibition of MPO did not reduce ROS levels, the murine ROS production seems to be rather independent of MPO or may have another cause, which will be discussed below in more

detail. Although MPO expression was reduced in lung PMN (**Figure 32**), extracellular MPO concentrations were slightly elevated (**Figure 34**), indicating an increased degranulation upon MPO inhibitor treatment. Based on the decreased MPO activity, observed upon MPO inhibitor treatment *in vitro*, it was highly unexpected not to see a reduction of extracellular MPO activity at day 35 p.i. at all. Further, no differences in cytokine expression could be observed upon *per os* MPO inhibitor treatment (**Figure 38**). Thus, the complete failure to reduce MPO activity and the lacking effect on other immune responses, indicates a possible ineffectiveness of the MPO inhibitors *in vivo*. This was unexpected, as the protocol and solvents for ABAH treatment have been established earlier [76], [178], [180] and the protocols used during this study were based on these publications. Thus, it seems unlikely that the absence of MPO inhibition is due to the application route or the vehicle used or its concentration. Therefore, another likely explanation is a wrong treatment start. This is also indicated by the enhanced LDH activity in the lung at day 25 p.i. compared to day 35 pi., at which the overall necrosis level was significantly lower (**Figure 33**). It seems like PMN induced necrosis peaks at an earlier time point and a more detailed analysis of disease development of a Mtb infection in C3HeB/FeJ mice could be required to answer these questions. We aimed to start treatment with the onset of chronic inflammatory responses. As discussed before, the first two weeks of infection are described to be similar between different mouse strains [110]. The onset of Mtb induced necrosis and leukocyte influx in C3HeB/FeJ start around day 30 p.i. [115], which is why the treatment start was set around that date. It might be more beneficial to inhibit MPO as early as at the initial onset of cellular recruitment and necrosis, e.g. day 15 p.i., to prevent subsequent pathology and tissue destruction. However, whether this is preventable in murine TB using MPO inhibition, remains questionable, as no reduction in MPO activity and necrosis was seen *in vitro* and *in vivo* upon MPO inhibitor treatment.

8.3.2 Immune response to a HDT using MPO inhibition and INH treatment

The classical host directed therapy (HDT) combines antimicrobial drug administration with treatment targeting the hosts immune system. Usually HDT aims to reduce inflammatory processes. Thus, we combined our approach of MPO inhibition with additional, low dose isoniazid (INH) co-treatment of 10 mg/kg in order to analyse effects, that might arise from the combination of HDT and classical antibiotic treatment. It has been shown before, that combination of anti-inflammatory and INH treatment enhance and improve effects of a HDT

drug. For example, a study showed, that targeting the release of cAMP by macrophages, a signalling molecule, that increases inflammatory cytokine levels, was only effective upon combination with INH treatment [183]. In contrast, the combination of different treatments can also result in a worsened outcome, as for example aspirin antagonized clearance of bacteria from the lung by INH when co-administered, while Ibuprofen did not cause this effect [184]. Usually INH is administered at 25 to 50 mg/kg [133], [134], [183]. The low-dose antibiotic treatment was chosen, to reduce the effects of the antibiotic which might mask effects of the MPO inhibitors. In turn, the moderate antibiotic pressure might improve effects from MPO inhibitors.

However, the additional antibiotic treatment could not improve treatment outcome. The health scores were not improved and although a reduction in CFU was seen for INH treated animals, this was solely based upon the antibiotic, as co-treatment of INH and MPO inhibitors fail to reduce the bacterial burden further (**Figure 30**). Additionally, the frequency of PMN, MPO expressing PMN and ROS producing PMN in the lungs of INH co-treated mice were found to be on the level of Captisol® vehicle treated mice, indicating no additional effects on the PMN response by the INH treatment (**Figure 32**). The same result was seen for MPO concentrations and activity in different organ samples. Only the extracellular lung MPO activity was slightly reduced in INH co-treated mice, but not in a significant manner (**Figure 34**).

The cellular immune response revealed some interesting alterations. Compared to animals that were only treated with MPO inhibitors, differences were found in the recruitment of other cell populations when INH treatment was included. The frequency of DCs was significantly reduced, while the frequency of alveolar macrophages was elevated upon additional INH treatment (**Figure 35**). Again, this was solely based on the INH treatment and not the combined HDT. The frequency of interstitial macrophages and NK cells, adaptive $CD4^+$, $CD8^+$ and NK T cells was, however, similar in all groups, independent of the applied treatment (**Figure 35, Figure 36**).

The lower number of the major antigen presenting cell population in INH treated mice might explain differences found in the activation of lymphocytes. Only MPO inhibitor treated mice showed an enhanced frequency of activated $CD4^+$ and $CD8^+$ T cell, while animals that received additional INH treatment did not show these effects (**Figure 36**). The enhanced activation of lymphocytes in MPO inhibitor treated animals was further reflected in an elevated production of IFNγ and TNFα upon re-stimulation. Of note, this increased cytokine

expression was also seen in Captisol® vehicle treated animals. In contrast, all INH treated animals had very low IFNγ and TNFα expressing T cell populations (**Figure 37**).

Taken together, this study could not show a beneficial effect using the combined HDT using MPO inhibition and INH treatment. Although the antibiotic treatment reduced the bacterial burden in the lung, PMN responses were not changed. Further, the adaptive immune response seemed to be impaired, shown by reduced T cell activation, which might lead to subsequent defects in clearing the infection, as T cell responses are essential for Mtb elimination [25], [185]. Conclusively, this data points towards a rather supressing effect by INH on the adaptive immunity, that was independent of additional MPO inhibition. Indeed, the reduced frequency of activated T cells in INH treated mice was described before. The antibiotic treatment with INH especially drove spleen derived, activated $CD4^+$ T cells into early cell death and, thus significantly reduced antibody mediated immune responses [186], which might explain the effects seen in our study.

8.3.3 MPO as a systemic, multifunctional player in shaping the immune response

The use of a different model organism might be helpful to further analyse the effect of MPO inhibition *in vivo*, while mice might not be a suitable model to target PMN in TB. The MPO activity in mice is significantly lower compared to hPMN, which is around 109 Units/$5x10^6$ cells. In comparison, C57 mice have an MPO activity of 20 Units/$5x10^6$ cells. However, none of the currently used model organisms has a similar high MPO activity of PMN like humans. Guinea pigs show an activity of 11 Units/$5x10^6$ cells and rabbits of 13 Units/$5x10^6$ cells. Not even human primates like rhesus monkeys showed a comparable MPO activity with only 38 Units/$5x10^6$ cells. Interestingly, squirrels (127 Units/$5x10^6$ cells) and dogs (95 Units/$5x10^6$ cells) have a comparable activity [187]. However, these species are not established models for pulmonary TB.

Besides the primary ROS producing activity of MPO, the enzyme executes a variety of different immune functions. For example, MPO can function as a host derived antigen for T cells in human and mouse. This is highlighted by the presence of anti-neutrophilic cytoplasmic antibodies (ANCA). As the name indicates, ANCA are antibodies targeting host derived cytoplasmic neutrophilic antigens like MPO or proteinase 3. Their occurrence is usually associated with autoimmune disorders like systemic vasculitis, which is an inflammation of blood vessels. In mouse and human systemic vasculitis, autoreactive anti-

MPO specific $CD4^+$ T cells were found, that proliferate in the presence of MPO and further induce MPO-ANCA production [188], [189]. In another model for glomerulonephritis, an inflammation of small vessels in the kidney, MPO immunized mice showed an Il-17A driven pathology, which was characterized by proliferation of $CD4^+$ T cells, elevated pro-inflammatory cytokines, recruitment of PMN and injurious effector macrophages [190].

In other situations, MPO did not act as autoantigen and was inhibiting inflammatory immune responses. Extracellular MPO was found to be able to suppress DC activation, which in turn downregulated T cell responses in the lymph nodes of mice [191]. Additionally, in a model of experimentally induced lupus nephritis, MPO KO mice showed an elevated inflammatory response, which was also associated with an increased $CD4^+$ T cell activity and proinflammatory cytokine production, suggesting an immune regulatory mechanism by MPO [192]. This is further supported by an increased susceptibility to develop systemic lupus erythematosus in humans, that express a G-463A allele, which is associated with a lower expression of MPO [193].

In this study, the use of MPO inhibitors enhanced the overall concentration of MPO in the lung of infected mice and additionally increased the activity and cytokine production of $CD4^+$ and $CD8^+$ T cells, while the frequency of DCs remained on the level of untreated mice. In INH treated mice, the overall concentration of MPO was reduced and no increased lymphocyte activation could be observed. For the situation of TB infected mice, this might point towards an autogenic function for MPO, rather than executing ROS production effector functions. However, the analysis in this study did not focus on this aspect of MPO function and further studies would be required to answer the upcoming questions.

8.3.4 Nitric oxide as the major effector molecules in the murine model

One likely explanation for the contradicting results seen in this study for MPO inhibition, might be based upon species dependent differences in gene expression and effector molecules of PMN in humans vs. mice. In hPMN, the enzyme activity of MPO is 5 times higher than in mice [187], suggesting an inferior role for MPO in the production of ROS in murine cells. Further, we used DHR123, a non-fluorescent molecule, to analyse ROS production. The molecule penetrates the cell membranes and localizes in the mitochondria. As a result of oxidative chemical reaction, DHR123 is reduced to rhodamine 123, which then becomes fluorescent. The reaction is not only induced by ROS, but also by reactive nitrogen intermediates (RNI) and a separation between the oxidative reagents is not possible

with this technique [194]. RNI are generated by a family of isoenzymes, called NO synthases (iNOS) and are a second unspecific, innate defence mechanism, that targets pathogen DNA, lipids and proteins.

In humans, RNI were previously described as vasodilating effector molecules relatively absent in monocytes and PMN of healthy patients [195]. However, RNI can be elevated in PMN upon inflammation, like in the context of cirrhosis [196] or upon bacterial infection, for example in patients with urinary tract infections [197]. Nevertheless, the contribution of RNI for the clearance of Mtb in human is usually solely attributed to macrophages and regarded as minor defence mechanism in hPMN [198].

In murine models of TB, however, reactive RNI play a more relevant role than ROS. In macrophages from mice that carried a genetic disruption of the $gp91^{phox}$ subunit of NADPH oxidase, which prevented ROS production, Mtb growth was elevated. Stimulation of these macrophages with IFNγ restored their ability to kill the pathogens, yet in an RNI dependent manner. In support, macrophages from iNOS KO mice were unable to contain the infection despite IFNγ stimulation [199]. Further, studies with *gp91*$^{phox-/-}$ and $NOS2^{-/-}$ mice showed that each system can compensate the other to a certain extent, as these models rarely develop spontaneous infections. However, during an infection with Mtb, a defect in iNOS leads to a rapid growth and subsequent killing of the mice while a defect in ROS production only had minor effect on the outcome, compared to wildtype mice [199], [200].

Strikingly, MPO inhibition was mainly tested in chronic inflammatory autoimmune diseases, while studies on infectious diseases are rare and often suggest a beneficial effect of MPO activity during infections. Indeed, one study on amoebic liver abscess in hamster questions the efficacy of MPO inhibition in the context of an infectious disease. The hepatic abscesses induced by *Entamoeba histolytica* (*E. histolytica*) shares some features that also drive an Mtb infection. The inflammatory pathology in susceptible animals was shown to be driven by PMN necrosis [201]. However, total depletion of PMN did not protect SCID mice from increased abscesses and further, resistant animals cleared the infection in a PMN dependent way, highlighting that a carefully balanced PMN response is essential [202]. During the course of infection of a susceptible hamster model with *E. histolytica* MPO was reduced, while resistant BALB/c mice, showed an increasing MPO kinetic. Interestingly, ABAH treatment did not reduce lesion size in the susceptible hamster model. However, BALB/c mice showed increased lesions and less damaged amoebas upon ABAH treatment. Despite the species dependent differences that have to be considered, the study concludes a

protective effect of MPO [203]. However, *E. histolytica* infections have a significantly reduced infection time of less than 48h, and are rather acute, than chronic, which differentiates them from Mtb infections. Nevertheless, the results indicate an importance of murine MPO early in infectious diseases. This is supported by findings on $p47^{phox}$ KO mice, that lack the ability to produce ROS due to a defect in the NADPH oxidase. These mice were unable to control increased bacterial growth during the initial phase after an aerosol infection. Interestingly, this initial detriment is overwritten, as soon as the IFNγ response initiates macrophage activation [204].

Nevertheless, the increased ROS production in lung PMN in infected mice, might be based on RNI induced rhodamine 123 fluorescence and indicate a compensatory mechanism for the MPO inhibition reduced ROS production and a minor role for MPO. This might further explain the increased necrosis, which in this situation might be based on the elevated RNI levels, and why the inhibition of MPO could not prevent this. Analysis of RNI production in different organs might answer this hypothesis.

8.4 Conclusion & outlook

For the first time, the lipidome of hPMN and the effects on the lipid composition of a Mtb induced, necrotic cell death were analysed. Using mass spectrometry, a reduction in TAGs was detected at 2 hpi upon Mtb infection. Treatment with the MPO inhibitor ABAH abrogated this reduction. However, this effect was seen before necrosis became evident and has therefore a different cause, unrelated to the cell death. TAGs are an important carbon and energy source for Mtb [93]–[95]. Active MPO or its products seems to be beneficial for Mtb facilitating access and lipid metabolizing, before the MPO products play a role in necrosis. At 6 hpi, ABAH treatment reduced the amount of cholesterol in infected hPMN. This is potentially linked to the cell's death. Apoptosis encloses the mycobacteria in vesicles, with may limited energy sources in the same way as seen in phagolysosomes in activated macrophages [149]. Cholesterol is usually accessed upon environmental pressure and the observed reduction could be a coping mechanism of Mtb to restricted nutrients in apoptotic vesicles. Conclusively, the data indicate a metabolization of host cell lipids almost immediate after infection. However, further studies are required to fully understand the lipid metabolizing processes occurring during an Mtb infection.

The translation of the findings in hPMN of an Mtb induced, MPO dependent, ROS driven necrotic cell death into a murine model, was facing some challenges. Murine PMN populations isolated from different organs showed great variations, regarding their effector functions upon a mycobacterial infection. Unmatured bone marrow derived PMN have a limited phagocytic ability and ROS production upon a mycobacterial infection. Maturation of bone marrow cells with murine G-CSF significantly increased these effector functions and drove the cells into necrotic cell death. Blood derived PMN were comparable to matured bone marrow derived PMN, but they can only be harvested in small numbers and showed greater inter experimental variances. This study shows, that murine PNM populations have distinct effector functions and highlights that these cell populations require further characterization to improve understanding of PMN development.

The inhibition of MPO in murine PMN had no effect on necrosis reduction *in vitro* and *in vivo*. Of note, neither *intraperitoneally* nor *per os* treatment was effective. No improvement of the health score, the pathology or a reduction of the MPO activity was detected in the organs of infected and ABAH treated mice. In contrast, MPO inhibition lead to an increased MPO extracellular protein concentrations and increased frequency of activated T cells. This might be connected and suggest an antigenic purpose of MPO in this context, where MPO increases the adaptive immune response in an ANCA dependent way, like seen in other models [188], [189]. However, to support this hypothesis a closer analysis of the adaptive immune response has to be conducted, like the evaluation of the frequency of MPO specific T cells and an analysis of ANCA levels in the animals.

The antibacterial INH treatment with or without MPO inhibitors, did reduce bacterial burden in a MPO inhibitor independent way, but failed to improve other measures of pathology. It even reduced activation of T cells in the lung. Because this effect has been described before, it would be important to further investigate the effects of INH treatment on the immune system. Especially, as an impairment of the adaptive immune response against Mtb could lead to severe constrains in long term clearance of the pathogen [25], [26].

Flow cytometry showed an enhanced frequency of rhodamine 123 positive and necrotic lung PMN upon MPO inhibitor treatment. In hPMN, ABAH treatment significantly reduced fluorescence of rhodamine 123 (unpublished data from our group), indicating, that the majority of oxidative intermediates in hPMN are ROS. The fluorescence detected in murine PMN this study, might be based upon the reactivity of DHR123 with RNI [194]. Thus, either

a compensation of ROS by RNI is more pronounced in mice than in hPMN or ROS play in general a minor role in antimicrobial murine PMN effector mechanisms. A thorough analysis of RNI production and underlying mechanisms in mice could answer this question. The inhibition of RNI production or the use of KO models could be a useful tool in this situation. Further, immunohistochemistry or detection of RNI levels in organs from these mice might be helpful.

Conclusively, based on the differences observed upon MPO inhibition in human and murine PMN, this study cannot exclude a beneficial effect of MPO inhibition for humans and other experimental analyses have to be conducted to answer this question. Thus, despite a human like pathology, marked by increased PMN accumulation and necrotizing granuloma in susceptible C3HeB/FeJ mice, this study provides strong evidence of fundamental, species dependent differences with regard to MPO inhibitory effects on necrotic cell death during TB.

9 ABBREVIATIONS

ABAH	Aminobenzoicacidhydrazide
AcOH	Acetic acid
APC	Allophycocyanin
Aqua det.	Aqua destillata
bm	Bone marrow
BSA	Bovine serum albumin
BV	Brilliant violet
Ca	Calcium
CCL	C-C-chemokine ligand
CER	Ceramide
$CHCl_3$	Chloroform
CE	Cholesteryl ester
CD	Cluster of differentiation
CFU	Colony forming units
Cy7	Cyanine-7
CXCL	C-X-C motif chemokine ligand
DHR123	Dihydrorhodamine 123
dsRed	*Discosoma* red
Na_2HPO	Disodium phosphate
ESAT-6	Early secretec antigenic target-6
ELISA	Enzyme-linked immunosorbent assay
EtOH	Ethanol
e.g.	Exempli gratia; for example
XDR-TB	Extensively drug-resistant Tuberculosis
FITC	Fluorescein
FACS	Fluorescence activated cell sortening
xg	G force
G	Gauge
g	Gramm
G-CSF	Granulocyte colony stimulating factor
h	Hour
hpi	Hours post infection
HCL	Hydrochloride
H2SO	Hydrogen thioperoxide
ICAM	Inter cellular adhesion molecule 1
IFNγ	Interferon gamma
IL	Interleukin
i.p.	*intraperitoneal*
KCl	Kaliumchloride
$KHCO_3$	Kaliumhydrogencarbonat
KO	Knock out
LDH	Lactatedehydrogenase
LC	Liquid chromatography
L	Liter
MAC1	Macrophage-1 antigen
Mg	Magnesium

MS	Mass spectrometry
MSD	Meso scale discovery
m	Meter
MeOH	Methanol
MTBE	Methyl-*tert*-butyl ether
µ	Micro
mL	Milliliter
min	Minute
M	Mol
KH_2PO_4	Monopotassium phosphate
MDR-TB	Multidrug-resistant Tuberculosis
Mtb	*Mycobacterium tuberculosis*
MTBC	Mycobaterium tuberculosis complex
MPO	Myeloperoxidase
NaN3	Natriumazide
NaCl	Natriumchloride
NaCl	Natriumchloride
$NaHCO_3$	Natriumhydrogencarbonat
NaOH	Natriumhydroxid
No.	Number
oN	Over night
PBS	Phosphate buffered saline
Pe	Phytoerythrin
PerCP	Peridinin chlorophyll
PG	Phosphatidylglycerol
p.i.	post infection
PMN	Polymorphal mononuclear neutrophils
Rb	Rabbit
RT	Room temperature
RPMI	Roswell park memorial institue
Nacl	Sodium chloride
$C_3H_3NaO_3$	Sodium pyruvate
sp.	Species
TAG	Triacylglycerols
TBS	Tris-buffered saline
TNF	Tumor necrosis factor
w/o	Without
ZN	Ziehl-neelson

10 LITERATURE

[1] World Health Organization, “Global Tuberculosis Report,” vol. 53, no. 9, 2020.

[2] T. M. Daniel and P. A. Iversen, “Hippocrates and tuberculosis,” *Int. J. Tuberc. Lung Dis.*, vol. 19, no. 4, pp. 373–374, 2015.

[3] I. Barberis, N. L. Bragazzi, L. Galluzzo, and M. Martini, “The history of tuberculosis: from the first historical records to the isolation of Koch’s bacillus,” 2017.

[4] M. Martini, N. Riccardi, A. Giacomelli, V. Gazzaniga, and G. Besozzi, “Tuberculosis: an ancient disease that remains a medical, social, economical and ethical issue.”

[5] R. Koch, *The etiology of tuberculosis*, 15th ed. Berliner Klinische Wochenschrift, 1882.

[6] J. P. Cegielski and D. N. McMurray, “The relationship between malnutrition and tuberculosis: Evidence from studies in humans and experimental animals,” *International Journal of Tuberculosis and Lung Disease*, vol. 8, no. 3. International Union Against Tuberculosis and Lung Disease, pp. 286–298, 2004.

[7] W. Kimbrough, V. Saliba, M. Dahab, C. Haskew, and F. Checchi, “The burden of tuberculosis in crisis-affected populations: a systematic review.,” *Lancet. Infect. Dis.*, vol. 12, no. 12, pp. 950–65, Dec. 2012.

[8] V. Eldholm *et al.*, “Armed conflict and population displacement as drivers of the evolution and dispersal of Mycobacterium tuberculosis,” *Proc. Natl. Acad. Sci. U. S. A.*, vol. 113, no. 48, pp. 13881–13886, Nov. 2016.

[9] M. B. Ismail, R. Rafei, F. Dabboussi, and M. Hamze, “Tuberculosis, war, and refugees: Spotlight on the Syrian humanitarian crisis Armed conflicts and forced population displacements markedly increase TB risk and selection of TB-resistant forms,” 2018.

[10] P. Nahid *et al.*, “Treatment of drug-resistant tuberculosis an official ATS/CDC/ERS/IDSA clinical practice guideline,” *Am. J. Respir. Crit. Care Med.*, vol. 200, no. 10, pp. E93–E142, Nov. 2019.

[11] World Health Organization, *Global TB report 2019*. 2019.

[12] K. A. Abrahams and G. S. Besra, “Mycobacterial cell wall biosynthesis: a multifaceted antibiotic target,” 2016.

[13] M. de Martino, L. Lodi, L. Galli, and E. Chiappini, “Immune Response to Mycobacterium tuberculosis: A Narrative Review,” *Front. Pediatr.*, vol. 7, p. 350, Aug. 2019.

[14] S. M. Behar *et al.*, “Apoptosis is an innate defense function of macrophages against Mycobacterium tuberculosis,” *Mucosal Immunology*, vol. 4, no. 3. Nature Publishing Group, pp. 279–287, 09-May-2011.

[15] H. E. Volkman, T. C. Pozos, J. Zheng, J. M. Davis, J. F. Rawls, and L. Ramakrishnan, “Tuberculous granuloma induction via interaction of a bacterial secreted protein with host epithelium,” *Science (80-.).*, vol. 327, no. 5964, pp. 466–469, Jan. 2010.

[16] M. I. Gröschel, F. Sayes, R. Simeone, L. Majlessi, and R. Brosch, “ESX secretion systems: Mycobacterial evolution to counter host immunity,” *Nature Reviews Microbiology*, vol. 14, no. 11. Nature Publishing Group, pp. 677–691, 01-Nov-2016.

[17] T. Dallenga *et al.*, “M. tuberculosis-Induced Necrosis of Infected Neutrophils Promotes Bacterial Growth Following Phagocytosis by Macrophages,” *Cell Host Microbe*, vol. 22, no. 4, pp. 519-530.e3, 2017.

[18] M. G. Harisinghani, T. C. McLoud, J. A. O. Shepard, J. P. Ko, M. M. Shroff, and P. R. Mueller, “Tuberculosis from head to toe,” *Radiographics*, vol. 20, no. 2, pp. 449–470, 2000.

[19] M. Akhtar and A. M. Hadeel, “Pathology of Tuberculosis,” *Tuberculosis*, pp. 153–161, 2004.

[20] L. Kozakiewicz, J. Phuah, J. Flynn, and J. Chan, “The role of B cells and humoral immunity in mycobacterium Tuberculosis infection,” *Adv. Exp. Med. Biol.*, vol. 783, pp. 225–250, 2013.

[21] D. SMITH, H. HÄNSCH, G. BANCROFT, and S. EHLERS, “T-cell-independent granuloma formation in response to *Mycobacterium avium* : role of tumour necrosis factor-α and interferon-γ,” *Immunology*, vol. 92, no. 4, pp. 413–421, Dec. 1997.

[22] J. L. Flynn and J. D. Ernst, “Immune responses in tuberculosis,” *Curr. Opin. Immunol.*, vol. 12, no. 4, pp. 432–436, 2000.

[23] S. Ehlers and U. E. Schaible, “The granuloma in tuberculosis: Dynamics of a host-pathogen collusion,” *Front. Immunol.*, vol. 3, no. JAN, pp. 1–9, 2012.

[24] D. V. Havlir and P. F. Barnes, “Tuberculosis in patients with human immunodeficiency virus infection,” *New England Journal of Medicine*, vol. 340, no. 5. Massachusetts Medical Society , p. 367, 04-Feb-1999.

[25] A. M. Cooper, “Cell-mediated immune responses in tuberculosis,” *Annual Review of Immunology*, vol. 27. NIH Public Access, pp. 393–422, 2009.

[26] D. H. Canaday, R. J. Wilkinson, Q. Li, C. V. Harding, R. F. Silver, and W. H. Boom, “ CD4 + and CD8 + T Cells Kill Intracellular Mycobacterium tuberculosis by a Perforin and Fas/Fas Ligand-Independent Mechanism ,” *J. Immunol.*, vol. 167, no. 5, pp. 2734–2742, Sep. 2001.

[27] M. Gonzalez-Juarrero, O. C. Turner, J. Turner, P. Marietta, J. V. Brooks, and I. M. Orme, “Temporal and spatial arrangement of lymphocytes within lung granulomas induced by aerosol infection with Mycobacterium tuberculosis,” *Infect. Immun.*, vol. 69, no. 3, pp. 1722–1728, Mar. 2001.

[28] D. Ordway *et al.*, “ The Cellular Immune Response to Mycobacterium tuberculosis Infection in the Guinea Pig ,” *J. Immunol.*, vol. 179, no. 4, pp. 2532–2541, Aug. 2007.

[29] P. J. Maglione, J. Xu, A. Casadevall, and J. Chan, “ Fcγ Receptors Regulate Immune Activation and Susceptibility during Mycobacterium tuberculosis Infection ,” *J. Immunol.*, vol. 180, no. 5, pp. 3329–3338, Mar. 2008.

[30] M. Guilliams, P. Bruhns, Y. Saeys, H. Hammad, and B. N. Lambrecht, “The function of Fcγ receptors in dendritic cells and macrophages,” *Nature Reviews Immunology*, vol. 14, no. 2. Nat Rev Immunol, pp. 94–108, Feb-2014.

[31] S. De Vallière, G. Abate, A. Blazevic, R. M. Heuertz, and D. F. Hoft, “Enhancement of innate and cell-mediated immunity by antimycobacterial antibodies,” *Infect. Immun.*, vol. 73, no. 10, pp. 6711–6720, Oct. 2005.

[32] S. K. Kumar, P. Singh, and S. Sinha, “Naturally produced opsonizing antibodies restrict the survival of Mycobacterium tuberculosis in human macrophages by augmenting phagosome maturation,” *Open Biol.*, vol. 5, no. 12, 2015.

[33] L. Encinales *et al.*, “Humoral immunity in tuberculin skin test anergy and its role in

high-risk persons exposed to active tuberculosis," *Mol. Immunol.*, vol. 47, no. 5, pp. 1066–1073, Feb. 2010.

[34] S. Balu *et al.*, "A Novel Human IgA Monoclonal Antibody Protects against Tuberculosis," *J. Immunol.*, vol. 186, no. 5, pp. 3113–3119, Mar. 2011.

[35] N. Olivares *et al.*, "Prophylactic effect of administration of human gamma globulins in a mouse model of tuberculosis," *Tuberculosis*, vol. 89, no. 3, pp. 218–220, May 2009.

[36] J. A. L. Flynn *et al.*, "Tumor necrosis factor-α is required in the protective immune response against mycobacterium tuberculosis in mice," *Immunity*, vol. 2, no. 6, pp. 561–572, 1995.

[37] K. Kasahara, I. Sato, K. Ogura, H. Takeuchi, K. Kobayashi, and M. Adachi, "Expression of Chemokines and Induction of Rapid Cell Death in Human Blood Neutrophils by Mycobacterium tuberculosis."

[38] M. Alemán *et al.*, "Activation of peripheral blood neutrophils from patients with active advanced tuberculosis," *Clin. Immunol.*, vol. 100, no. 1, pp. 87–95, 2001.

[39] A. Dorhoi, M. Iannaccone, J. Maertzdorf, G. Nouailles, J. Weiner, and S. H. E. Kaufmann, "Reverse translation in tuberculosis: Neutrophils provide clues for understanding development of active disease," *Frontiers in Immunology*, vol. 5, no. FEB. Frontiers Research Foundation, 2014.

[40] P. E. Newburger and D. C. Dale, "Evaluation and Management of Patients with Isolated Neutropenia," 2013.

[41] D. Kreisel *et al.*, "In vivo two-photon imaging reveals monocyte-dependent neutrophil extravasation during pulmonary inflammation," *Proc. Natl. Acad. Sci. U. S. A.*, vol. 107, no. 42, pp. 18073–18078, Oct. 2010.

[42] E. Kolaczkowska and P. Kubes, "Neutrophil recruitment and function in health and inflammation," *Nature Reviews Immunology*, vol. 13, no. 3. Nature Publishing Group, pp. 159–175, 25-Mar-2013.

[43] T. N. Mayadas, X. Cullere, and C. A. Lowell, "The Multifaceted Functions of Neutrophils," *Annu. Rev. Pathol. Mech. Dis*, vol. 9, pp. 181–218, 2014.

[44] S. Geng *et al.*, "Emergence, origin, and function of neutrophil-dendritic cell hybrids in experimentally induced inflammatory lesions in mice," *Blood*, vol. 121, no. 10,

pp. 1690–1700, Mar. 2013.

[45] H. Matsushima *et al.*, "Neutrophil differentiation into a unique hybrid population exhibiting dual phenotype and functionality of neutrophils and dendritic cells," *Blood*, vol. 121, no. 10, pp. 1677–1689, Mar. 2013.

[46] I. Puga *et al.*, "B cell-helper neutrophils stimulate the diversification and production of immunoglobulin in the marginal zone of the spleen," *Nat. Immunol.*, vol. 13, no. 2, pp. 170–180, Feb. 2012.

[47] B. N. Jaeger *et al.*, "Neutrophil depletion impairs natural killer cell maturation, function, and homeostasis," *J. Exp. Med.*, vol. 209, no. 3, pp. 565–580, Mar. 2012.

[48] C. J. Darcy *et al.*, "Neutrophils with myeloid derived suppressor function deplete arginine and constrain T cell function in septic shock patients," 2014.

[49] C. T. N. Pham, "Neutrophil serine proteases fine-tune the inflammatory response," *International Journal of Biochemistry and Cell Biology*, vol. 40, no. 6–7. NIH Public Access, pp. 1317–1333, Jun-2008.

[50] Y. Zhang *et al.*, "Enhanced interleukin-8 release and gene expression in macrophages after exposure to Mycobacterium tuberculosis and its components," *J. Clin. Invest.*, vol. 95, no. 2, pp. 586–592, 1995.

[51] M. Phillipson and P. Kubes, "The neutrophil in vascular inflammation," *Nature Medicine*, vol. 17, no. 11. Nat Med, pp. 1381–1390, Nov-2011.

[52] K. Ley, C. Laudanna, M. I. Cybulsky, and S. Nourshargh, "Getting to the site of inflammation: The leukocyte adhesion cascade updated," *Nature Reviews Immunology*, vol. 7, no. 9. Nature Publishing Group, pp. 678–689, Sep-2007.

[53] P. M. Murphy, "The molecular biology of leukocyte chemoattractant receptors," *Annual Review of Immunology*, vol. 12. Annual Reviews Inc., pp. 593–633, 1994.

[54] J. G. HIRSCH and Z. A. COHN, "Degranulation of polymorphonuclear leucocytes following phagocytosis of microorganisms.," *J. Exp. Med.*, vol. 112, no. 6, pp. 1005–1014, 1960.

[55] G. Weiss and U. E. Schaible, "Macrophage defense mechanisms against intracellular bacteria," *Immunol. Rev.*, vol. 264, no. 1, pp. 182–203, 2015.

[56] S. R. Coughlin and E. Camerer, "PARticipation in inflammation," *Journal of*

Clinical Investigation, vol. 111, no. 1. The American Society for Clinical Investigation, pp. 25–27, 2003.

[57] A. Belaaouaj *et al.*, "Mice lacking neutrophil elastase reveal impaired host defense against gram negative bacterial sepsis," *Nat. Med.*, vol. 4, no. 5, pp. 615–618, May 1998.

[58] E. P. Reeves *et al.*, "Killing activity of neutrophils is mediated through activation of proteases by K+ flux," *Nature*, vol. 416, no. 6878, pp. 291–297, 2002.

[59] D. L. Carden and R. J. Korthuis, "Protease inhibition attenuates microvascular dysfunction in postischemic skeletal muscle," *Am. J. Physiol. - Hear. Circ. Physiol.*, vol. 271, no. 5 40-5, 1996.

[60] J. A. Delyani, T. Murohara, and A. M. Lefer, "Novel recombinant serpin, LEX-032, attenuates myocardial reperfusion injury in cats," *Am. J. Physiol. - Hear. Circ. Physiol.*, vol. 270, no. 3 39-3, 1996.

[61] S. Pierre Benoit Champagne, P. Tremblay, and A. Cantin, "Neutrophil Elastase Proteolytic Cleavage of ICAM-1 by Human," 1998.

[62] O. Robledo *et al.*, "ICAM-1 isoforms: specific activity and sensitivity to cleavage by leukocyte elastase and cathepsin G," *Eur. J. Immunol.*, vol. 33, no. 5, pp. 1351–1360, May 2003.

[63] N. Shimoda, N. Fukazawa, K. Nonomura, and R. L. Fairchild, "Cathepsin G Is Required for Sustained Inflammation and Tissue Injury after Reperfusion of Ischemic Kidneys," *Cell Inj.*, vol. 170, pp. 930–940, 2007.

[64] J. F. Chmiel and P. B. Davis, "State of the art: Why do the lungs of patients with cystic fibrosis become infected and why can't they clear the infection?," *Respiratory Research*, vol. 4, no. 1. Respir Res, 27-Aug-2003.

[65] C. C. Taggart, C. M. Greene, T. P. Carroll, S. J. O'Neill, and N. G. McElvaney, "Elastolytic proteases: Inflammation resolution and dysregulation in chronic infective lung disease," *American Journal of Respiratory and Critical Care Medicine*, vol. 171, no. 10. American Thoracic Society, pp. 1070–1076, 15-May-2005.

[66] T. J. Moraes *et al.*, "Abnormalities in the pulmonary innate immune system in cystic fibrosis," *Am. J. Respir. Cell Mol. Biol.*, vol. 34, no. 3, pp. 364–374, Mar. 2006.

[67] C. Benarafa, G. P. Priebe, and E. Remold-O'Donnell, "The neutrophil serine protease inhibitor serpinb1 preserves lung defense functions in Pseudomonas aeruginosa infection," *J. Exp. Med.*, vol. 204, no. 8, pp. 1901–1909, Aug. 2007.

[68] B. S. van der Veen, M. P. de Winther, and P. Heeringa, "Myeloperoxidase: molecular mechanisms of action and their relevance to human health and disease," *Antioxidants Redox Signal.*, vol. 11, no. 11, pp. 2899–2937, 2009.

[69] J. Bylund, K. L. Brown, C. Movitz, C. Dahlgren, and A. Karlsson, "Intracellular generation of superoxide by the phagocyte NADPH oxidase: How, where, and what for?," *Free Radic. Biol. Med.*, vol. 49, no. 12, pp. 1834–1845, 2010.

[70] L. A. Marquez, J. T. Huang, and H. B. Dunford, "Spectral and Kinetic Studies on the Formation of Myeloperoxidase Compounds I and II: Roles of Hydrogen Peroxide and Superoxide1," 1994.

[71] P. G. Furtmuller, U. Burner, and C. Obinger, "Reaction of myeloperoxidase compound I with chloride, bromide, iodide, and thiocyanate," *Biochemistry*, vol. 37, no. 51, pp. 17923–17930, 1998.

[72] S. J. Klebanoff, "Myeloperoxidase : friend and foe," *J. Leukoc. Biol.*, vol. 77, no. 5, pp. 598–625, 2005.

[73] J. M. Albrich, J. H. Gilbaugh, K. B. Callahan, and J. K. Hurst, "Effects of the putative neutrophil-generated toxin, hypochlorous acid, on membrane permeability and transport systems of Escherichia coli," *J. Clin. Invest.*, vol. 78, no. 1, pp. 177–184, 1986.

[74] W. M. Nauseef, "How human neutrophils kill and degrade microbes: an integrated view," *Immunol. Rev.*, vol. 219, no. 1, pp. 88–102, Oct. 2007.

[75] F. C. Fang, "Antimicrobial reactive oxygen and nitrogen species: Concepts and controversies," *Nature Reviews Microbiology*, vol. 2, no. 10. Nature Publishing Group, pp. 820–832, Oct-2004.

[76] R. Forghani *et al.*, "Demyelinating Diseases : Myeloperoxidase as an Imaging," *Radiology*, vol. 263, no. 2, pp. 451–460, 2012.

[77] M. Laforge *et al.*, "Tissue damage from neutrophil-induced oxidative stress in COVID-19," *Nature Reviews Immunology*, vol. 20, no. 9. Nature Research, pp. 515–516, 29-Jul-2020.

[78] P. J. Barnes, “Oxidative stress-based therapeutics in COPD,” *Redox Biology*, vol. 33. Elsevier B.V., 01-Jun-2020.

[79] B. Corleis, D. Korbel, R. Wilson, J. Bylund, R. Chee, and U. E. Schaible, “Escape of Mycobacterium tuberculosis from oxidative killing by neutrophils,” *Cell. Microbiol.*, vol. 14, no. 7, pp. 1109–1121, 2012.

[80] A. C. Doran, A. Yurdagul, and I. Tabas, “Efferocytosis in health and disease,” *Nature Reviews Immunology*, vol. 20, no. 4. Nature Research, pp. 254–267, 01-Apr-2020.

[81] E. Boada-Romero, J. Martinez, B. L. Heckmann, and D. R. Green, “The clearance of dead cells by efferocytosis,” *Nature Reviews Molecular Cell Biology*, vol. 21, no. 7. Nature Research, pp. 398–414, 01-Jul-2020.

[82] J. M. McCracken and L. A. H. Allen, “Regulation of human neutrophil apoptosis and lifespan in health and disease,” *J. Cell Death*, vol. 7, no. 1, pp. 15–23, May 2014.

[83] T. Dallenga and U. E. Schaible, “Neutrophils in tuberculosis-first line of defence or booster of disease and targets for host-directed therapy?,” *Pathog. Dis.*, vol. 74, no. 3, pp. 1–8, 2016.

[84] K. Segawa and S. Nagata, “An Apoptotic ‘Eat Me’ Signal: Phosphatidylserine Exposure,” *Trends Cell Biol.*, vol. 25, no. 11, pp. 639–650, 2015.

[85] S. J. Kim, D. Gershov, X. Ma, N. Brot, and K. B. Elkon, “I-PLA2 activation during apoptosis promotes the exposure of membrane lysophosphatidylcholine leading to binding by natural immunoglobulin M antibodies and complement activation,” *J. Exp. Med.*, vol. 196, no. 5, pp. 655–665, Sep. 2002.

[86] B. Luo *et al.*, “Erythropoeitin Signaling in Macrophages Promotes Dying Cell Clearance and Immune Tolerance,” *Immunity*, vol. 44, no. 2, pp. 287–302, Feb. 2016.

[87] T. P. Mikołajczyk *et al.*, “Characterization of the impairment of the uptake of apoptotic polymorphonuclear cells by monocyte subpopulations in systemic lupus erythematosus,” *Lupus*, vol. 23, no. 13, pp. 1358–1369, 2014.

[88] R. Fernandez-Boyanapalli *et al.*, “Impaired Phagocytosis of Apoptotic Cells by Macrophages in Chronic Granulomatous Disease Is Reversed by IFN-γ in a Nitric

Oxide-Dependent Manner," *J. Immunol.*, vol. 185, no. 7, pp. 4030–4041, 2010.

[89] E. Niki, "Lipid peroxidation: Physiological levels and dual biological effects," *Free Radic. Biol. Med.*, vol. 47, no. 5, pp. 469–484, Sep. 2009.

[90] G. Carlin and R. Djurs?ter, "Peroxidation of Phospholipids Promoted by Myeloperoxidase," *Free Radic. Res. Commun.*, vol. 4, no. 4, pp. 251–257, Jan. 1988.

[91] S. Claster, D. T. Chiu, A. Quintanilha, and B. Lubin, "Neutrophils mediate lipid peroxidation in human red cells," *Blood*, vol. 64, no. 5, pp. 1079–1084, 1984.

[92] R. Piga, Y. Saito, Y. Yoshida, and E. Niki, "Cytotoxic effects of various stressors on PC12 cells: Involvement of oxidative stress and effect of antioxidants," *Neurotoxicology*, vol. 28, no. 1, pp. 67–75, Jan. 2007.

[93] H. BLOCH and W. SEGAL, "Biochemical differentiation of Mycobacterium tuberculosis grown in vivo and in vitro.," *J. Bacteriol.*, vol. 72, no. 2, pp. 132–141, Aug. 1956.

[94] D. G. Russell, P. J. Cardona, M. J. Kim, S. Allain, and F. Altare, "Foamy macrophages and the progression of the human tuberculosis granuloma," *Nature Immunology*, vol. 10, no. 9. NIH Public Access, pp. 943–948, 2009.

[95] J. Daniel, H. Maamar, C. Deb, T. D. Sirakova, and P. E. Kolattukudy, "Mycobacterium tuberculosis Uses Host Triacylglycerol to Accumulate Lipid Droplets and Acquires a Dormancy-Like Phenotype in Lipid-Loaded Macrophages," *PLoS Pathog.*, vol. 7, no. 6, p. e1002093, Jun. 2011.

[96] D. G. Russell *et al.*, "Mycobacterium tuberculosis wears what it eats."

[97] T. Ulrichs and S. H. E. Kaufmann, "New insights into the function of granulomas in human tuberculosis," *Journal of Pathology*, vol. 208, no. 2. John Wiley & Sons, Ltd, pp. 261–269, 01-Jan-2006.

[98] A. Brzostek, B. Dziadek, A. Rumijowska-Galewicz, J. Pawelczyk, and J. Dziadek, "Cholesterol oxidase is required for virulence of Mycobacterium tuberculosis," 2007.

[99] R. K. Maurya, S. Bharti, and M. Y. Krishnan, "Triacylglycerols: Fuelling the hibernating mycobacterium tuberculosis," *Front. Cell. Infect. Microbiol.*, vol. 9, no. JAN, p. 450, 2019.

[100] K. Kasahara, I. Sato, K. Ogura, H. Takeuchi, K. Kobayashi, and M. Adachi, "Expression of Chemokines and Induction of Rapid Cell Death in Human Blood Neutrophils by Mycobacterium tuberculosis."

[101] S. Y. Eum *et al.*, "Neutrophils are the predominant infected phagocytic cells in the airways of patients with active pulmonary TB," *Chest*, vol. 137, no. 1, pp. 122–128, 2010.

[102] S. Pokkali and S. D. Das, "Augmented chemokine levels and chemokine receptor expression on immune cells during pulmonary tuberculosis," *Hum. Immunol.*, vol. 70, no. 2, pp. 110–115, Feb. 2009.

[103] M. P. R. Berry *et al.*, "An interferon-inducible neutrophil-driven blood transcriptional signature in human tuberculosis," *Nature*, vol. 466, no. 7309, pp. 973–977, 2010.

[104] R. Gopal *et al.*, "S100A8/A9 proteins mediate neutrophilic inflammation and lung pathology during tuberculosis," *Am. J. Respir. Crit. Care Med.*, vol. 188, no. 9, pp. 1137–1146, 2013.

[105] I. Kramnik, W. F. Dietrich, P. Demant, and B. R. Bloom, "Genetic control of resistance to experimental infection with virulent Mycobacterium tuberculosis," 2000.

[106] E. Kondratieva, N. Logunova, K. Majorov, M. Averbakh, and A. Apt, "Host Genetics in Granuloma Formation: Human-Like Lung Pathology in Mice with Reciprocal Genetic Susceptibility to M. tuberculosis and M. avium," *PLoS One*, vol. 5, no. 5, p. e10515, May 2010.

[107] V. Yeremeev, I. Linge, T. Kondratieva, and A. Apt, "Neutrophils exacerbate tuberculosis infection in genetically susceptible mice," *Tuberculosis*, vol. 95, no. 4, pp. 447–451, 2015.

[108] C. Keller, R. Hoffmann, R. Lang, S. Brandau, C. Hermann, and S. Ehlers, "Genetically determined susceptibility to tuberculosis in mice causally involves accelerated and enhanced recruitment of granulocytes," *Infect. Immun.*, vol. 74, no. 7, pp. 4295–4309, 2006.

[109] I. Kramnik, P. Demant, and B. B. Bloom, "Susceptibility to tuberculosis as a complex genetic trait: Analysis using recombinant congenic strains of mice," *Novartis Found. Symp.*, no. 217, pp. 120–137, 1998.

[110] J. A. L. Flynn, “Lessons from experimental Mycobacterium tuberculosis infections,” *Microbes and Infection*, vol. 8, no. 4. Elsevier Masson, pp. 1179–1188, 01-Apr-2006.

[111] E. R. Rhoades, “Progression of chronic pulmonary tuberculosis in mice aerogenically infected with virulent Mycobacterium tuberculosis,” *Tuber. Lung Dis.*, vol. 78, no. 1, pp. 57–66, Jan. 1997.

[112] I. Kramnik, W. F. Dietrich, P. Demant, and B. R. Bloom, “Genetic control of resistance to experimental infection with virulent Mycobacterium tuberculosis.,” *Proc. Natl. Acad. Sci. U. S. A.*, vol. 97, pp. 8560–8565, 2000.

[113] S. M. Irwin *et al.*, “Presence of multiple lesion types with vastly different microenvironments in C3HeB/FeJ mice following aerosol infection with Mycobacterium tuberculosis.,” *Dis. Model. Mech.*, vol. 8, no. 6, pp. 591–602, 2015.

[114] A. V Pichugin, B.-S. Yan, A. Sloutsky, L. Kobzik, and I. Kramnik, “Immunopathology and Infectious Diseases Dominant Role of the sst1 Locus in Pathogenesis of Necrotizing Lung Granulomas during Chronic Tuberculosis Infection and Reactivation in Genetically Resistant Hosts,” *Am. J. Pathol.*, vol. 174, no. 6, pp. 2190–2201, 2009.

[115] E. R. Driver *et al.*, “Evaluation of a mouse model of necrotic granuloma formation using C3HeB/FeJ mice for testing of drugs against Mycobacterium tuberculosis,” *Antimicrob. Agents Chemother.*, vol. 56, no. 6, pp. 3181–3195, 2012.

[116] E. R. Rhoades, “Progression of chronic pulmonary tuberculosis in mice aerogenically infected with virulent Mycobacterium tuberculosis,” *Tuber. Lung Dis.*, vol. 78, no. 1, pp. 57–66, Jan. 1997.

[117] A. V Pichugin, B. S. Yan, A. Sloutsky, L. Kobzik, and I. Kramnik, “Dominant role of the sst1 locus in pathogenesis of necrotizing lung granulomas during chronic tuberculosis infection and reactivation in genetically resistant hosts,” *Am J Pathol*, vol. 174, no. 6, pp. 2190–2201, 2009.

[118] C. Lavebratt, A. S. Apt, B. V. Nikonenko, M. Schalling, and E. Schurr, “Severity of Tuberculosis in Mice is Linked to Distal Chromosome 3 and Proximal Chromosome 9,” *J. Infect. Dis.*, vol. 180, no. 1, pp. 150–155, Jul. 1999.

[119] B. V. Nikonenko, M. M. Averbakh, A. S. Apt, C. Lavebratt, and E. Schurr,

"Comparative analysis of mycobacterial infections in susceptible I/St and resistant A/Sn inbred mice," *Tuber. Lung Dis.*, vol. 80, no. 1, pp. 15–25, Jan. 2000.

[120] F. Sánchez *et al.*, "Multigenic control of disease severity after virulent Mycobacterium tuberculosis infection in mice," *Infect. Immun.*, vol. 71, no. 1, pp. 126–131, Jan. 2003.

[121] M. K. K. Niazi *et al.*, "Lung necrosis and neutrophils reflect common pathways of susceptibility to Mycobacterium tuberculosis in genetically diverse, immune-competent mice," 2015.

[122] S. Aly *et al.*, "Oxygen status of lung granulomas inMycobacterium tuberculosis-infected mice," *J. Pathol.*, vol. 210, no. 3, pp. 298–305, Nov. 2006.

[123] J. J. Linderman, N. A. Cilfone, E. Pienaar, C. Gong, and D. E. Kirschner, "A multi-scale approach to designing therapeutics for tuberculosis," *Integr. Biol. (United Kingdom)*, vol. 7, no. 5, pp. 591–609, 2015.

[124] A. Kolloli and S. Subbian, "Host-directed therapeutic strategies for tuberculosis," *Front. Med.*, vol. 4, no. OCT, 2017.

[125] E. Niki, "Lipid peroxidation: Physiological levels and dual biological effects," *Free Radic. Biol. Med.*, vol. 47, no. 5, pp. 469–484, 2009.

[126] A. De Jong *et al.*, "CD1a autoreactive T cells recognize natural skin oils that Function As Headless Antigens," vol. 15, no. 2, pp. 177–185, 2014.

[127] I. Van Rhijn *et al.*, "Human autoreactive T cells recognize CD1b and phospholipids," *Proc. Natl. Acad. Sci.*, vol. 113, no. 2, p. 201520947, 2015.

[128] P. Y. Lee, J.-X. Wang, E. Parisini, C. C. Dascher, and P. A. Nigrovic, "Ly6 family proteins in neutrophil biology," *J. Leukoc. Biol.*, vol. 94, no. 4, pp. 585–594, 2013.

[129] T. Itou, L. V. Collins, F. B. Thorén, C. Dahlgren, and A. Karlsson, "Changes in activation states of murine polymorphonuclear leukocytes (PMN) during inflammation: A comparison of bone marrow and peritoneal exudate PMN," *Clin. Vaccine Immunol.*, vol. 13, no. 5, pp. 575–583, May 2006.

[130] B. Uhl *et al.*, "Aged neutrophils contribute to the first line of defense in the acute inflammatory response," *Blood*, vol. 128, no. 19, pp. 2327–2337, Nov. 2016.

[131] N. Fine *et al.*, "Primed PMNs in healthy mouse and human circulation are first responders during acute inflammation," *Blood Adv.*, vol. 3, no. 10, pp. 1622–1637,

2019.

[132] E. B. Eruslanov *et al.*, "Neutrophil Responses to Mycobacterium tuberculosis Infection in Genetically Susceptible and Resistant mice," *Society*, vol. 73, no. 3, pp. 1744–1753, 2005.

[133] A. J. M. Lenaerts, V. Gruppo, J. V Brooks, and I. M. Orme, "NOTES Rapid In Vivo Screening of Experimental Drugs for Tuberculosis Using Gamma Interferon Gene-Disrupted Mice," *Antimicrob. Agents Chemother.*, vol. 47, no. 2, pp. 783–785, 2003.

[134] M. Gonzalez-Juarrero, L. K. Woolhiser, E. Brooks, M. A. DeGroote, and A. J. Lenaerts, "Mouse model for efficacy testing of antituberculosis agents via intrapulmonary delivery," *Antimicrob. Agents Chemother.*, vol. 56, no. 7, pp. 3957–3959, Jul. 2012.

[135] P. E. Simms and T. M. Ellis, "Utility of flow cytometric detection of CD69 expression as a rapid method for determining poly- and oligoclonal lymphocyte activation," *Clin. Diagn. Lab. Immunol.*, vol. 3, no. 3, pp. 301–304, 1996.

[136] P. S. Penglis, L. G. Cleland, M. Demasi, G. E. Caughey, and M. J. James, "Differential Regulation of Prostaglandin E_2 and Thromboxane A_2 Production in Human Monocytes: Implications for the Use of Cyclooxygenase Inhibitors," *J. Immunol.*, vol. 165, no. 3, pp. 1605–1611, Aug. 2000.

[137] J. E. Kyle *et al.*, "Cell type-resolved human lung lipidome reveals cellular cooperation in lung function," vol. 8, p. 13455, 2018.

[138] Y. Zheng *et al.*, "Inflammatory responses relate to distinct bronchoalveolar lavage lipidome in community-acquired pneumonia patients: A pilot study," *Respir. Res.*, vol. 20, no. 1, 2019.

[139] J. C. Alarcon-Barrera *et al.*, "Lipid metabolism of leukocytes in the unstimulated and activated states," *Anal. Bioanal. Chem.*, vol. 412, no. 10, pp. 2353–2363, Apr. 2020.

[140] S. E. Horvath and G. Daum, "Lipids of mitochondria," *Prog. Lipid Res.*, vol. 52, no. 4, pp. 590–614, 2013.

[141] C. Osman, M. Haag, F. T. Wieland, B. Brügger, and T. Langer, "A mitochondrial phosphatase required for cardiolipin biosynthesis: the PGP phosphatase Gep4," *EMBO J.*, vol. 29, no. 12, pp. 1976–1987, Jun. 2010.

[142] J. A. Poveda *et al.*, “Lipid modulation of ion channels through specific binding sites,” *Biochimica et Biophysica Acta - Biomembranes*, vol. 1838, no. 6. Elsevier, pp. 1560–1567, 01-Jun-2014.

[143] A. Tong *et al.*, “Direct binding of phosphatidylglycerol at specific sites modulates desensitization of a Ligand-gated ion channel,” *Elife*, vol. 8, Nov. 2019.

[144] M. Knight, J. Braverman, K. Asfaha, K. Gronert, and S. Stanley, “Lipid droplet formation in Mycobacterium tuberculosis infected macrophages requires IFN-γ/HIF-1α signaling and supports host defense,” *PLoS Pathog.*, vol. 14, no. 1, Jan. 2018.

[145] S. T. Cole *et al.*, “Deciphering the biology of mycobacterium tuberculosis from the complete genome sequence,” *Nature*, vol. 393, no. 6685. Nature, pp. 537–544, 11-Jun-1998.

[146] IOM (Institute of Medicine), *The Causes and Impacts of Neglected Tropical and Zoonotic Diseases : Opportunities for Integrated Intervention Strategies: Workshop Summary*. 2011.

[147] N. Brandenburg, J., Marwitz, S., Tazoll, SC., Waldow, F., Karlsdorf, B., Vierbuchen, T., Scholzen, T., Gross, A., Goldenbaum, S., Hölscher, A., Hein, M., Linnemann, L., Reimann, M., Kispert, A., Leitges, M., Rupp, J., Lange, C., Niemann, S., Behrends, J., Go, “Mycobacterium tuberculosis exploits WNT6-induced Acetyl-CoA Carboxylase-2 driven perturbation of host lipid homeostasis to facilitate growth in macrophages,” pp. 1–56, 2020.

[148] A. Brzostek, J. Pawelczyk, A. Rumijowska-Galewicz, B. Dziadek, and J. Dziadek, “Mycobacterium tuberculosis is able to accumulate and utilize cholesterol,” *J. Bacteriol.*, vol. 191, no. 21, pp. 6584–6591, Nov. 2009.

[149] A. K. Pandey and C. M. Sassetti, “Mycobacterial persistence requires the utilization of host cholesterol,” *Proc. Natl. Acad. Sci. U. S. A.*, vol. 105, no. 11, pp. 4376–4380, Mar. 2008.

[150] M. Swamydas, Y. Luo, M. E. Dorf, and M. S. Lionakis, “Isolation of mouse neutrophils,” *Curr. Protoc. Immunol.*, vol. 2015, pp. 3.20.1-3.20.15, 2015.

[151] R. Boxio, C. Bossenmeyer-Pourié, N. Steinckwich, C. Dournon, and O. Nüße, “Mouse bone marrow contains large numbers of functionally competent neutrophils,” *J. Leukoc. Biol.*, vol. 75, no. 4, pp. 604–611, 2003.

[152] M. Swamydas and M. S. Lionakis, “Isolation, purification and labeling of mouse bone marrow neutrophils for functional studies and adoptive transfer experiments.,” *J. Vis. Exp.*, no. 77, p. e50586, 2013.

[153] S. Basu, G. Hodgson, M. Katz, and A. R. Dunn, “Evaluation of role of G-CSF in the production, survival, and release of neutrophils from bone marrow into circulation,” *Blood*, vol. 100, no. 3, pp. 854–861, 2002.

[154] D. Metcalf, “Control of granulocytes and macrophages: Molecular, cellular, and clinical aspects,” *Science*, vol. 254, no. 5031. Science, pp. 529–533, 1991.

[155] G. D. Demetri and J. D. Griffin, “Granulocyte colony-stimulating factor and its receptor,” *Blood*, vol. 78, no. 11. pp. 2791–2808, 1991.

[156] L. J. Campbell *et al.*, “Marrow proliferation and the appearance of giant neutrophils in response to recombinant human granulocyte colony stimulating factor (rhG-CSF),” *Br. J. Haematol.*, vol. 80, no. 3, pp. 298–304, Mar. 1992.

[157] M. R. Shalaby, B. B. Aggarwal, E. Rinderknecht, L. P. Svedersky, B. S. Finkle, and M. A. Palladino, “Activation of human polymorphonuclear neutrophil functions by interferon-gamma and tumor necrosis factors.,” *J. Immunol.*, vol. 135, no. 3, 1985.

[158] L. F. Marchi, R. Sesti-Costa, M. D. C. Ignacchiti, S. Chedraoui-Silva, and B. Mantovani, “In vitro activation of mouse neutrophils by recombinant human interferon-gamma: Increased phagocytosis and release of reactive oxygen species and pro-inflammatory cytokines,” *Int. Immunopharmacol.*, vol. 18, no. 2, pp. 228–235, 2014.

[159] T. N. Ellis and B. L. Beaman, “Interferon-γ activation of polymorphonuclear neutrophil function,” *Immunology*, vol. 112, no. 1. Wiley-Blackwell, pp. 2–12, May-2004.

[160] B. D. Hansen and D. S. Finbloom, “Characterization of the interaction between recombinant human interferon-γ and its receptor on human polymorphonuclear leukocytes,” *J. Leukoc. Biol.*, vol. 47, no. 1, pp. 64–69, 1990.

[161] J. Larrick, D. Graham, K. Toy, L. Lin, G. Senyk, and B. Fendly, “Recombinant tumor necrosis factor causes activation of human granulocytes,” *Blood*, vol. 69, no. 2, pp. 640–644, Feb. 1987.

[162] J. L. Salyer, J. F. Bohnsack, W. A. Knape, A. O. Shigeoka, E. R. Ashwood, and H.

R. Hill, “Mechanisms of tumor necrosis factor-α alteration of PMN adhesion and migration,” *Am. J. Pathol.*, vol. 136, no. 4, pp. 831–841, 1990.

[163] A. L. Corbi, T. K. Kishimoto, L. J. Miller, and T. A. Springer$, “THE JOURNAL OF BIOLOGICAL CHEMISTRY The Human Leukocyte Adhesion Glycoprotein Mac-1 (Complement Receptor Type 3, CDllb) a! Subunit CLONING, PRIMARY STRUCTURE, AND RELATION TO THE INTEGRINS, VON WILLEBRAND FACTOR AND FACTOR B*,” 1988.

[164] D. C. Anderson *et al.*, “The severe and moderate phenotypes of heritable Mac-1, LFA-1 deficiency: Their quantitative definition and relation to leukocyte dysfunction and clinical features,” *J. Infect. Dis.*, vol. 152, no. 4, pp. 668–689, Oct. 1985.

[165] D. C. Anderson and T. A. Springer, “Leukocyte adhesion deficiency: an inherited defect in the Mac-1, LFA-1, and p150,95 glycoproteins.,” *Annu. Rev. Med.*, vol. 38, pp. 175–194, 1987.

[166] R. Kettritz, M. Choi, S. Rolle, M. Wellner, and F. C. Luft, “Integrins and Cytokines Activate Nuclear Transcription Factor-κB in Human Neutrophils,” *J. Biol. Chem.*, vol. 279, no. 4, pp. 2657–2665, Jan. 2004.

[167] K. O. Kisich, M. Higgins, G. Diamond, and L. Heifets, “Tumor necrosis factor alpha stimulates killing of Mycobacterium tuberculosis by human neutrophils,” *Infect. Immun.*, vol. 70, no. 8, pp. 4591–4599, 2002.

[168] K. B. Boyle *et al.*, “ Class IA Phosphoinositide 3-Kinase β and δ Regulate Neutrophil Oxidase Activation in Response to Aspergillus fumigatus Hyphae ,” *J. Immunol.*, vol. 186, no. 5, pp. 2978–2989, Mar. 2011.

[169] M. Evrard *et al.*, “Developmental Analysis of Bone Marrow Neutrophils Reveals Populations Specialized in Expansion, Trafficking, and Effector Functions,” *Immunity*, vol. 48, no. 2, pp. 364-379.e8, 2018.

[170] Y. P. Zhu *et al.*, “Identification of an Early Unipotent Neutrophil Progenitor with Pro-tumoral Activity in Mouse and Human Bone Marrow,” *Cell Rep.*, vol. 24, no. 9, pp. 2329-2341.e8, 2018.

[171] J. Pillay *et al.*, “Functional heterogeneity and differential priming of circulating neutrophils in human experimental endotoxemia,” *J. Leukoc. Biol.*, vol. 88, no. 1, pp. 211–220, Jul. 2010.

[172] R. Taneja, A. P. Sharma, M. B. Hallett, G. P. Findlay, and M. R. Morris, "IMMATURE CIRCULATING NEUTROPHILS IN SEPSIS HAVE IMPAIRED PHAGOCYTOSIS AND CALCIUM SIGNALING," *Shock*, vol. 30, no. 6, pp. 618–622, Dec. 2008.

[173] A. Churg *et al.*, "Late intervention with a myeloperoxidase inhibitor stops progression of experimental chronic obstructive pulmonary disease," *Am. J. Respir. Crit. Care Med.*, vol. 185, no. 1, pp. 34–43, 2012.

[174] A. J. Kettle, C. A. Gedye, and C. C. Winterbourn, "Mechanism of inactivation of myeloperoxidase by 4-aminobenzoic acid hydrazide.," *Biochem. J.*, vol. 321 (Pt 2, pp. 503–508, 1997.

[175] V. T. V. Dao *et al.*, "Pharmacology and Clinical Drug Candidates in Redox Medicine," *Antioxidants and Redox Signaling*, vol. 23, no. 14. Mary Ann Liebert Inc., pp. 1113–1129, 10-Nov-2015.

[176] D. Venturelli *et al.*, "Nucleic Acids Research Nucleotide sequence of cDNA for murine myeloperoxidase A cDNA encoding murine myeloperoxidase (MPO) was cloned and sequenced from a PUC19 library derived from a hemopoietic progenitor cell line induced to differentiate into sequen," vol. 17, no. 14, p. 15213, 1989.

[177] Y. C. Patry, P. H. Nachman, M. A. P. Audrain, R. J. Falk, K. Meflah, and V. L. M. Esnault, "Difference in antigenic determinant profiles between human and rat myeloperoxidase," *Clin. Exp. Immunol.*, vol. 132, no. 3, pp. 505–508, Jun. 2003.

[178] H. J. Kim *et al.*, "Myeloperoxidase inhibition increases neurogenesis after ischemic stroke," *J. Pharmacol. Exp. Ther.*, vol. 359, no. 2, pp. 262–272, Nov. 2016.

[179] H. J. Kim, Y. Wei, G. R. Wojtkiewicz, J. Y. Lee, M. A. Moskowitz, and J. W. Chen, "Reducing myeloperoxidase activity decreases inflammation and increases cellular protection in ischemic stroke."

[180] H. J. Kim, Y. Wei, G. R. Wojtkiewicz, J. Y. Lee, M. A. Moskowitz, and J. W. Chen, "Reducing myeloperoxidase activity decreases inflammation and increases cellular protection in ischemic stroke," *J. Cereb. Blood Flow Metab.*, vol. 39, no. 9, pp. 1864–1877, Sep. 2019.

[181] P. V. Turner, T. Brabb, C. Pekow, and M. A. Vasbinder, "Administration of substances to laboratory animals: Routes of administration and factors to consider,"

Journal of the American Association for Laboratory Animal Science, vol. 50, no. 5. American Association for Laboratory Animal Science, pp. 600–613, Sep-2011.

[182] R. E. Lewis, A. L. Kunz, and R. E. Bell, "Error of intraperitoneal injections in rats.," *Lab. Anim. Care*, vol. 16, no. 6, pp. 505–509, 1966.

[183] M.-S. Koo *et al.*, "Phosphodiesterase 4 Inhibition Reduces Innate Immunity and Improves Isoniazid Clearance of Mycobacterium tuberculosis in the Lungs of Infected Mice," *PLoS One*, vol. 6, no. 2, p. e17091, Feb. 2011.

[184] S. T. Byrne, S. M. Denkin, and Y. Zhang, "Aspirin Antagonism in Isoniazid Treatment of Tuberculosis in Mice," *Antimicrob. Agents Chemother.*, vol. 51, no. 2, pp. 794–795, 2007.

[185] D. H. Canaday *et al.*, "CD4 þ T cell polyfunctional pro fi le in HIV-TB coinfection are similar between individuals with latent and active TB infection," *Tuberculosis*, vol. 95, no. 4, pp. 470–475, 2015.

[186] D. K. Singh, S. Ahmad, P. Moodley, M. Bhattacharyya, L. Van Kaer, and G. Das, "Isoniazid Induces Apoptosis Of Activated CD4 T Cells IMPLICATIONS FOR POST-THERAPY TUBERCULOSIS REACTIVATION AND REINFECTION * Sultan Tousif ‡1," 2014.

[187] G. Rausch PG, Moore, "Granule enzymes of polymorphonuclear neutrophils: A phylogenetic comparison," *Blood*, vol. 46, no. 6, pp. 913–9, 1975.

[188] M. E. Griffith, A. Coulthart, and C. D. Pusey, "T cell responses to myeloperoxidase (MPO) and proteinase 3 (PR3) in patients with systemic vasculitis," *Clin. Exp. Immunol.*, vol. 103, no. 2, pp. 253–258, 1996.

[189] J. D. Ooi *et al.*, "The immunodominant myeloperoxidase T-cell epitope induces local cell-mediated injury in antimyeloperoxidase glomerulonephritis," *Proc. Natl. Acad. Sci. U. S. A.*, vol. 109, no. 39, p. E2615, Sep. 2012.

[190] P. Y. Gan *et al.*, "Th17 cells promote autoimmune anti-myeloperoxidase glomerulonephritis," *J. Am. Soc. Nephrol.*, vol. 21, no. 6, pp. 925–931, Jun. 2010.

[191] D. Odobasic *et al.*, "Neutrophil myeloperoxidase regulates T-cell2driven tissue inflammation in mice by inhibiting dendritic cell function," *Blood*, vol. 121, pp. 4195–4204, 2013.

[192] D. Odobasic *et al.*, "Suppression of Autoimmunity and Renal Disease in Pristane-

Induced Lupus by Myeloperoxidase," *Arthritis Rheumatol.*, vol. 67, no. 7, pp. 1868–1880, Jul. 2015.

[193] H. Bouali *et al.*, "Association of the G-463A myeloperoxidase gene polymorphism with renal disease in African Americans with systemic lupus erythematosus," *J. Rheumatol.*, vol. 34, no. 10, pp. 2028–2034, Oct. 2007.

[194] B. S. Chalam KV, "An In vitro Assay to Quantify Nitrosative Component of Oxidative Stress," *J. Mol. Genet. Med.*, vol. 08, no. 03, 2014.

[195] S. Moncada, R. M. Palmer, and E. A. Higgs, "Nitric oxide: physiology, pathophysiology, and pharmacology.," *Pharmacol. Rev.*, vol. 43, no. 2, 1991.

[196] G. Laffi *et al.*, "Increased production of nitric oxide by neutrophils and monocytes from cirrhotic patients with ascites and hyperdynamic circulation," *Hepatology*, vol. 22, no. 6, pp. 1666–1673, Dec. 1995.

[197] M. A. Wheeler, R. M. Weiss, and W. C. Sessa, "Bacterial infection induces nitric oxide synthase in human neutrophils," *J Clin Invest*, vol. 99, no. 1, p. 110, 1997.

[198] C. Nathan and M. U. Shiloh, "Reactive oxygen and nitrogen intermediates in the relationship between mammalian hosts and microbial pathogens," *Proc. Natl. Acad. Sci. U. S. A.*, vol. 97, no. 16, pp. 8841–8848, Aug. 2000.

[199] L. B. Adams, M. C. Dinauer, D. E. Morgenstern, and J. L. Krahenbuhl, "Comparison of the roles of reactive oxygen and nitrogen intermediates in the host response to Mycobacterium tuberculosis using transgenic mice," *Tuber. Lung Dis.*, vol. 78, no. 5–6, pp. 237–246, Jan. 1997.

[200] J. D. Macmicking, R. J. North, R. Lacourse, J. S. Mudgett, S. K. Shah, and C. F. Nathan, "Identification of nitric oxide synthase as a protective locus against tuberculosis (Mycobacterium tuberculosisinfectious disease)," 1997.

[201] V. Tsutsumi, R. Mena-Lopez, F. Anaya-Velazquez, and A. Martinez-Palomo, "Cellular bases of experimental amebic liver abscess formation," *Am. J. Pathol.*, vol. 117, no. 1, pp. 81–91, 1984.

[202] K. B. Seydel, T. Zhang, and J. Stanley, "Neutrophils play a critical role in early resistance to amebic liver abscesses in severe combined immunodeficient mice," *Infect. Immun.*, vol. 65, no. 9, pp. 3951–3953, 1997.

[203] A. Cruz-Baquero *et al.*, "Different behavior of myeloperoxidase in two rodent

amoebic liver abscess models," *PLoS One*, vol. 12, no. 8, Aug. 2017.

[204] A. M. Cooper, B. H. Segal, A. A. Frank, S. M. Holland, and I. M. Orme, "Transient loss of resistance to pulmonary tuberculosis in p47(phox-/-) mice," *Infect. Immun.*, vol. 68, no. 3, pp. 1231–1234, 2000.

11 LIST OF FIGURES

12 SUPPLEMENTARY MATERIAL

12.1 Isotype control for MPO-DAB immunostaining

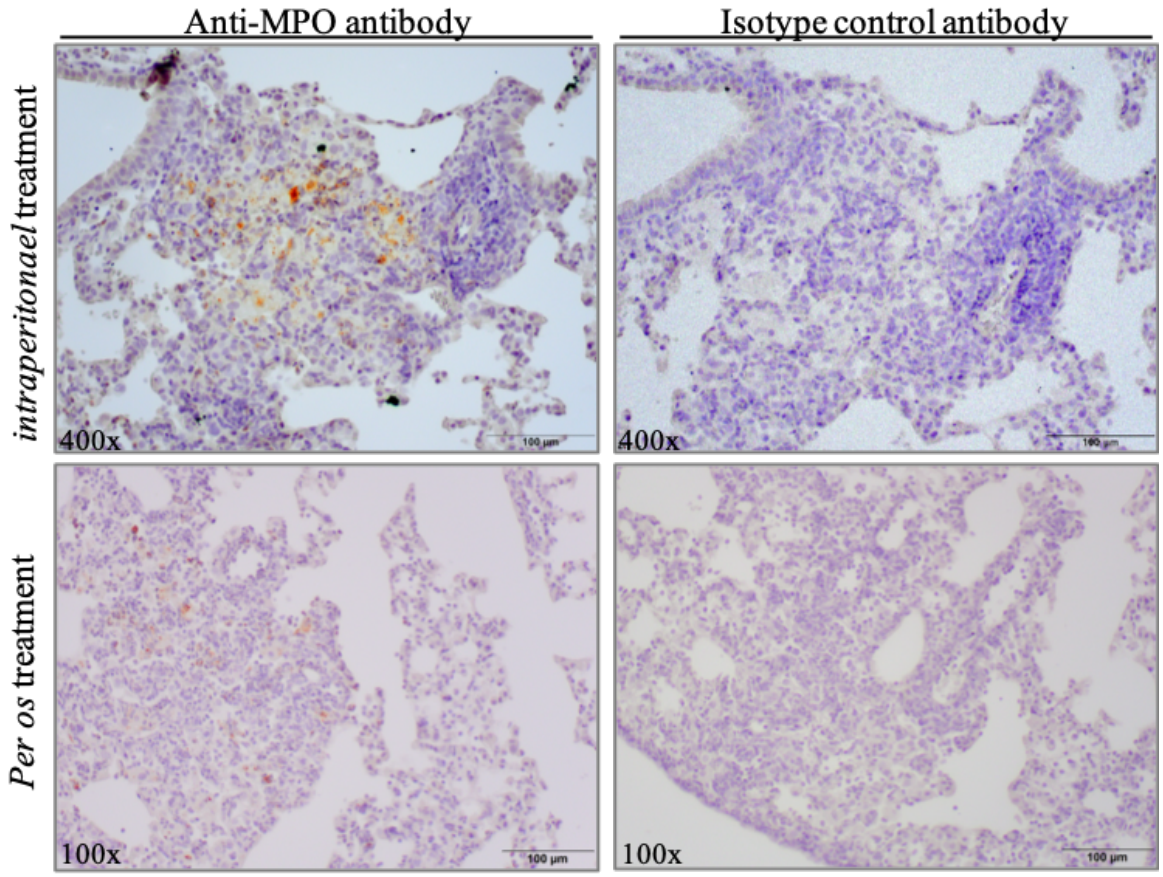

Figure 39 Isotype control stain for MPO-DAB stain. C3HeB/FeJ mice were infected with an infection dose of 100 – 150 Mtb H37Rv via aerosol inhalation, treated *intraperitoneally* for a 9-day period with 40 mg/kg ABAH and sacrificed at day 41 p.i., respectively or treated *per os* for a 10-day period with 80 mg/kg ABAH and were killed at day 36 p.i. Lungs were removed, embedded in parafin and processed for immunostaining for MPO. Shown are isotype controls for each treatment. Brown spots mark positive MPO identification.

12.2 Flow cytometry gating scheme for *in vivo* analysis of PMN and myeloid cells

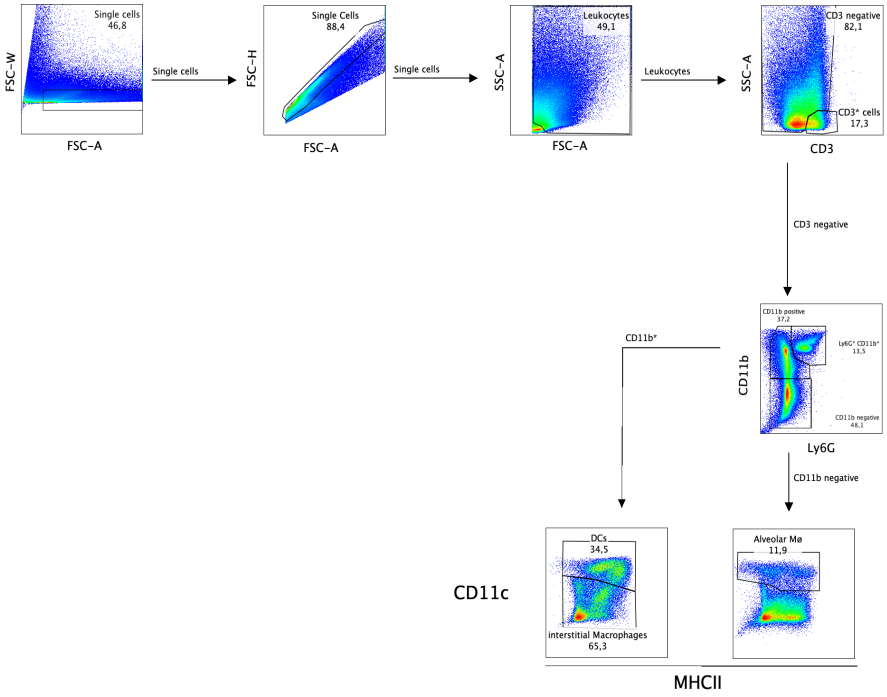

Figure 40 Flow cytometry gating scheme for *in vivo* analysis of PMN and other myeloid cells. After debris, doublet and $CD3^+$ lymphocyte exclusion, PMN were defined as $Ly6G^+$. Further PMN gating for Mtb infection, ROS production and necrosis can be found in gating scheme **Figure 12**. $Ly6G^-$ cells were further gated into alveolar macrophages ($CD11b^-/CD11c^+$, Frequency of $CD3^-$), interstitial macrophages ($CD11b^-/CD11c^{med/-}$, Frequency of $CD3^-$) and Dendritic cells (DC) ($CD11b^+/CD11c^+$, Frequency of $CD3^-$). In the gating scheme, a '*' symbolizes a positive cell culture ('$^+$')

12.3 Flow cytometry gating scheme for *in vivo* analysis of PMN MPO expression and T and NKT cells

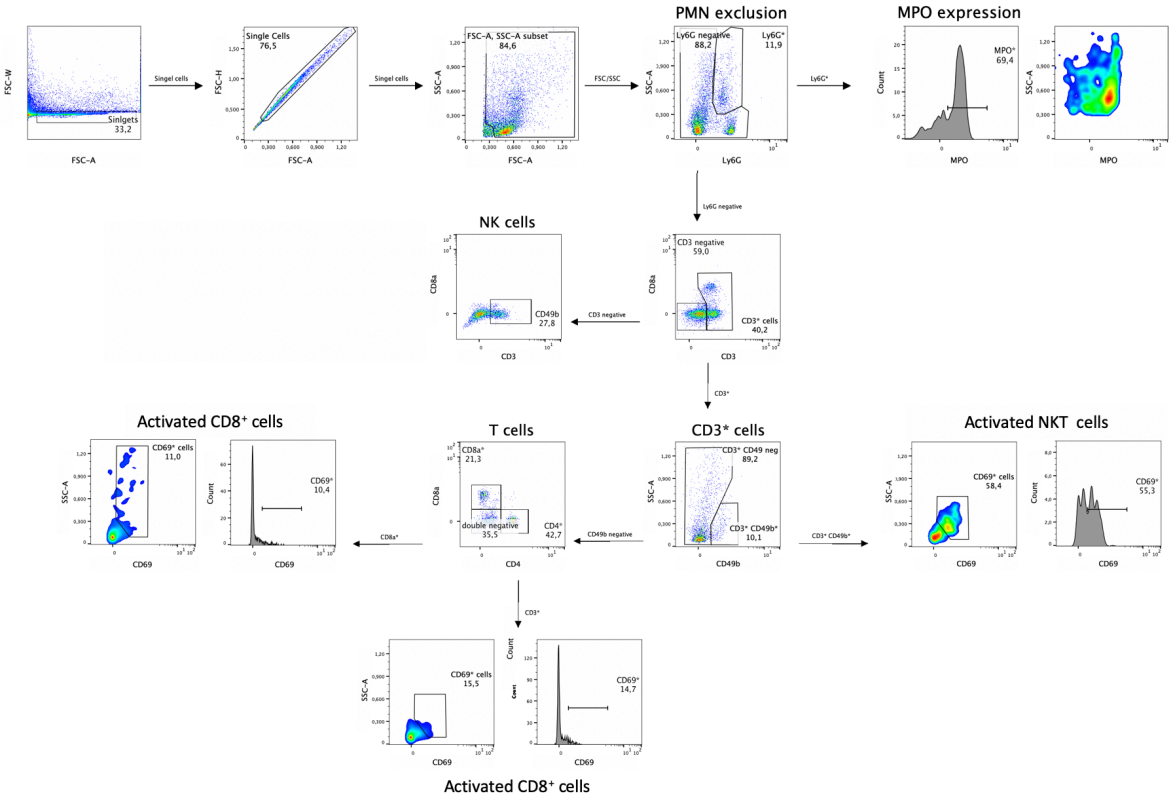

Figure 41 Flow cytometry gating scheme for in vivo analysis of PMN MPO expression and T and NKT cells. After debris, doublet exclusion, PMN were defined as $Ly6G^{+}/SSC\text{-}A^{high}$. From this population the frequency of MPO^{+} cells were analysed. $CD3^{+}/Ly6G^{-}$ cells were again gated for $CD3^{+}$ cells. The $CD3^{-}$ cell population was gated for NK cells as $CD3^{-}/CD49b^{+}$, Frequency of $FSC\text{-}A^{+}/SSC\text{-}A^{+}$. The $CD3^{+}$ population was gated for $CD3^{+}/CD49b^{+}$ cells as NKT cells. $CD3^{+}/CD49b^{-}$ cells were then gated for $CD4^{+}$ and $CD8^{+}$ T cells. NKT cells, $CD4^{+}$ and $CD8^{+}$ T cells were then each gated for activated cells in each cell population as $CD69^{+}$ cells. In the gating scheme, a '*' symbolizes a positive cell culture ('+').

12.4 Detailed presentation of different lipid classes

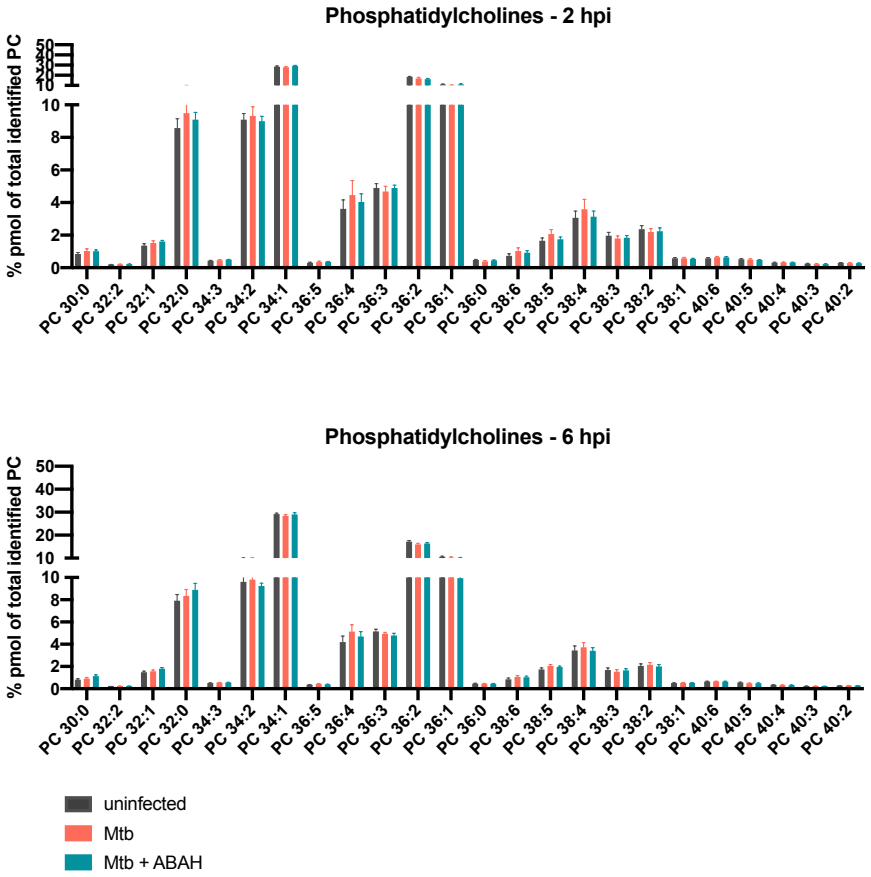

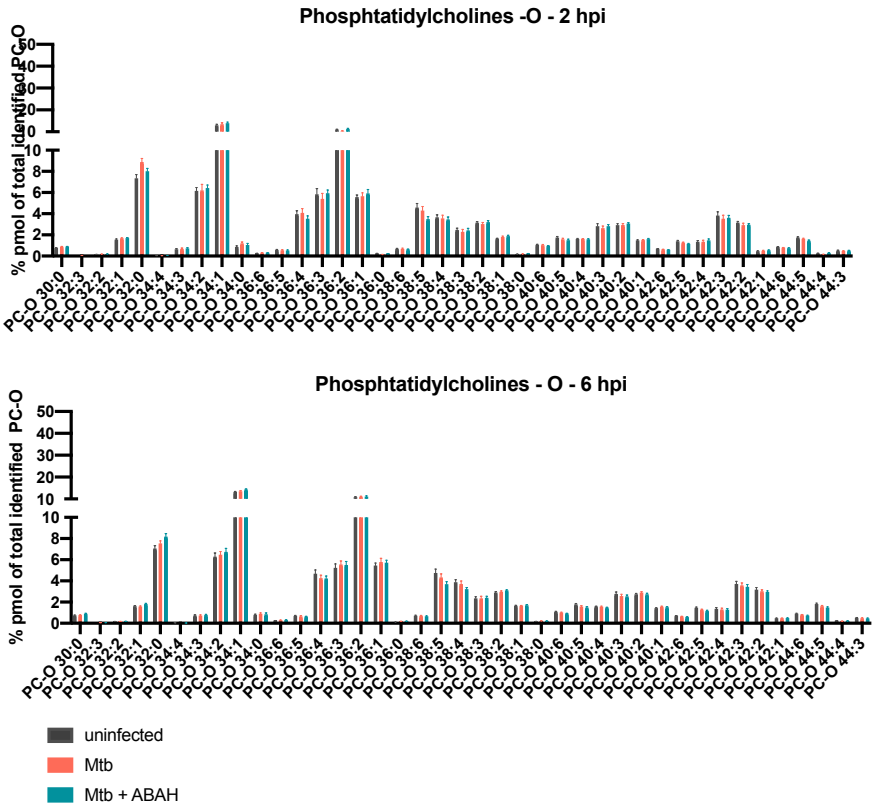

Figure 42 Phosphatidylcholine lipid species distribution in hPMN upon H37Rv Mtb infection and additional MPO inhibition. Lipids were isolated from hPMN *in vitro* cultures at 2 and 6 hpi, which were either uninfected, infected with H37Rv or infected and treated with the MPO inhibitor ABAH. For detailed analysis of Phosphatidylcholine (PC) lipid species, normalization to the total amount of Phosphatidylcholine lipids was made. Depicted are 5 independent experiments. Error bars indicate mean with SEM.

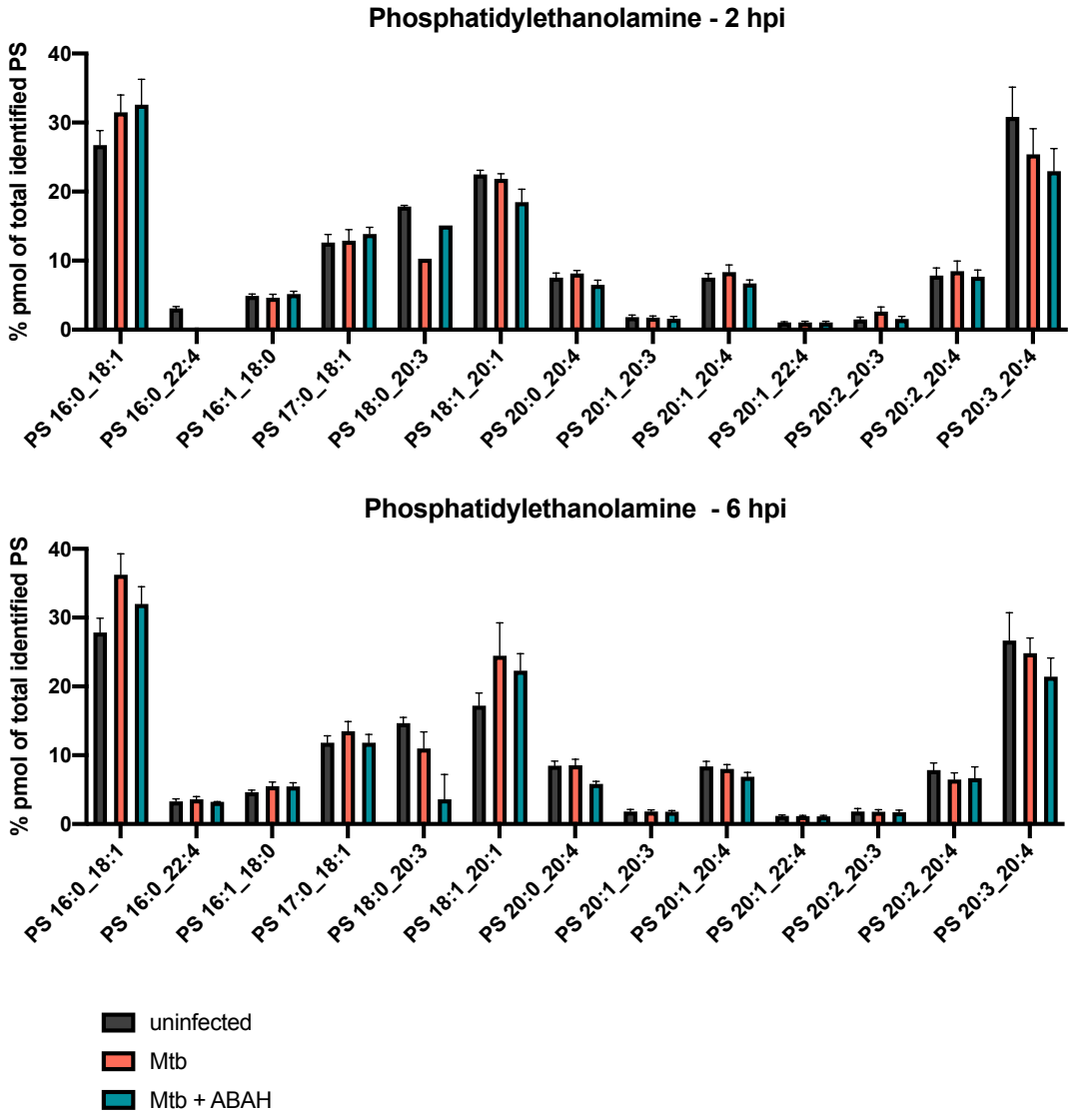

Figure 43 Phosphatidylethanolamine lipid species distribution in hPMN upon H37Rv Mtb infection and additional MPO inhibition. Lipids were isolated from hPMN *in vitro* cultures at 2 and 6 hpi, which were either uninfected, infected with H37Rv or infected and treated with the MPO inhibitor ABAH. For detailed analysis of Phosphatidylethanolamine (PS) lipid species, normalization to the total amount of Phosphatidylethanolamine lipids was made. Depicted are 5 independent experiments. Error bars indicate mean with SEM.

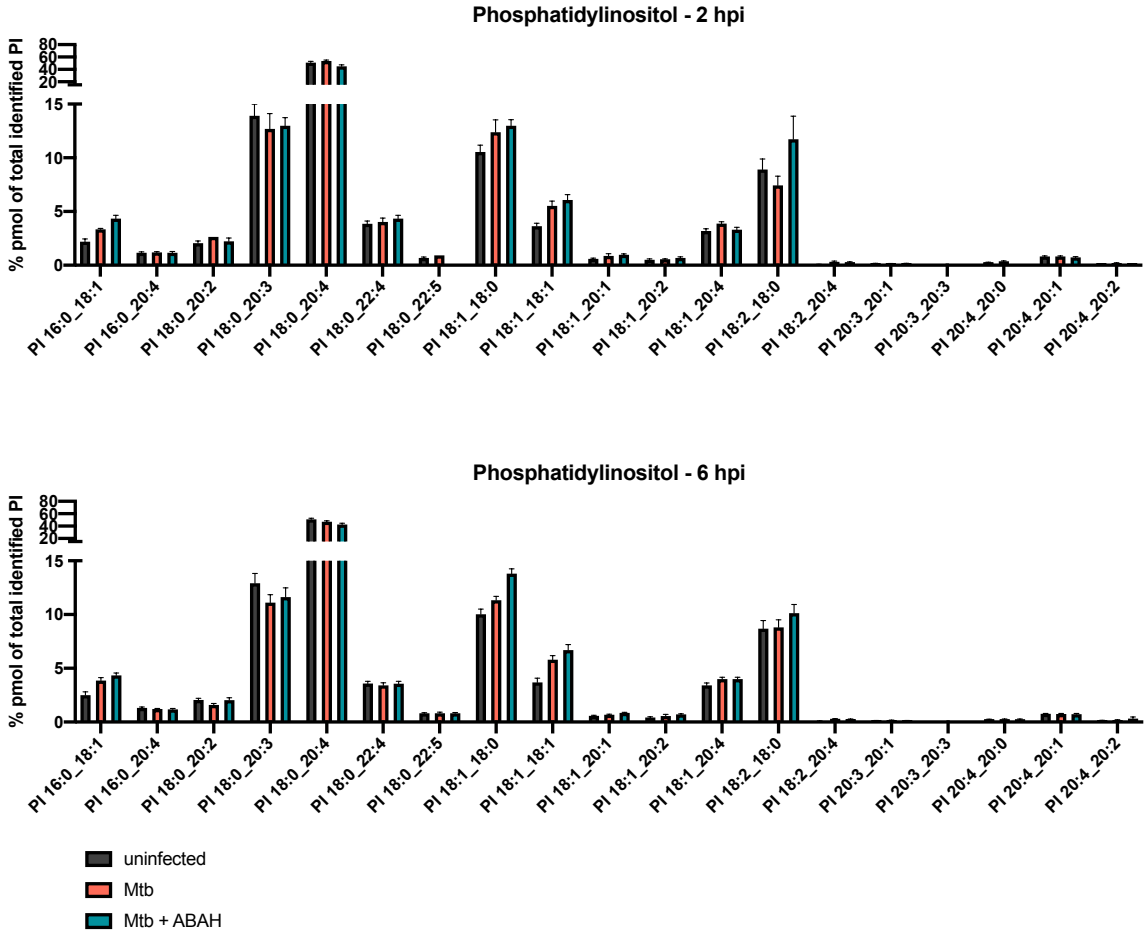

Figure 44 Phosphatidylinositol lipid species distribution in hPMN upon H37Rv Mtb infection and additional MPO inhibition. Lipids were isolated from hPMN *in vitro* cultures at 2 and 6 hpi, which were either uninfected, infected with H37Rv or infected and treated with the MPO inhibitor ABAH. For detailed analysis of Phosphatidylinositol (PI) lipid species, normalization to the total amount of Phosphatidylinositol lipids was made. Depicted are 5 independent experiments. Error bars indicate mean with SEM.

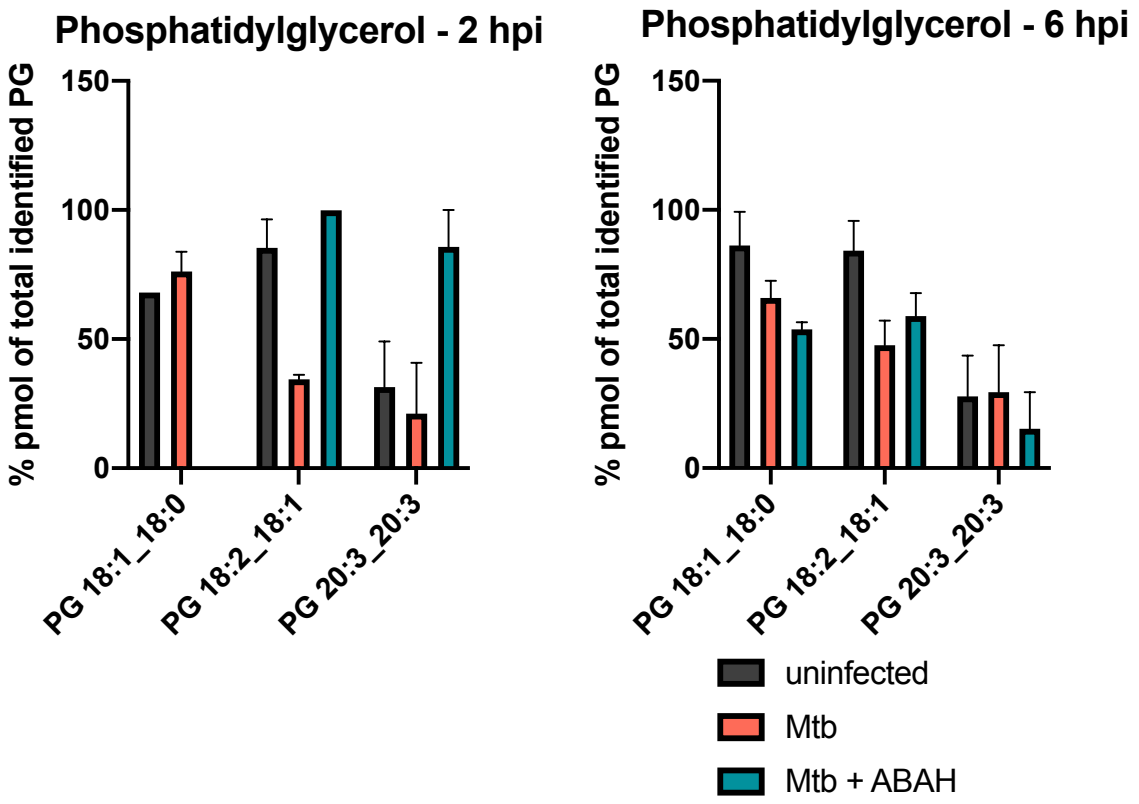

Figure 45 Phosphatidylglycerol lipid species distribution in hPMN upon H37Rv Mtb infection and additional MPO inhibition. Lipids were isolated from hPMN *in vitro* cultures at 2 and 6 hpi, which were either uninfected, infected with H37Rv or infected and treated with the MPO inhibitor ABAH. For detailed analysis of Phosphatidylglycerol (PI) lipid species, normalization to the total amount of Phosphatidylglycerol lipids was made. Depicted are 5 independent experiments. Error bars indicate mean with SEM.

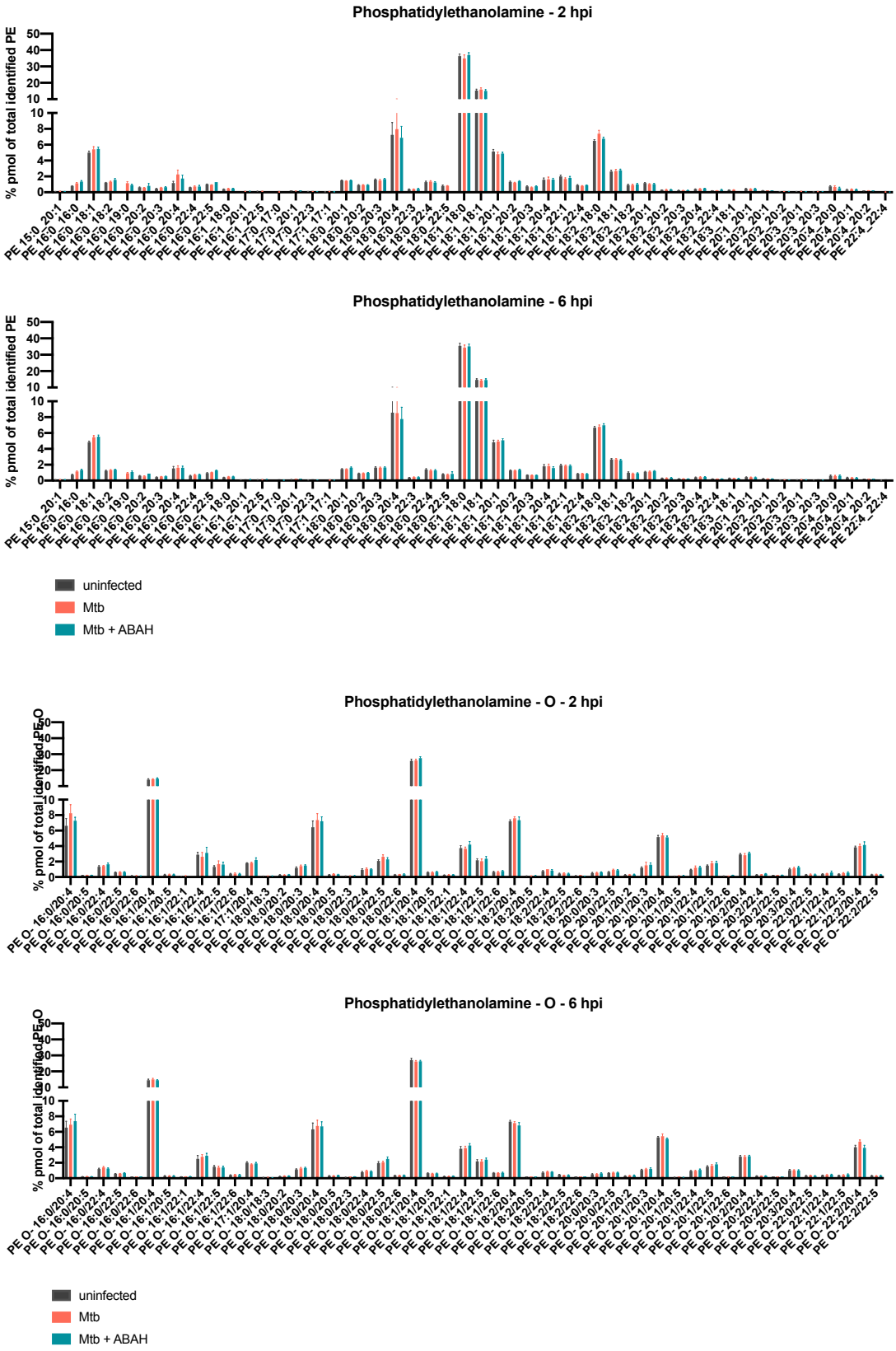

Figure 46 Phosphatidylethanolamine lipid species distribution in hPMN upon H37Rv Mtb infection and additional MPO inhibition. Lipids were isolated from hPMN *in vitro* cultures at 2 and 6 hpi, which were either uninfected, infected with H37Rv or infected and treated with

the MPO inhibitor ABAH. For detailed analysis of Phosphatidylethanolamine (PE) lipid species, normalization to the total amount of Phosphatidylethanolamine lipids was made. Depicted are 5 independent experiments. Error bars indicate mean with SEM.

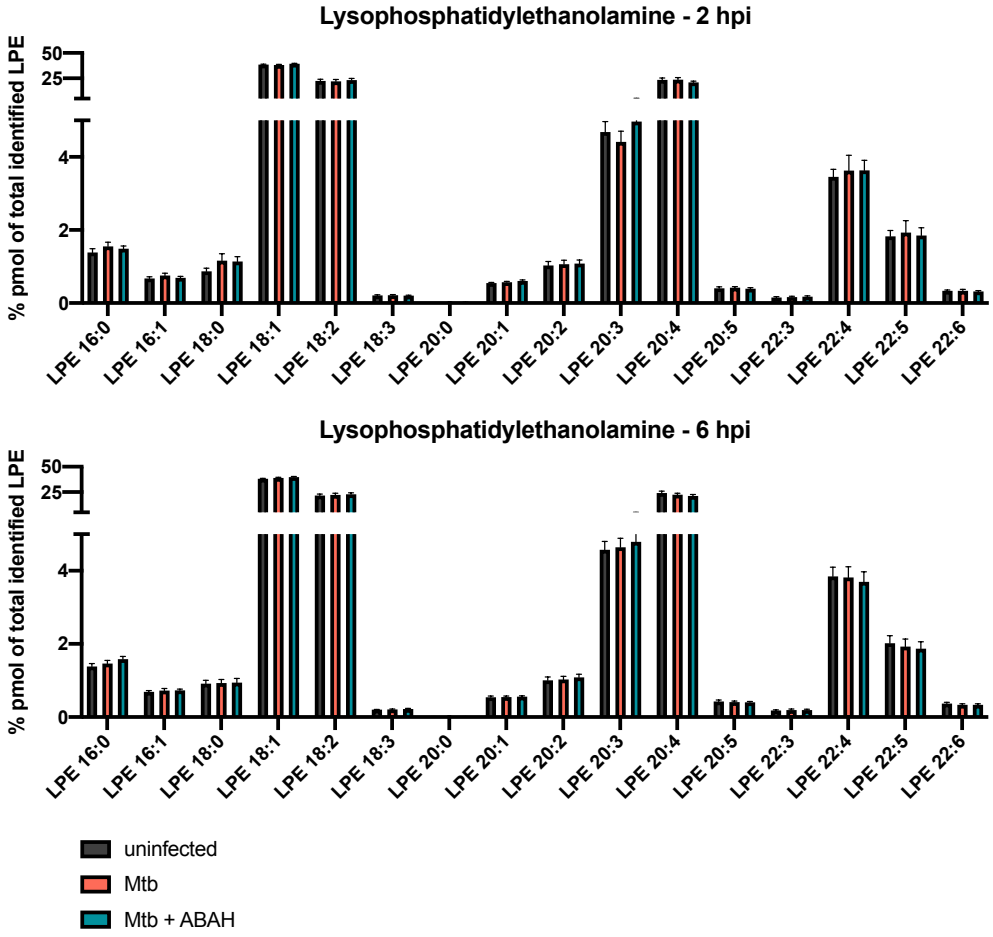

Figure 47 **Lysophosphatidylethanolamine lipid species distribution in hPMN upon H37Rv Mtb infection and additional MPO inhibition.** Lipids were isolated from hPMN *in vitro* cultures at 2 and 6 hpi, which were either uninfected, infected with H37Rv or infected and treated with the MPO inhibitor ABAH. For detailed analysis of Lysophosphatidylethanolamine (LPE) lipid species, normalization to the total amount of Lysophosphatidylethanolamine lipids was made. Depicted are 5 independent experiments. Error bars indicate mean with SEM.

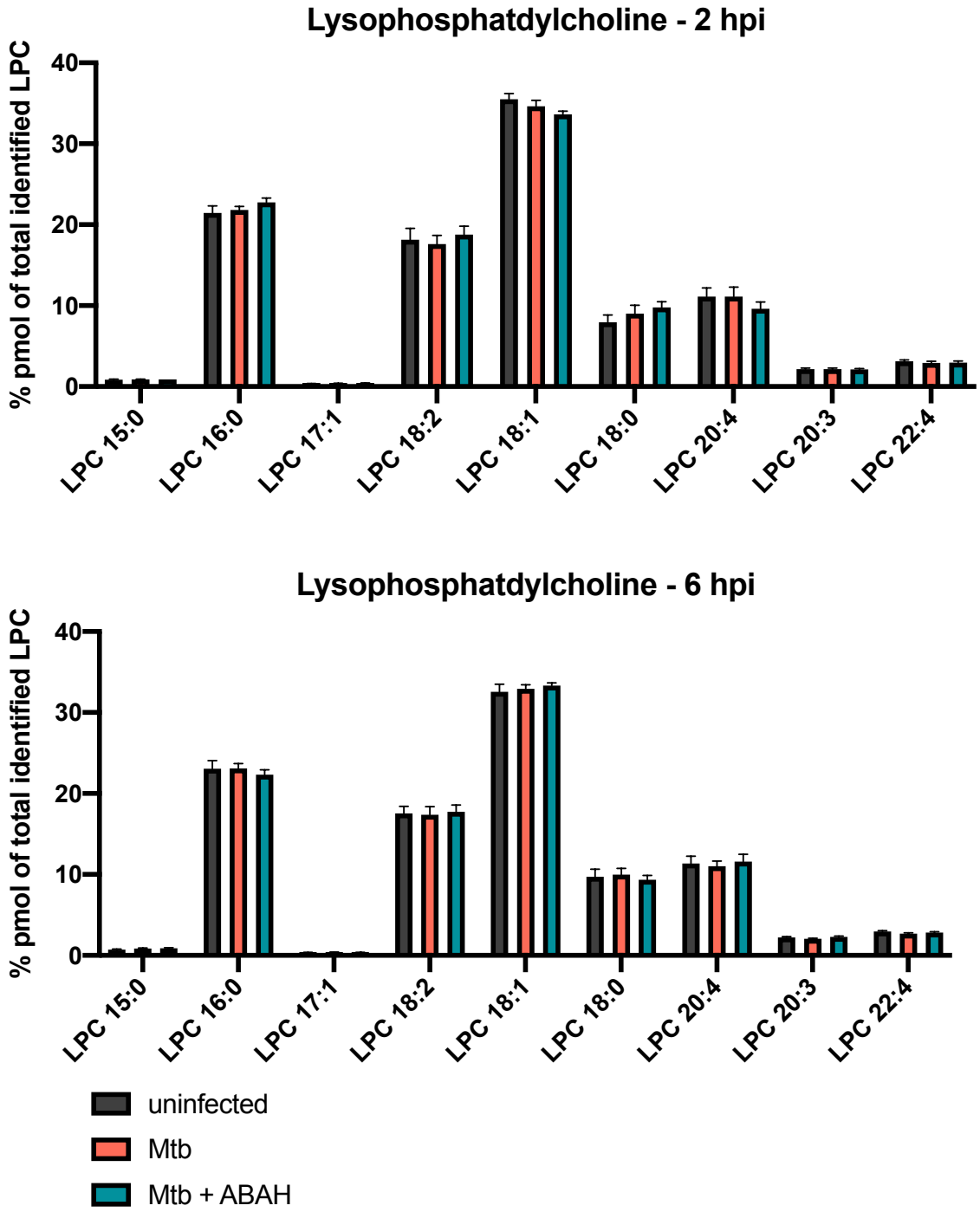

Figure 48 Lysophosphatidylcholine lipid species distribution in hPMN upon H37Rv Mtb infection and additional MPO inhibition. Lipids were isolated from hPMN *in vitro* cultures at 2 and 6 hpi, which were either uninfected, infected with H37Rv or infected and treated with the MPO inhibitor ABAH. For detailed analysis of Lysophosphatidylcholine (LPC) lipid species, normalization to the total amount of Lysophosphatidylcholine lipids was made. Depicted are 5 independent experiments. Error bars indicate mean with SEM.

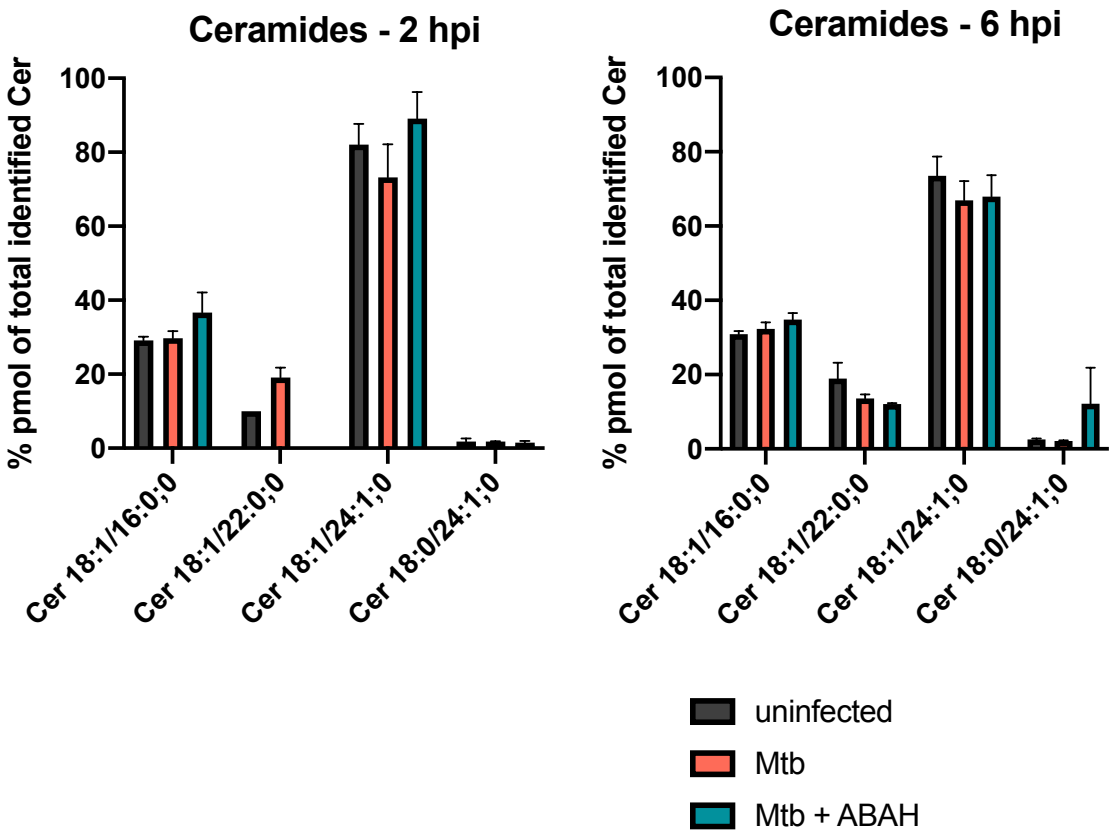

Figure 49 Ceramides lipid species distribution in hPMN upon H37Rv Mtb infection and additional MPO inhibition. Lipids were isolated from hPMN *in vitro* cultures at 2 and 6 hpi, which were either uninfected, infected with H37Rv or infected and treated with the MPO inhibitor ABAH. For detailed analysis of Ceramides (CER) lipid species, normalization to the total amount of Ceramides lipids was made. Depicted are 5 independent experiments. Error bars indicate mean with SEM.

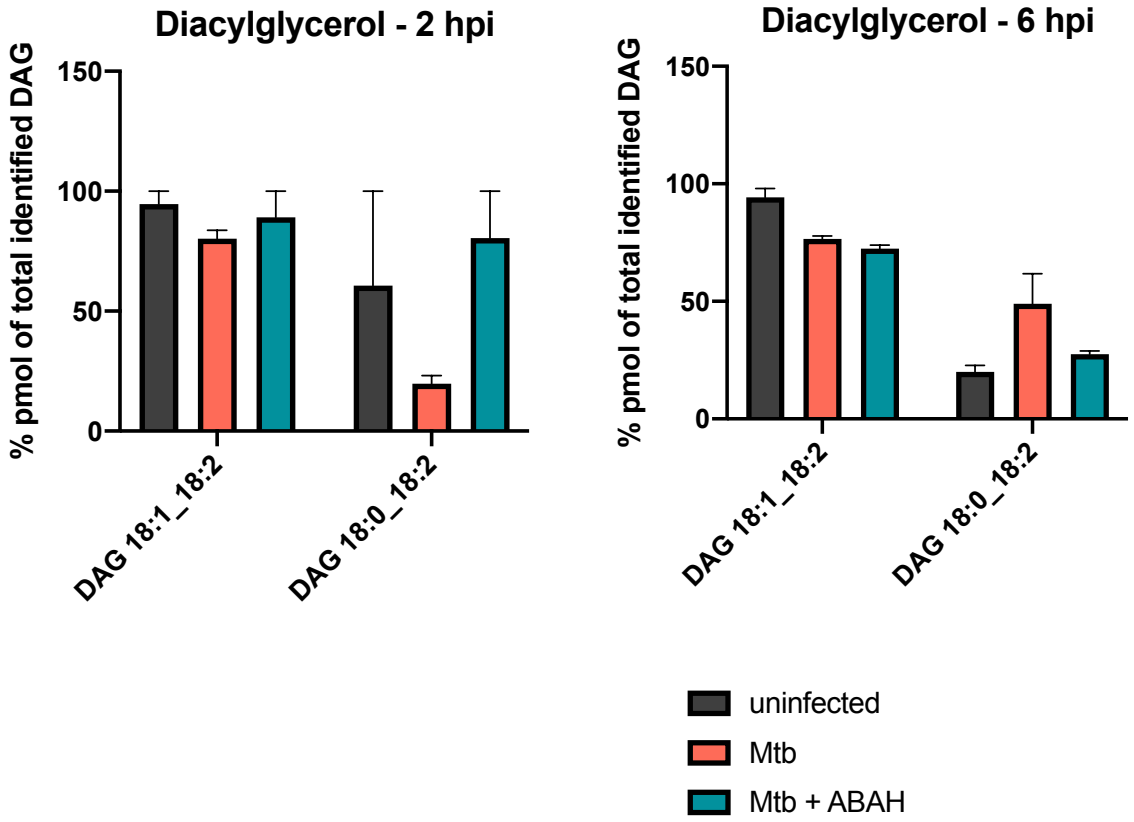

Figure 50 Diacylglycerols lipid species distribution in hPMN upon H37Rv Mtb infection and additional MPO inhibition. Lipids were isolated from hPMN *in vitro* cultures at 2 and 6 hpi, which were either uninfected, infected with H37Rv or infected and treated with the MPO inhibitor ABAH. For detailed analysis of Diacylglycerol (DAG) lipid species, normalization to the total amount of Diacylglycerol lipids was made. Depicted are 5 independent experiments. Error bars indicate mean with SEM.

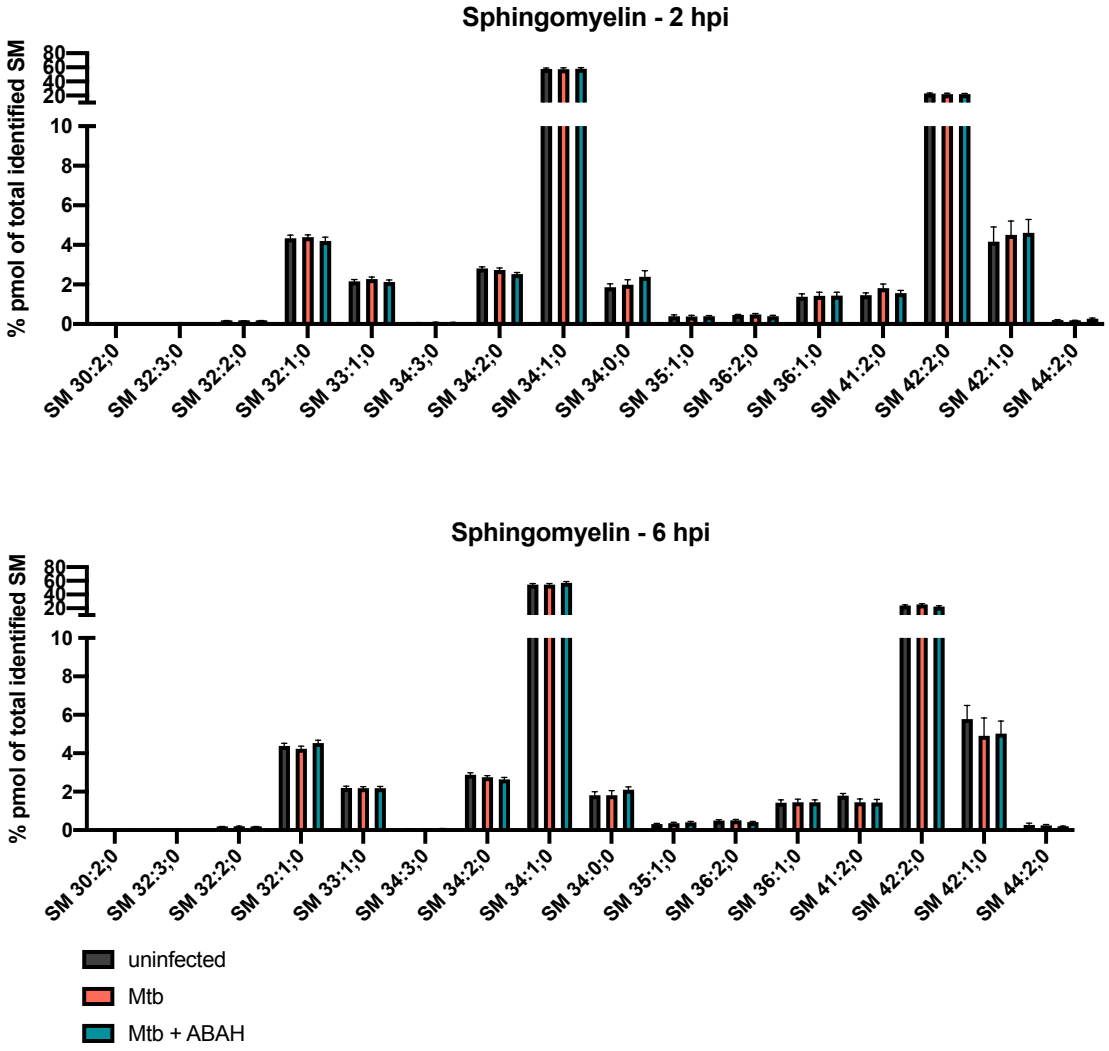

Figure 51 Sphingomyelin lipid species distribution in hPMN upon H37Rv Mtb infection and additional MPO inhibition. Lipids were isolated from hPMN *in vitro* cultures at 2 and 6 hpi, which were either uninfected, infected with H37Rv or infected and treated with the MPO inhibitor ABAH. For detailed analysis of Sphingomyelin (SM) lipid species, normalization to the total amount of Sphingomyelin lipids was made. Depicted are 5 independent experiments. Error bars indicate mean wit

13 DANKSAGUNG

Ich möchte mich zunächst bei Herrn Prof. Dr. **Ulrich Schaible** für das Bereitstellen meines Promotionsthemas bedanken. Darüber hinaus, war die Möglichkeit in deiner Arbeitsgruppe und in Borstel zu arbeiten, eine wunderschöne Erfahrung, die ich nicht missen möchte. Die Diskussionen und Gespräche waren immer inspirierend, begeisternd und motivierend.

Prof. Dr. **Kathrin Kalies** möchte ich danken, dass sie die Zweitbegutachtung meiner Promotion übernimmt, sowie bei Prof. Dr. **Norbert Tautz**, dass er sich bereit erklärt hat, den Vorsitz für meine mündliche Prüfung zu übernehmen.

Dr. **Christoph Hölscher**, der mich im Rahmen des Doktorandenprogramms des ITRG1911 mit seinen Ideen und Erfahrungen zu Mausversuchen immer sehr unterstützt hat. Darüber hinaus gilt mein Dank **Shouxiong Huang**, PhD, der mich während meines Auslandsaufenthaltes an der Universität von Cincinnati sehr herzlich in seine Arbeitsgruppe aufgenommen hat. Die Diskussionen und Erfahrung die ich dort in Bezug auf Lipidbiologie, T Zellen und FACS Analysen erfahren habe, haben mich weitergebracht.

PD Dr. **Dominik Schwudke** möchte ich dafür danken, dass er mir die Faszination für Biochemie und Lipide nähergebracht hat. Zu Beginn war es ein mir fremdes Thema, für welches ich mich, auch dank unserer zahlreichen Diskussionen, inzwischen begeistern kann. Ohne deine große Unterstützung, Expertise und Ratschläge hätte ich das nicht stemmen können. Dabei möchte ich natürlich nicht die Menschen aus seiner Arbeitsgruppe vergessen, die stets bereit waren, mich bei meinen Arbeiten in der Biochemie, zu unterstützen. Ohne **Michael**, **Verena** und **Franzi**. wäre ich nicht so schnell und gut vorangekommen. Ich habe mich dort immer Willkommen gefühlt.

Auf einer ganz anderen Ebene möchte ich mich dazu noch einmal bei **Dominik Schwudke** bedanken. Ich denke sehr gerne an unsere gemeinsamen Musikabende zurück. Du hast mich nach Jahren des Solo-spielens wieder dazu gebracht mein Geigenspiel mit anderen zu teilen. Die Möglichkeit, dass ich auf der Weihnachtsfeier 2019 vom Forschungszentrum Teil der Band sein konnte, ist etwas ganz Besonderes gewesen!

Von der Arbeitsgruppe ‚Mikrobielle Grenzflächenbiologie' möchte ich PD Dr. **Norbert Reiling** danken, mit dem ich ebenfalls inspirierende Gespräche und Diskussionen hatte.

Großer Dank geht natürlich auch an unsere tolle Arbeitsgruppe der zellulären Mikrobiologie! Ihr wart ein tolles Team! Allen voran **Tobi**, danke für deine Unterstützung

und Einarbeitung in das Thema und den Oidorno Diskussionen. **Christoph**, ich werde unsere Diskussionen und gemeinsames Haare raufen sehr vermissen! Viel Erfolg bei deinem Endspurt! **Julia**, vielen Dank für unsere Gemeinsame Zeit, Waldspaziergänge und den immer freien Sofaplatz, wenn ich es nicht mehr nach Hamburg geschafft habe. **Jacqueline**, ohne dich wäre die Zeit im IRTG und in Cincinnati nicht das gewesen, was es war. Ich werde unsere Cinci-WG und die Gespräche mit dir vermissen. Hau rein, dann hast du es auch bald geschafft! Dazu möchte ich mich noch einmal bei meinem Masterstudenten **Diego** bedanken, der mit großem Interesse einen Teil meines Projektes vorangetrieben hat. Viel Erfolg für deine PhD-Zukunft! Ohne die große Hilfe von **Jacqueline, Kristine, Nina** und **Vivien** wäre ich oft ‚lost im lab' gewesen und ohne eure Hilfe bei den Organentnahmen hätten diese Tage gedauert! Ein Besonderer Dank geht dabei noch an **Dagmar**, die mir unglaublich bei der Verarbeitung der Organe und deren Färbung geholfen hat**.** Vergessen möchte ich auch nicht **Ola**, **Jessica** und **Pit**, viel Erfolg euch und vielen Dank euch allen für euren Support!

Ich hätte diese Arbeit zudem nicht ohne die Unterstützung meiner Freund*innen und Familie geschafft. Es sind zu viele Menschen, die ich jetzt aufzählen könnte, deswegen danke ich zunächst stellvertretend der **Julio Lopez Gruppe**. Nach Corona stoßen wir noch einmal gemeinsam an!

Liebe Proseccotherapie - **Annika, Bini** und **Miri** - die bezaubernde Unterstützung, die ich moralisch und emotional von euch bekommen habe, hat mich durch die vier Jahre getragen und wird es weiter tun!

Meinen Eltern, **Regine** und **Michael**, möchte ich besonders danken, dass ihr mir von klein auf, die Faszination an Wissenschaft und Natur mitgegeben habt. Das, und ihr, wart mir stets eine Inspiration! Herzlichen Glückwunsch an meine Schwester **Doris**, die nun doch noch vor mir mit ihrer Promotion fertig geworden ist, und meinen Bruder **Falk**. Ich bin froh, dass ihr da seid!

Julius, ich freue mich mehr als alles andere auf unsere gemeinsame Zukunft!

14 EIDESSTATTLICHE ERKLÄRUNG

Hiermit versichere ich, dass ich die Dissertation ohne fremde Hilfe angefertigt und keine anderen als die angegebenen Hilfsmittel verwendet habe. Weder vorher noch gleichzeitig habe ich andernorts einen Zulassungsantrag gestellt oder diese Dissertation vorgelegt. Ich habe mich bisher noch keinem Promotionsverfahren unterzogen.

Hamburg, den. _____

_____

Lara Christine Linnemann